HIGH TEMPERATURE ELASTICITY OF FLUORIDE AND OXIDE ANALOGUES

by

Leonie Ellen Ann Jones

A thesis submitted for the degree of

Doctor of Philosophy

to the

Australian National University

Research School of Earth Sciences

April, 1976

"Beware of the man who works hard to learn something, learns it and finds himself no wiser than before ..... He is full of murderous resentment of people who are ignorant without having come by their ignorance the hard way."

Kurt Vonnegut, Cat's Cradle.

The experimental programme reported in this thesis was carried out by the author in the Research School of Earth Sciences, A.N.U., from March 1972 to January 1976. Some of the material presented in Chapter 5 is a result of collaboration with Dr. R. C. Liebermann and was published in Jones and Liebermann (1974). All other discussions and interpretations are my own work except as acknowledged.

Leonie E. Jones

Leonie E. Jones

ACKNOWLEDGEMENTS

My thanks go foremost to Dr. R. C. Liebermann for his constant and untiring supervision and guidance. To Dr. Liebermann I owe the development of my ability as a research scientist. I am also grateful to Prof. A. E. Ringwood for his interest in my work and for suggesting the application of the Goldschmidt fluoride-oxide modelling scheme to high temperature elasticity.

I would also like to extend my thanks to members of the technical staff of the R.S.E.S. for their friendship and willing advice on various matters, in particular W. H. Hibberson, A. Major, D. J. Mayson, and E. H. Pedersen. I thank Dr. R. A. Eggleton of the Geology Department, A.N.U. for use of his laboratory and assistance with transmission X-ray techniques.

I have also profitted through interaction with members of staff and student contemporaries. I am particularly grateful to Drs. T. J. Fitch and J. F. Gettrust and to J. Mills for discussions on data analysis and computer techniques. During my time at the A.N.U., I have valued the friendship of student contemporaries including G. Brey, M. P. Gorton, K. L. Harris, I. N. S. Jackson, G. Lister, P. M. Martin, T. Mori and D. J. Whitford.

I would like to express my gratitude to my family for the educational opportunities that they provided for me. The assistance of the Australian Government through a Commonwealth Post-Graduate Research Award (supplemented by the A.N.U.) is greatly appreciated.

Finally I would like to thank Mrs. A. Howarth for her patience and care in typing this thesis.

ABSTRACT

The precise ultrasonic pulse superposition technique has been employed to determine the elastic moduli as a function of temperature from T = 298-650°K for single crystal fluorides crystallising in the rocksalt (LiF and NaF), fluorite (CaF_2, SrF_2 and BaF_2), rutile (MgF_2) and perovskite ($KMgF_3$) structures. The pressure derivatives of the elastic moduli were also measured for $KMgF_3$. These new data are consistent with low temperature (T < 298°K) data obtained by other ultrasonic pulse techniques and are superior to previous high temperature data from resonance experiments. We employ these new data to consider the fluoride-oxide modelling scheme based on Goldschmidt's crystal chemical considerations and to evaluate the use of fluorides as models for the high temperature elastic behaviour of their oxide analogues.

The elastic moduli, c, are represented by quadratic functions in T over the experimental temperature range; however, the curvature is not in the same sense for all the crystals. For CaF_2, SrF_2, BaF_2 and MgF_2, the curvature is consistent with the predictions of classical lattice dynamics that the c-T plot at constant volume should be linear in T at high temperatures. The behaviour of the c' and c_{11} modes for LiF and NaF contradicts these predictions. The fluorides do not appear to exhibit high temperature elastic behaviour at significantly lower absolute temperatures than their oxide analogues.

The bulk moduli of equivolume oxides and fluorides in a particular structure are scaled as $4S^2$, where $S = Z^O/Z^F$ is the ratio of the effective unit charges and is approximately 75% for all the crystal structures. For the rocksalt-structure fluorides and oxides, the similar values for $|(\partial c/\partial T)_P|$ for the members of an analogue pair and their decrease with increasing molar volume are explained in terms of nearest neighbour distance in a model incorporating Mitskevich's theory

with K-V systematics. Such similarities do not exist in the values of $(\partial c/\partial T)_P$ for fluorides and oxides with the fluorite, rutile and perovskite structures and trends are absent for the last two structures. For compounds in all four structures, $(\partial K_S/\partial T)_P$ is dominated by the extrinsic temperature dependence, whereas for $(\partial \mu/\partial T)_P$, the intrinsic is at least as important as the extrinsic contribution.

CONTENTS

TABLES

FIGURES

CHAPTER 1

INTRODUCTION

CHAPTER 1

INTRODUCTION

Seismological studies provide the most direct information on the earth's interior in the form of elastic wave velocities and density as a function of depth. Mineral physics, the application of the concepts and techniques of solid state physics to the study of materials of importance in geophysics, bridges the gap between petrological models of the earth's interior and earth models derived from seismological evidence. Knowledge of the elastic moduli and their pressure and temperature derivatives is important not only for establishing an equation of state for the earth, but also for examining detailed problems, such as the nature of the low-velocity zone and elastic wave velocities in the descending lithospheric slab at plate margins.

Laboratory elasticity studies which employ ultrasonic techniques to determine the elastic wave velocities are limited in the attainable temperature and pressure range ($T < 1200^{\circ}C$, $P < 40$ kbar). The approach adopted in this thesis involves the study of analogue compounds under conditions accessible in the laboratory, to estimate the high pressure and high temperature properties of earth-forming compounds.

1.1 Fluoride-oxide modelling scheme and its application to high temperature elasticity

The concept of analogue compounds was first introduced on the basis of crystal chemical considerations by Goldschmidt (1927) who demonstrated that ionic size is one of the most important factors governing crystal structure. Ringwood (1970) has made extensive use of the germanates as high pressure models for the physical and crystal chemical properties of their silicate analogues. The larger size of the germanium ion with respect to silicon means that the germanates

should transform to high pressure phases at lower pressures than the corresponding silicates. Germanates have also been useful as models for the elasticity of high pressure phases of silicates (e.g., Liebermann, 1972, 1974b, 1975).

Another aspect of Goldschmidt's (1927) modelling concept concerns fluoride and oxide analogue compounds and is also based on crystal chemical considerations: (a) the similarity in ionic radii of O^{2-} and F^-; (b) the applicability of the rigid ion model to compounds containing the O^{2-} and F^- ions, which have relatively low polarisabilities resulting in their ionic radii being almost independent of co-ordination number; and (c) the correspondence of the crystal structures of oxide and fluoride compounds in which the cations are also of comparable ionic radii, but for which the cationic charge of the fluoride is half that of the oxide.

In the table below we illustrate the central feature of the entire modelling scheme: the similarity of the ionic radii of O^{2-} and F^- for various co-ordination numbers (after Shannon and Prewitt, 1969, 1970). The comparisons also demonstrate that the ionic radii of O^{2-} and F^- are almost independent of co-ordination number. Notable examples of simple

Co-ordination number	Ionic radii (Å)	
	O^{2-}	F^-
II	1.35	1.285
III	1.36	1.30
IV	1.38	1.31
VI	1.40	1.33

fluorides which exhibit structural correspondences are LiF-MgO (rocksalt structure), CaF_2-ThO_2 (fluorite structure), MgF_2-TiO_2 (rutile structure) and BeF_2-SiO_2 (α-quartz and coesite structures). The relative ionic sizes for fluorides and oxides in the rocksalt structure are illustrated

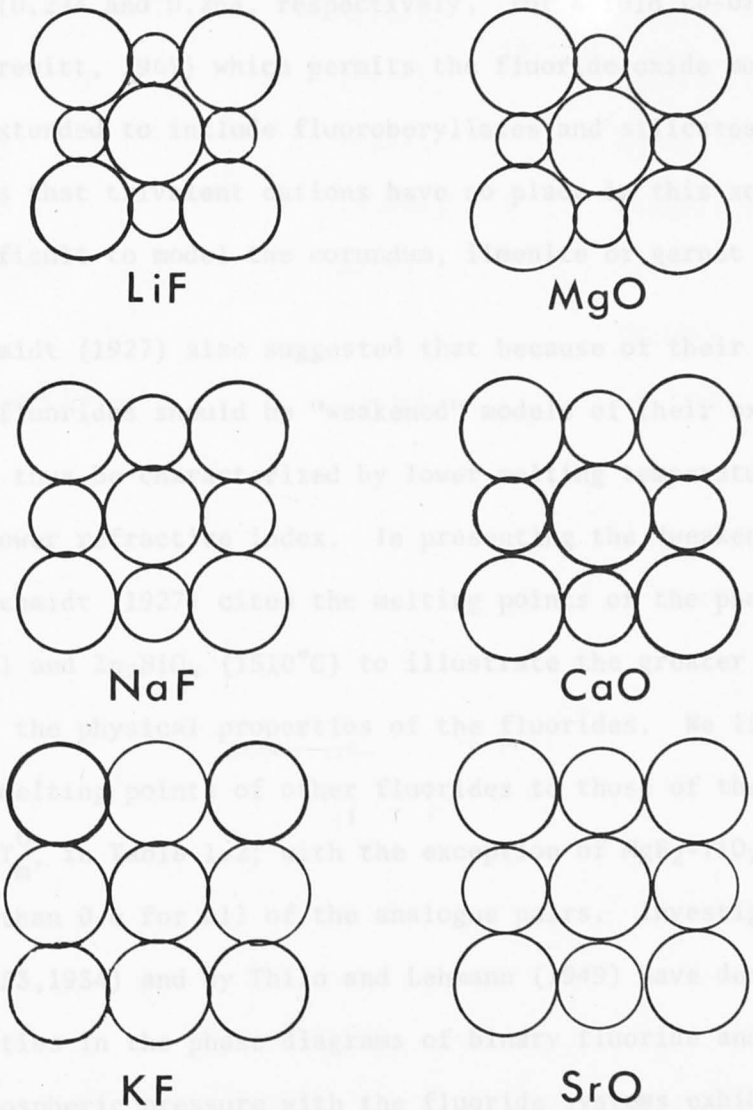

Figure 1.1: Diagram of the cubic face layers for the rocksalt structure illustrating the relative ionic sizes for fluoride-oxide analogue pairs. The ionic radii and the interionic distances are to scale.

in Figure 1.1. In addition, a number of binary compounds with crystal structures of interest to geophysical discussions of the earth's interior are consistent with this modelling scheme and are listed in Table 1.1. Of particular interest is the close correspondence of the ionic radii of Be^{2+} and Si^{4+} (0.27Å and 0.26Å, respectively, for 4-fold co-ordination) (Shannon and Prewitt, 1969) which permits the fluoride-oxide modelling system to be extended to include fluoroberyllates and silicates. One disadvantage is that trivalent cations have no place in this scheme, so that it is difficult to model the corundum, ilmenite or garnet structures.

Goldschmidt (1927) also suggested that because of their lower ionic charge, fluorides should be "weakened" models of their oxide analogues, and thus be characterized by lower melting temperature, lower hardness and lower refractive index. In presenting the "weakened" model concept, Goldschmidt (1927) cited the melting points of the phenacites Li_2BeF_4 (470°C) and Zn_2SiO_4 (1510°C) to illustrate the greater temperature sensitivity of the physical properties of the fluorides. We list the ratios of the melting points of other fluorides to those of their oxide analogues, T_m^F/T_m^O, in Table 1.2; with the exception of MgF_2-TiO_2, this ratio is less than 0.6 for all of the analogue pairs. Investigations by Roy et al. (1953,1954) and by Thilo and Lehmann (1949) have demonstrated close similarities in the phase diagrams of binary fluoride and oxide systems at atmospheric pressure with the fluoride systems exhibiting much lower solidus and liquidus temperatures. Recently, Jackson and Liebermann (1974) have shown that the fusion curves of rocksalt fluorides and oxides at high pressure may be correlated in a similar manner. In a study which parallels that reported in this thesis, Jackson (1976) employed fluoride and oxide analogue systems in an investigation of phase equilibria and melting relationships.

The idea that the fluorides might be models for the high temperature elasticity of their oxide analogues was prompted by the

Table 1.1:

Crystal Structure	Fluoride	Oxide
Olivine	Na_2BeF_4	Ca_2SiO_4
Phenacite	Li_2BeF_4	Zn_2SiO_4
Pyroxene	$LiBeF_3$	$MgSiO_3$
Diopside	$LiNaBe_2F_6$	$CaMgSi_2O_6$
Perovskite	$KMgF_3$	$SrTiO_3$
Spinel	Li_2NiF_4	Mg_2SnO_4
Strontium plumbate	Na_2NiF_4	Ca_2SnO_4

TABLE 1.2: Ratios of Melting Temperatures (T_m) for Fluoride-Oxide Analogue Pairs†

Pair	T_m^F/T_m^O
LiF-MgO	0.36
NaF-CaO	0.44
KF-SrO	0.42
RbF-BaO	0.46
KF-BaO	0.49
CaF_2-ThO_2	0.48
MgF_2-TiO_2	0.73
MnF_2-SnO_2	0.59
$KMgF_3$-$SrTiO_3$	0.56

† The melting temperatures for these fluorides and oxides are listed completely in Table 5.1.

the greater temperature sensitivity of the physical properties of the fluorides and by the fact that germanates have been used as models for the high pressure elasticity of silicates. Classical lattice dynamical theories (e.g., Leibfried and Ludwig, 1961) predict that the elastic moduli should depend linearly on temperature for temperatures greater than the Debye temperature; Anderson (1966) referred to this as the regime of high temperature elastic behaviour. The temperature derivative of the bulk modulus in the high temperature regime is an important input parameter to theoretical equations of state. The evaluation of the use of fluorides to predict the high temperature elastic behaviour of their oxide analogues involves two approaches. (1) Determination of whether the fluorides exhibit high temperature elastic behaviour at lower absolute temperatures than their oxide analogues, which would enable measurement of high temperature derivatives of the elastic moduli at temperatures attainable in laboratory experiments. (2) Examination of the elastic moduli and their temperature derivatives in terms of elastic moduli systematics to determine whether measured values for the fluorides can be used to predict those of the oxides.

The quality and the temperature range of the available elasticity data from the literature precluded evaluation of the high temperature modelling concept. One of the most promising systems for testing the validity of the high temperature modelling concept is the rocksalt analogue pair LiF-MgO. Reliable elasticity data for MgO exist for the temperature range 73°K to 1200°K (Anderson and Andreatch, 1966; Spetzler, 1969, 1970). However the high temperature data for LiF from the resonance experiments of Susse (1961) and Chernov and Stepanov (1961) were not suited to detailed comparison with MgO. The only other fluorides for which single crystal elastic moduli have been determined at high temperatures ($T > 300°K$) are NaF (rocksalt) and CaF_2 (fluorite), both of which were studied by resonance techniques (Nikanorov and Stepanov,

1963; Nikanorov et al., 1968; Vidal, 1974). The uncertainties in the data for LiF determined by such techniques did not encourage reliance on the data for NaF and CaF_2.

We have therefore undertaken a programme to determine the elastic moduli of LiF and its isomorph NaF, and of CaF_2 and its isomorphs SrF_2 and BaF_2, by ultrasonic pulse techniques to temperatures well above room temperature. In addition, we have studied the temperature dependence of the elastic moduli of the rutile-structure MgF_2, and the perovskite-structure $KMgF_3$, which are of great interest as structural analogues of two possible lower mantle phases (see Ringwood, 1970; Liu, 1975, 1976).

1.2 Outline of thesis

The purpose of this thesis is to report new and precise values of the single crystal elastic moduli as a function of temperature from 298°K to approximately 650°K for fluorides in the rocksalt, fluorite, rutile and perovskite structures, and to examine the data within the framework of high temperature equations of state and elastic modulus systematics in order to evaluate the fluorides as models for the high temperature elastic behavior of the oxides. In Chapter 2, we describe the experimental techniques employed to determine the elastic wave velocities and hence the elastic moduli as a function of temperature and pressure. The elasticity data versus temperature are presented in Chapter 3 for LiF, NaF, CaF_2, SrF_2, BaF_2, MgF_2 and $KMgF_3$. These new data are shown to be internally consistent throughout the temperature range and are compared with existing data from previous investigators. Various high temperature equations of state are employed in Chapter 4 for the discussion of the temperature behaviour of our elastic moduli, and for comparison of the onset of high temperature elastic behaviour

for fluoride and oxide analogues. In Chapter 5, fluoride and oxide elastic moduli and their pressure and temperature derivatives are examined in terms of elastic modulus systematics. Chapter 6 contains a summary and final conclusions on the value of the fluoride-oxide modelling scheme with regard to high temperature elasticity.

1.3 Extent of publication

Some of the material in this thesis has been published or submitted for publication while more is being prepared for publication.

1. Jones, L. E. A. and Liebermann, R. C., 1974. Elastic and thermal properties of fluoride and oxide analogues in the rocksalt, fluorite, rutile and perovskite structures, Phys. Earth Planet. Interiors., 9:101-107.
2. Jones, L. E. A., 1976. High temperature behavior of the elastic moduli of LiF and NaF; comparison with MgO and CaO, submitted to Phys. Earth Planet. Interiors.
3. Jones, L. E. A., 1976. High temperature elasticity of the fluorite structure compounds, CaF_2, SrF_2 and MgF_2, in preparation.
4. Jones, L. E. A., 1976. High temperature elasticity of rutile structure MgF_2, in preparation.
5. Jones, L. E. A., 1976. Elastic moduli of $KMgF_3$-perovskite as a function of temperature and pressure, in preparation.

CHAPTER 2

EXPERIMENTAL TECHNIQUES

2.1 Introduction

Ultrasonic pulse techniques were employed in determining the elastic wave velocities in several single crystal fluorides as a function of temperature and pressure. For the temperature measurements, a controlled atmosphere furnace capable of $T \lesssim 1000^{\circ}C$ was specially designed and built. Existing apparatus of our laboratory was utilized for the pressure measurements to $P \lesssim 3$ kbar.

2.2 Sample description and preparation

Single crystal specimens of LiF, NaF, CaF_2, BaF_2 and MgF_2 were purchased from Harshaw Chemical Company (Cleveland, Ohio, U.S.A.) while single crystals of SrF_2 and $KMgF_3$ were obtained from Atomergic Chemetals (Carle Place, New York, U.S.A.). The bulk densities were determined hydrostatically, using toluene as the density reference fluid, and agree to within 0.1% with the X-ray densities (Table 2.1); the former were employed in the calculation of the elastic moduli in Chapter 3.

For the materials of cubic symmetry (all of the above except MgF_2) it was necessary to prepare two sets of crystallographic faces for ultrasonic measurement to determine and cross-check the three independent elastic moduli. The LiF, NaF and CaF_2 crystals were received as {100} oriented cubes which required further orientation and cutting to provide a pair of (110) faces and a pair of (001) faces; the SrF_2 and $KMgF_3$ crystals were purchased in this configuration. Due to the appearance of a small crack, the BaF_2 crystal was not altered from its original configuration which included a pair of (110) faces and a pair of $(1\bar{1}1)$ faces.

The tetragonal MgF_2 crystal was purchased as a 1 inch cube with a pair of faces perpendicular to the c-axis, [001]. To enable the determination and cross-checking of the six independent elastic moduli,

TABLE 2.1: Comparison of bulk and X-ray densities

Crystal	Bulk density ($gm.cm^{-3}$)	X-ray density ($gm.cm^{-3}$)
LiF	2.641±0.003	2.639[1]
NaF	2.806±0.003	2.804[1]
CaF_2	3.183±0.003	3.181[2]
SrF_2	4.282±0.004	4.277[3]
BaF_2	4.887±0.005	4.886[2]
MgF_2 (crystal A)	3.178±0.003	3.178[4]
MgF_2 (crystal B)	3.177±0.003	3.178[4]
$KMgF_3$	3.151±0.003	3.15[5]

1. Miller and Smith (1964)
2. Wong and Schuele (1968)
3. Gerlich (1964b)
4. Haussühl (1968)
5. Rosenberg and Wigmore (1967)

this specimen was oriented and cut to provide the two crystals illustrated in Figure 2.1; crystal A, which consisted of a cube with a pair of (001) faces and a pair of (110) faces; and crystal B, which was a cube with a pair of (100) faces and a pair of faces at 45° to the (001) and (010) crystallographic planes. Since the purchased crystal of MgF_2 was misaligned from the c-axis by 5°, the resultant errors in the orientations of crystals A and B were corrected in the polishing process.

The physical dimensions of the approximately cubical specimens lay between 6.3 mm and 7.5 mm for all crystals except $KMgF_3$, for which the edge length was approximately 5 mm. Lengths at room temperature and atmospheric pressure were determined with a micrometer and are accurate to $\pm 3 \times 10^{-3}$ mm. Opposite faces were polished with 8 μm diamond paste to a flatness of within 0.0005 cm and to a parallelness of better than 0.013°.

The final orientations for LiF and NaF were verified by transmission X-ray techniques to be correct to within 0.3°. Back reflection X-ray techniques verified that the orientations were correct to within 1.5° for CaF_2, SrF_2 and the (110) face for BaF_2. The $(1\bar{1}1)$ face of BaF_2 was found to have a misalignment of 3.5°. Similar determinations for MgF_2 demonstrated that the orientations were correct to within 1°. The misorientation angles for each of the seven crystals are detailed completely in Appendix A. The effect of these misorientations on the elastic moduli and their temperature derivatives is discussed later in Chapter 3.

2.3 Ultrasonic Techniques

The pulse superposition technique of McSkimin (1961, 1962) was employed in determining the elastic wave velocities as a function of temperature and pressure. A block diagram of the electronic equipment

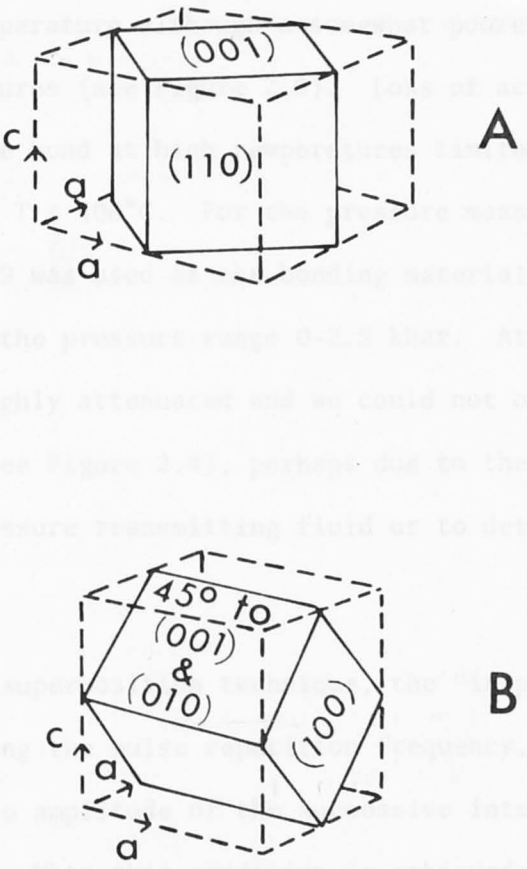

Figure 2.1: Diagram showing the orientation of MgF_2 crystals A and B relative to the crystallographic axes for tetragonal crystals.

used is shown in Figure 2.2. The 20 MHz quartz transducers (X-cut for compressional and AC-cut for shear waves, both co-axially-plated and ¼ inch diameter) were bonded directly to the specimens for the temperature and pressure measurements. A high temperature lubricating grease Extemp 9901 (Frisillo and Barsch, 1972) facilitated excellent acoustic coupling at room temperature although a somewhat poorer signal resulted at elevated temperatures (see Figure 2.3). Loss of acoustic coupling due to failure of the bond at high temperatures limited the experimental temperature range to $T \lesssim 400°C$. For the pressure measurements, Dow-Chemical Resin 276-V9 was used as the bonding material and provided an excellent signal in the pressure range 0-2.5 kbar. At higher pressures, the signal became highly attenuated and we could not obtain systematic, reproducible data (see Figure 2.4), perhaps due to the increased viscocity of the pressure transmitting fluid or to deterioration of the bonding resin.

In the pulse superposition technique, the "in phase" echo condition is obtained by varying the pulse repetition frequency, f_R, until a maximum occurs in the amplitude of the successive internal acoustic echoes within the specimen. When this condition is achieved:

$$\delta = (1/f_R p) - (1/f_c)[n/p - \gamma/360] \qquad (2.1)$$

where δ is the round trip delay in the specimen alone, f_c is the carrier frequency (20 MHz) and γ is a phase angle associated with reflections at the transducer-specimen interface. In these experiments, pulses were applied for each round trip in the specimen, corresponding to the $p = 1$ condition. The value of f_R associated with $n = 0$ was determined by measuring the spectrum of repetition frequencies corresponding to integer increments in n for 10 MHz, 20 MHz and 30 MHz transducers. Unresolved ambiguities were eliminated by a pulse transmission technique (Liebermann et al., 1975). For a thin acoustic bond, the phase angle γ should be of the order of a few degrees (McSkimin, 1961, 1962; Schreiber et al., 1973).

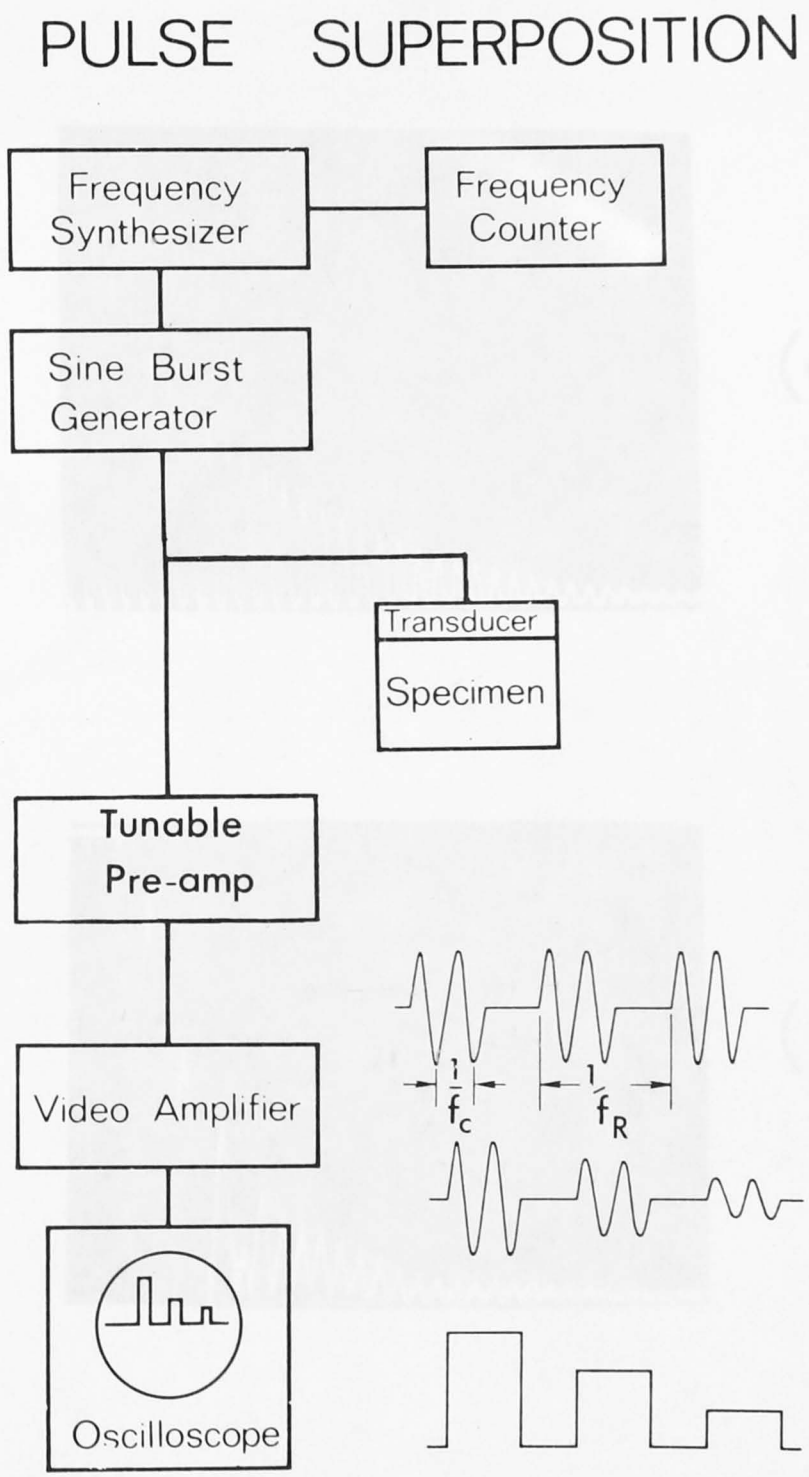

Figure 2.2: Block diagram of the pulse superposition apparatus in operation with one transducer. The relationship between the pulse repetition frequency (f_R) and the carrier frequency (f_c) is illustrated schematically.

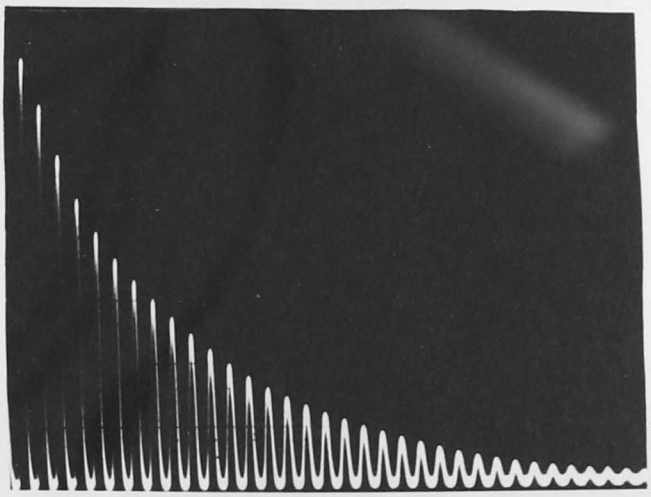

(a)

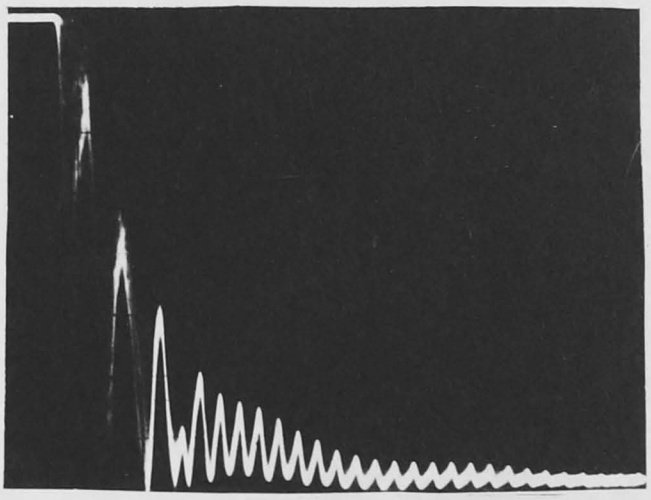

(b)

Fig.2.3 Photos of typical ultrasonic pulse superposition signals for LiF at room temperature (a) and at high temperature (350°C)(b). The deterioration of the signal with increasing temperature is due to the failure of the Extemp bond. The carrier frequency is approximately 20MHz and the mode of propagation is C_{44} shear mode in the [001] direction.

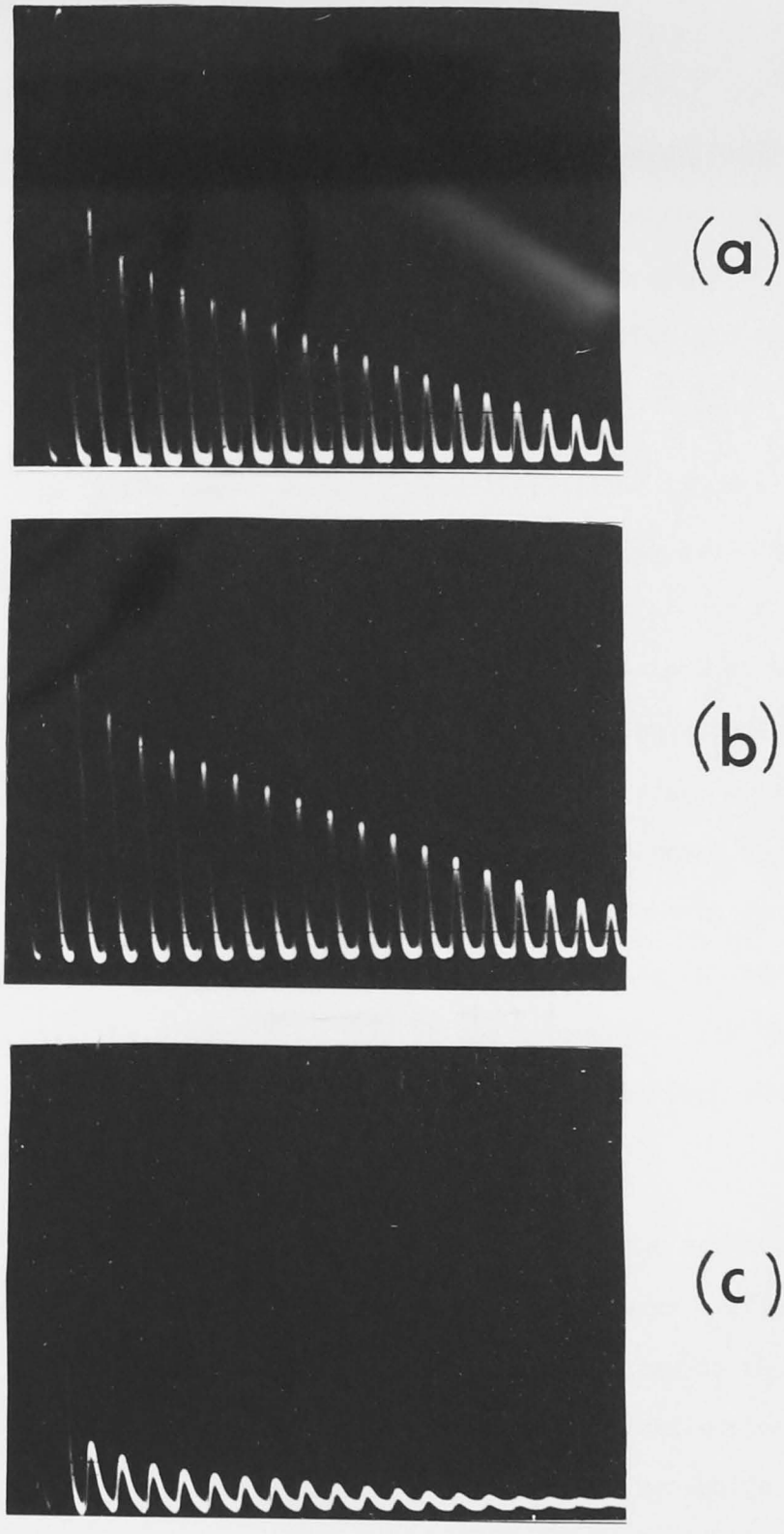

Fig.2.4 Photos of typical ultrasonic pulse superposition signals for $KMgF_3$ at ambient pressure (a), at 1 kbar (b) and at 3 kbar(c). The increased attenuation and decrease in the signal quality at 3 kbar are indicative of bonding problems at higher pressures. The carrier frequency is approximately 20 MHz and the mode of propagation is the C_{44} shear mode in the [110] direction

The resultant errors in δ would lie between 1×10^{-3} and 1×10^{-4} for the compressional and shear modes measured. The variation of the phase angle γ with pressure and temperature was minimized by maintaining the transducer-bond assemblage at its resonant frequency (McSkimin, 1961). Herein lies the advantage of the pulse superposition technique in its sensitivity to small changes in the elastic wave velocities due to changing environmental conditions (P, T, etc.).

Ambiguities in the measurement of pulse repetition frequencies were observed due to extraneous interference effects which produced multiple maxima in pulse amplitudes instead of the ideal single maximum. In addition, not all the displayed echoes peaked in amplitude at the same frequency, a condition we refer to as "phasing". The uncertainties in f_R, which tended to be larger for the compressional modes, were estimated on the basis of the separation of the multiple peaks and were comparable to the errors in δ due to phase changes at the transducer-bond-sample interfaces. Uneven bond thicknesses resulting in varying phase angles across the transducer could be one explanation for the multiple peaking and "phasing". This is supported by the fact that the pattern of peaks does vary with temperature.

Non-parallellism and departure from flatness of the acoustically reflecting faces could also result in extraneous interference effects. Another contributing factor could be diffraction which results in beam spreading and possible side wall reflections as well as reflection of a non-planar wave front from the far end of the sample. The choice of 20 MHz transducers is a tradeoff between minimising the effects of non-parallelism (less significant at lower frequencies) and those of diffraction (less significant at higher frequencies). At the carrier frequency of 20 MHz the previously quoted parallelism figures of better than 0.013° and flatness of better than 0.0005 cm lie on the borderline of detectable effect (Truell et al., 1969, chapter 2.2). The effects of

diffraction are small for $a/\lambda >> 1$, where a is the transducer radius and λ is the wavelength of the carrier (McSkimin, 1964). For compressional waves, $a/\lambda \sim 12$ and for shear waves, $a/\lambda \sim 25$. Hence diffraction effects are more likely to be non-negligible for compressional than for shear waves. The small departures of the echo pattern from exponential decay at room temperature are typical of the effects of non-parallelism and diffraction (Truell et al., 1969, chapters 2.1, 2.2). That the extraneous interferences could be due to the side wall reflections allied with diffraction is supported by the fact that the occurrence of multiple peaking was greatly reduced with the change of boundary conditions upon immersion of the sample in the pressure medium.

The observed multiple peaking and "phasing" probably arise from a combination of diffraction and bond effects. However, despite the errors ascribed to f_R on the basis of peak separation, it was, in general, possible to track a particular peak as a function of temperature, resulting in a much more systematic data set than the errors would imply. The absolute accuracy of f_R at any P, T is better than $\pm 1 \times 10^{-3}$; however the relative precision of f_R at successive T or P in a particular run is better than $\pm 1 \times 10^{-4}$.

2.4 Furnace and specimen holder

A small furnace was specially constructed to our design for the measurement of elastic wave velocities as a function of temperature. One requirement was a thermal inertia low enough to facilitate a flexible range of heating rates, yet high enough to prevent short term temperature fluctuations. The stipulation that the temperature gradient across the sample be as small as possible demanded the provision of a large uniform "hot spot" at the centre of the furnace. Provision also had to be made for the maintenance of an inert gas atmosphere.

A schematic drawing of the furnace is shown in Figure 2.5, illustrating the furnace casing built by our workshop, the furnace core and the packing arrangement. The furnace core consisted of a mullite tube of 5/8 inch internal diameter which we wound with platinum 20% rhodium wire of 0.020 inch diameter. The windings were spaced closer at the ends (approximately 13 turns per inch) than at the centre (approximately 10 turns per inch) and were anchored in place with alumina cement. This gradation in winding was intended to produce a large uniform "hot spot". The ends of the mullite tube extended beyond the furnace so that gas seals could be easily made with the specimen holder and opposing end piece in place. We completed assembly of the furnace by packing in powdered alumina and magnesium oxide as thermal insulation.

The specimen holder (Figures 2.6, 2.7) was designed to support the sample, to supply the electrical signal to the co-axial transducer bonded directly to the sample, and to provide spring loading on the transducer-sample interface. This last was necessary to maintain good acoustical coupling as a function of temperature. The opposing end piece was employed as a thermal and gas seal as well as a means of introducing the platinum-platinum 10% rhodium thermocouple which was seated directly against the specimen. A schematic drawing of both the specimen holder and end piece is shown in Figure 2.6 which also illustrates their placement in the furnace core. Figure 2.7 is a photograph of the assembled specimen holder while Figure 2.8 is a photograph of the furnace with both specimen holder and opposing end piece in place.

The temperature distribution along the axis of the furnace and the exact position of the "hot spot" were determined with the complete assemblage shown in Figure 2.8, but with the introduction of a second thermocouple down the axis of the signal pin. The difference between the fixed reference thermocouple and the movable one enabled precise determination of the temperature distribution. For the final determination, a dummy specimen with a hole for the thermocouple bored

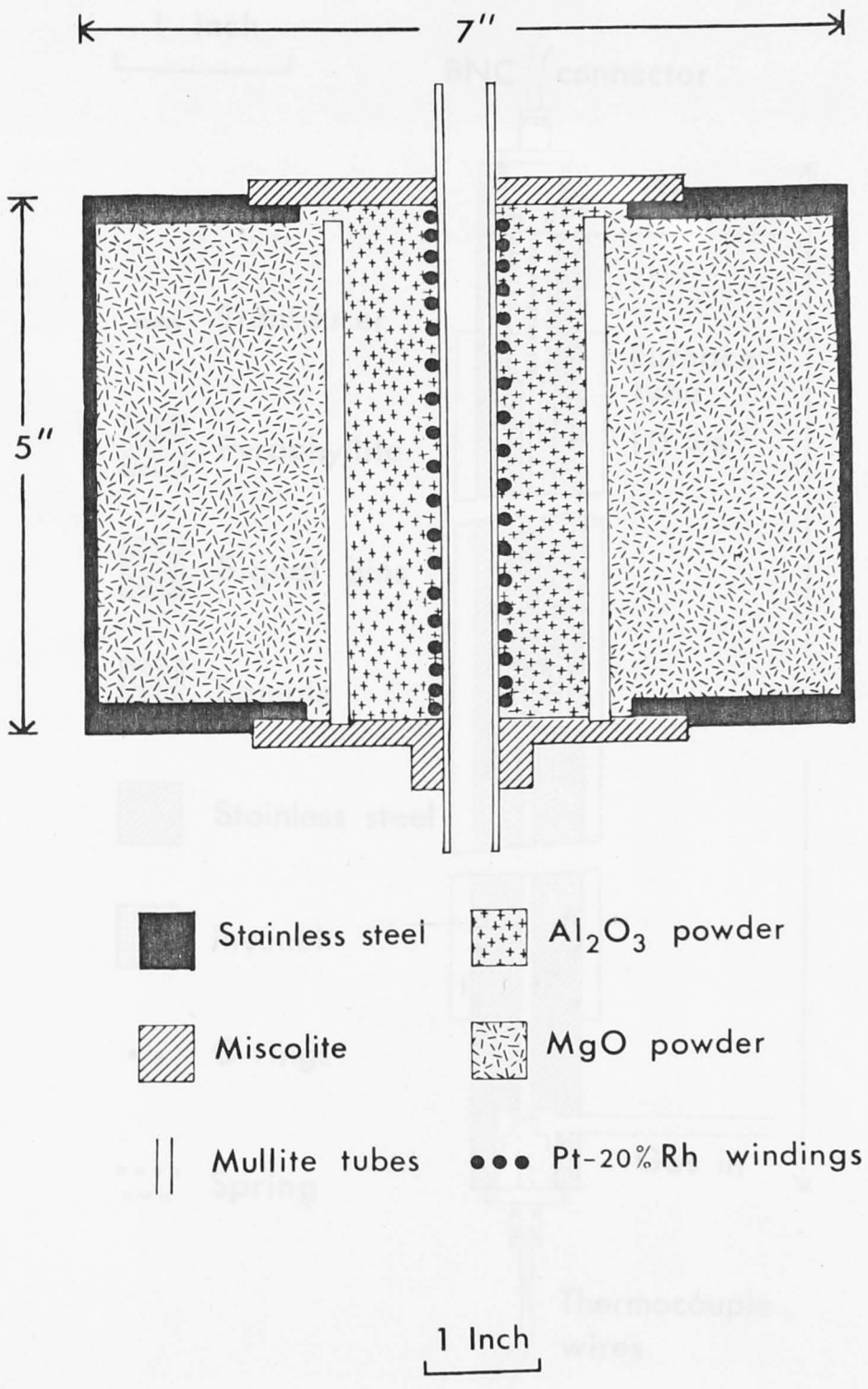

Figure 2.5: Vertical section through the furnace showing the furnace casing, the furnace core and the packing arrangement of the insulating material.

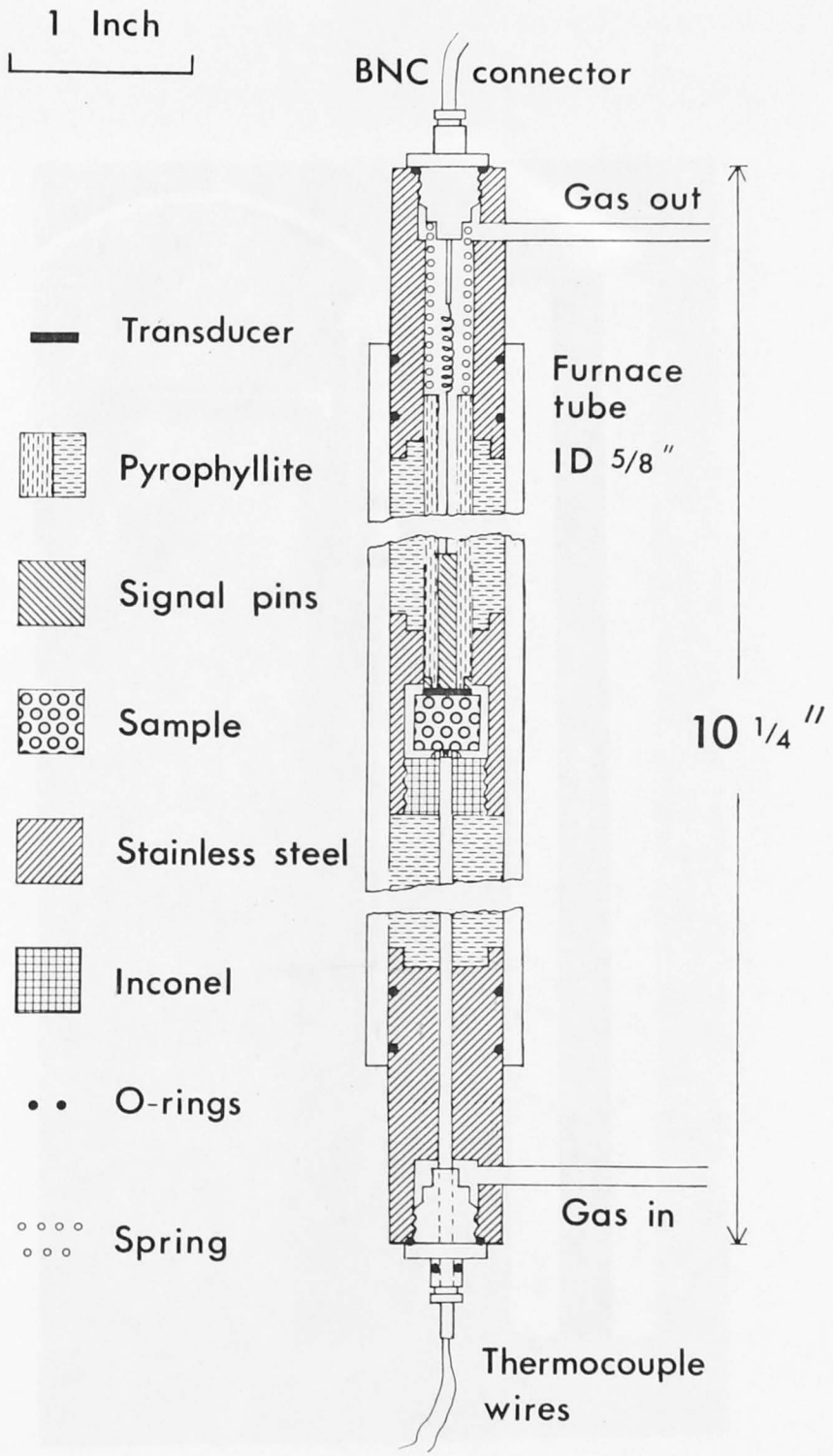

Figure 2.6: Schematic drawing of the specimen holder and opposing end piece in situ in the furnace bore. The drawing is to scale except where broken in the vertical dimension, and except for schematic representation of the transducer, springs, screw-thread and O-rings.

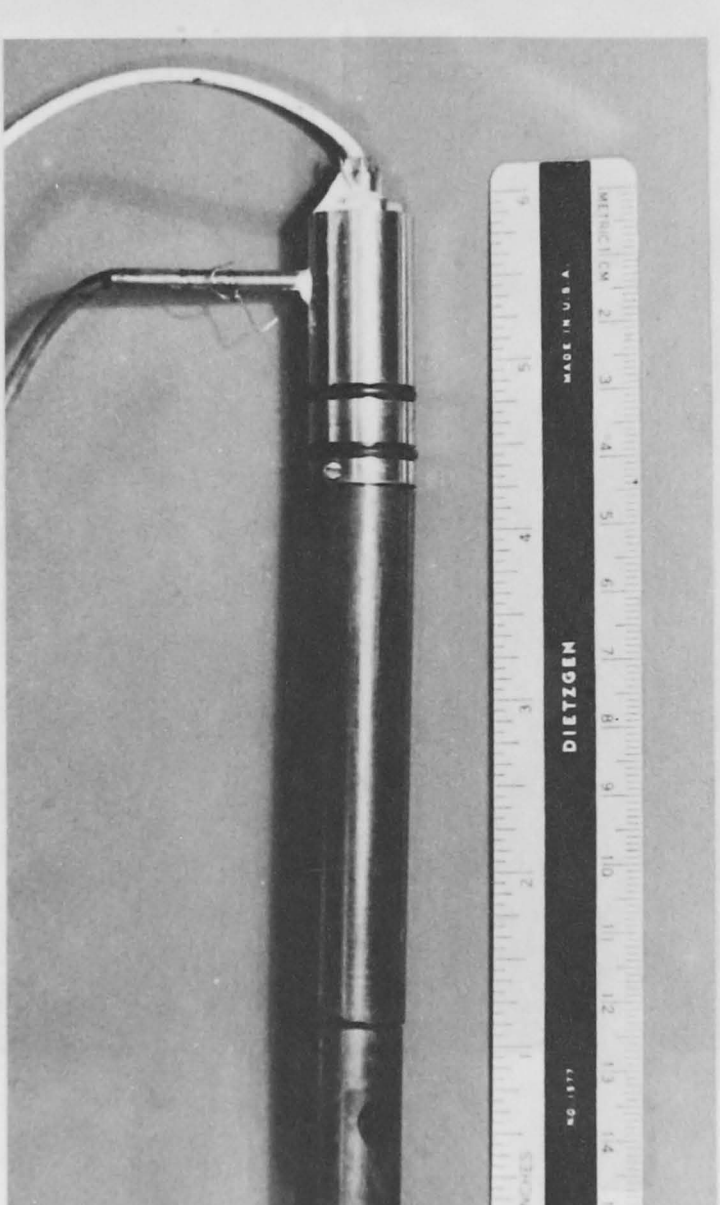

Fig. 2.7: Photo of the assembled specimen holder

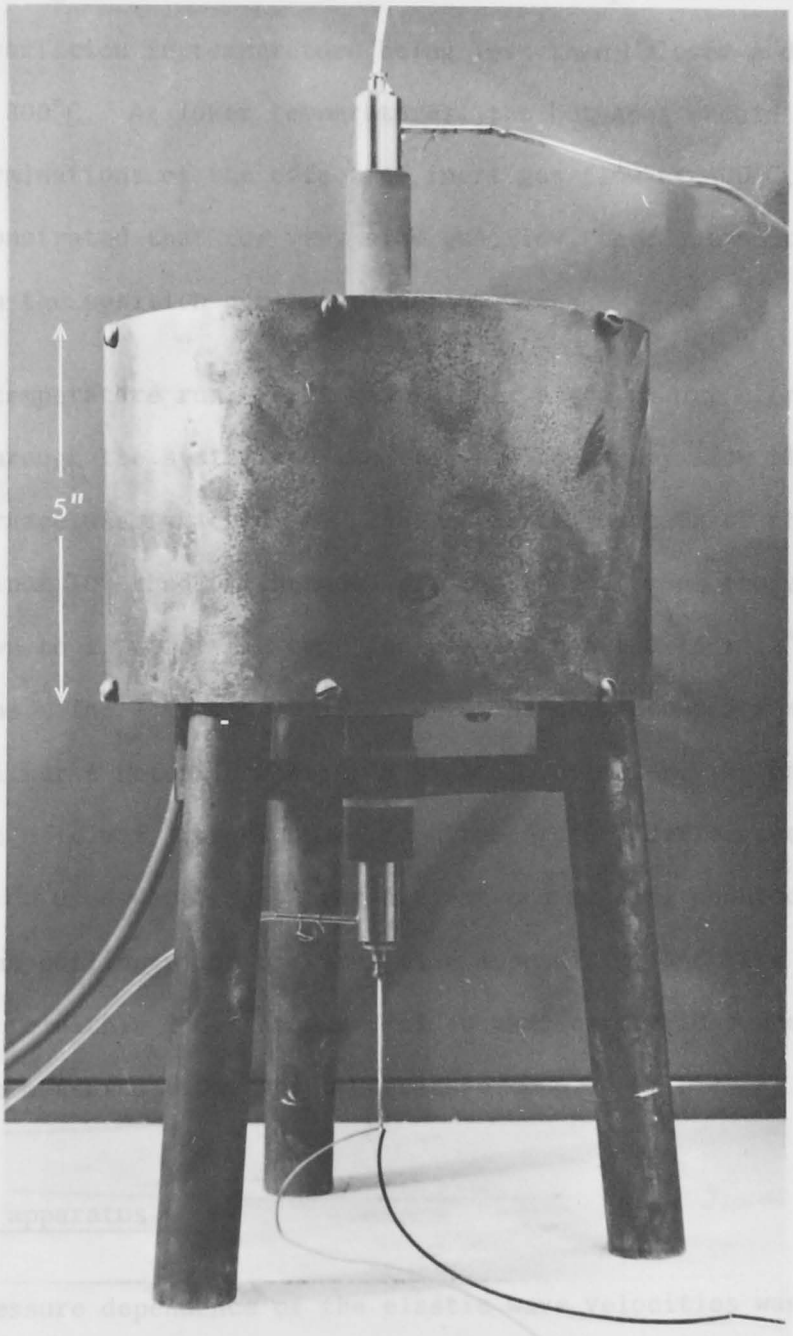

Fig. 2.8 Photo of the furnace assembly with the specimen holder and opposing end piece in place. The signal cable can be seen at the very top of the photo. Gas input and output tubes are attached to horizontal tubes on the assembly. The thermocouple leads enter from the bottom.

along its axis was employed as this simulated the experimental arrangement more closely. Figure 2.9 demonstrates that the hot spot is indeed very uniform, the variation in temperature being less than 1°C over a distance of 12.5 mm at 800°C. At lower temperatures, the hot spot should be even larger. Determinations of the effect of inert gas flow at 400°C, 600°C and 800°C demonstrated that for very slow gas flow, the "hot spot" was unaltered from the position determined at 800°C.

For a temperature run, inert gas (either argon or dry nitrogen) was flushed through the system and then reduced to a very slow flow before the furnace was switched on. The reference junction of the platinum-platinum 10% rhodium thermocouple remained at room temperature which was known to ±1°C for the runs for LiF and NaF and to ±0.2°C for subsequent runs. The e.m.f. associated with the thermocouple was measured by either a potentiometer or a digital voltmeter; the uncertainty in measurement of e.m.f. corresponded to a temperature difference of 0.5°C. The thermocouples used were calibrated against the melting point of gold and against the boiling point of water (see Appendix B) and were found to be correct to within 2°C. It was decided that corrections need not be made to the measured values of temperature.

2.5 Pressure apparatus

The pressure dependence of the elastic wave velocities was determined by placing the specimen in a standard specimen holder in a liquid medium apparatus (Figure 2.10) built by Harwood Engineering Company according to the specifications of this laboratory (Liebermann et al., 1975). Silicone oil (Dow-Corning DC-200, 5 centistoke viscosity) was the pressure medium and the pressure was determined from the millivolt output of a manganin pressure gauge with a precision of ±0.01 kbar. Temperature was not controlled but was monitored by a copper-constantan thermocouple with a reference of 0°C in an ice-water slurry. With each

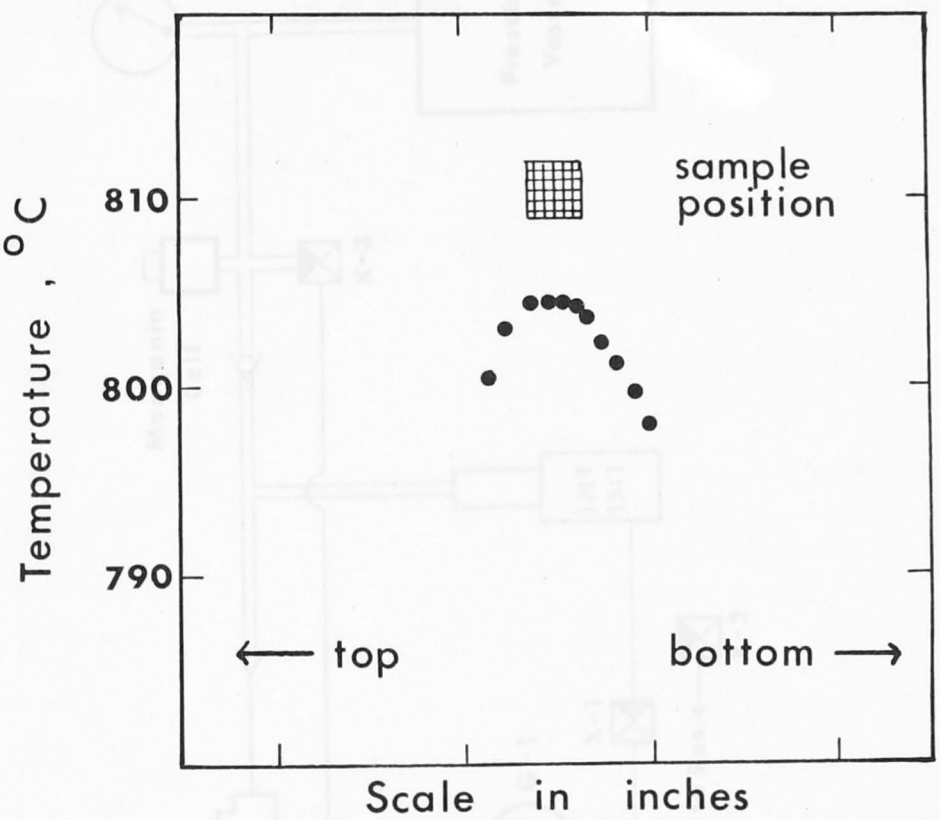

Figure 2.9: The axial temperature distribution across the centre of the furnace. The position of the specimen is indicated.

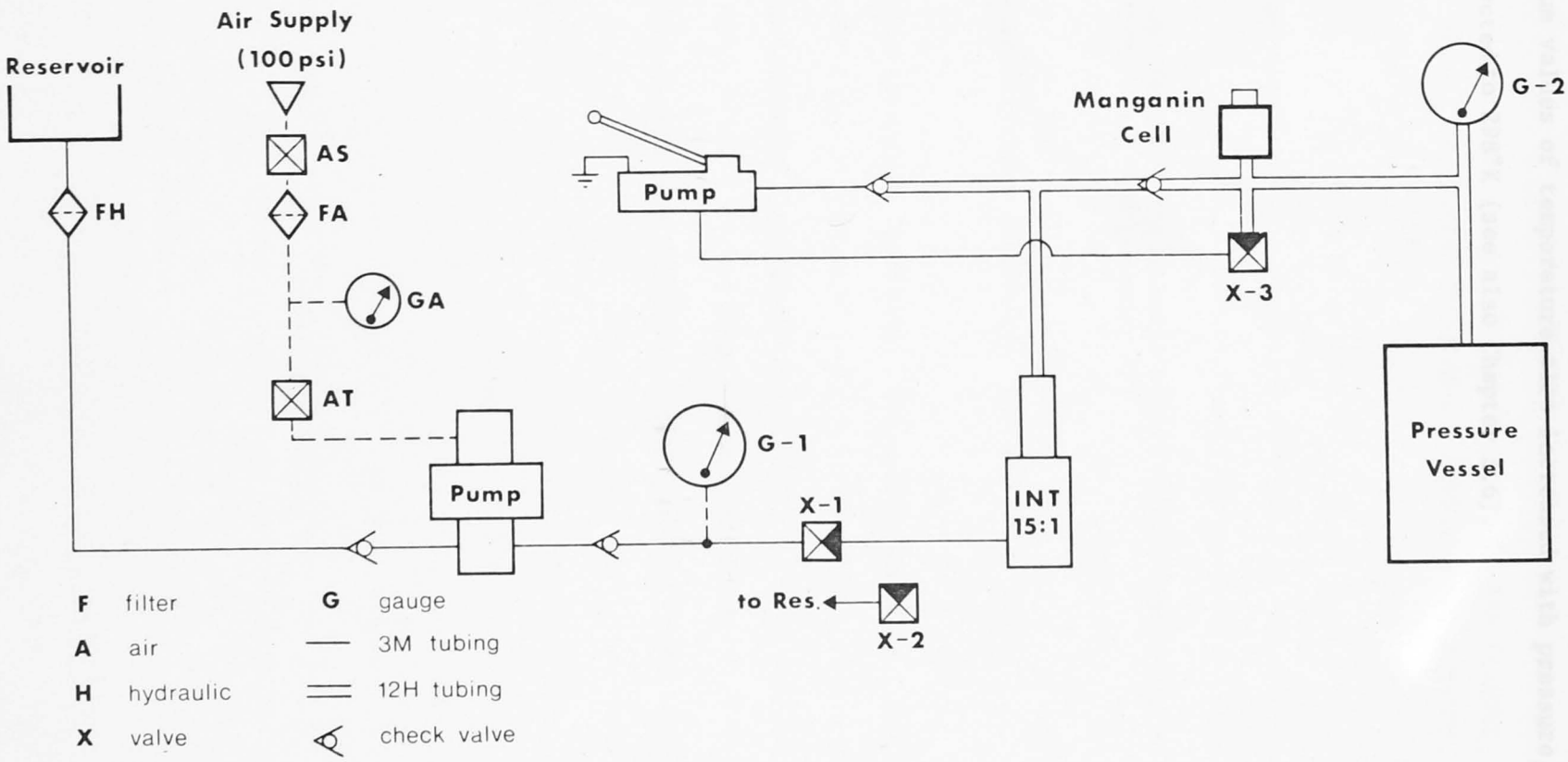

Figure 2.10: Block diagram of the pressure vessel system.

increase in pressure, the temperature also increased and time to reach equilibrium was allowed before measurements were taken. Since the equilibrium values of temperature also increased with pressure, the data were corrected to 298°K (see also Chapter 3.6).

CHAPTER 3

TEMPERATURE AND PRESSURE DEPENDENCE OF THE ELASTIC MODULI OF SEVERAL FLUORIDES: EXPERIMENTAL RESULTS

CHAPTER 3

TEMPERATURE AND PRESSURE DEPENDENCE OF THE ELASTIC MODULI OF SEVERAL FLUORIDES: EXPERIMENTAL RESULTS

3.1 Introduction

The single crystal elastic moduli were determined as a function of temperature using the experimental techniques described in Chapter 2, for fluorides which crystallize in the rocksalt, fluorite, rutile and perovskite structures. Measurements were performed in the range 298°K to approximately 650°K for LiF and NaF (rocksalt), CaF_2, SrF_2 and BaF_2 (fluorite), and MgF_2 (rutile). The temperature range of the measurements for $KMgF_3$ (perovskite) lay between 298°K and approximately 550°K. The single crystal elastic moduli of $KMgF_3$ were also determined as a function of pressure from 1 bar to 2.5 kbar.

Propagation of shear and compressional waves in the [110] and [001] directions for the cubic crystals LiF, NaF, CaF_2 and SrF_2 enabled the determination and cross-checking of the three independent elastic moduli (Table 3.1) as a function of temperature. For BaF_2 and $KMgF_3$, the three independent elastic moduli were determined by the propagation of compressional and shear waves in the [110] direction, with the room temperature crosschecks for BaF_2 being provided by measurements for the $[1\bar{1}1]$ direction (Table 3.1). The six independent elastic moduli for MgF_2, together with crosschecks to 370°K, were determined by the propagation of shear and compressional waves in the [100], [110] and [001] directions, and in a direction at 45° to the [001] and [010] directions (Table 3.2).

3.2 Data analysis for the elastic moduli (c) as a function of temperature (T) and pressure (P)

The elastic wave velocities as a function of temperature are determined from the primary data, the pulse repetition frequencies, f_R,

Table 3.1: Modes of propagation in cubic crystals used for determining the single crystal elastic constants

Mode velocity	Elastic Constant	Direction	Mode
v_1	c_{11}	[001]	P
v_2	c_{44}	[001]	S random polarisation
v_3	$^1c'$	[110]	S pol $[1\bar{1}0]$
v_4	c_{44}	[110]	S pol [001]
v_5	$^2c''$	[110]	P
v_6	^3c_L	$[1\bar{1}1]$	P
v_7	^4c_T	$[1\bar{1}1]$	S random polarisation

1. $c' = (c_{11} - c_{12})/2$
2. $c'' = (c_{11} + c_{12} + 2c_{44})/2$
3. $c_L = (c_{11} + 2c_{12} + 4c_{44})/3$
4. $c_T = (c_{11} - c_{12} + c_{44})/3$

Table 3.2: Modes of propagation used for determining the single crystal elastic constants for the rutile structure

Mode velocity	Elastic constant	Direction	Mode
v_1	c_{11}	[100]	P
v_2	c_{66}	[100]	S pol. [010]
v_3	c_{44}	[100]	S pol. [001]
v_4	$^1c_{L_1}$	[110]	P
v_5	$^2c'$	[110]	S pol. $[1\bar{1}1]$
v_6	c_{44}	[110]	S pol. [001]
v_7	c_{33}	[001]	P
v_8	c_{44}	[001]	S random polarisation
v_9	$^3c_{L_2}$	45° to [001] and [010]	P (quasi)
v_{10}	$^4c_{T_2}$	45° to [001] and [010]	S (quasi)
v_{11}	$^5c_{T_1}$	45° to [001] and [010]	S pol. [100]

1. $c_{L_1} = (c_{11} + c_{12} + 2c_{66})/2$

2. $c' = (c_{11} - c_{12})/2$

3. $c_{L_2} = \frac{1}{4}\{c_{11} + c_{33} + 2c_{44} + [(c_{11} - c_{33})^2 + 4(c_{13} + c_{44})^2]^{\frac{1}{2}}\}$

4. $c_{T_2} = \frac{1}{4}\{c_{11} + c_{33} + 2c_{44} - [(c_{11} - c_{33})^2 + 4(c_{13} + c_{44})^2]^{\frac{1}{2}}\}$

5. $c_{T_1} = (c_{44} + c_{66})/2$

which are measured during very slow heating (less than 0.5°C per minute). The values of f_R thus obtained are indistinguishable from equilibrium measurements. The inherent precision of the pulse superposition technique is reduced by other experimental uncertainties, in particular those associated with bond and diffraction effects (Chapter 2). For the purposes of a least squares analysis, it is assumed that the uncertainties in the pulse repetition frequency are instrumental and are all equal (relative error = 1×10^{-4} for most of the measured modes), and that the random errors in the measurement of temperature can be neglected.

The pulse repetition frequencies, f_R, the elastic wave velocities, v, and the elastic moduli, c, at any temperature are related by

$$v = 2\ell f_R$$

$$c = \rho v^2 = 4\rho\ell^2 f_R^2 \qquad (3.1)$$

For cubic crystals, ρ, the specimen density, and ℓ, the specimen length in the direction of propagation, are related to their respective room temperature values, ρ_o and ℓ_o, by

$$\rho = \rho_o\left(\frac{\ell_o}{\ell}\right)^3 \qquad (3.2)$$

$$\ell = \ell_o(a_1 + a_2T + a_3T^2 + a_4T^3) \qquad (3.3)$$

The coefficients a_i in the polynomial expression for the length, together with the bulk density used in the calculation of the elastic moduli, are given in Table 3.3 for LiF and NaF, and in Table 3.4 for CaF_2, SrF_2 and BaF_2. For tetragonal crystals for which the thermal expansion is anisotropic, the corresponding relationships between ℓ and ℓ_o for the [100] and [110] directions is given by

$$\left(\frac{\ell}{\ell_o}\right) = \left(\frac{\ell^a}{\ell^a{}_o}\right) = (a_1 + a_2T + a_3T^2) \qquad (3.4)$$

and for the [001] direction by

Table 3.3: Basic data for LiF and NaF

Data	LiF	NaF
Molecular Weight	25.94	41.99
Molar Volume, cm^3	9.83	14.98
Bulk Density, $gm.cm^{-3}$	2.641	2.806
X-ray Density, $gm.cm^{-3}$	2.639[1]	2.804[1]
a_1	0.9925[2]	0.9924[2]
a_2, $deg^{-1} \times 10^{-4}$	0.1845[2]	0.1896[2]
a_3, $deg^{-2} \times 10^{-7}$	0.2360[2]	0.2263[2]

1. Miller and Smith (1964)
2. $\ell(T) = \ell(298)\ [a_1 + a_2T + a_3T^2]$, where a_1, a_2, and a_3 are calculated from b_1, b_2 and b_3 of Srivastava and Merchant (1973) where $a^*(T) = b_1 + b_2T + b_3T^2$, a^* being the lattice parameter.

Table 3.4: Basic data for CaF_2, SrF_2 and BaF_2

Data	CaF_2	SrF_2	BaF_2
Molecular Weight	78.08	125.62	175.34
Molar Volume, cm^3	24.55	29.37	35.89
Bulk Density, $gm.cm^{-3}$	3.183	4.282	4.887
X-ray Density, $gm.cm^{-3}$	3.181[1]	4.277[2]	4.886[1]
a_1	0.9957[3]	0.9943[3]	0.9950[3]
a_2, $deg^{-1} \times 10^{-4}$	0.0727	0.2616	0.1371
a_3, $deg^{-2} \times 10^{-7}$	0.2863	- 0.3509	0.090
a_4, $deg^{-3} \times 10^{-10}$	- 0.1567	0.390	0.050

1. Wong and Schuele (1968)
2. Gerlich (1964b)
3. $\ell(T) = \ell(298)\ (a_1 + a_2T + a_3T^2 + a_4T^3)$ where ℓ is the length and the a_i are determined from the thermal expansion data of Sirdeshmukh and Deshpande (1964).

$$\left(\frac{\ell}{\ell_o}\right) = \left(\frac{\ell^c}{\ell^c{}_o}\right) = (c_1 + c_2T + c_3T^2) \qquad (3.5)$$

and between ρ and ρ_o by

$$(\rho/\rho_o) = \left(\frac{\ell^a{}_o}{\ell^a}\right)^2\left(\frac{\ell^c{}_o}{\ell^c}\right) \qquad (3.6)$$

where ℓ^a and ℓ^c are lengths along the a and c axes respectively. For propagation in the direction at 45° to the [001] and [010] directions, the relationship between ℓ and ℓ_o is

$$\left(\frac{\ell}{\ell_o}\right)^2 = \tfrac{1}{2}\left[\left(\frac{\ell^a}{\ell^a{}_o}\right)^2 + \left(\frac{\ell^c}{\ell^c{}_o}\right)^2\right] \qquad (3.7)$$

The coefficients a_i and c_i, and the bulk density are given in Table 3.5 for MgF_2. The raw pulse repetition frequency data and the elastic moduli calculated from equation (2.1) at each temperature data point are listed in Appendix C for each of the measured modes for LiF, NaF, CaF_2, SrF_2, BaF_2 and MgF_2. For $KMgF_3$, only the pulse repetition frequencies and corresponding temperatures are listed in Appendix C.

The values of the elastic moduli, c, calculated from equation (2.1), versus temperature were fitted by polynomials in T using the method of least squares. The standard F-test (Bevington, 1969, chapter 10-2) was applied in determining the statistical significance of adding further terms to the fitted polynomials. This was used in conjunction with a standard χ^2-test (Bevington, 1969, chapter 10-1) to determine the degree of the polynomial that should be fitted to the c-T data. In general, it was found that the statistical significance of adding a further term to the polynomial became marginal at the point where the reduced χ^2-value became approximately equal to unity, indicating that the scatter of the data about the fitted polynomial was comparable with the estimated experimental uncertainties. In the absence of thermal expansion data for $KMgF_3$, the polynomial fitting procedure was applied

Table 3.5: Basic data for MgF_2

Data		
Molecular Weight		62.31
Molar Volume, cm^3		19.61
Bulk Density, $gm.cm^{-3}$	crystal A	3.178
	crystal B	3.177
X-ray Density, $gm.cm^{-3}$		3.178[1]
a_1		0.997019^2
a_2, $deg^{-1} \times 10^{-4}$		0.087794^2
a_3, $deg^{-1} \times 10^{-7}$		0.040547^2
c_1		0.99584^2
c_2, $deg^{-1} \times 10^{-4}$		0.125943^2
c_3, $deg^{-1} \times 10^{-7}$		0.043968^2

1. Haussühl (1968)
2. $\ell_a(T) = \ell_a(298)\ [a_1 + a_2T + a_3T^2]$ and $\ell_c(T) = \ell_c(298)\ [c_1 + c_2T + c_3T^2]$ where ℓ_a, ℓ_c are lengths along the a-axes and c-axis respectively. The a_i and c_i are determined from the thermal expansion data of Bailey et al. (1975).

directly to the f_R-T data.

The values of the elastic moduli and their temperature derivatives were evaluated at 298°K from the polynomial equations in T. The associated errors were determined from the uncertainties in the polynomial coefficients (Bevington, 1969, chapters 6-5, 8-1) together with the uncertainties in ρ_o ($\sim$ 0.1%) and ℓ_o ($\sim$ 0.05%). Since the uncertainties in the polynomial coefficients are not independent, the calculated errors in the elastic moduli and their temperature derivatives probably overestimate the actual uncertainties.

The effect of crystal misorientations (Chapter 2) on the elastic moduli and their temperature derivatives was calculated from the expressions for the orientation dependence of the elastic wave velocities given by Waterman (1959). The expression used in conjunction with Waterman's equations for calculating the error in the temperature derivatives is given in Appendix A.

The primary pressure data are the pulse repetition frequencies, f_R, measured as a function of pressure under equilibrium and quasi-isothermal conditions and corrected to 298°K, using data for the temperature dependence of the f_R. The precision of the measurement of f_R is 2×10^{-4} for the compressional mode and 1×10^{-4} for the shear modes. The uncertainties can also be roughly estimated from the degree of reproducibility attained in different runs. For the purposes of a least squares analysis, it is assumed that the uncertainties in f_R are instrumental and are all equal, and that the random errors in the measurement of pressure can be neglected.

The pulse repetition frequencies versus pressure were fitted by straight lines using the method of least squares. The linear relationship for f_R-P simplified the application of the formula introduced by Cook (1957) for the relative length change with pressure,

$$\left(\frac{\ell}{\ell_o}\right) = 1 + \frac{(1 + \Delta)}{12\rho_o\ell_o^2} \int_0^P \frac{dP}{f_5^2 - f_4^2 - f_3^2/3} \qquad (3.8)$$

where f_3, f_4, f_5 are the pulse repetition frequencies corresponding to v_3, v_4 and v_5 in Table 3.1 and where Δ is given by

$$\Delta = \alpha_v \gamma T \qquad (3.9)$$

In (3.9), α_v is the volumetric thermal expansion and γ is the thermal Grüneisen parameter

$$\gamma = \frac{\alpha_v K_S}{\rho C_P} \qquad (3.10)$$

K_S being the adiabatic bulk modulus and C_P, the specific heat per gram at constant pressure. Since the f_R depend linearly on P, equation (3.8) can be rewritten as

$$\left(\frac{\ell}{\ell_o}\right) = 1 + \frac{(1 + \Delta)}{12\rho_o\ell_o^2} \int_0^P \frac{dP}{AP^2 + BP + C} \qquad (3.11)$$

The integral in equation (3.11) can be evaluated (e.g., see Abramowitz and Stegun, 1965) as follows:

$$\int \frac{dP}{AP^2 + BP + C} = \frac{1}{(B^2 - 4AC)^{1/2}} \ln \left| \frac{2AP + B - (B^2 - 4AC)^{1/2}}{2AP + B + (B^2 - 4AC)^{1/2}} \right|$$

$$(B^2 - 4AC > 0)$$

$$= \frac{-2}{2AP + B} \qquad (B^2 - 4AC = 0)$$

$$= \frac{2}{(4AC - B^2)^{1/2}} \arctan \frac{2AP + B}{(4AC - B^2)^{1/2}}$$

$$(B^2 - 4AC < 0) \qquad (3.12)$$

The elastic moduli were calculated at 1 bar and the maximum experimental pressure from equations (3.1), (3.2), (3.11) and (3.12) using the values of f_R derived from the linear fits to the f_R-P data.

The bulk density used in the calculation is listed in Table 3.6. In (3.11), $(1 + \Delta)$ was replaced by unity for $KMgF_3$. This has a negligible effect on ℓ/ℓ_o since $\Delta \sim 0.05$ and the second term in (3.11) is of the order 1×10^{-3} at 2.5 kbar. The pressure derivatives of the elastic moduli were determined by assuming a linear dependence on pressure for the elastic moduli. The errors in the elastic moduli and their pressure derivatives were estimated from the uncertainties in the coefficients of the linear equations satisfying the f_R-P data.

3.3 Rocksalt-structure fluorides: LiF and NaF. c(T).

The elastic moduli calculated from equation (3.1) for LiF and NaF are plotted for all five modes in Figures 3.1 and 3.2 respectively. Also shown are the fitted polynomial equations (see also Table 3.7). For all modes except c'' for LiF and NaF, the addition of a quadratic term to the fitted polynomial equation was statistically significant at the 99.9% confidence level. For c'', a cubic polynomial was required for LiF although a linear fit was sufficient for the NaF data. However, the uncertainty for c'' is larger than that for the other modes due to difficulties in identifying the correct peak as a function of temperature. In view of this it was decided that only a second degree polynomial was justified by the data for LiF.

The values of the elastic moduli and their temperature derivatives, calculated by evaluating the polynomials at 298°K, are listed in Table 3.8 for LiF and NaF, together with the associated errors. The effects of misorientation were found to be negligible. The crosschecks are provided by comparing c_{44} from ν_2 and ν_4 and by comparing c'' (measured) and c'' (calculated from c_{11}, c' and c_{44}); in all cases the agreement for the elastic moduli is better than 0.5% and for the temperature derivatives is within 5%. These differences for c_{44} and c'' and their temperature derivatives are well within the calculated uncertainties for the

Table 3.6: Basic data for $KMgF_3$

Data	
Molecular Weight	120.41
Molar Volume, cm^3	38.23
Bulk Density, $gm.cm^{-3}$	3.151
X-ray Density, $gm.cm^{-3}$	3.15[1]

1. Rosenberg and Wigmore (1967)

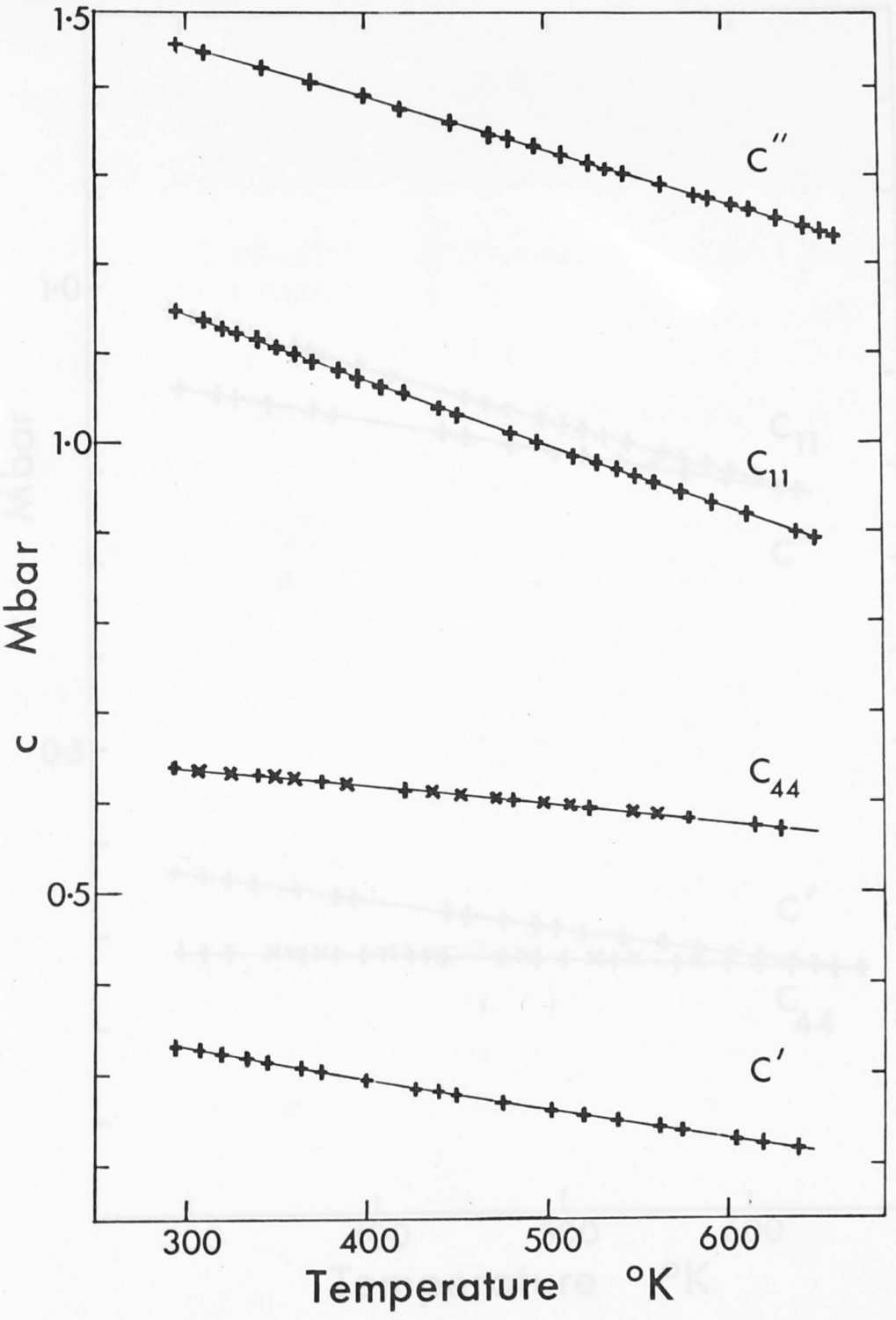

Figure 3.1: Elastic moduli versus temperature for the modes c_{11}, c'', c_{44} and c' for LiF. The solid lines represent the fitted second degree polynomials. For the c_{44} shear mode, the polynomial curve for the [001] direction cannot be distinguished from the plotted curve for the [110] direction. Data points for the crosscheck for c_{44} from the [001] direction are indicated by X. For reasons of clarity, not all the data points used in the fitting procedure are plotted.

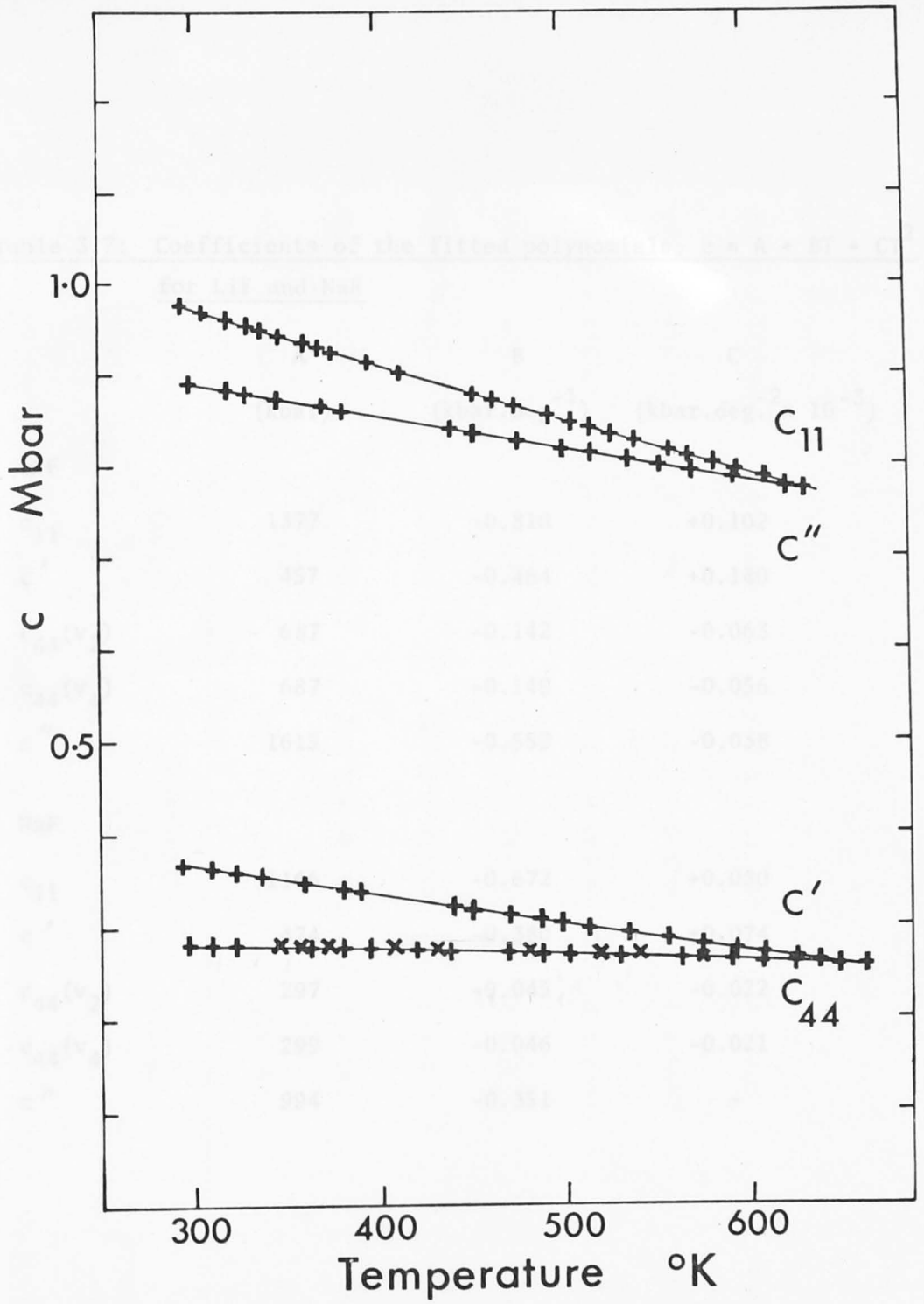

Figure 3.2: Elastic moduli versus temperature for the modes c_{11}, c'', c_{44} and c' for NaF. The solid lines represent the fitted polynomials (quadratics for c_{11}, c' and c_{44} and a straight line for c''). For the c_{44} shear mode, the polynomial curve for the [110] direction cannot be distinguished from the plotted curve for the [001] direction. Data points for the crosscheck for c_{44} from the [110] direction are indicated by X. For reasons of clarity, not all the data points used in the fitting procedure are plotted.

Table 3.7: Coefficients of the fitted polynomials, $c = A + BT + CT^2$ for LiF and NaF

	A (kbar)	B (kbar.deg.$^{-1}$)	C (kbar.deg.$^{-2}$ x 10^{-3})
LiF			
c_{11}	1377	-0.810	+0.102
c'	457	-0.464	+0.140
$c_{44}(v_2)$	687	-0.142	-0.063
$c_{44}(v_4)$	687	-0.149	-0.056
c''	1615	-0.552	-0.038
NaF			
c_{11}	1166	-0.672	+0.080
c'	474	-0.380	+0.074
$c_{44}(v_2)$	297	-0.045	-0.022
$c_{44}(v_4)$	299	-0.046	-0.021
c''	994	-0.351	-

Table 3.8: Single crystal elastic moduli and their temperature derivatives at 298°K for LiF and NaF

Mode	Velocity	LiF c (kbar)	LiF $\left(\frac{\partial c}{\partial T}\right)_P$ (kbar.deg.$^{-1}$)	NaF c (kbar)	NaF $\left(\frac{\partial c}{\partial T}\right)_P$ (kbar.deg.$^{-1}$)
c_{11}	v_1	1144 ± 3	-0.749 ± 0.005	973 ± 3	-0.624 ± 0.006
c'	v_3	331 ± 1	-0.380 ± 0.002	368 ± 1	-0.336 ± 0.002
c_{44}	v_2	639 ± 3	-0.179 ± 0.002	282 ± 2	-0.058 ± 0.003
	v_4	637 ± 2	-0.183 ± 0.004	284 ± 2	-0.059 ± 0.004
c''	v_5	1447 ± 7	-0.575 ± 0.012	890 ± 3	-0.354 ± 0.003
	calc.	1453 ± 4	-0.555 ± 0.009	888 ± 5	-0.347 ± 0.008
K_S	calc.	704 ± 4	-0.242 ± 0.008	483 ± 4	-0.177 ± 0.009

respective modes.

In Table 3.9, values of the elastic moduli from other investigations are listed for comparison with our data for LiF and NaF at 298°K. For LiF, the agreement is good with the exception of the values of Briscoe and Squire (1957) and Susse (1961) which tend to be very much lower. Similarly for NaF the agreement is generally good with the exception of the elastic moduli data of Nikanorov and Stepanov (1963).

Also compared in Table 3.9 are the values of the temperature derivatives of the elastic moduli $(\partial c/\partial T)_P$ at 298°K. For both LiF and NaF the agreement between our values and those of Haussühl (1960) is remarkably good, the discrepancy being less than 1%. The agreement with the NaF data of Vallin et al. (1966) and Bensch (1972) is only fair.

The comparison of our elastic moduli with those of other investigators can be carried out over a wider range of temperatures in Figures 3.3 and 3.4 which are plots of adiabatic bulk modulus, K_S, versus temperature from 0-1000°K for LiF and 0-800°K for NaF, respectively. The data of Briscoe and Squire (1957) for LiF define a smooth curve offset to lower K_S values than ours but with a compatible gradient at 298°K. The data point at 298°K from Haussühl (1960) is in agreement with our curve both in absolute value and indicated gradient. The resonance data of Chernov and Stepanov (1961) and Susse (1961) deviate markedly from our curve at higher temperatures even though the former intersects our curve in the neighbourhood of 300°K.

For NaF, there is good agreement between our data (300-650°K) and those of Vallin et al. (1966) (0-300°K) and Lewis et al. (1967) (0-300°K). In addition the room temperature value of K_S and the temperature gradient of Haussühl (1960) are in agreement with our curve. The values of the bulk modulus from the resonance experiments of Nikanorov and Stepanov (1963) are consistently lower at all temperatures and the absolute value

Table 3.9: Comparison of room temperature values of c and $(\partial c/\partial T)_P$ from various investigators for LiF and NaF

	c_{11}	c'	c_{44}	K_S	$\left(\frac{\partial c_{11}}{\partial T}\right)_P$	$\left(\frac{\partial c'}{\partial T}\right)_P$	$\left(\frac{\partial c_{44}}{\partial T}\right)_P$	$\left(\frac{\partial K_S}{\partial T}\right)_P$	Reference
	(kbar)				(kbar.deg.$^{-1}$)				
LiF	1144	331	639	704	-0.749	-0.380	-0.183	-0.242	This work
	1137	331	637	696					Miller and Smith (1964)
	1136	330	635	696	-0.749	-0.377	-0.178	-0.247	Haussühl (1960)
	1130	327	637	694					Chernov and Stepanov (1961)
	1111	345	630	651					Briscoe and Squire (1957)
	913	276	598	622					Susse (1961)
NaF	973	368	282	483	-0.624	-0.336	-0.059	-0.177	This work
	970	366	282	482					Miller and Smith (1964)
	970	364	283	485	-0.618	-0.331	-0.059	-0.177	Haussühl (1960)
	970	367	282	481	-0.60	-0.325	-0.085	-0.166	Vallin et al. (1966)
	963	359	279	485					Lewis et al. (1967)
	963	362	276	482	-0.584	-0.308	-0.045	-0.173	Bensch (1972)
	943	372	283	447					Nikanorov and Stepanov (1963)

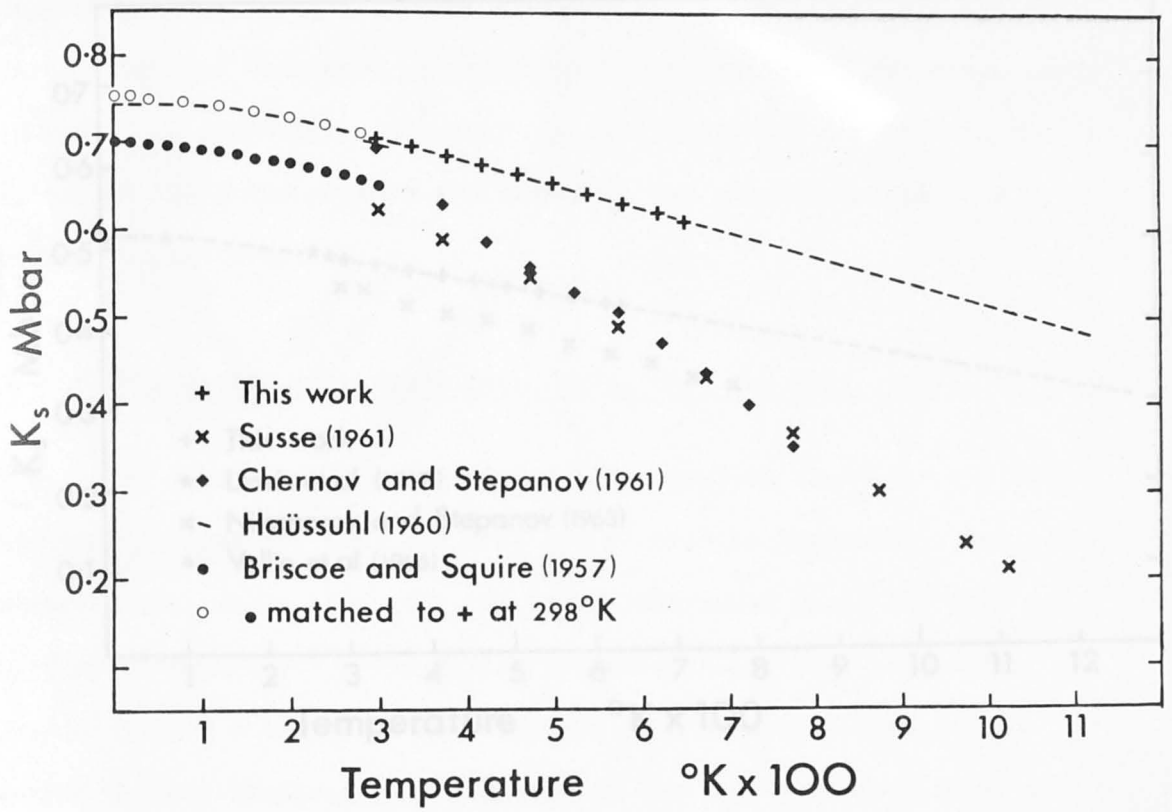

Figure 3.3: Bulk modulus versus temperature for LiF. The dashed curve will be discussed later, when this figure is presented again as Figure 4.10.

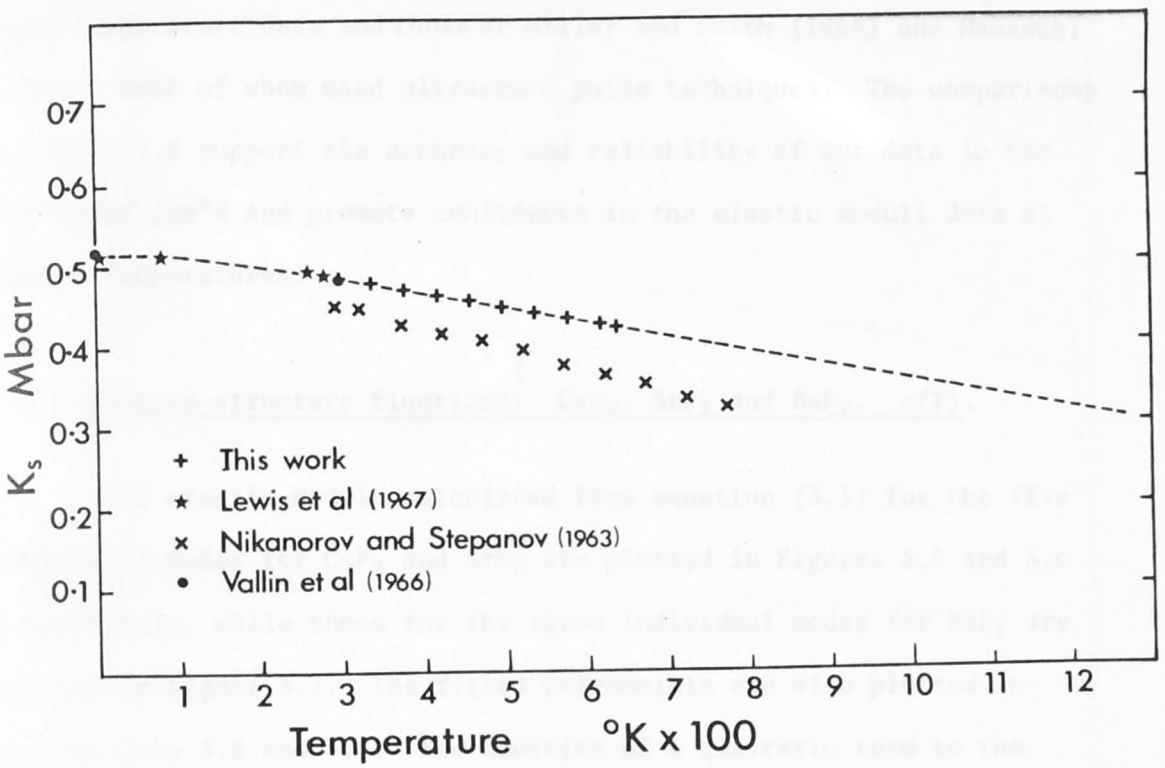

Figure 3.4: Bulk modulus versus temperature for NaF. The dashed curve will be discussed later, when this figure is presented again as Figure 4.11.

of their gradient is 50% higher than that of other investigators.

Of particular note in Table 3.9 is the good agreement between our room temperature data and those of Miller and Smith (1964) and Haussühl (1960), both of whom used ultrasonic pulse techniques. The comparisons in Table 3.9 support the accuracy and reliability of our data in the region of 298°K and promote confidence in the elastic moduli data at higher temperatures.

3.4 Fluorite-structure fluorides: CaF_2, SrF_2 and BaF_2. c(T).

The elastic moduli calculated from equation (3.1) for the five individual modes for CaF_2 and SrF_2 are plotted in Figures 3.5 and 3.6 respectively, while those for the three individual modes for BaF_2 are plotted in Figure 3.7. The fitted polynomials are also plotted in Figures 3.5, 3.6 and 3.7. The addition of a quadratic term to the linear fit was statistically significant (at the 99.9% confidence level) for all modes except for c_{44} (v_4) for CaF_2. For consistency and comparison with the c_{44} (v_2) mode, the quadratic term for c_{44} (v_4) was retained. For some modes, the addition of a cubic term was marginally significant; however, simultaneous application of the χ^2-test indicated that the reduced χ^2 value was less than unity for the quadratic fit, which implies that the average scatter of the data about the fitted polynomial was less than the estimated experimental uncertainty. In view of this it was decided that the data required only a second degree polynomial. The polynomial coefficients for all three crystals are listed in Table 3.10.

The values of the elastic moduli and their temperature derivatives calculated by evaluating the polynomials at 298°K are given in Table 3.11 for CaF_2 and SrF_2. In Table 3.12 are listed the calculated values (from the polynomial) of the elastic moduli and their temperature

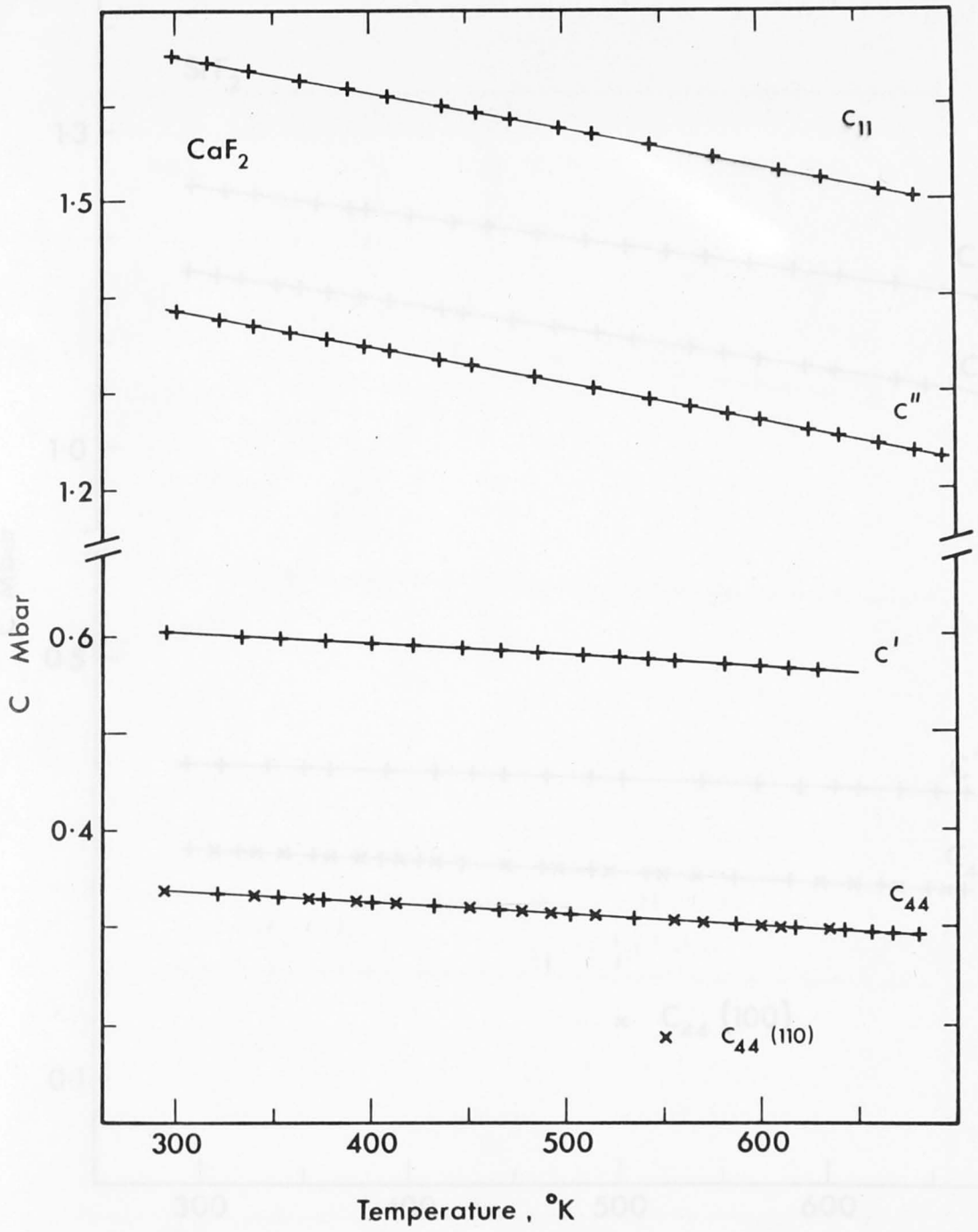

Figure 3.5: Elastic moduli versus temperature for the modes c_{11}, c'', c_{44} and c' for CaF_2. The solid lines represent the fitted second degree polynomials for c_{11}, c'', c_{44} (v_2) and c'. For the c_{44} shear mode, the polynomial curve for the [110] direction cannot be distinguished from the plotted curve for the [001] direction. Data points for the crosscheck for c_{44} from the [110] direction are indicated by X. For reasons of clarity, not all the data points used in the fitting procedure are plotted.

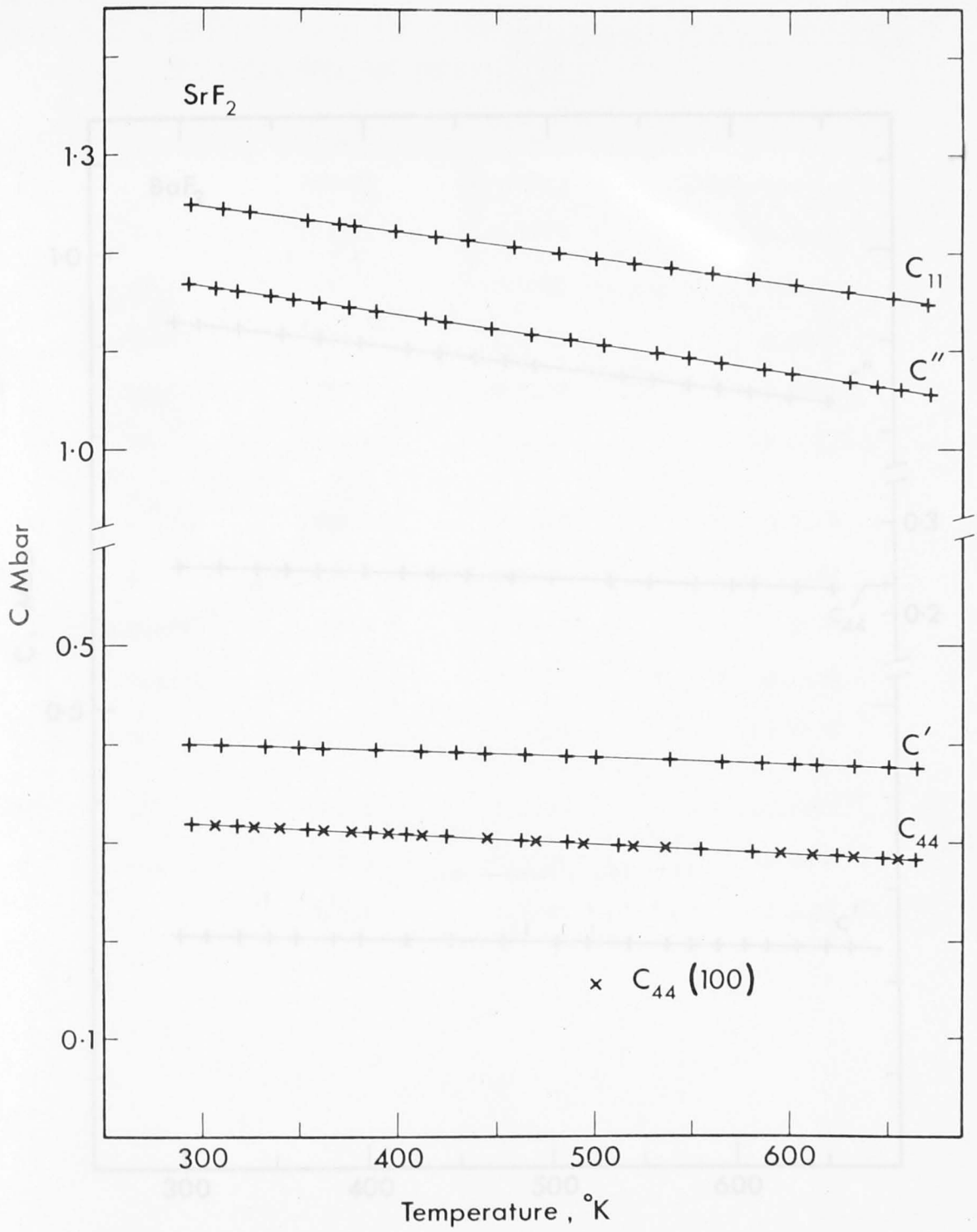

Figure 3.6: Elastic moduli versus temperature for the modes c_{11}, c'', c_{44} and c' for SrF_2. The solid lines represent the fitted second degree polynomials for c_{11}, c'', c_{44} (v_4) and c'. For the shear mode c_{44}, the polynomial curve for the [001] direction is indistinguishable from the plotted curve for the [110] direction. Data points for the crosscheck from the [001] direction are indicated by X. For reasons of clarity, all of the data points used in the fitting procedure were not plotted.

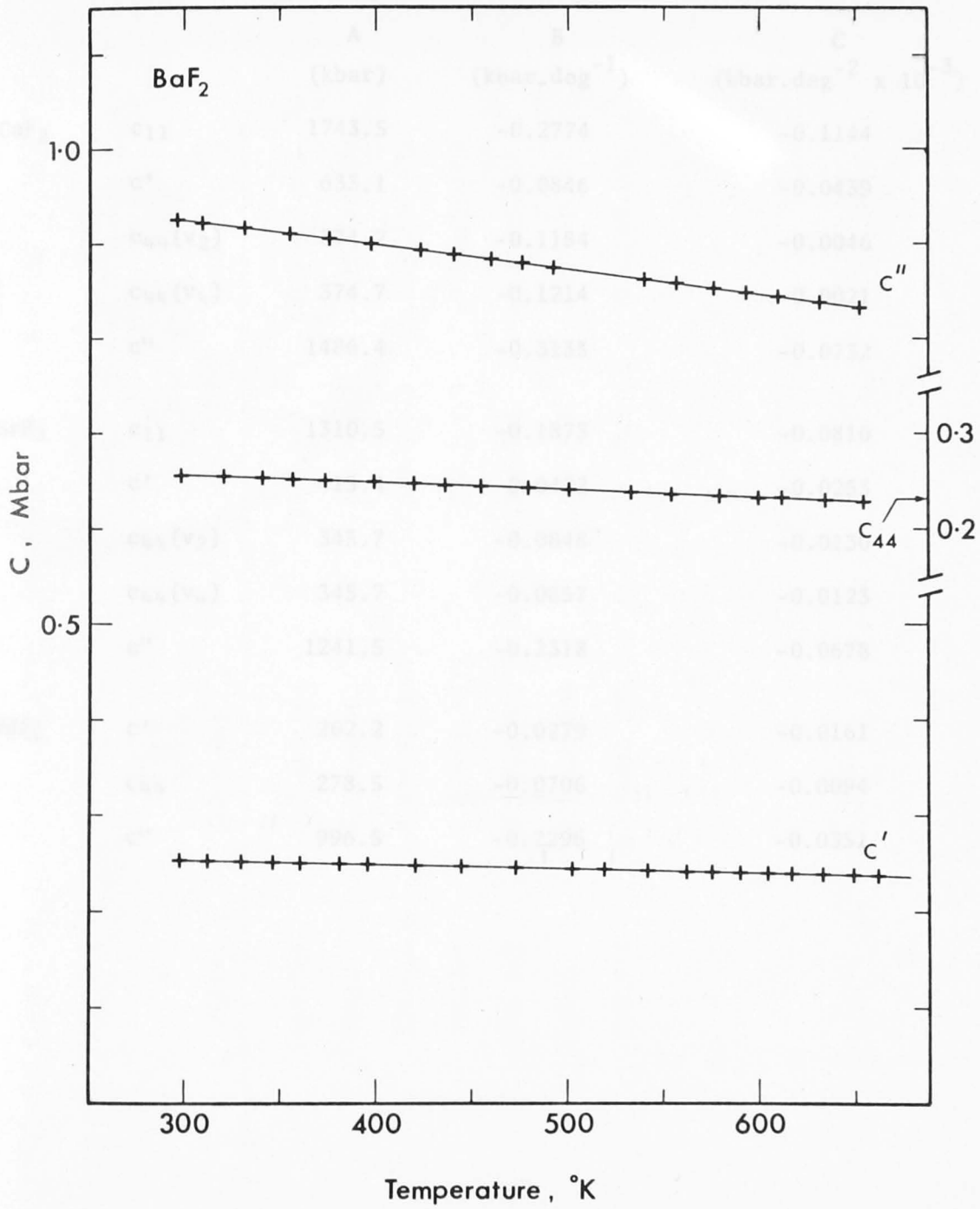

Figure 3.7: Elastic moduli versus temperature for the modes c'', c' and c_{44} (v_4) for BaF_2. The fitted polynomials are represented by the solid lines. For reasons of clarity, it was not possible to plot all the data points used in the fitting procedure.

Table 3.10: Coefficients of the fitted polynomials, $c = A + BT + CT^2$, for CaF_2, SrF_2 and BaF_2

		A (kbar)	B (kbar.deg^{-1})	C (kbar.deg^{-2} x 10^{-3})
CaF_2	c_{11}	1743.5	-0.2774	-0.1144
	c'	633.1	-0.0846	-0.0439
	$c_{44}(v_2)$	374.2	-0.1184	-0.0046
	$c_{44}(v_4)$	374.7	-0.1214	-0.0021
	c''	1486.4	-0.3135	-0.0732
SrF_2	c_{11}	1310.5	-0.1873	-0.0810
	c'	415.4	-0.0422	-0.0253
	$c_{44}(v_2)$	345.7	-0.0848	-0.0130
	$c_{44}(v_4)$	345.7	-0.0857	-0.0123
	c''	1241.5	-0.2318	-0.0678
BaF_2	c'	262.2	-0.0279	-0.0161
	c_{44}	278.5	-0.0706	-0.0094
	c''	996.5	-0.2296	-0.0351

Table 3.11: Single crystal elastic moduli and their temperature derivatives at 298°K for CaF_2 and SrF_2

		CaF_2		SrF_2	
Mode	Velocity	c (kbar)	$\left(\frac{\partial c}{\partial T}\right)_P$ (kbar.deg^{-1})	c (kbar)	$\left(\frac{\partial c}{\partial T}\right)_P$ (kbar.deg^{-1})
c_{11}	v_1	1650.7±3	-0.346±0.004	1247.5±2	-0.236±0.002
c'	v_3	604±1	-0.111±0.001	400.6±0.7	-0.0573±0.0007
c_{44}	v_2	338.5±0.6	-0.1212±0.0007	319.3±0.8	-0.0925±0.001
	v_4	338.3±1	-0.1226±0.0015	319.1±0.7	-0.093±0.0008
c''	v_5	1386.5±1	-0.357±0.003	1166.4±2	-0.272±0.002
	calc.	1385±5	-0.356±0.006	1166.2±4	-0.271±0.004
K_S	calc.	845.4±4	-0.198±0.005	713.4±3	-0.159±0.003

Table 3.12: Single crystal elastic moduli and their temperature derivatives at 298°K for BaF_2

Mode	Velocity	c (kbar)	$\left(\frac{\partial c}{\partial T}\right)_P$ (kbar.deg^{-1})
c'	v_3	252.4±0.5	-0.0376±0.006
c_{44}	v_4	256.7±0.5	-0.0761±0.0005
c''	v_5	925.0±2	-0.251±0.002
c_L	v_6	927.5±1.4	-
	calc.	926.4±2	-
c_T	v_7	253.8±0.4	-
	calc.	253.8±0.5	-
K_S	calc.	581.2±3	-0.162±0.005

derivatives for BaF_2, together with the measured values of $C_L(v_6)$ and $C_T(v_7)$ at room temperature.

The effect of misorientation on the elastic moduli and their temperature derivatives was determined as described in Appendix A, and these errors when significant were incorporated into those listed in Tables 3.11 and 3.12. For CaF_2, the misorientation errors were comparable with other experimental uncertainties for the elastic moduli (0.2%) and very much less for the derivatives (0.1%). For SrF_2, the errors arising from misorientation were negligible (< 0.03% for the elastic moduli and < 0.05% for their derivatives). The large misorientation angle of 3.5° for the [110] direction in BaF_2 resulted in errors of less than 0.03% for the elastic moduli and 0.5% for the derivatives, while the effect of misorientation in the $[1\bar{1}1]$ direction was negligible. The insensitivity of the elastic wave velocities of BaF_2 to misorientation results from its near isotropy (i.e., $c' \approx c_{44}$).

For CaF_2 and SrF_2, the crosschecks are provided by comparing c_{44} from v_2 and v_4 and by comparing c'' (measured) and c'' (calculated from c_{11}, c' and c_{44}); the agreement is better than 0.1% for the elastic moduli and 2% for the derivatives, well within the calculated uncertainties. For BaF_2, the room temperature crosschecks are provided by comparing the calculated and measured values of C_L and C_T which agree to approximately 0.1%. Crosschecks for the temperature derivatives were not possible because development of the crack in the specimen prevented further high-temperature measurements.

In Table 3.13, values of the elastic moduli from other investigators are listed for comparison with our new data for CaF_2, SrF_2 and BaF_2 at 298°K. For CaF_2 and SrF_2, the value tabulated for c_{44} is the average of the values from v_2 and v_4 in Table 3.11. The agreement is good for CaF_2 with the exception of the values of Nikanorov et al. (1968) and Huffman

Table 3.13: Comparison of room temperature values of c and $(\partial c/\partial T)_P$ from various investigators for CaF_2, SrF_2 and BaF_2

	c_{11}	c'	c_{44}	K_S	$\left(\frac{\partial c_{11}}{\partial T}\right)_P$	$\left(\frac{\partial c'}{\partial T}\right)_P$	$\left(\frac{\partial c_{44}}{\partial T}\right)_P$	$\left(\frac{\partial K_S}{\partial T}\right)_P$	
	(kbar)				(kbar.deg^{-1})				Reference
CaF_2	1651	604	338	845	-0.346	-0.111	-0.122	-0.198	This work
	1642	601.2	337.0	841	-0.318	-0.107	-0.122	-0.176	Wong and Schuele (1968)
	1635.7	597.8	339.2	838.6	-0.335	-0.104	-0.116	-0.197	Haussühl (1963)
	1649.4	601.6	338.0	847.3					Ho and Ruoff (1967)
	1652	599	337	853.3					Brielles and Vidal (1975)
	1652.6	599	337.5	854					Vidal (1974)
	1700	590	341	913.3					Nikanorov et al. (1968)
	1640	555	337.0	900					Huffman and Norwood (1960)
SrF_2	1247.5	400.6	319	713.7	-0.236	-0.057	-0.093	-0.159	This work
	1236	402.3	313.2	699.6	-0.198	-0.017	-0.085	-0.175	Gerlich (1964b)
	1246.1	399.9	318.74	713.0	-0.239	-0.057	-0.092	-0.162	Alterovitz and Gerlich (1970)
BaF_2	920.8	252.4	256.7	581.2	-0.212	-0.0375	-0.076	-0.162	This work
	919.9	252.1	256.8	583.8	-0.204	-0.0368	-0.0734	-0.155	Wong and Schuele (1968)
	912.2	248.7	255.1	580.6	-0.206	-0.0359	-0.0735	-0.158	Haussühl (1963)
	894.8	254.7	249.5	555.2					Gerlich (1968)
	891.5	245.7	253.5	594.3					Gerlich (1964a)

and Norwood (1960). Similarly for BaF_2, the agreement is generally good with the exception of the values of Gerlich (1964a, 1968). Our values of the elastic moduli for SrF_2 agree very well with those of Alterovitz and Gerlich (1970), but not as well with those of Gerlich (1964b).

Also compared in Table 3.13 are the values of the temperature derivatives of the elastic moduli, $(\partial c/\partial T)_P$ at 298°K. Our values of $(\partial c_{44}/\partial T)_P$ for CaF_2 and SrF_2 are obtained by averaging the values from v_2 and v_4 listed in Table 3.11. For CaF_2, there is good agreement between our values and those of Wong and Schuele (1968) and Haussühl (1963); in particular, there is striking agreement between our value of $(\partial K_S/\partial T)_P$ and that of Haussühl (1963). The values of Alterovitz and Gerlich (1970) for SrF_2 agree exceptionally well with all of our values for $(\partial c/\partial T)_P$; the agreement is much better than for the earlier data of Gerlich (1964b). For BaF_2, there is good agreement among the values of $(\partial c/\partial T)_P$ from the present work and those of Wong and Schuele (1968) and Haussühl (1963).

As for LiF and NaF, the available high T data from various sources may be readily compared in Figure 3.8 which is a plot of adiabatic bulk modulus, K_S, versus temperature from different investigators from 0-1123°K for CaF_2, and from 0-650°K for SrF_2 and BaF_2. The low temperature values of K_S for CaF_2 calculated from c_{11} and c_{12} of Huffman and Norwood (1960) do not follow a smooth curve and are offset to higher K_S values than ours, as are the high temperature resonance data of Nikanorov et al. (1968). The K_S values from both these studies were considerably higher than those of all other investigators at 298°K in Table 3.13. However the K_S-T data of Nikanorov et al. (1968) does follow the general trend of the present K_S-T data. The K_S-T data from Vidal (1974) obtained by resonance techniques is considerably different in gradient from our curve (approximately 50% difference in $(\partial K_S/\partial T)_P$) although there is agreement with our curve at room temperature. However,

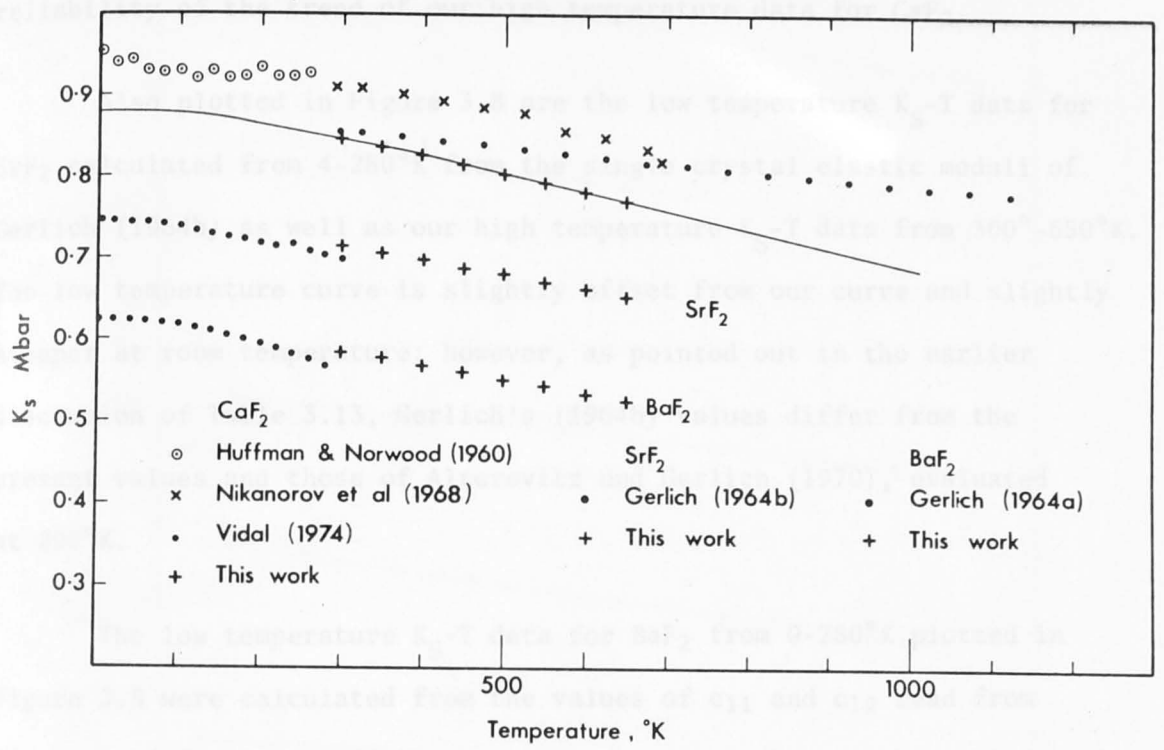

Figure 3.8: Bulk modulus versus temperature for CaF_2, SrF_2 and BaF_2. The solid line for CaF_2 will be discussed later in Figure 4.12.

the agreement of our values for $(\partial c/\partial T)_P$ at 298°K with other data obtained by ultrasonic pulse techniques in Table 3.13 support the reliability of the trend of our high temperature data for CaF_2.

Also plotted in Figure 3.8 are the low temperature K_S-T data for SrF_2 calculated from 4-280°K from the single crystal elastic moduli of Gerlich (1964b) as well as our high temperature K_S-T data from 300°-650°K. The low temperature curve is slightly offset from our curve and slightly steeper at room temperature; however, as pointed out in the earlier discussion of Table 3.13, Gerlich's (1964b) values differ from the present values and those of Alterovitz and Gerlich (1970), evaluated at 298°K.

The low temperature K_S-T data for BaF_2 from 0-280°K plotted in Figure 3.8 were calculated from the values of c_{11} and c_{12} read from Figure 1 of Gerlich (1964a). Even though such values are not likely to be very accurate they are sufficient to indicate the trend of the low temperature data curve which is offset from our curve at 298°K and also somewhat steeper in slope. Comparisons of the various data in Table 3.13 indicate that the room temperature value and gradient for our K_S-T curve is reliable and promote confidence in the high temperature data for BaF_2.

3.5 Rutile-structure fluorides: MgF_2. c(T).

The elastic moduli calculated from equation (3.1) for MgF_2 are plotted in Figure 3.9 for all eleven modes in Table 3.2 together with the fitted polynomials (Table 3.14). The primary modes for c_{11}, c_{66}, c', c_{33}, c_{44} (v_8) and C_{L_2} were measured from 298-650°K while the modes for the crosschecks, c_{44} (v_3 and v_6), C_{L_1}, C_{T_1}, and C_{T_2} were measured from 298-370°K. The fitted polynomials were determined to be quadratics in T at a confidence level of better than 99.9% for all modes by the simultan-

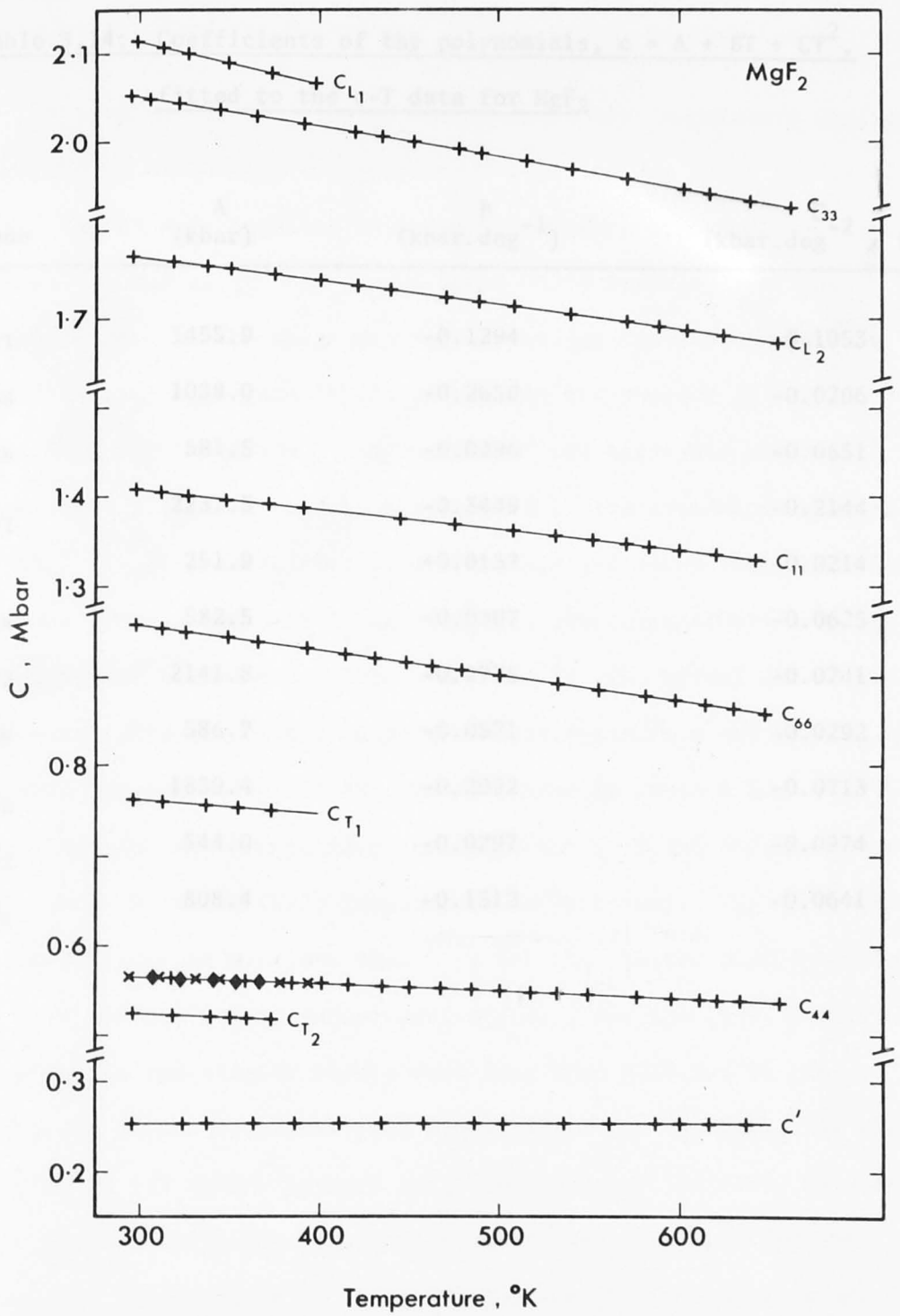

Figure 3.9: Elastic moduli versus temperature from 298°-650°K for the modes c_{11}, c_{66}, c', c_{33}, c_{44} (v_8) and C_{L_2} for MgF_2 and from 298°-373°K for the crosscheck modes, C_{L_1}, c_{44} (v_3 and v_6), C_{T_1} and C_{T_2}. The solid lines represent the fitted polynomials (not plotted for c_{44} (v_3 and v_6)). Data points for the crosscheck for c_{44} from the [100] direction are indicated by ♦ and from the [110] direction by X. For reasons of clarity not all the data points used in the fitting procedure were plotted.

Table 3.14: Coefficients of the polynomials, $c = A + BT + CT^2$, fitted to the c-T data for MgF_2

Mode	A (kbar)	B (kbar.deg^{-1})	C (kbar.deg^{-2} x 10^{-3})
c_{11}	1455.9	-0.1294	-0.1053
c_{66}	1038.0	-0.2650	-0.0206
c_{44}	581.5	-0.0296	-0.0651
c_{L_1}	2237.3	-0.3449	-0.2144
c'	251.9	+0.0137	-0.0214
c_{44}	582.5	-0.0307	-0.0625
c_{33}	2141.8	-0.2775	-0.0741
c_{44}	586.7	-0.0571	-0.0292
c_{L_2}	1839.4	-0.2092	-0.0713
c_{T_2}	544.0	-0.0297	-0.0974
c_{T_1}	808.4	-0.1312	-0.0641

eous application of the F-test and χ^2-test described previously.

The values of the elastic moduli and their temperature derivatives calculated by evaluating the polynomial equations at 298°K are listed in Table 3.15 for MgF_2 together with the appropriate errors. The value of K_S is calculated as the VRH (Voigt-Reuss-Hill) average, i.e. the arithmetic mean of the Voigt and Reuss averages for the moduli of a polycrystalline aggregate (Hill, 1952). In the absence of a theoretical formulation for the P and T derivatives of the aggregate moduli, it was assumed that $(\partial K_S/\partial T)$ could be represented by the arithmetic mean of the values of $(\partial K_S/\partial T)$ calculated from the Voigt and Reuss formulae. The upper and lower bounds for K_S and $(\partial K_S/\partial T)$ are respectively 1023 and 1015 kbar, and 0.1604 and 0.1599 kbar. deg^{-1}. The errors due to misorientation were calculated as described in Appendix A and when significant were incorporated into the errors listed in Table 3.15. For the [001] direction the errors were insignificant (< 0.04% for the elastic moduli and < 0.1% for their temperature derivatives). The errors for the [100] direction are less than 0.2% for the elastic moduli and less than 0.5% for their temperature derivatives. For the [110] direction, the errors in the elastic moduli were less than 0.2% and in their temperature derivatives less than 0.02% except for $(\partial c'/\partial T)_P$ for which the error is 13% (which appears large only because $(\partial c'/\partial T)_P$ is near zero). Consequently, the misorientation of less than 0.3° for the propagation direction at 45° to the [100] and [010] directions was assumed to have negligible effect on the elastic moduli and their temperature derivatives.

For MgF_2, the crosschecks are provided by the comparison of c_{44} from v_3, v_6 and v_8, and by the comparison of the measured values of C_{L_1}, C_{T_1} and C_{T_2} with those calculated from the six primary modes. The crosschecks for the elastic moduli are good to within 0.25%. For $(\partial c_{44}/\partial T)_P$ the values from v_3 and v_6 agree to within 0.6% whereas the

Table 3.15: Single crystal elastic moduli and their temperature derivatives at 298°K for MgF_2

Mode	Velocity	c (kbar)	$\left(\frac{\partial c}{\partial T}\right)_P$ (kbar.deg^{-1})
c_{11}	v_1	1408±6	-0.192±0.007
c_{66}	v_2	957±5	-0.277±0.007
c'	v_5	254±1	+0.0009±0.0004
c_{33}	v_7	2053±6	-0.322±0.006
c_{44}	v_8	567±1	-0.0746±0.0007
c_{L_2}	v_9	1771±5	-0.252±0.005
c_{12}	calc.	900±5	-0.194±0.007
c_{13}	calc.	635±11	-0.086±0.025
K_S	calc.	1019±7	-0.160±0.015
c_{44}	v_3	567±3	-0.0683±0.007
	v_6	568±2	-0.0679±0.004
c_{L_1}	v_4	2115±21	-0.473±0.071
	calc.	2111±9	-0.470±0.012
c_{T_2}	v_{10}	527±8	-0.088±0.026
	calc.	527±13	-0.080±0.019
c_{T_1}	v_{11}	764±7	-0.169±0.017
	calc.	762±3	-0.176±0.004

values from v_6 and v_8 agree to within 10%. The calculated and measured values of $(\partial C_{L_1}/\partial T)_P$, $(\partial C_{T_1}/\partial T)_P$ and $(\partial C_{T_2}/\partial T)_P$ all agree to within 10%. The errors associated with the measured crosscheck modes are large due to the limited temperature range and the small number of data points used in the polynomial fitting procedure; the large errors in the calculation of these elastic moduli and their temperature derivatives result from the propagation of errors, since these elastic moduli are complicated functions of the six independent elastic moduli. In view of this, the crosschecks are quite satisfactory.

In Table 3.16, values of the elastic moduli from other investigators are listed for comparison with our new data for MgF_2 at 298°K. The agreement is generally good with the exception of the values of Cutler et al. (1968) which are all too low (except for c' and c_{66}). Our value of the isotropic bulk modulus (VRH average) compares favourably with the polycrystalline data of Bailey et al. (1975).

Also compared in Table 3.16 are the values of $(\partial c/\partial T)_P$ at 298°K from various investigators. The values attributed to Aleksandrov et al. (1969) are determined from their values at 20°C and -100°C together with their statement that the elastic moduli depend linearly on temperature in this range. The agreement between the various values is generally satisfactory.

In Figure 3.10, the present values of K_S versus T are compared with those of Bailey et al. (1975). The values of K_S for Bailey et al. (1975) were calculated from their linear equations in T for the average compressional and shear velocities of a number of polycrystalline samples. Our values of K_S are the VRH averages calculated at each temperature from the single crystal moduli. The difference between the Voigt and Reuss aggregate averages is indicated in Figure 3.10. Also plotted in Figure 3.10 are the two data points calculated from the single

Table 3.16: Comparison of room temperature values of c and $(\partial c/\partial T)_P$ for MgF_2 from various investigators

	c_{11}	c_{33}	c_{12}	c_{13}	c_{44}	c_{66}	c'	K_S	Reference
c (kbar)	1408	2053	900	635	567	957	254	1019	This work
	1395	2041	897	625	564	951	249	1010	Aleksandrov et al. (1969)
	1237	1770	732	536	552	978	252	869	Cutler et al. (1968)
	1427	2040	922	641	567	935	252	1030	Davies (1976)
	1399	2042	893	637	570	954	253	1015	Haussühl (1968)
	-	-	-	-	-	-	-	1035	Bailey et al. (1975)
$\left(\frac{dc}{dT}\right)_P$ ($kbar.deg^{-1}$)	-0.192	-0.322	-0.194	-0.086	-0.075	-0.277	+0.0009	-0.160	This work
	-0.233	-0.308	-0.183	-0.050	-0.058	-0.308	-0.025	-0.151	Aleksandrov et al. (1969)
	-0.215	-0.294	-0.223	-0.051	-0.063	-0.267	+0.004	-0.155	Haussühl (1968)
	-	-	-	-	-	-	-	-0.176	Bailey et al. (1975)

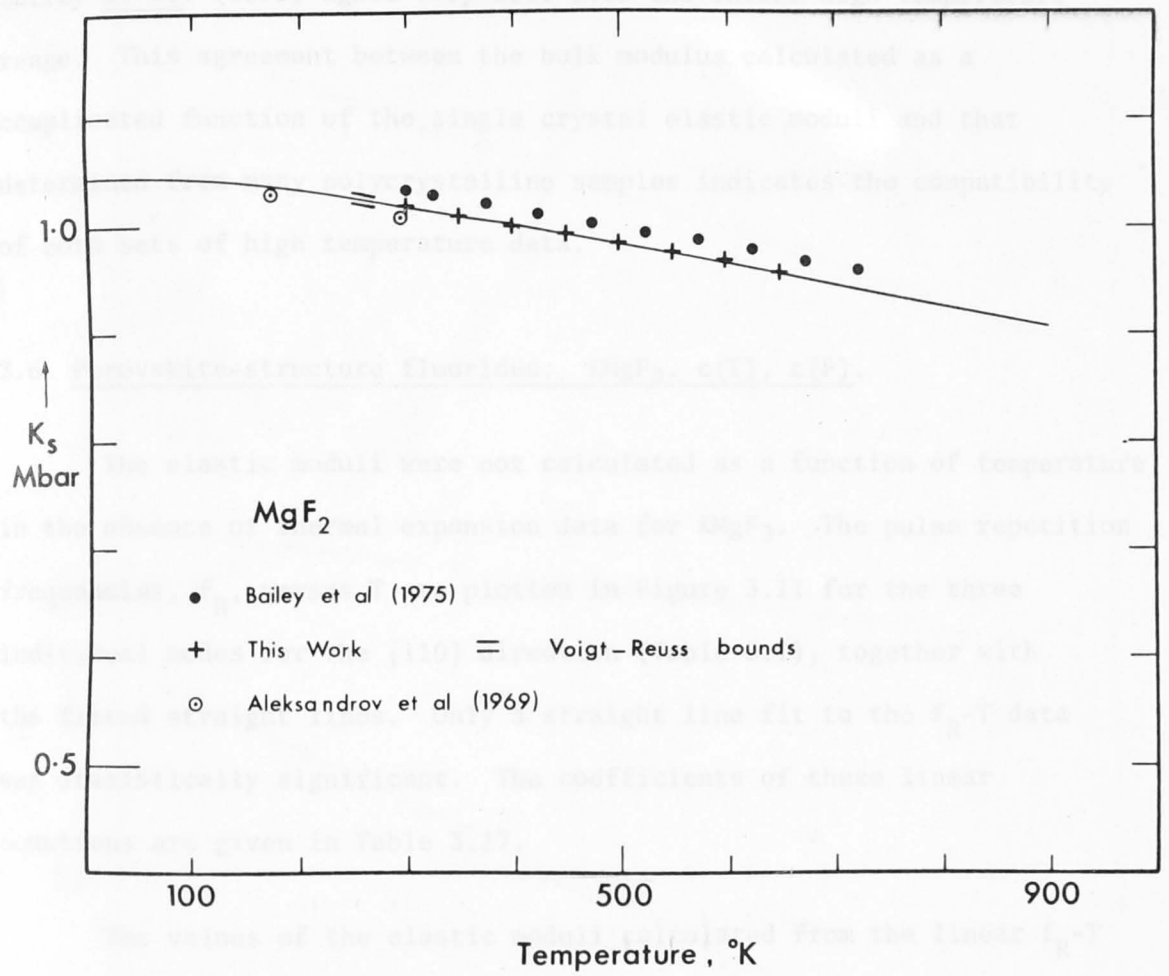

Figure 3.10: Bulk modulus versus temperature for MgF_2. The solid curve will be discussed later, when this figure is presented again as Figure 4.13.

crystal elastic moduli of Aleksandrov et al. (1969) at 173°K and 293°K. Except for a slight offset, the present K_S-T data curve and that from Bailey et al. (1975) agree very well over the entire high temperature range. This agreement between the bulk modulus calculated as a complicated function of the single crystal elastic moduli and that determined from many polycrystalline samples indicates the compatibility of both sets of high temperature data.

3.6 Perovskite-structure fluorides: $KMgF_3$. c(T), c(P).

The elastic moduli were not calculated as a function of temperature in the absence of thermal expansion data for $KMgF_3$. The pulse repetition frequencies, f_R, versus T are plotted in Figure 3.11 for the three individual modes for the [110] direction (Table 3.1), together with the fitted straight lines. Only a straight line fit to the f_R-T data was statistically significant. The coefficients of these linear equations are given in Table 3.17.

The values of the elastic moduli calculated from the linear f_R-T equations at 298°K are given in Table 3.18. The errors due to misorientation were negligible. The temperature dependence of the elastic moduli was expressed in the form

$$\left(\frac{d \ln c}{dt}\right) = -\alpha + 2\left(\frac{d \ln f_R}{dT}\right) \qquad (3.13)$$

where α is the linear coefficient of thermal expansion. Equation (3.13) is obtained by differentiating equation (3.1) with respect to T and then by dividing the resultant equation by equation (3.1). The temperature dependence of the elastic moduli at 298°K can then be found directly from equation (3.13), once the value of the thermal expansion coefficient is known. In Table 3.18 are listed the values of $(\partial \ln f_R/\partial T)_P$ together with the appropriate errors. If the linear thermal expansion coefficient

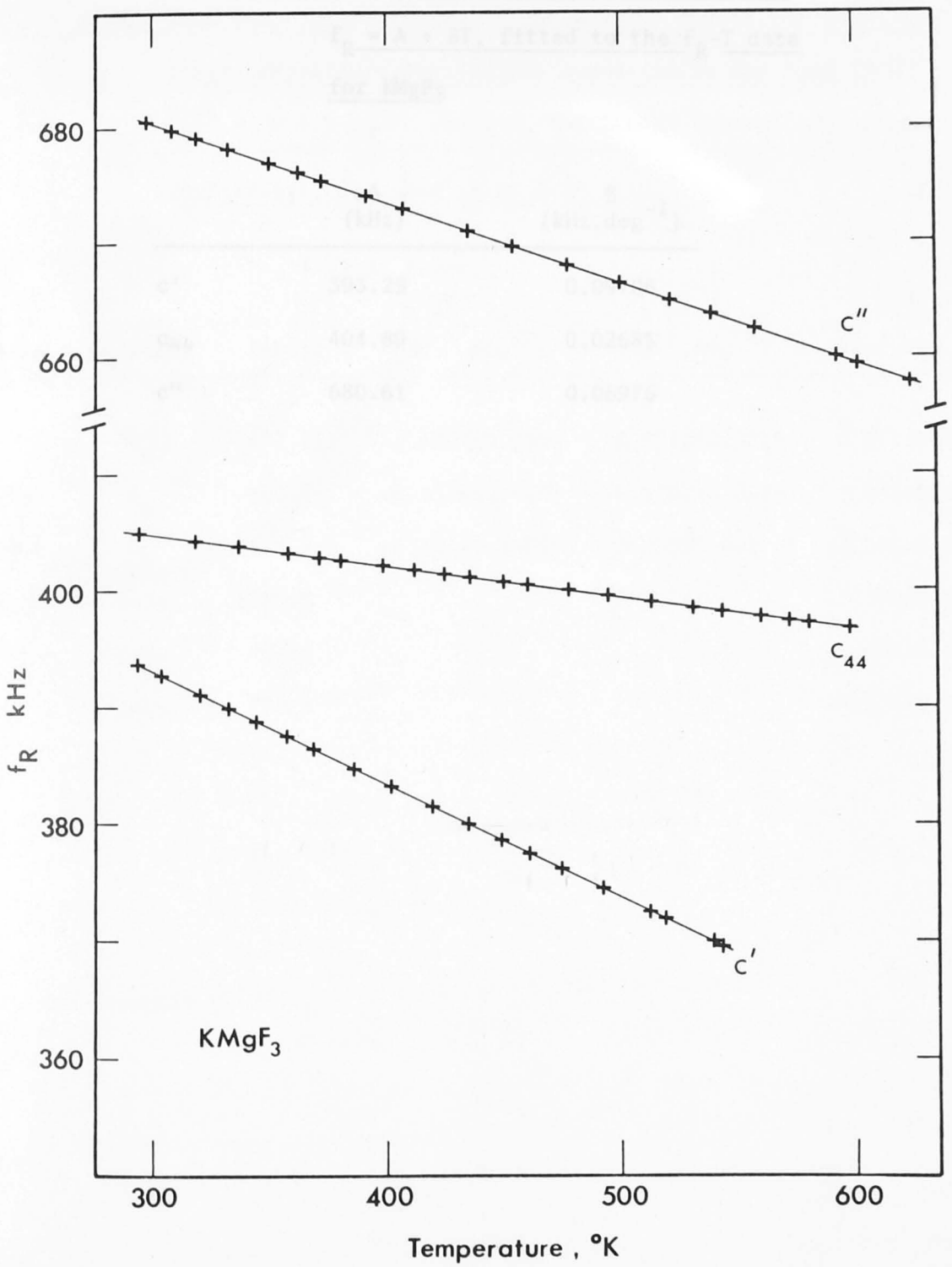

Figure 3.11: Pulse repetition frequency, f_R, versus temperature for the c'', c' and c_{44} modes for $KMgF_3$. Not all the data points were plotted for reasons of clarity.

Table 3.17: Coefficients of the straight lines, $f_R = A + BT$, fitted to the f_R-T data for $KMgF_3$

	A (kHz)	B ($kHz.deg^{-1}$)
c'	393.29	0.09708
c_{44}	404.89	0.02685
c''	680.61	0.06976

Table 3.18: Room temperature values of the elastic moduli for $KMgF_3$ and their temperature derivatives expressed in the form $\frac{d\ln c}{dT} = -\alpha + 2\frac{d\ln f_R}{dT}$ where α, the linear thermal expansion coefficient, is taken to be 3.76×10^{-5} deg^{-1} †

Mode	Velocity	c (kbar)	$\left(\frac{d\ln f_R}{dT}\right)_P$ (10^{-3} deg^{-1})	$\left(\frac{d\ln c}{dT}\right)_P$ (10^{-3} deg^{-1})	$\left(\frac{dc}{dT}\right)_P$ (kbar.deg^{-1})
c'	v_3	471.9±1	-0.4937±0.0006	-0.5313±0.0013	-0.251±0.001
c_{44}	v_4	500.1±1	-0.1326±0.0003	-0.1702±0.0008	-0.085±0.001
c''	v_5	1413.3±3	-0.205±0.0008	-0.243±0.002	-0.343±0.004
c_{11}	calc.	1385±5			-0.509±0.006
c_{12}	calc.	441±5			-0.007±0.006
K_S	calc.	756±4			-0.174±0.005

† See Footnote p. 29.

is assumed to be 3.76×10^{-5} deg^{-1} for $KMgF_3$[†] (see footnote), values for $(\partial \ln c/\partial T)_P$ and $(\partial c/\partial T)_P$ can be calculated at 298°K and these are also tabulated in Table 3.18.

The values of f_R versus pressure to 2.5 kbar for $KMgF_3$ are plotted in Figures 3.12, 3.13 and 3.14 for c', c_{44} and c'' respectively, together with the fitted straight lines (Table 3.19). Only a linear fit to the data was justified for the small number of data points which span a limited pressure range. For c', run 2 data was analysed in preference to run 1 data, since the decreasing P data points for run 1 did not exactly follow the trend for increasing P. In addition, f_R evaluated at 1 bar and 298°K from run 2 is in much better agreement with the corresponding value from the temperature run. The data for run 3 for c_{44} (see Figure 3.13) were taken as the primary f_R-P data since these data are more numerous and reproducible than for runs 1 and 2. The data for c'' versus pressure are reproducible within the limit of experimental uncertainty in determining f_R, which was larger for this mode. The above pressure measurements are limited to 2.5 kbars, since at higher pressures the data are not reproducible.

In Table 3.20 are listed values of the elastic moduli and their pressure derivatives for $KMgF_3$ at 298°K. The elastic moduli at 298°K determined from the pressure runs agree to within 0.06% of those determined from the temperature runs (Table 3.18), which is of the order of the uncertainty expected from the straight line fitting procedure. (The larger errors listed in Tables 3.18 and 3.20 result from the incorporation

---

[†] This value of α for $KMgF_3$ is determined by multiplying by 4 the value of α for $SrTiO_3$ (Lytle, 1964). This follows from the thermal expansion studies of Megaw (1939) and Austin (1952) which demonstrated that for compounds with the same structure, α is proportional to $Z_c Z_a$ where Z_c, Z_a are the cationic and anionic valence charges respectively.

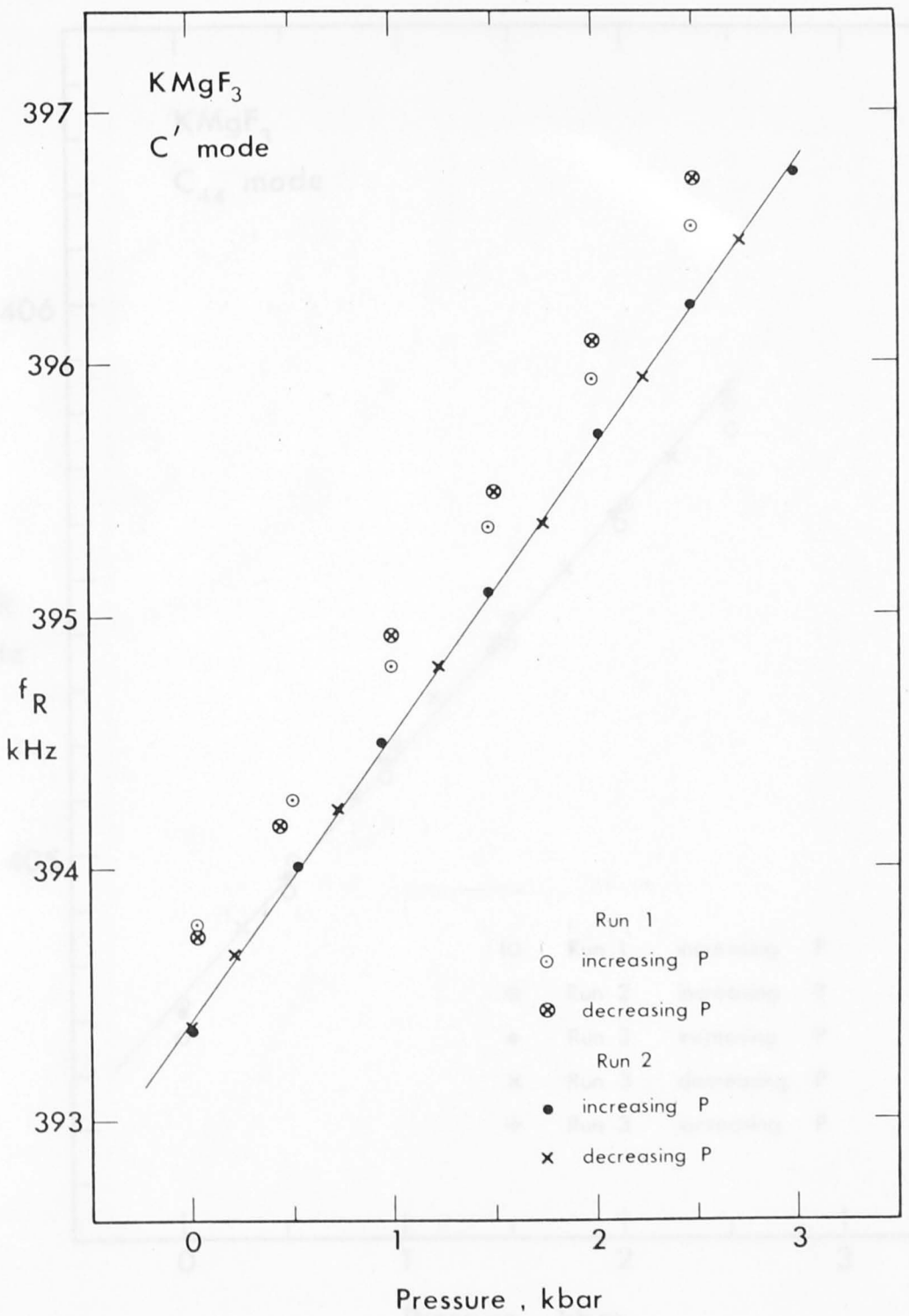

Figure 3.12: Pulse repetition frequency, f_R, versus pressure for c' for $KMgF_3$.

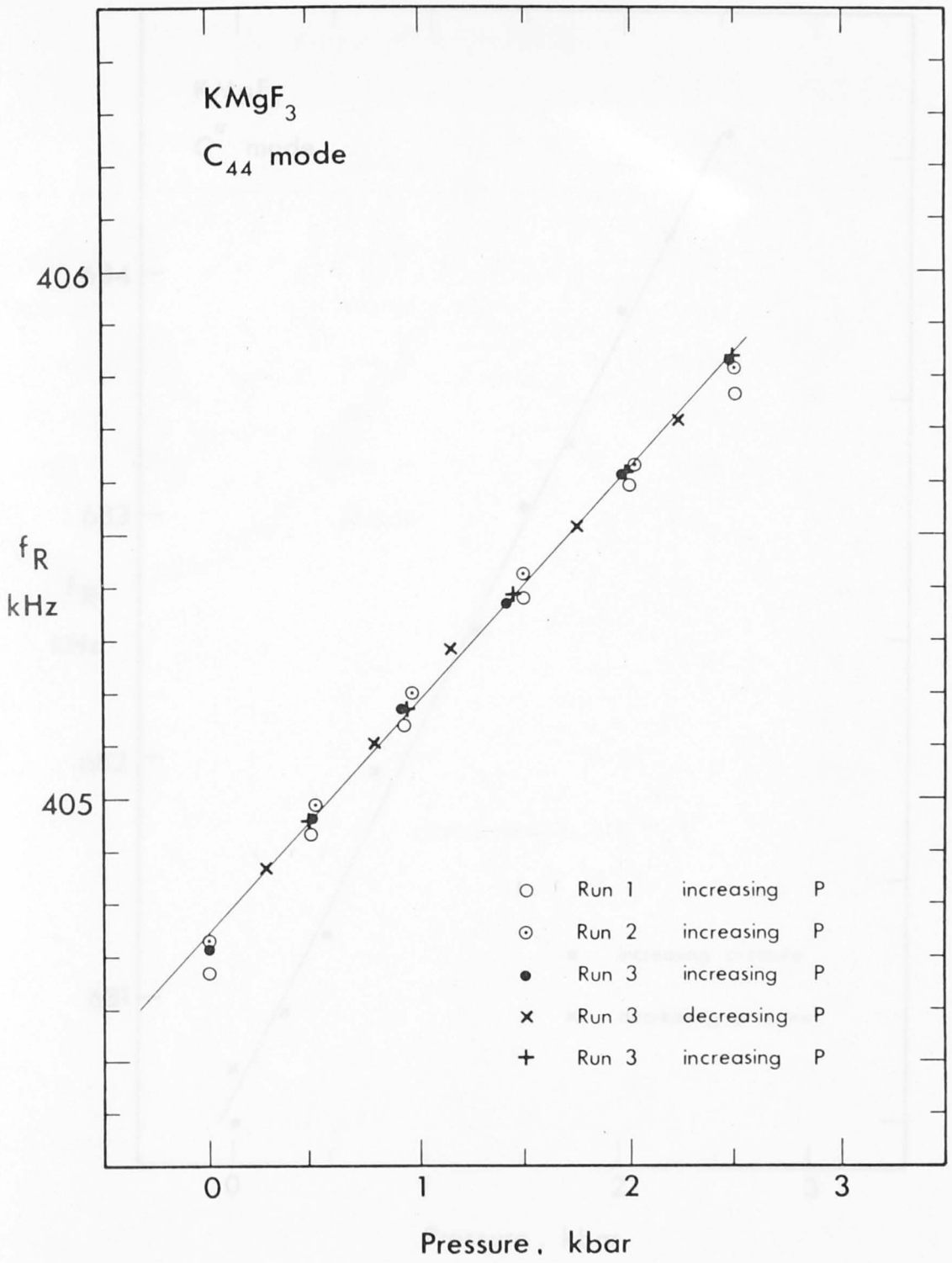

Figure 3.13: Pulse repetition frequency, f_R, versus pressure for c_{44} for $KMgF_3$.

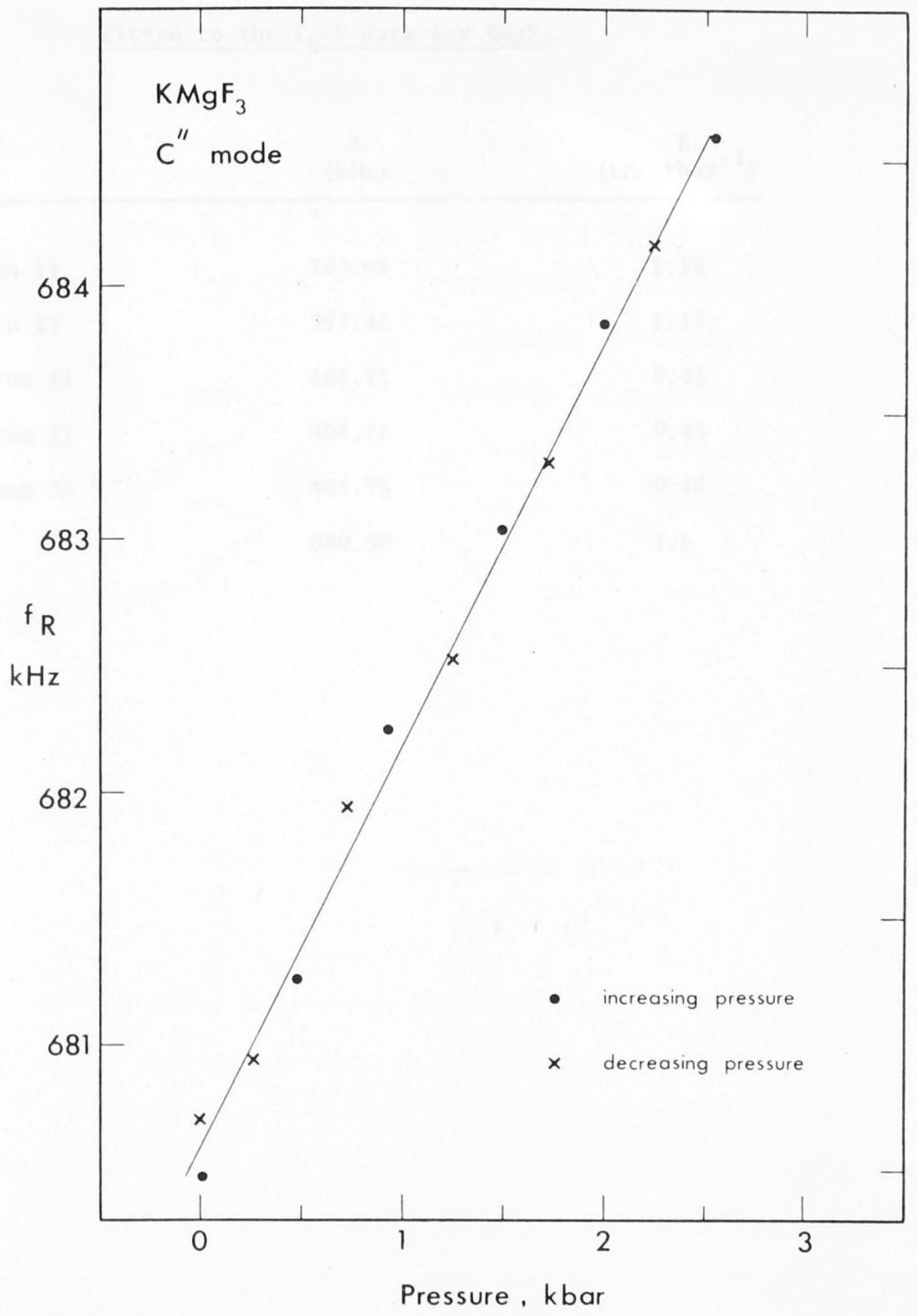

Figure 3.14: Pulse repetition frequency, f_R, versus pressure for c'' for $KMgF_3$.

Table 3.19: Coefficients of the straight lines, $f_R = A + BP$, fitted to the f_R-P data for $KMgF_3$

	A (kHz)	B ($kHz.kbar^{-1}$)
c' (run 1)	393.69	1.18
c' (run 2)	393.40	1.13
c_{44} (run 1)	404.71	0.43
c_{44} (run 2)	404.76	0.43
c_{44} (run 3)	404.75	0.44
c''	680.59	1.6

Table 3.20: Elastic moduli and their pressure derivatives at 1 bar and 298°K for $KMgF_3$

Mode	Velocity	c (kbar)	$\frac{dc}{dp}$
c'	v_3	472.2±1	2.94±0.12
c_{44}	v_4	499.8±1	1.31±0.03
c''	v_5	1413.2±3	7.3±0.4
c_{11}	calc.	1386±5	8.93±0.55
c_{12}	calc.	441±5	3.05±0.55
K_S	calc.	756±4	5.01±0.47

of the measurement errors for ρ_o and ℓ_o). It is worth pointing out that the values of $(\partial c/\partial P)_T$ calculated from the less reliable runs for c' and c_{44} lie within the uncertainty limits on the values of $(\partial c/\partial P)_T$ listed in Table 3.20.

In Table 3.21, our values of the elastic moduli at 298°K for $KMgF_3$ are compared with those of other investigators. There is very good agreement between our values and those of Reshchikova (1969) while the values of Rosenberg and Wigmore (1967) all appear too low.

The values of $(\partial c/\partial T)_P$ at 298°K are also compared in Table 3.21. The agreement between our values of $(\partial c/\partial T)_P$ calculated neglecting thermal expansion and those of Reshchikova (1969), who also ignored thermal expansion, is excellent. Table 3.21 also illustrates that the effect of neglecting thermal expansion is an error of approximately 10% in all the $(\partial c/\partial T)_P$ except for the smaller magnitude $(\partial c_{44}/\partial T)_P$ for which the error is approximately 25%.

3.7 Conclusion

Utilising the precise technique of pulse superposition, we have measured as a function of temperature (and pressure) the single crystal elastic moduli of several fluorides crystallising in the rocksalt, fluorite, rutile and perovskite structures. The reliability of our data is supported by its internal consistency and compatability with other data. In general, crosschecks are good to within 0.25% for the elastic moduli and 5% for their temperature derivatives for LiF, NaF, CaF_2, SrF_2 and MgF_2. These results are evidence for the reliability of our data for $KMgF_3$ (no crosschecks) and BaF_2 (room temperature crosschecks only).

The agreement between our values of the elastic moduli and their temperature derivatives at 298°K and those of other investigators using ultrasonic pulse techniques attests to the reliability of our data in

Table 3.21: Comparison of the room temperature values of c and $(\partial c/\partial T)_P$ for $KMgF_3$ from various investigators

c_{11}	c'	c_{44}	K_S	Reference
	(kbar)			
1385	472	500	756	This work
1380.1	471.8	498.3	751.1	Reshchikova (1969)
1320	462	485	704	Rosenberg and Wigmore (1967)
$\left(\frac{\partial c_{11}}{\partial T}\right)_P$	$\left(\frac{\partial c'}{\partial T}\right)_P$	$\left(\frac{\partial c_{44}}{\partial T}\right)_P$	$\left(\frac{\partial K_S}{\partial T}\right)_P$	
	(kbar.deg^{-1})			
-0.509	-0.251	-0.085	-0.174	This work
-0.46	-0.23	-0.066	-0.153	This work neglecting thermal expansion
-0.47	-0.23	-0.061	-0.163	Reshchikova (1969)

the room temperature region and promotes confidence in our elastic moduli data at higher temperatures. Our high temperature data appear to be superior to the existing high temperature elastic data determined from resonance experiments.

These precise new data will be central to the discussions of high temperature elastic behaviour (Chapter 4) and elastic modulus systematics (Chapter 5).

CHAPTER 4

HIGH TEMPERATURE ELASTICITY

CHAPTER 4

HIGH TEMPERATURE ELASTICITY

4.1 Introduction

Many workers, both in the fields of solid state physics and earth sciences, have been interested in the characterisation of the temperature dependence of the elastic moduli; such studies have involved either experimental determinations or theoretical derivations (or both). There are many reasons for this interest. The parameters in various interatomic force models can be further constrained by information on the behaviour of the elastic moduli, c, versus temperature, leading to a greater understanding of the nature of the short range repulsive forces in the lattice. Such an approach assumes that the elastic behaviour versus temperature is correctly described by the particular lattice dynamical model; for instance, Garber and Granato (1975) expressed the temperature dependence of the second-order elastic constants in terms of second-order, third-order and fourth-order elastic constants. Alternatively, the experimentally determined values of c-T can be employed in testing the validity of certain lattice dynamical approaches as well as in supporting semi-empirical derivations. An understanding of the dynamic lattice is essential in assessing thermal and finite compression effects so that physical properties can be extrapolated to pressures and temperatures beyond the accessible laboratory ranges; these extrapolations have special importance in geophysical discussions of the Earth's interior, where pressures of 3.5 Mbar and temperatures of greater than 3000°K are achieved.

The regimes of low- and high-temperature elasticity have received particular attention in theoretical studies of the solid state. Here "low" temperature refers roughly to the "T^3" region in the Debye theory of specific heat and "high" temperature refers to temperatures above which all of the lattice vibrational modes are activated and the

classical Dulong-Petit specific heat limit is attained (.i.e., for $T > \theta_D$, the Debye temperature). Various formulations of finite strain equations of state depend on the knowledge of the high temperature value of $(\partial K/\partial T)_P$ in the reference state so that thermal effects can be incorporated (e.g., Thomsen and Anderson, 1969; Thomsen, 1970, 1972; Davies, 1973). The temperature derivatives of the elastic moduli, $(\partial c/\partial T)_P$, at high temperatures are also important to discussions of lattice instability theories of melting (e.g., Jackson and Liebermann, 1974).

The dependence of the elastic moduli on pressure and temperature is a direct consequence of lattice anharmonicity. Such behaviour is not predicted by harmonic theories which are based on the assumption that the interatomic potential energy can be expanded as a power series in atomic displacements terminated after the quadratic term. Harmonic theories predict that the elastic moduli should be independent of temperature and pressure and that the thermal expansion should be zero (see Kittel, 1971, chapter 6; Leibfried and Ludwig, 1961).

Anharmonic effects were considered by Grüneisen (1926) in his explanation of the thermal expansion of solids. Born and his co-workers[†] presented a thorough thermodynamical characterisation of solids in which calculations of the elastic moduli versus temperature were carried out for various values of the exponents m and n in the power law potential, $\Phi = \frac{A}{r^m} + \frac{B}{r^n}$. The approaches of both Born and Grüneisen were restricted by the use of such a simple, power law interatomic potential.

Leibfried and Hahn (1958) employed a more generalized approach to arrive at the now commonly accepted result that the elastic moduli are linearly decreasing in temperature at high temperatures ($T >> \theta_D$, where θ_D is the Debye temperature) and are approximately constant with temperature at low temperatures ($T << \theta_D$) (see Figure 4.1). This

---

[†] e.g., Born (1943), Born and Bradburn (1943), Bradburn (1943), Furth (1944), Gow (1944).

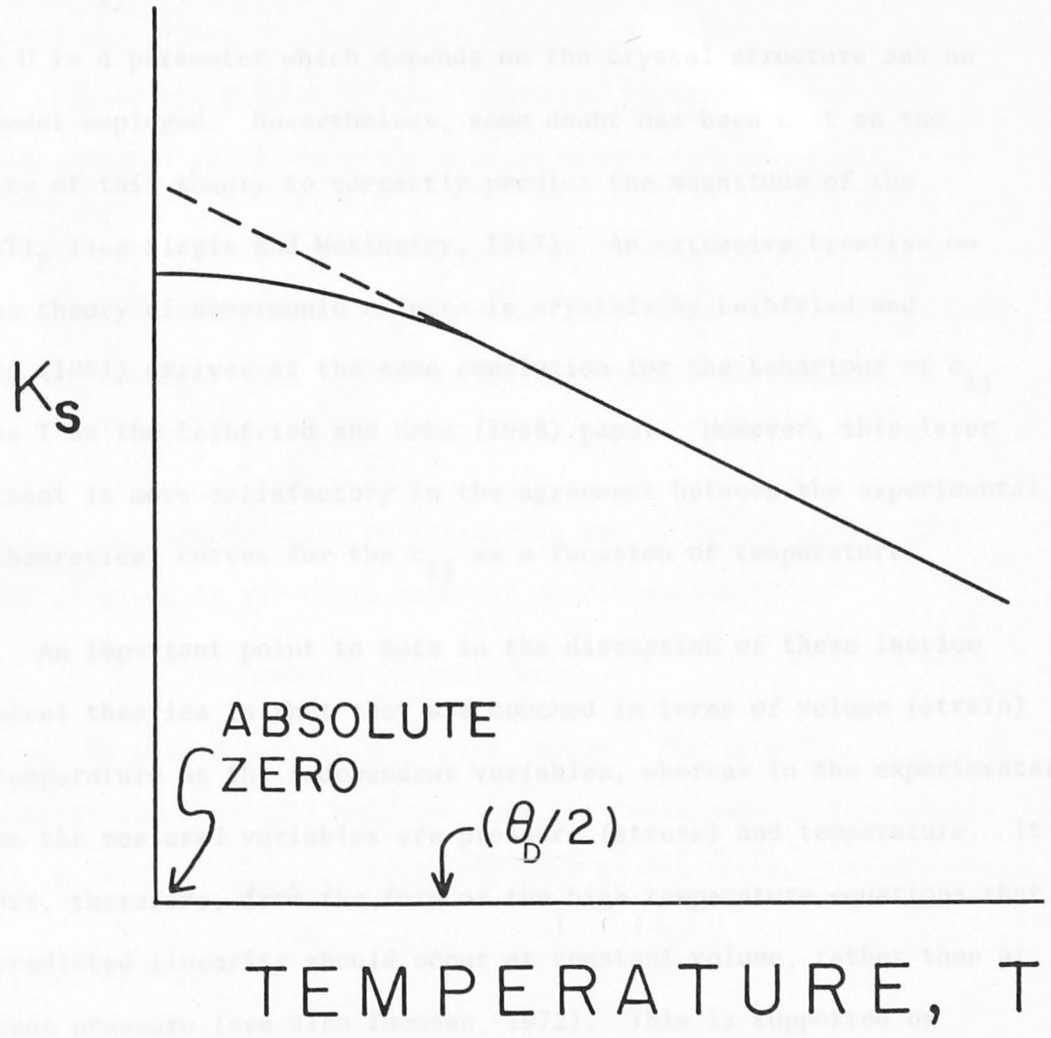

Figure 4.1: Plot of K_S versus T demonstrating the general behaviour of the elastic moduli as a function of temperature. At very low temperatures, K_S is approximately constant while at high temperatures K_S is almost linear in T.

results from their expression for the elastic moduli, c_{ij}, in terms of the internal vibrational energy, $\bar{\varepsilon}$

$$c_{ij} = c_o(1 - D\bar{\varepsilon}) \qquad (4.1)$$

where D is a parameter which depends on the crystal structure and on the model employed. Nevertheless, some doubt has been cast on the ability of this theory to correctly predict the magnitude of the $(\partial c/\partial T)_p$ (see Slagle and McKinstry, 1967). An extensive treatise on on the theory of anharmonic effects in crystals by Leibfried and Ludwig (1961) arrives at the same conclusion for the behaviour of c_{ij} versus T as the Leibfried and Hahn (1958) paper. However, this later treatment is more satisfactory in the agreement between the experimental and theoretical curves for the c_{ij} as a function of temperature.

An important point to note in the discussion of these lattice dynamical theories is that they are couched in terms of volume (strain) and temperature as the independent variables, whereas in the experimental regime the measured variables are pressure (stress) and temperature. It appears, therefore, from the form of the high temperature equations that the predicted linearity should occur at constant volume, rather than at constant pressure (see also Thomsen, 1972). This is supported by Stern's (1958) theory of the anharmonic properties of solids which is formulated in terms of stress and temperature. Stern demonstrated that the temperature derivative of the adiabatic compressibility was proportional to the specific heat at constant pressure which increases with temperature; this implies that the adiabatic bulk modulus should not depend linearly on temperature at constant pressure.

The theories of Garber and Granato (1975) and Mitskevich (1965) also illustrate the high temperature linearity of the elastic moduli as a function of temperature, without the restriction of Leibfried and Hahn (1958) that the temperature dependent part of the elastic moduli should

be proportional to the vibrational energy. Finite strain theories of Thomsen (1970, 1972) and Davies (1973), the so-called 4th order anharmonic theories, extend the considerations of Leibfried and Ludwig (1961) who discussed the effect of temperature and infinitesimal strain. This should obviate the difficulty that classical theories of lattice dynamics are not valid where the strains become larger.

However, all of the preceding theories are limited by their reliance on the quasi-harmonic approximation. This can be illustrated briefly as follows. The isothermal elastic moduli are defined as

$$c_{ijkl}^{T} = \frac{1}{V_o}\left(\frac{\partial^2 F}{\partial \eta_{ij}\partial \eta_{kl}}\right)_T \qquad i,j,k,l = 1,2,3 \qquad (4.2)$$

where η_{ij}, η_{kl} are measures of the strain and F, the Helmholtz free energy, is given in the quasi-harmonic approximation by

$$F = \Phi_o + F_{harmonic} + F_{anharmonic} \qquad (4.3)$$

Φ_o being the static lattice potential energy. The term $F_{anharmonic}$ is an explicit function of T only and does not contribute to the elastic moduli in (4.2). $F_{harmonic}$ is represented by the harmonic expression

$$F_{harmonic} = \sum_k \{\frac{\hbar\omega}{2} + kT \ln [1 - \exp (-\frac{\hbar\omega}{kT})]\} \qquad (4.4)$$

with the proviso that the vibrational frequencies, ω, are now explicit functions of volume (strain). The validity of this quasi-harmonic approximation may be subject to doubt at temperatures where the thermal vibrations become large (e.g. Leibfried and Ludwig, 1961).

Semi-empirical equations of state, for example Anderson's (1966) version of Wachtman's equation, avoid the difficulty of correctly describing the anharmonic effects by relating the elastic moduli to the measured values of other properties which reflect the contributions of high temperature anharmonicity (e.g., the enthalpy data). This approach has also been followed by Madan (1971) and will be discussed later in this Chapter.

Our new experimental data for the elastic moduli at high temperatures will be discussed in terms of the theories of high temperature elasticity for the rocksalt, fluorite, rutile and perovskite structures. Particular attention will be paid to the question of the relative onset of the high temperature elastic regime for the fluorides and their oxide analogues.

4.2 Intrinsic and extrinsic temperature dependence of the elastic moduli

To evaluate the various theoretical predictions of the high temperature behaviour of the elastic moduli, it is useful to express the measured temperature dependence as a combination of intrinsic and extrinsic components:

$$\left(\frac{\partial c}{\partial T}\right)_P = \left(\frac{\partial c}{\partial T}\right)_V + \left(\frac{\partial c}{\partial P}\right)_T \left(\frac{\partial P}{\partial V}\right)_T \left(\frac{\partial V}{\partial T}\right)_P$$

intrinsic extrinsic

$$= \left(\frac{\partial c}{\partial T}\right)_V - \alpha_V K_T \left(\frac{\partial c}{\partial P}\right)_T \qquad (4.5)$$

$$= \left(\frac{\partial c}{\partial T}\right)_V - \frac{\alpha_V K_S}{(1 + \alpha_V \gamma T)} \left(\frac{\partial c}{\partial P}\right)_T$$

where Volume thermal expansion $\alpha_V = \frac{1}{V}\left(\frac{\partial V}{\partial T}\right)_P$

Isothermal bulk modulus $K_T = -V\left(\frac{\partial P}{\partial V}\right)_T$

Adiabatic bulk modulus $K_S = K_T\ (1 + \alpha_V \gamma T)$

Thermal Grüneisen parameter $\gamma = \frac{\alpha_V K_S}{\rho C_P}$

Specific heat (per gram) at constant P $= C_P$

Values of C_P and γ for LiF, NaF, CaF_2, SrF_2, BaF_2 and MgF_2 are listed in Table 4.1. The extrinsic temperature dependence of the elastic moduli

TABLE 4.1: Thermodynamic Data

	C_p (cal. deg^{-1} $mole^{-1}$)	γ
LiF	9.978[1]	1.63
NaF	11.198[2]	1.51
CaF_2	16.393[1]	1.83
SrF_2	18.1[3]	1.31
BaF_2	17.020[4]	1.80
MgF_2	14.73[1]	1.21

1. Douglas (1959)
2. JANAF (1971)
3. Touloukian (1967)
4. Wicks and Block (1963)

in (4.5) arises through their dependence on volume and its dependence on temperature.

Equation (4.5) is strictly applicable only to solids with cubic symmetry. Fritz (1974) has shown that for the rutile structure the equivalent expression is

$$\left(\frac{\partial c}{\partial T}\right)_P = \left(\frac{\partial c}{\partial T}\right)_V - \frac{\alpha_V K_S}{(1 + \alpha_V \gamma T)} \left(\frac{\partial c}{\partial P}\right)_T + \beta c \qquad (4.6)$$

where β is a correction term involving the axial thermal expansion coefficients, the axial compressibilities and the uniaxial strain derivatives of the elastic moduli. The magnitude of β is discussed in section 4.5 for MgF_2.

4.3 $(\partial c/\partial T)_P$ versus T for LiF and NaF

The intrinsic and extrinsic temperature dependence of the elastic moduli for LiF and NaF is illustrated in Figures 4.2 and 4.3 which are plots versus temperature of $(\partial c/\partial T)_P$, determined from the polynomial equations (Table 3.7), and $(\partial c/\partial T)_V$ calculated from equation (4.5), for the moduli c_{11}, c'', c' c_{44} and K_S. Our experimental values for K_S and those of Srivastava and Merchant (1973) for α_V as a function of temperature were used in the calculations in equation (4.5). For simplicity, it was assumed that γ and $(\partial c/\partial P)_T$ are independent of temperature, the values for the latter being taken from Miller and Smith (1964). Figure 4.2 and Figure 4.3 also demonstrate that the crosschecks described earlier (Chapter 3) for c'' and c_{44} are valid over the entire temperature range, T = 300°-650°K.

The linear temperature dependence of $(\partial c/\partial T)_P$ for all moduli is a direct consequence of fitting the data by a second degree polynomial. For both LiF and NaF, $|(\partial c_{11}/\partial T)_P|$ and $|(\partial c'/\partial T)_P|$ decrease with T while

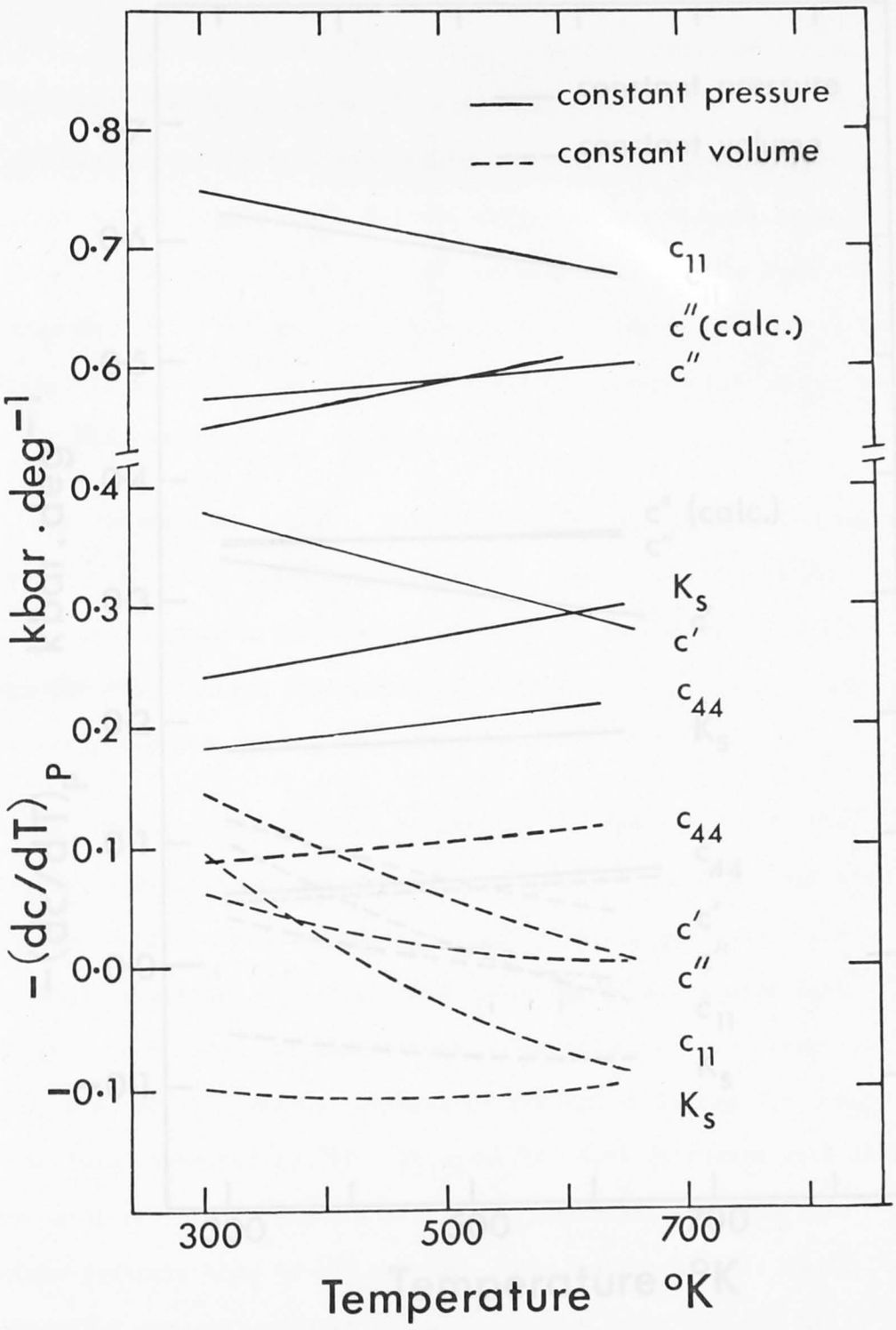

Figure 4.2: $-(\partial c/\partial T)$ versus temperature for LiF. The values of $(\partial c/\partial T)_P$, represented by the solid lines, are determined from the fitted polynomial equations. The dashed lines represent the values of $(\partial c/\partial T)_V$ calculated from equation (4.5). The crosscheck for $(\partial c_{44}/\partial T)_P$ obtained from the [001] direction cannot be distinguished from the plotted line for the [110] direction.

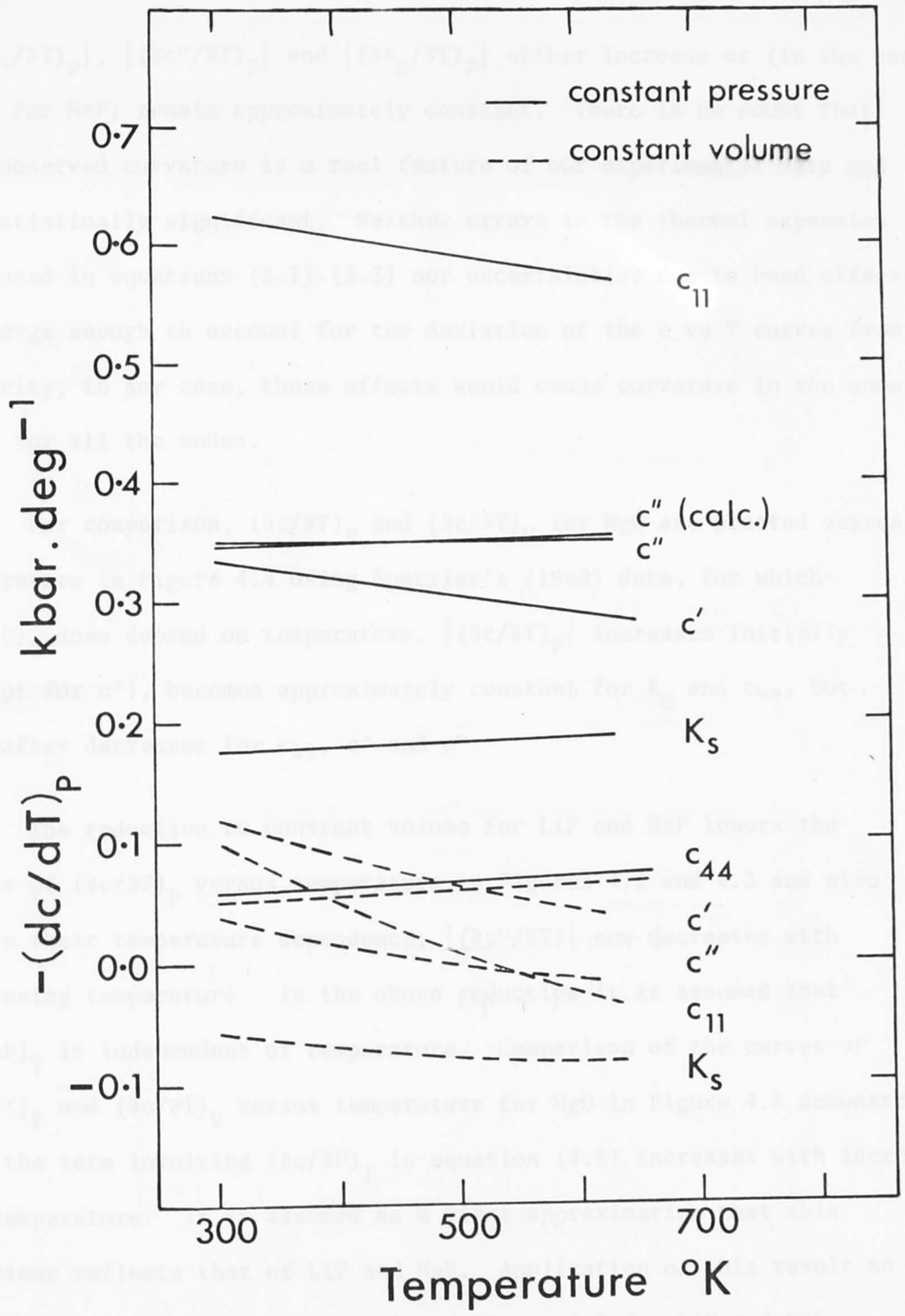

Figure 4.3: - $(\partial c/\partial T)$ versus temperature for NaF. The values of $(\partial c/\partial T)_P$, represented by the solid lines, are determined from the fitted polynomial equations. The dashed lines represent the values of $(\partial c/\partial T)_V$ calculated from equation (4.5). The crosscheck for $(\partial c_{44}/\partial T)_P$ obtained from the [110] direction cannot be distinguished from the plotted line for the [001] direction.

$|(\partial c_{44}/\partial T)_P|$, $|(\partial c''/\partial T)_P|$ and $|(\partial K_S/\partial T)_P|$ either increase or (in the case of c'' for NaF) remain approximately constant. There is no doubt that this observed curvature is a real feature of our experimental data and is statistically significant. Neither errors in the thermal expansion data used in equations (3.1)-(3.3) nor uncertainties due to bond effects are large enough to account for the deviation of the c vs T curves from linearity; in any case, these effects would cause curvature in the same sense for all the modes.

For comparison, $(\partial c/\partial T)_P$ and $(\partial c/\partial T)_V$ for MgO are plotted versus temperature in Figure 4.4 using Spetzler's (1969) data, for which $(\partial c/\partial P)_T$ does depend on temperature. $|(\partial c/\partial T)_P|$ increases initially (except for c'), becomes approximately constant for K_S and c_{44}, but thereafter decreases for c_{11}, c' and c''.

The reduction to constant volume for LiF and NaF lowers the curves of $(\partial c/\partial T)_P$ versus temperature in Figures 4.2 and 4.3 and also alters their temperature dependence; $|(\partial c''/\partial T)|$ now decreases with increasing temperature. In the above reduction it is assumed that $(\partial c/\partial P)_T$ is independent of temperature. Comparison of the curves of $(\partial c/\partial T)_P$ and $(\partial c/\partial T)_V$ versus temperature for MgO in Figure 4.4 demonstrates that the term involving $(\partial c/\partial P)_T$ in equation (4.5) increases with increasing temperature. It is assumed as a first approximation that this behaviour reflects that of LiF and NaF. Application of this result to the $(\partial c/\partial T)$-T curves in Figure 4.2 and Figure 4.3 for LiF and NaF indicates that although the temperature dependence of $(\partial c/\partial T)_V$ may be eliminated for the modulus c_{44} (resulting in a linear c-T plot at constant volume), that for the moduli c_{11}, c' and c'' will be accentuated.

Several interesting comparisons emerge from Figures 4.2-4.4. Firstly, $|(\partial c_{11}/\partial T)_V|$ and $|(\partial c'/\partial T)_V|$ for MgO decrease with temperature as they did for LiF and NaF. Secondly, the reduction to

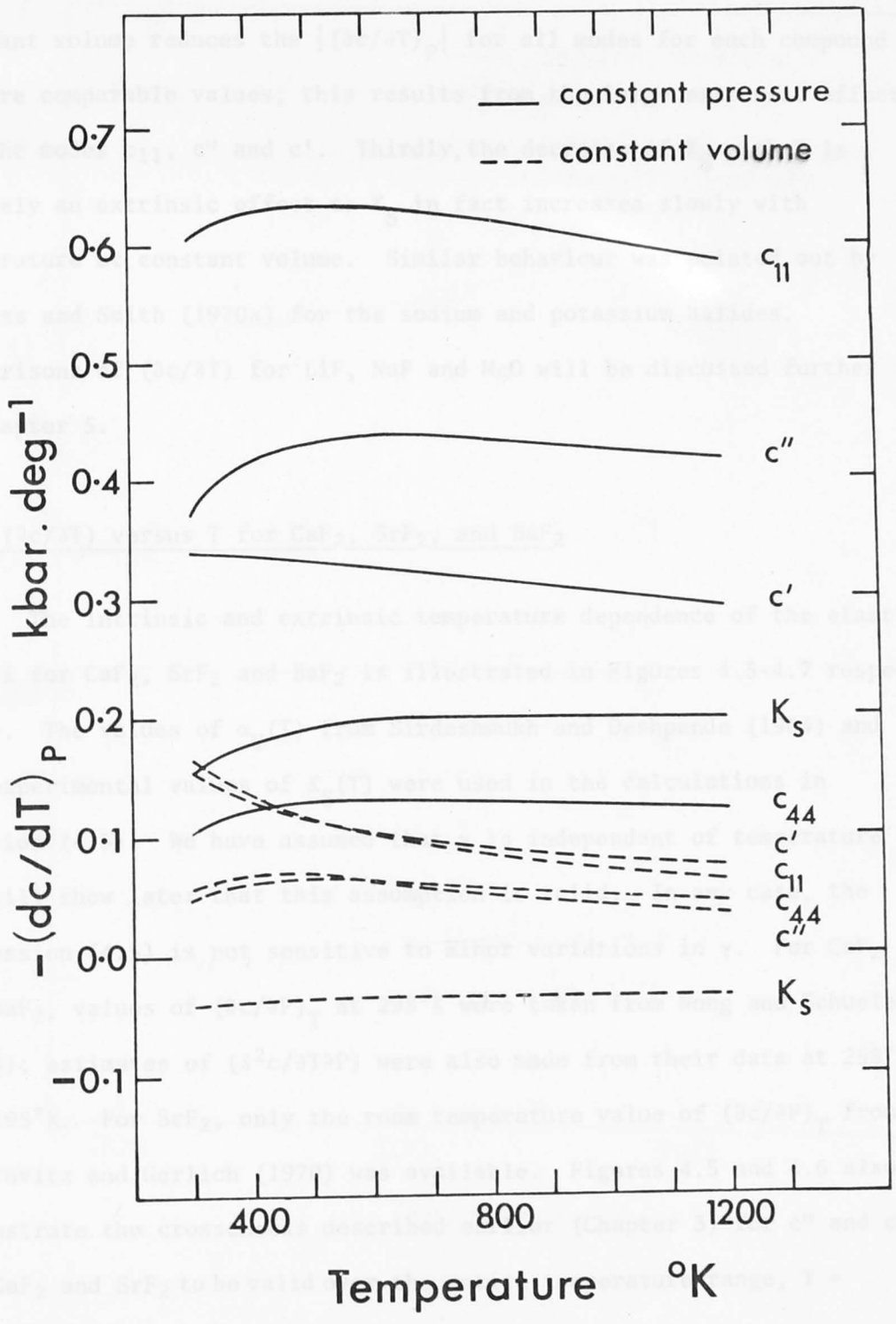

Figure 4.4: $-(\partial c/\partial T)$ versus temperature for MgO. The values of $(\partial c/\partial T)_P$, represented by the solid lines, are taken from Spetzler (1969). The dashed lines represent the values of $(\partial c/\partial T)_V$ calculated from equation (4.5) using Spetzler's (1969) data.

constant volume reduces the $|(\partial c/\partial T)_P|$ for all modes for each compound to more comparable values; this results from the large extrinsic effect for the modes c_{11}, c'' and c'. Thirdly, the decrease of K_S with T is entirely an extrinsic effect as K_S in fact increases slowly with temperature at constant volume. Similar behaviour was pointed out by Roberts and Smith (1970a) for the sodium and potassium halides. Comparisons of $(\partial c/\partial T)$ for LiF, NaF and MgO will be discussed further in Chapter 5.

4.4 $(\partial c/\partial T)$ versus T for CaF_2, SrF_2, and BaF_2

The intrinsic and extrinsic temperature dependence of the elastic moduli for CaF_2, SrF_2 and BaF_2 is illustrated in Figures 4.5-4.7 respectively. The values of $\alpha_V(T)$ from Sirdeshmukh and Deshpande (1964) and the experimental values of $K_S(T)$ were used in the calculations in equation (4.5). We have assumed that γ is independent of temperature and will show later that this assumption is valid. In any case, the expression (4.5) is not sensitive to minor variations in γ. For CaF_2 and BaF_2, values of $(\partial c/\partial P)_T$ at 298°K were taken from Wong and Schuele (1968); estimates of $(\partial^2 c/\partial T \partial P)$ were also made from their data at 298°K and 195°K. For SrF_2, only the room temperature value of $(\partial c/\partial P)_T$ from Alterovitz and Gerlich (1970) was available. Figures 4.5 and 4.6 also demonstrate the crosschecks described earlier (Chapter 3) for c'' and c_{44} for CaF_2 and SrF_2 to be valid over the entire temperature range, T = 300-650°K.

The linearity of the $(\partial c/\partial T)_P$ curves in T for all moduli is again a direct consequence of fitting the data by second degree polynomials (Table 3.10). For all of the moduli for CaF_2, SrF_2 and BaF_2, $|(\partial c/\partial T)_P|$ either increases with T or remains approximately constant. This is in contrast to the behaviour for LiF and NaF (section 4.3) where $|(\partial c/\partial T)_P|$ for some moduli actually decreases with temperature. As discussed

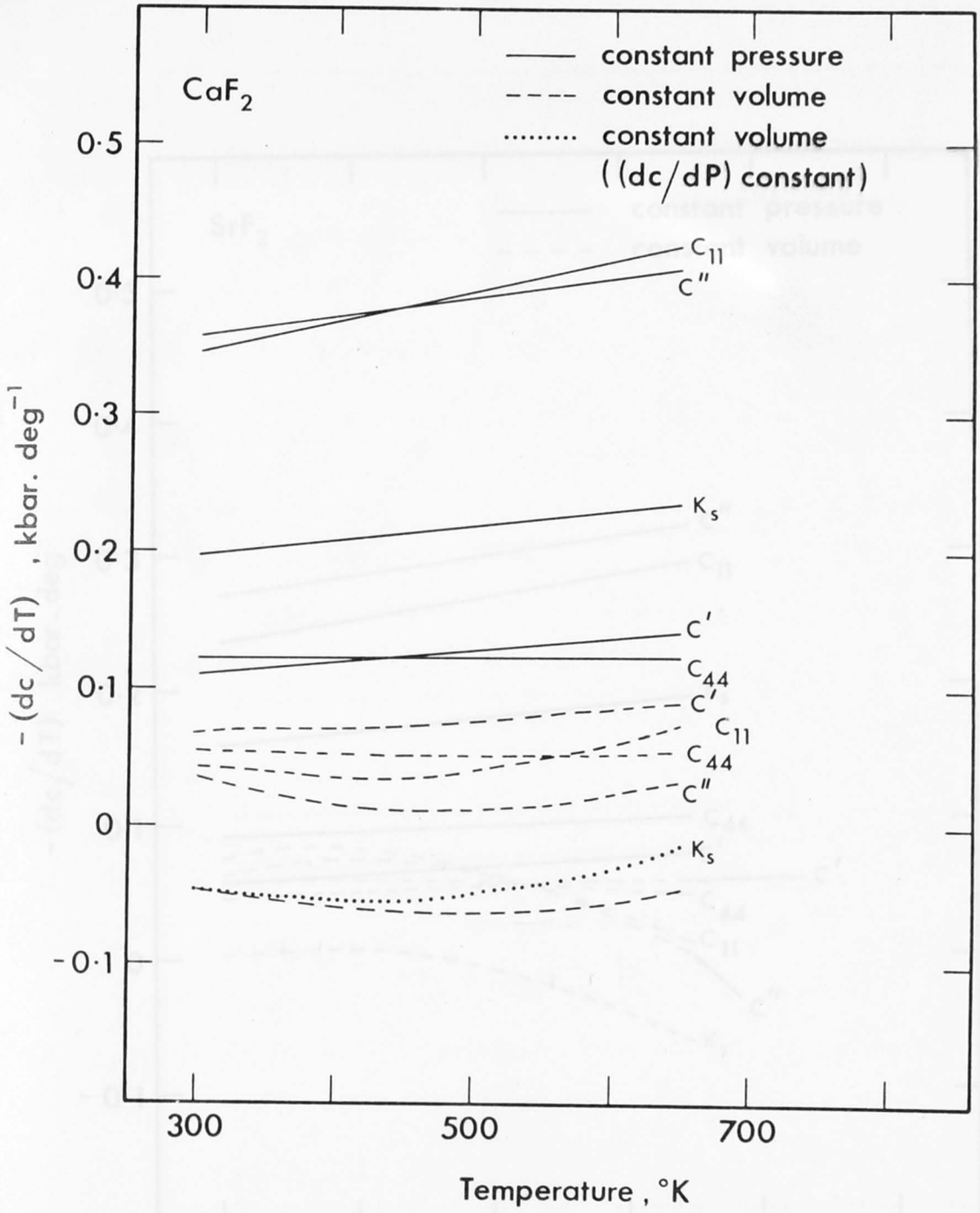

Figure 4.5: $-(\partial c/\partial T)$ versus temperature for CaF_2. The values of $(\partial c/\partial T)_P$, represented by the solid lines, are determined from the fitted polynomial equations. The dashed lines represent the values of $(\partial c/\partial T)_V$ calculated from (4.5). The dotted line for K_S illustrates the effect of a constant value for $(\partial c/\partial P)_T$. The crosschecks for $(\partial c_{44}/\partial T)_P$ (v_4) and $(\partial c''/\partial T)_P$ (calculated) cannot be distinguished from the respective plotted lines.

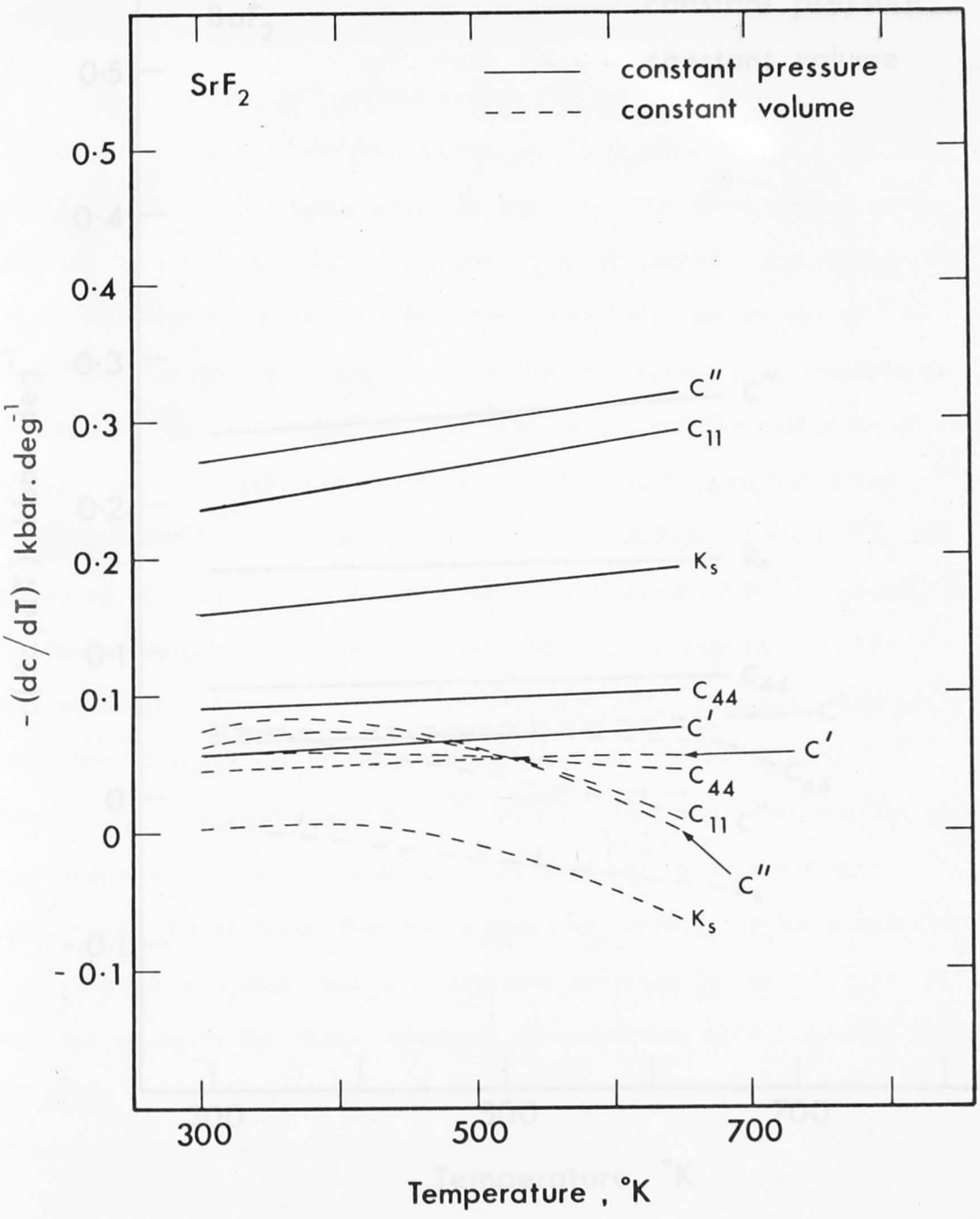

Figure 4.6: - $(\partial c/\partial T)$ versus temperature for SrF_2. The values of $(\partial c/\partial T)_P$ represented by the solid lines are determined from the fitted polynomial equations. The dashed lines represent the values of $(\partial c/\partial T)_V$ which are calculated from (4.5). The crosschecks for $(\partial c_{44}/\partial T)_P$ (v_2) and $(\partial c''/\partial T)_P$ calculated cannot be distinguished from the respective plotted lines.

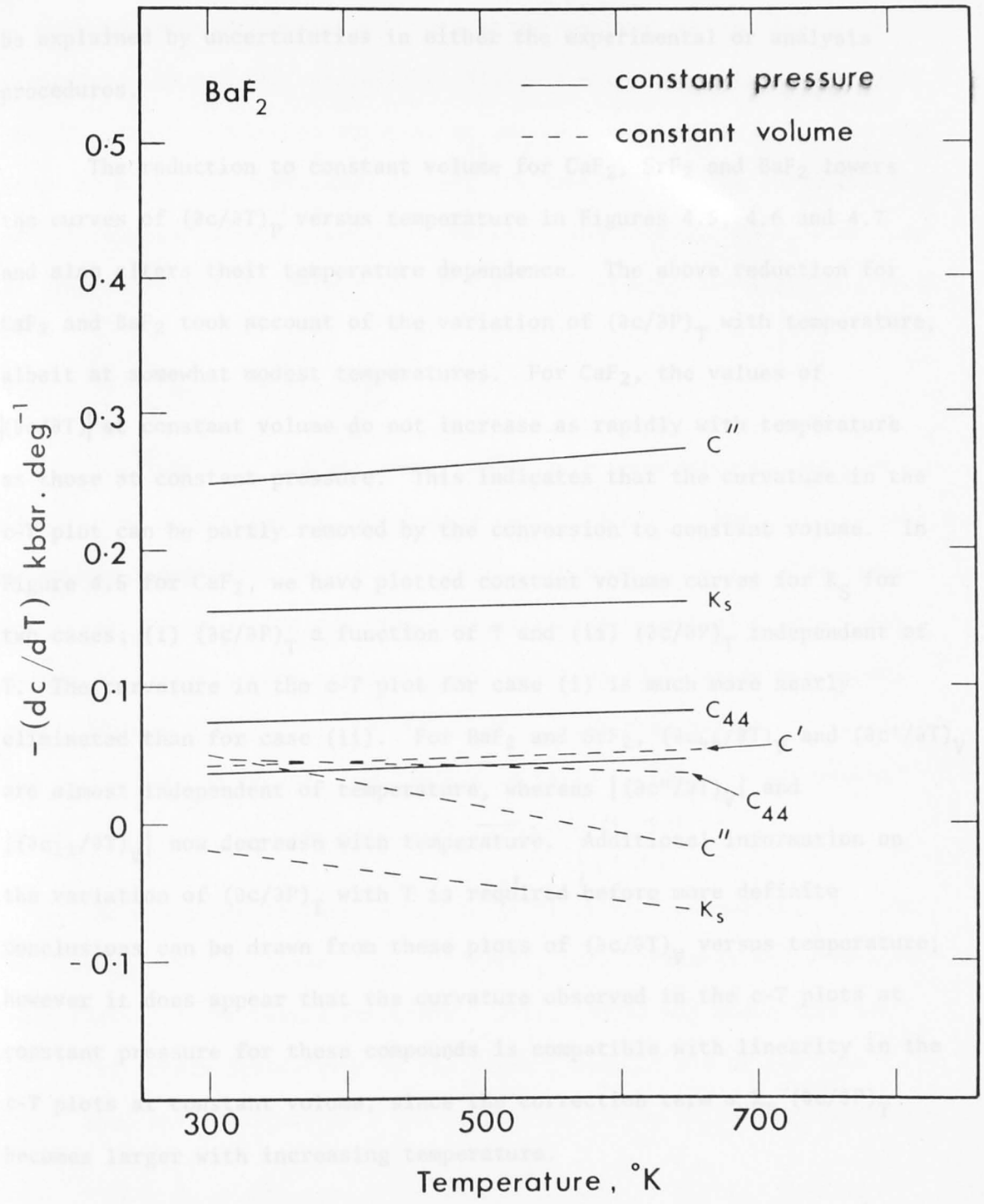

Figure 4.7: - $(\partial c/\partial T)$ versus temperature for BaF_2. The values of $(\partial c/\partial T)_p$, represented by the solid lines, are determined from the fitted polynomial equations. The dashed lines represent the values of $(\partial c/\partial T)_V$ which are calculated from (4.5).

earlier, the observed curvature is a real feature of the data and cannot be explained by uncertainties in either the experimental or analysis procedures.

The reduction to constant volume for CaF_2, SrF_2 and BaF_2 lowers the curves of $(\partial c/\partial T)_P$ versus temperature in Figures 4.5, 4.6 and 4.7 and also alters their temperature dependence. The above reduction for CaF_2 and BaF_2 took account of the variation of $(\partial c/\partial P)_T$ with temperature, albeit at somewhat modest temperatures. For CaF_2, the values of $|(\partial c/\partial T)|$ at constant volume do not increase as rapidly with temperature as those at constant pressure. This indicates that the curvature in the c-T plot can be partly removed by the conversion to constant volume. In Figure 4.5 for CaF_2, we have plotted constant volume curves for K_S for two cases; (i) $(\partial c/\partial P)_T$ a function of T and (ii) $(\partial c/\partial P)_T$ independent of T. The curvature in the c-T plot for case (i) is much more nearly eliminated than for case (ii). For BaF_2 and SrF_2, $(\partial c_{44}/\partial T)_V$ and $(\partial c'/\partial T)_V$ are almost independent of temperature, whereas $|(\partial c''/\partial T)_V|$ and $|(\partial c_{11}/\partial T)_V|$ now decrease with temperature. Additional information on the variation of $(\partial c/\partial P)_T$ with T is required before more definite conclusions can be drawn from these plots of $(\partial c/\partial T)_V$ versus temperature; however it does appear that the curvature observed in the c-T plots at constant pressure for these compounds is compatible with linearity in the c-T plots at constant volume, since the correction term $\alpha_V K_T (\partial c/\partial P)_T$ becomes larger with increasing temperature.

Several other interesting features can be seen in Figures 4.5-4.7. Firstly, the curvature in the c-T plot, as indicated by the gradient of the $(\partial c/\partial T)_P$-T plots, is largest for CaF_2 and smallest for BaF_2. This behaviour is in accord with the magnitude of the Debye temperatures (514°K for CaF_2, 380°K for SrF_2 and 282°K for BaF_2) since the predicted linear behaviour of c vs T should occur for temperatures greater than the Debye temperature. Secondly, the magnitudes of $(\partial c'/\partial T)_P$ and $(\partial c_{44}/\partial T)_P$

are very similar, indicating that the degree of anisotropy should not be very temperature sensitive. This is in contrast to the alkali fluorides, LiF and NaF, where $|(\partial c'/\partial T)|_P$ is much larger than $|(\partial c_{44}/\partial T)_P|$. Thirdly, the reduction to constant volume reduces the $|(\partial c/\partial T)_P|$ for all modes to much more comparable values; the results from the large extrinsic effect for the modes c_{11} and c". Fourthly, the decrease of K_S with T is entirely an extrinsic effect as $(\partial K_S/\partial T)_V$ is actually small and positive.

4.5 $(\partial c/\partial T)$ versus T for MgF_2

The intrinsic and extrinsic temperature dependence for MgF_2 is illustrated in Figure 4.8, which is a plot of $(\partial c/\partial T)_P$ and $(\partial c/\partial T)_V$ versus T for the independent single crystal elastic moduli and K_S. The values of $(\partial c/\partial T)_P$ were determined from the polynomial equations (Table 3.14); values of $(\partial c/\partial T)_V$ were calculated via equation (4.5) using our experimental values of K_S vs T, the values of α_V vs T from Bailey et al. (1975) and the values of $(\partial c/\partial P)_T$ at 298°K from Davies (1976). γ was assumed to be independent of temperature.

As mentioned earlier, equation (4.6) is the appropriate equation for the approximate separation of $(\partial c/\partial T)_P$ into intrinsic and extrinsic components for the rutile structure. Fritz (1974) has shown that if the axial strain derivatives of the elastic modulus are of the same sign, then the magnitude of β can be bounded in the following inequality,

$$0 \leq \left|\frac{c\beta}{\alpha_V K_S (\partial c/\partial P)_T}\right| \leq \left|2\frac{(\alpha_a \chi_c - \alpha_c \chi_a) K_S}{\alpha_V}\right| \qquad (4.7)$$

where α_a, α_c are the coefficients of axial thermal expansion, and $\chi_a = -(\partial \ln \ell^a/\partial P)_T$, $\chi_c = -(\partial \ln \ell^c/\partial P)_T$, are the axial compressibilities. From the stress-strain relationship involving the single crystal elastic constants (e.g. Musgrave, 1970, chapter 4.4), it can be shown that

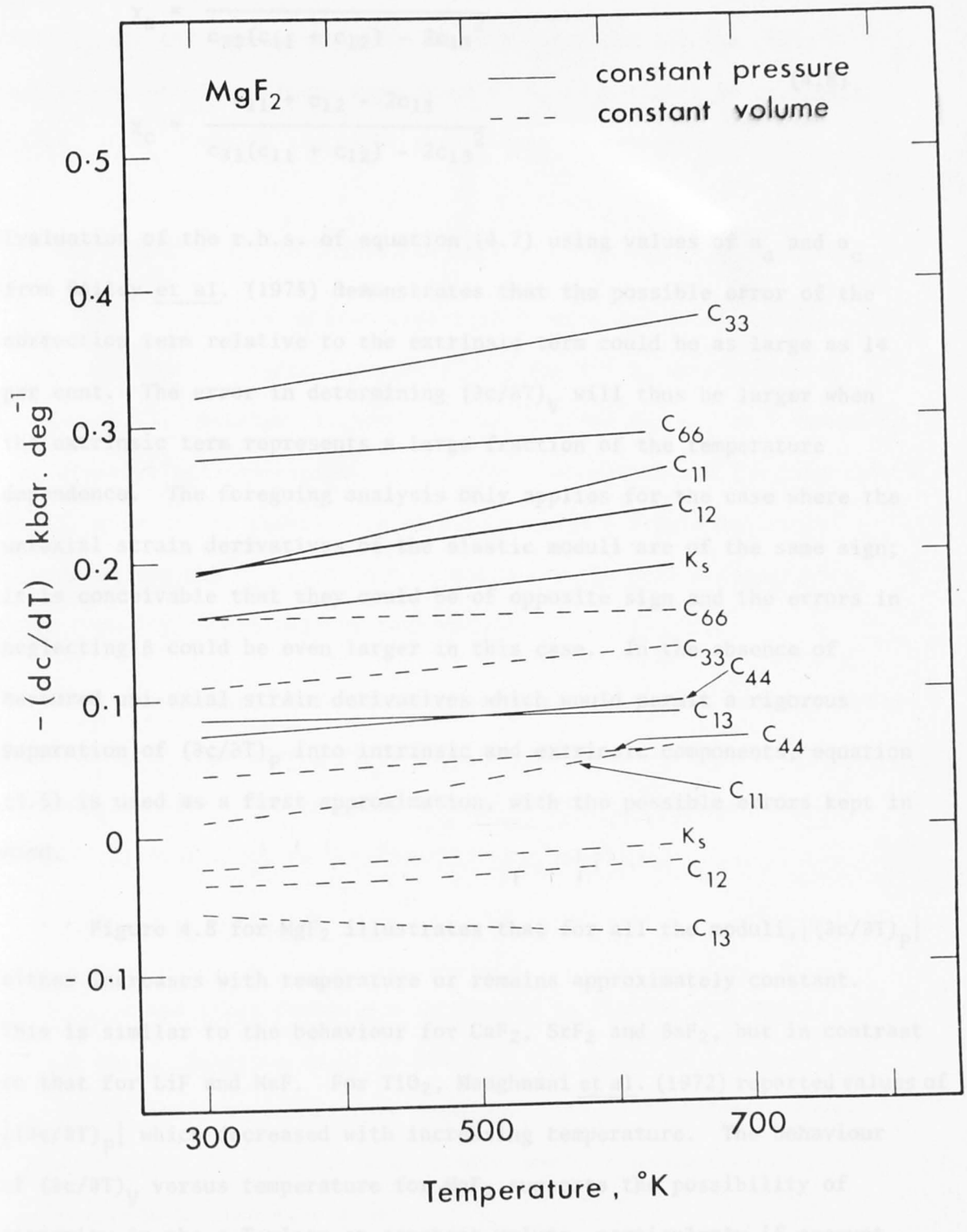

Figure 4.8: $-(\partial c/\partial T)$ versus temperature for MgF_2. The values of $(\partial c/\partial T)_P$, represented by the solid lines, are determined from the fitted polynomial equations. The dashed lines represent the values of $(\partial c/\partial T)_V$ which are calculated from (4.5).

$$\chi_a = \frac{c_{33} - c_{13}}{c_{33}(c_{11} + c_{12}) - 2c_{13}^2}$$

$$\chi_c = \frac{c_{11} + c_{12} - 2c_{13}}{c_{33}(c_{11} + c_{12}) - 2c_{13}^2} \qquad (4.8)$$

Evaluation of the r.h.s. of equation (4.7) using values of α_a and α_c from Bailey et al. (1975) demonstrates that the possible error of the correction term relative to the extrinsic term could be as large as 14 per cent. The error in determining $(\partial c/\partial T)_V$ will thus be larger when the extrinsic term represents a large fraction of the temperature dependence. The foregoing analysis only applies for the case where the uniaxial strain derivatives of the elastic moduli are of the same sign; it is conceivable that they could be of opposite sign and the errors in neglecting β could be even larger in this case. In the absence of measured uni-axial strain derivatives which would permit a rigorous separation of $(\partial c/\partial T)_P$ into intrinsic and extrinsic components, equation (4.5) is used as a first approximation, with the possible errors kept in mind.

Figure 4.8 for MgF_2 illustrates that for all the moduli, $|(\partial c/\partial T)_P|$ either increases with temperature or remains approximately constant. This is similar to the behaviour for CaF_2, SrF_2 and BaF_2, but in contrast to that for LiF and NaF. For TiO_2, Manghnani et al. (1972) reported values of $|(\partial c/\partial T)_P|$ which decreased with increasing temperature. The behaviour of $(\partial c/\partial T)_V$ versus temperature for MgF_2 supports the possibility of linearity in the c-T plots at constant volume, particularly if account could be taken of the temperature dependence of $(\partial c/\partial P)_T$. As discussed earlier in sections 4.3 and 4.4, an increase in the correction term with temperature would tend to reduce the slope of the $(\partial c/\partial T)$-T curves.

The remarks made previously for the rocksalt and fluorite fluorides regarding the similarity in magnitude of the $(\partial c/\partial T)_V$ vs T curves do not

apply for MgF_2. There seems to be no simple trend relating $(\partial c/\partial T)_P$ and $(\partial c/\partial T)_V$ for the various moduli. However, as noted for the other structures, the temperature dependence of K_S is entirely an extrinsic effect, as K_S actually increases very slowly at constant volume.

4.6 High temperature equations of state

The predictions of many classical lattice dynamical theories that c_{ij} should exhibit linear dependence on T for $T > \theta_D$ were discussed earlier (4.1). However, although the expressions for c_{ij} vs T reduce to simple analytical expressions in the high temperature and low temperature limits, none of the theories is able to furnish a simple analytical expression for the c_{ij} vs T that is valid for the entire temperature range from 0°K to the melting temperature.

In the absence of an exact theoretical equation of state, recourse may be made to equations derived on a semi-empirical or approximate theoretical basis. For example, Varshni (1970) has claimed some theoretical justification for the following equation

$$c = c_o + s/(e^{t/T} - 1) \qquad (4.9)$$

where c_o, s and t are parameters determined by fitting the equation to the c-T data. Equation (4.9) is based on the result of Leibfried and Hahn (1958) that the temperature dependent part of the elastic moduli is proportional to the internal vibrational energy $\bar{\varepsilon}$ (equation 4.1), as obtained from the Einstein model,

$$\bar{\varepsilon} = \tfrac{1}{2}\hbar\omega + \frac{\hbar\omega}{e^{\hbar\omega/kT} - 1} \qquad (4.10)$$

where h is Planck's constant, $\hbar = \frac{h}{2\pi}$ and k is Boltzmann's constant. Varshni demonstrated good agreement of (4.9) with the experimental data for metals and ionic compounds (some alkali halides and BaF_2). Attempts to fit equation (4.9) to the present c-T data for LiF and NaF indicated

that it was incompatible with the data for the modes c_{11} and c'. Analysis of the functional form of equation (4.9) revealed that it cannot accommodate data for which $(\partial c/\partial T)$ is negative and increasing, i.e., data for which the c-T plot is concave upward. Equation (4.9) is functionally compatible with the c-T data of CaF_2, SrF_2, BaF_2 and MgF_2; however it was decided not to fit the data by this equation since the parameters are not well constrained by the c-T values in the high temperature region and are extremely sensitive to small differences in slope. This occurs in the absence of constraining data on the parameters at lower temperatures ($T << \theta_D$) where a significant fraction of the curvature occurs (see Figure 4.1 for the general shape of c-T curves).

Another semi-empirical equation of state has been proposed by Wachtman et al. (1961)

$$E = E_0 - bT \exp(-T_0/T) \tag{4.11}$$

where E is Young's modulus and b and T_0 are the parameters to be determined from the data. Anderson (1966) has placed this equation on a firmer theoretical basis for K_S and has demonstrated that K_S is linear in T for $T > \theta_D/2$ (which he defines as the regime of high temperature elastic behaviour). Anderson's final form of the Wachtman equation (Soga, Schreiber and Anderson, 1966) is expressed in terms of the enthalpy data H^T and is given by

$$K_S^T - K_S^{298} = -\frac{\gamma\delta}{V^{298}}(H^T - H^{298})\left(1 - \frac{\alpha_V T}{2}\right) \tag{4.12}$$

where V^{298} is the volume at 298°K and δ is another dimensionless Grüneisen parameter defined by

$$\delta = -\left(\frac{\partial \ln K_S}{\partial T}\right)_P \Big/ \left(\frac{\partial \ln V}{\partial T}\right)_P = -\frac{1}{\alpha_V K_S}\left(\frac{\partial K_S}{\partial T}\right)_P \tag{4.13}$$

On theoretical grounds (Anderson, 1966; Madan, 1971), δ should lie approximately between 3 and 4 for alkali halides; this is verified in Figure 4.9 for some of our fluoride compounds. These theoretical

derivations depend on assumptions on the nature of the interatomic potential; nevertheless their advantage is that equation (4.12) can be used to extrapolate K_S to high temperatures in the absence of a value for $(\partial K_S/\partial T)$.

The derivation of (4.12) assumes that γ and δ are independent of temperature, an assumption which has been demonstrated to be valid for MgO, Mg_2SiO_4 and $MgSiO_3$ (Anderson, 1966; Soga and Anderson, 1967). In Figure 4.9, we have illustrated the temperature dependence of γ and δ for several fluorides of the present study, and demonstrated that γ and δ are indeed approximately constant over the range T = 300-650°K. The product $\gamma\delta$ varies even less over this temperature range, perhaps since the product is independent of both K_S and α_V. This observation is particularly interesting since it is sufficient in deriving (4.12) that $\gamma\delta$ be independent of temperature.

Figures 4.10 and 4.11 compare the experimental values of K_S for LiF and NaF with those calculated from 0°K to the melting point from the enthalpy data via equation (4.12). The calculated curves are matched in value and slope to our data curves at 298°K, since K_S^{298} and $(\partial K_S/\partial T)_P$ are input parameters to (4.12). Figures 4.10 and 4.11 demonstrate the excellent agreement between our data and the calculated curve for T > 300°K. This provides additional support for the reliability of our high temperature data, particularly since our values of K_S and $(\partial K_S/\partial T)_P$ at 298°K were earlier demonstrated to be in excellent agreement with the most reliable results of other investigators (Chapter 3). For LiF, the calculated curve between 0°K and 300°K follows the general trend of the offset Briscoe and Squire (1957) data (Figure 4.10). The agreement between the low temperature curves is better illustrated by adjusting Briscoe and Squire's data to agree with ours at 298°K. For NaF, the calculated low temperature curve agrees remarkably well with the low temperature data of Lewis et al. (1967) and Vallin et al. (1966). This

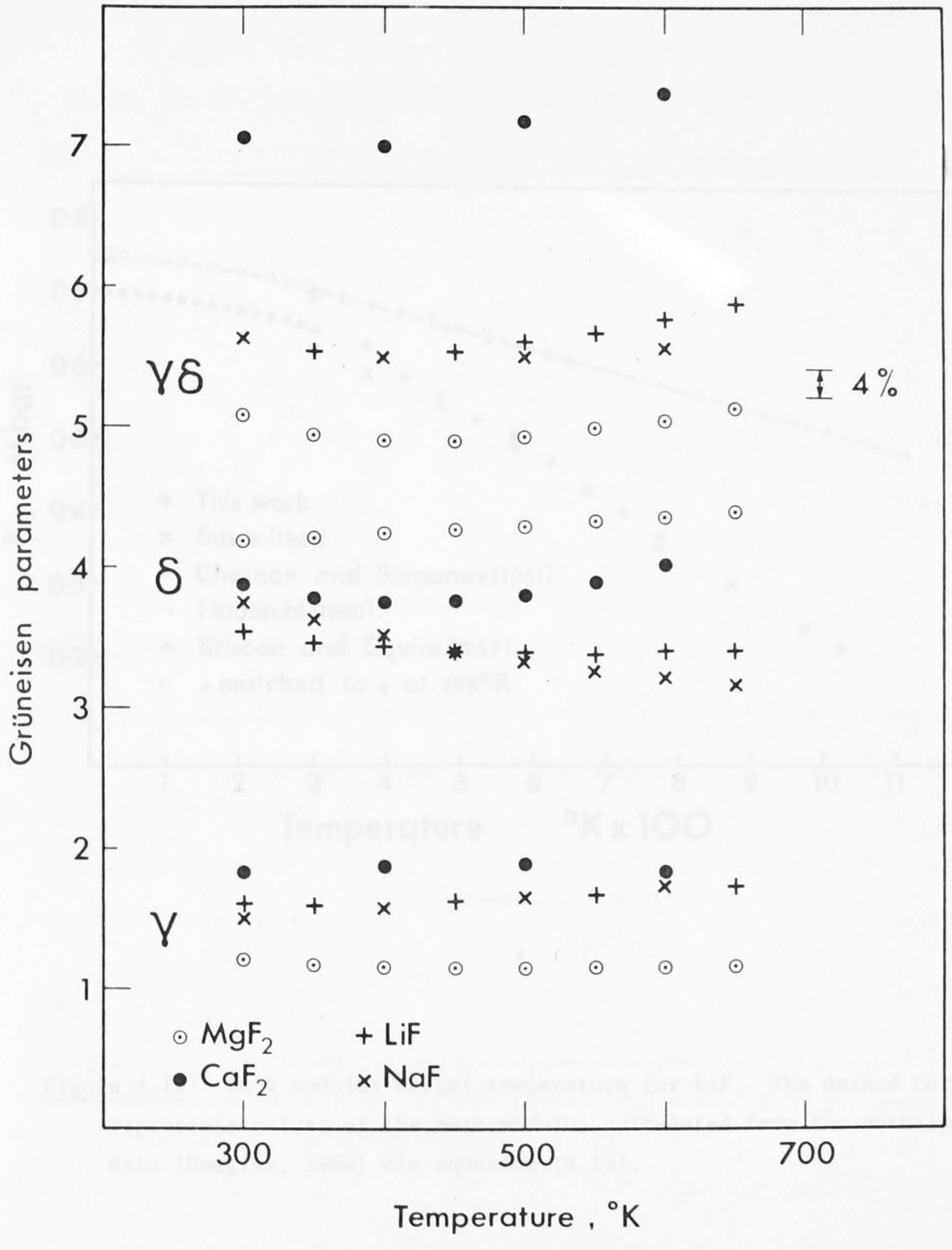

Figure 4.9: The Grüneisen paramaters, γ, δ and their product, $\gamma\delta$, versus temperature for LiF, NaF, CaF_2 and MgF_2. γ and δ were calculated using our experimental values of K_S and $(\partial K_S/\partial T)_P$ as a function of temperature, together with values of $C_P(T)$ from Douglas (1959) for LiF and MgF_2, and from JANAF (1971) for NaF and CaF_2. $\rho(T)$ was calculated from the data in Tables 3.3-3.5; values of the thermal expansion, $\alpha_V(T)$, were taken from the appropriate references in Tables 3.3-3.5.

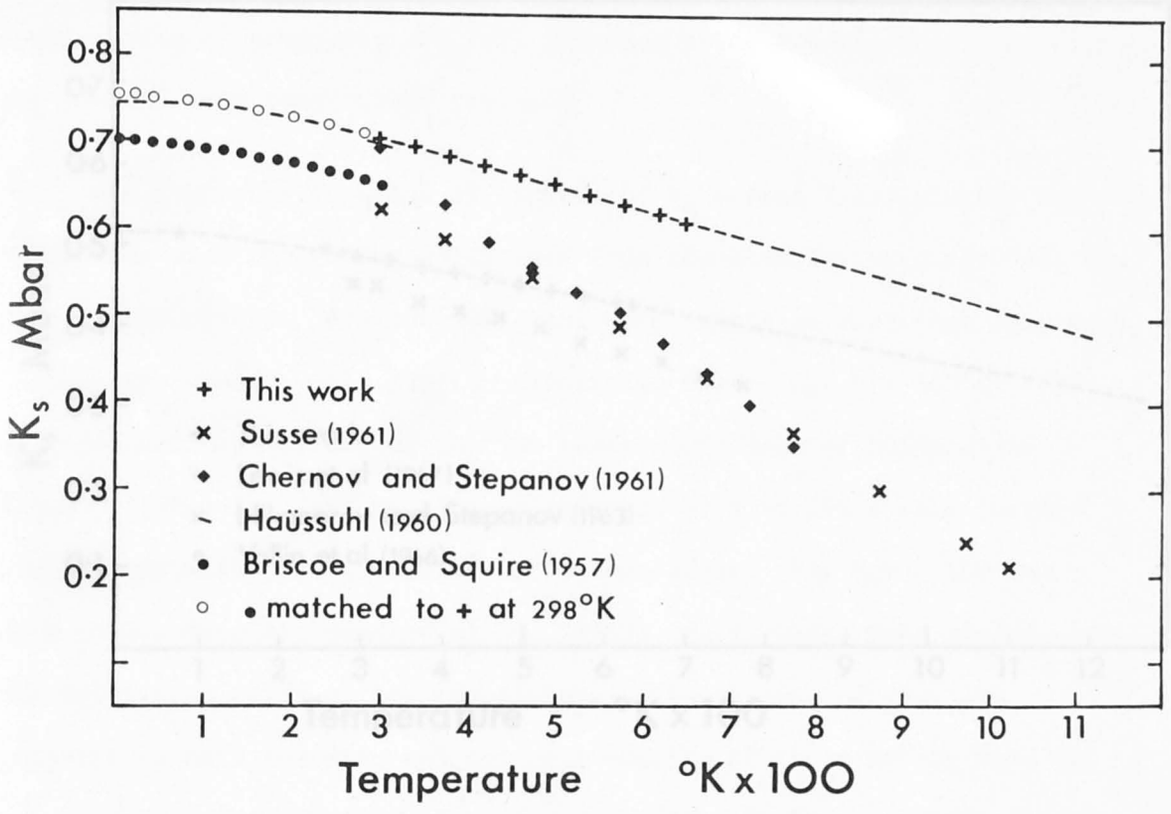

Figure 4.10: Bulk modulus versus temperature for LiF. The dashed curve represents values of the bulk modulus calculated from the enthalpy data (Douglas, 1959) via equation (4.12).

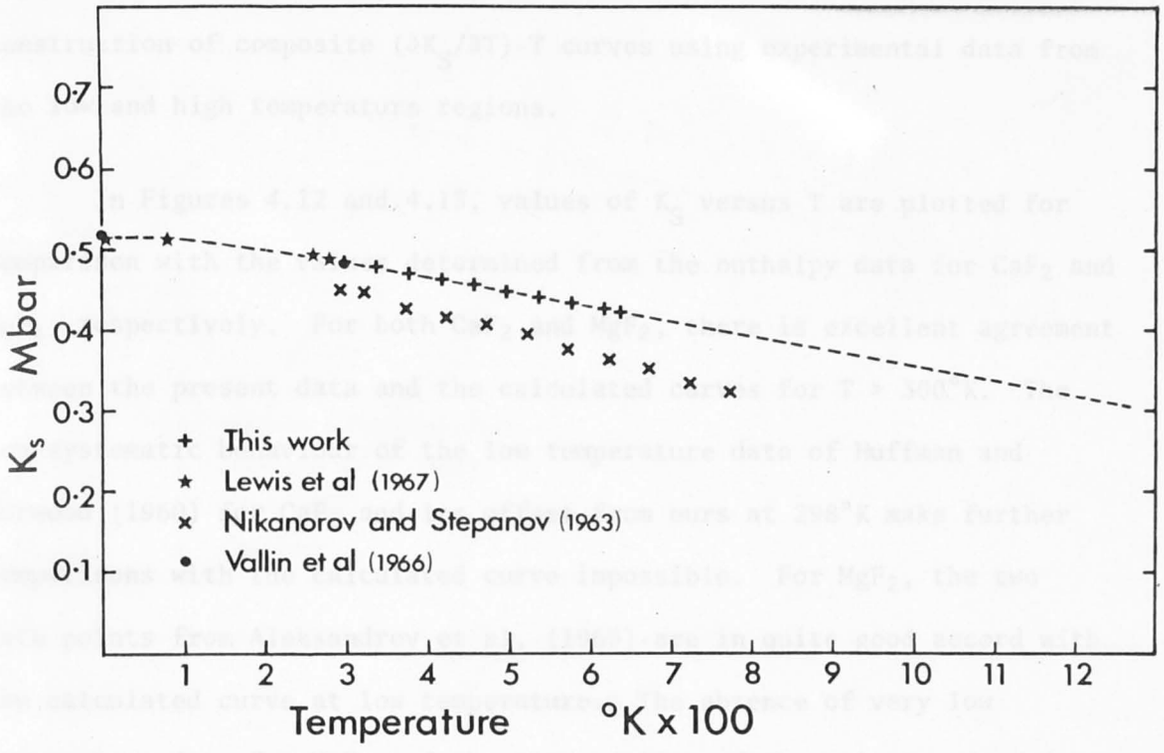

Figure 4.11: Bulk modulus versus temperature for NaF. The dashed curve represents values of the bulk modulus calculated from the enthalpy data (JANAF, 1971) via equation (4.12).

further supports our earlier claim (Chapter 3) that our high temperature data for LiF and NaF are in accord with the low temperature data of other experimenters using ultrasonic pulse techniques and lends credence to the construction of composite $(\partial K_S/\partial T)$-T curves using experimental data from the low and high temperature regions.

In Figures 4.12 and 4.13, values of K_S versus T are plotted for comparison with the values determined from the enthalpy data for CaF_2 and MgF_2, respectively. For both CaF_2 and MgF_2, there is excellent agreement between the present data and the calculated curves for T > 300°K. The non-systematic behaviour of the low temperature data of Huffman and Norwood (1960) for CaF_2 and its offset from ours at 298°K make further comparisons with the calculated curve impossible. For MgF_2, the two data points from Aleksandrov et al. (1969) are in quite good accord with the calculated curve at low temperature. The absence of very low temperature data for MgF_2 and the poor quality of the existing data for CaF_2 preclude construction of a composite $(\partial K_S/\partial T)$-T curve using experimental data.

Plots of $(\partial K_S/\partial T)_P$ versus temperature provide a much more sensitive way of examining the temperature behaviour of the bulk modulus since the high temperature linearity of the K_S-T plot is reflected by $(\partial K_S/\partial T)_P$ attaining a constant value (e.g., Anderson and Andreatch, 1966). In Figure 4.14, the measured $(\partial K_S/\partial T)_P$ is plotted versus temperature for LiF, NaF, and MgO in order to determine the onset of high temperature elastic behaviour. For comparison, $(\partial K_S/\partial T)_P$ calculated from the enthalpy data for LiF and NaF are also given in Figure 4.14 and the acoustic Debye temperatures, θ_D, are indicated (see Chapter 5.6 for θ_D).

The combined measured and calculated data in Figure 4.14 for LiF and NaF exhibit a very rapid increase of $|(\partial K_S/\partial T)_P|$ with temperature at low temperatures followed by a levelling out to constant values at high

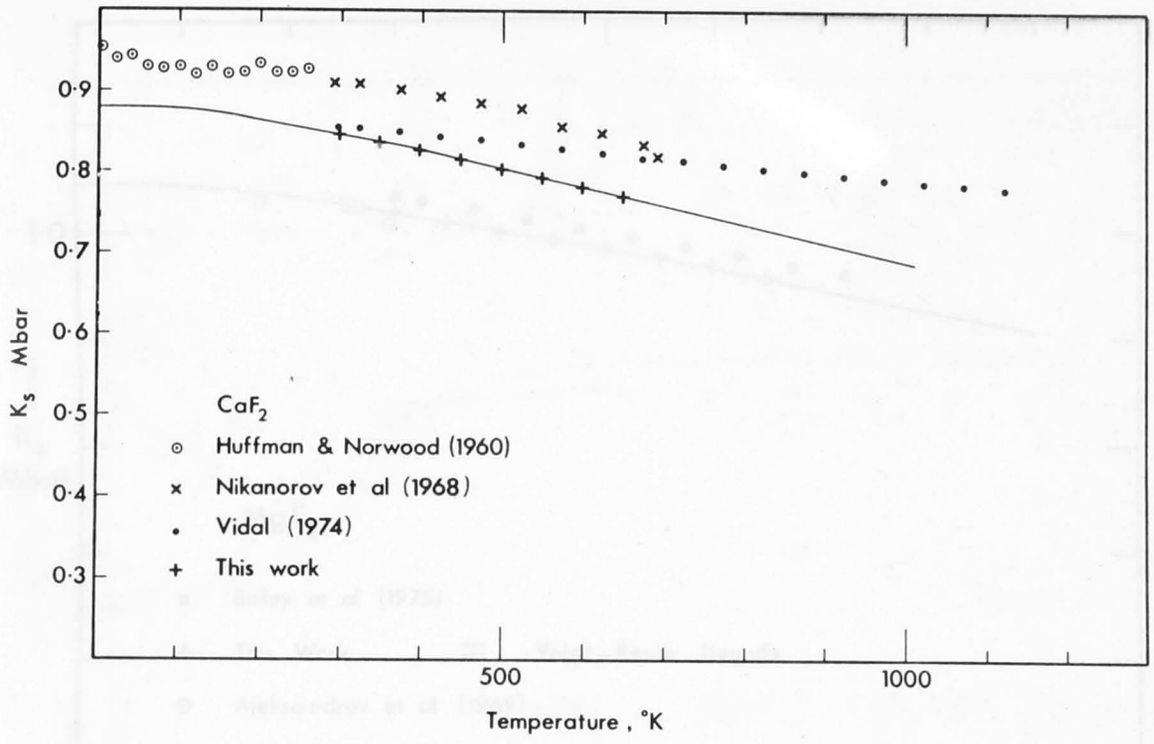

Figure 4.12: Bulk modulus versus temperature for CaF_2. The dashed curve represents values of the bulk modulus calculated from the enthalpy data (JANAF, 1971) via equation (4.12).

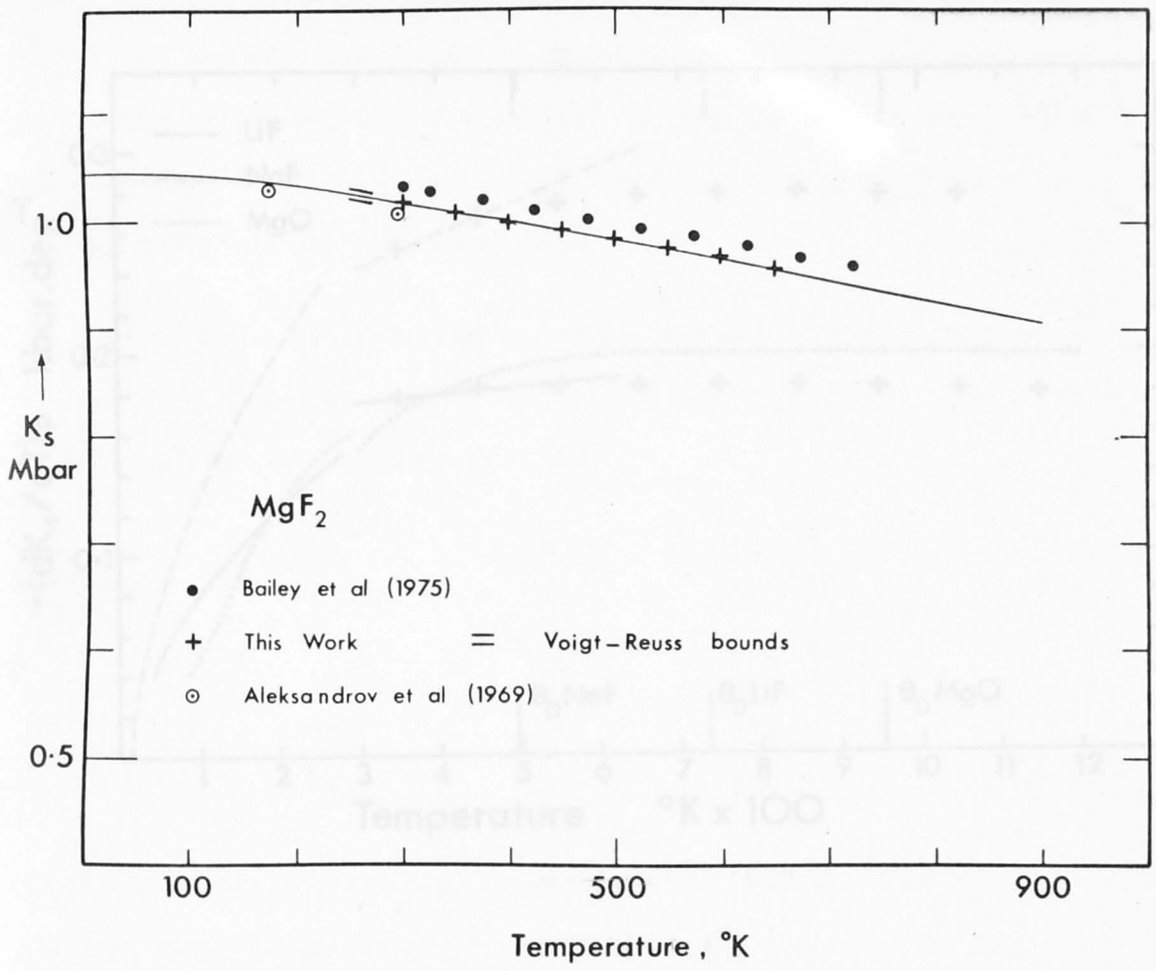

Figure 4.13: Bulk modulus versus temperature for MgF_2. The dashed curve represents values of the bulk modulus calculated from the enthalpy data (Douglas, 1959) via equation (4.12).

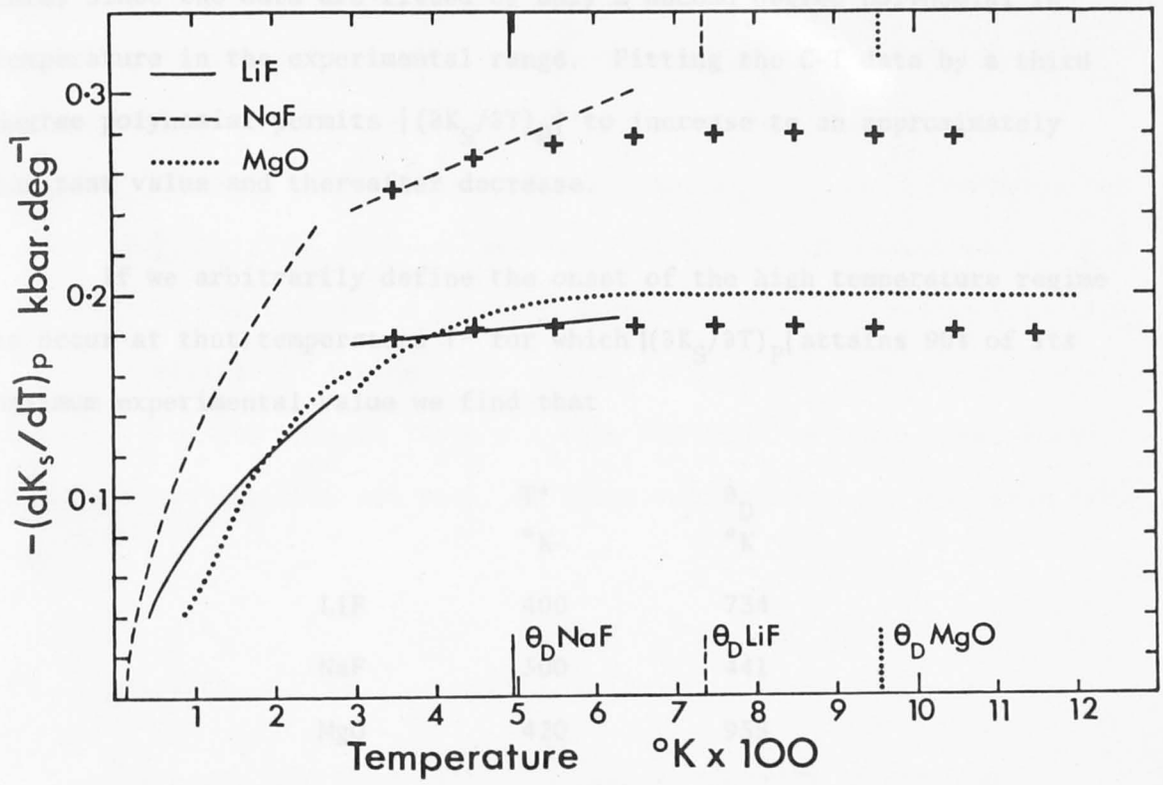

Figure 4.14: $-(\partial K_S/\partial T)_P$ versus temperature for LiF, NaF and MgO. Values of $(\partial K_S/\partial T)_P$ for LiF and NaF for T > 300°K were determined from the polynomial fit to our data. For T < 300°K, $(\partial K_S/\partial T)_P$ for LiF and NaF are determined stepwise from the data of Briscoe and Squire (1957) and Lewis et al. (1967) respectively, the temperature intervals being selected to eliminate large scatter. For MgO the $(\partial K_S/\partial T)_P$ values for T < 300°K are listed by Anderson and Andreatch (1966) and $(\partial K_S/\partial T)_P$ for T = 300°K to 1200°K are taken from Spetzler (1969). The values of $(\partial K_S/\partial T)_P$ calculated from the enthalpy data (Douglas, 1959 for LiF and JANAF, 1971 for NaF) via equation (4.12) are indicated by +. The Debye temperatures, θ_D, are indicated on the temperature axis for LiF, NaF and MgO.

temperature, similar to the behaviour of MgO (Figure 4.4). Our experimental curves for T = 298-650°K demonstrate that $|(\partial K_S/\partial T)_P|$ increases from its value for T < 300°K but does not attain a constant value at high temperatures since the data are fitted by only a second degree polynomial in temperature in the experimental range. Fitting the C-T data by a third degree polynomial permits $|(\partial K_S/\partial T)_P|$ to increase to an approximately constant value and thereafter decrease.

If we arbitrarily define the onset of the high temperature regime to occur at that temperature T* for which $|(\partial K_S/\partial T)_P|$ attains 90% of its maximum experimental value we find that

	T* °K	θ_D °K
LiF	400	734
NaF	300	441
MgO	420	955

Comparison of the experimental curves with the calculated data points indicates that the values of T* are likely to be too large for LiF and NaF. Nevertheless, these values of T* are in fair agreement with the theoretical prediction that the high temperature regime commences for $T > \theta_D/2$, although we might have anticipated a greater contrast in T* for LiF and MgO.

Similar comparisons based on high temperature elastic data are not able to be made for the fluorite structure fluorides and oxides. High temperature data exist only for polycrystalline ThO_2 specimens of varying degrees of porosity (Spinner et al., 1963) and are not presented in a suitable form for analysis or comparison. The low temperature data curves for CaF_2, SrF_2 and BaF_2 are not sufficiently continuous with our data curves at 298°K (see Figure 3.8) to permit the construction of composite $(\partial K_S/\partial T)_P$-T curves.

Comparisons of the relative onset of high temperature elasticity can also be made for the rutiles, MgF_2 and TiO_2. The single crystal elastic data of Manghnani et al. (1972) for TiO_2 permit the calculation of K_S and $(\partial K_S/\partial T)_P$ in the range, 298°-573°K, via the Voigt-Reuss-Hill averaging procedure (Hill, 1952). In Table 4.2, $(\partial K_S/\partial T)_P$ is listed at various temperatures above 298°K for MgF_2 and TiO_2. The values of $(\partial K_S/\partial T)_P$ for TiO_2 vary little over the temperature range. For MgF_2, the values of $|(\partial K_S/\partial T)_P|$ increase gradually with T; as discussed earlier for LiF and NaF, the fitting of a second degree polynomial prevents detection of any levelling off in the value of $(\partial K_S/\partial T)_P$ with T. We can conclude at least from the data in Table 4.2 that the onset of high temperature elastic behaviour does not occur at lower temperatures for MgF_2 than for TiO_2.

4.7 Conclusion

The prediction from lattice dynamical theories of the high temperature linearity of the c-T plot is more valid in constant volume rather than constant pressure space. The experimental results for CaF_2, SrF_2, BaF_2 and MgF_2 support this interpretation; at constant pressure, the c-T curves exhibit concave downward curvature, which can be largely eliminated by the correction to constant volume. However, since the curvature is in the opposite sense for the c_{11} and c' modes for LiF and NaF, correction to constant volume merely increases the deviation from linearity and accentuates the variance with the theory. A similar concave upward curvature in the c-T plot appears in the results of Slagle and McKinstry (1967) for NaCl, KCl and KBr and Manghnani et al. (1972) for TiO_2. Slagle and McKinstry fitted their data with polynomials in T, with the justification that the elastic moduli can be expanded as power series in the vibrational energy (equal to kT at high temperatures). The quadratic and higher order terms in this expansion were neglected by

TABLE 4.2: Comparison of $(\partial K_S/\partial T)_P$ versus temperature for MgF_2 and TiO_2

	T (°K)	$(\partial K_S/\partial T)_P$ (kbar deg^{-1})
MgF_2 [1]	298	-0.160
	348	-0.165
	398	-0.170
	448	-0.174
	498	-0.179
	548	-0.184
	598	-0.189
	648	-0.194
TiO_2 [2]	300.5	-0.571
	313	-0.517
	333	-0.495
	358	-0.525
	423	-0.501
	523	-0.458

1. This work
2. Manghnani et al. (1972)

Leibfried and Hahn (1958).

Detailed studies of the behaviour of the elastic moduli as a function of temperature have important implications for lattice dynamical theories. In particular, in the high temperature regime, the validity of the quasi-harmonic approximation requires further evaluation in the light of our new experimental data. For geophysical discussions of the earth's interior, the high temperature value of $(\partial K_S/\partial T)_P$ is an important parameter. The deviations from the predicted linear behaviour will result in some uncertainty in $(\partial K_S/\partial T)_P$; however since $|(\partial K_S/\partial T)_P|$ is a small quantity numerically, and since the extrapolations in equations of state are carried out over a pressure range which is very much larger than the temperature range, the resultant uncertainties will be of secondary importance.

Our rationale in measuring the temperature dependence for fluorides was the expectation that the fluorides would exhibit high temperature elastic behaviour at lower absolute temperatures than their oxide analogues; this would enable evaluation of high temperature derivatives in the accessible experimental temperature range. However, the comparisons for the model pairs LiF-MgO and MgF_2-TiO_2 indicate that the onset of high temperature elastic behaviour does not occur at significantly lower temperatures for the fluorides.

The precision of our data for the temperature dependence of the elastic moduli for LiF, NaF, CaF_2, SrF_2, BaF_2 and MgF_2 enables predictions of equations of state at high temperature to be tested. These data are also important in providing information on the elastic moduli and their temperature derivatives for crystal structures of interest in the earth's mantle. In Chapter 5, we will examine the possibility of employing our data for the fluorides to predict the elastic properties of their oxide analogues.

CHAPTER 5

SYSTEMATIC RELATIONSHIPS GOVERNING THE ELASTIC MODULI AND THEIR TEMPERATURE AND PRESSURE DERIVATIVES

CHAPTER 5

SYSTEMATIC RELATIONSHIPS GOVERNING THE ELASTIC MODULI AND THEIR TEMPERATURE AND PRESSURE DERIVATIVES

5.1 Introduction

Systematic relationships between the elastic properties and crystallographic parameters of minerals have been useful in geophysics in estimating the elasticity of unmeasured phases, in relating seismic velocities to density in order to draw compositional inferences about the earth's mantle, and in elucidating the nature of the interatomic forces in the crystalline lattice.

One of the first examples of such a relationship was the demonstration by Birch (1960, 1961a, 1961b) that the compressional velocity, v_p, is a function only of density, ρ, and mean atomic weight, $\bar{M}$. For many minerals and rocks, the following linear relationship holds:

$$v_p = a(\bar{M}) + b\rho \qquad (5.1)$$

where a is a function only of $\bar{M}$ and b is a constant. In view of the large number of possible variables, e.g., composition, structure, bonding type, etc., it is a rather surprising result that the velocity can be described in terms of only two parameters. Birch also conjectured that for a chemically homogeneous material, the velocity should depend only on density, irrespective of whether density variations were due to changes in temperature, pressure or crystallographic phase. The recent availability of data on the temperature and pressure dependence of the elastic moduli, and on the elasticity of the low- and high-pressure polymorphs of various phase transformations has enabled evaluation of Birch's hypothesis (D. L. Anderson et al., 1971; Liebermann and Ringwood, 1973; Liebermann, 1974b, 1975). Birch's initial formulation of the linear law (5.1) has been developed further by many workers; including

its recent formulation as a power law in which the parameters are derived from crystallographic and thermodynamic considerations (e.g., D. L. Anderson, 1967; Shankland, 1972; O. L. Anderson, 1973; Shankland and Chung, 1974).

Much recent interest has also centred on systematics cast in terms of elastic moduli and volume, V, rather than velocity and density. Several studies have demonstrated that the relationship KV = constant holds for isostructural series of halides, oxides, sulphides, selenides and tellurides (O. L. Anderson and Nafe, 1965; O. L. Anderson and Soga, 1967; D. L. Anderson and O. L. Anderson, 1970; and O. L. Anderson, 1972). In addition to the isostructural trends, O. L. Anderson and Soga (1967) have demonstrated that for compounds with the same mean atomic weight, $\overline{M}$, the relationship KV^4 = constant is appropriate and that this is merely a restatement of Birch's law.

Isostructural relationships for the shear modulus, μ, as a function of volume have been discussed by Davies (1975) who demonstrated that the relationship $\mu V^{4/3}$ = constant holds for many simple compounds. Davies also examined possible systematics in the pressure derivatives $(\partial K/\partial P)_T$ and $(\partial \mu/\partial P)_T$. Such systematics are also of interest in providing constraints for the interpretation of shock wave data for high pressure phases of rocks and minerals (e.g., D. L. Anderson and Kanamori, 1968; Davies and Gaffney, 1973).

The relationship between the bulk moduli of fluorides and their oxide analogues is examined in the existing framework of bulk modulus-volume systematics. Relationships are also investigated for the temperature and pressure derivatives of the elastic moduli as a function of volume, structure and composition. The earlier observation (Chapter 4) that the Debye temperatures of oxides and fluorides do not differ so markedly as the melting temperatures is explained in terms of systematics

in the Debye temperatures.

5.2 Bulk modulus-volume systematics

The empirical relationship KV = constant is consistent with a simple Born-Mie interatomic potential with a power law repulsion leading to $KV^{4/3}$ = constant, which is indistinguishable from the empirical result. O. L. Anderson (1972) has demonstrated that for a general repulsive potential v(r), the following equation is true,

$$K_0 = \frac{2}{9V_0}\frac{A}{r_0}\left[1 + \frac{v''(r_0)r_0}{2v'(r_0)}\right] \qquad (5.2)$$

where $A = A_m Z_c Z_a e^2$, A_m is the Madelung constant and Z_c, Z_a are the valence charges of the cation and anion respectively. The zero subscripts refer to values for the lattice in equilibrium. For a suitable definition of the Madelung constant, A_m is essentially independent of structure and the variation in A is contained in the valence product $Z_c Z_a$. Taking the logarithm of equation (5.2) gives

$$\ln K_0 = \ln Z_c Z_a - x \ln V_0 + \text{constant} \qquad (5.3)$$

where x empirically is close to one. If the term in brackets in equation (5.2) were independent of r_0, then x would equal 4/3 (the result for the Born-Mie potential). Equation (5.3) leads directly to the result (dropping the zero subscripts for convenience)

$$\frac{KV^*}{Z_c Z_a e^2} = \text{constant} \qquad (5.4)$$

Following Anderson and Nafe (1965), the data of Table 5.1 are presented in Figure 5.1 as a log-log plot of bulk modulus versus molar volume per ion pair ($V^* = 2\bar{M}/\rho = 2\bar{V}$, where $\bar{M}$ and $\bar{V}$ are the mean atomic weight and volume, respectively) for oxides and fluorides crystallising in the rocksalt, fluorite and rutile structures. For clarity the data for the perovskite oxides and fluorides are plotted in Figure 5.2.

Table 5.1: Summary of elastic and thermal properties of fluorides and oxides

Structure	Compound	CN	Ionic Radii[1,2] Å		Z_cZ_a	Molar Volume	M	ρ	Elastic Moduli Mbar		ψ[a]	T_m	θ_D	A[b]
			Cation(s)	Anion		cm^3		gm/cm^3	K_s	μ_s		°K	°K	
Rocksalt	LiF	6-6	0.74	1.33	1	9.83	25.94	2.639[3]	0.704[40]	0.491[40]	0.270	1120[31]	734[34]	57
	NaF		1.02	"	"	14.98	41.99	2.804[3]	0.483[40]	0.314[40]	0.283	1269[32]	491[35]	56
	KF		1.38	"	"	23.00	58.10	2.526[4]	0.323[4]	0.164[4]	0.289	1130[31]	327[4]	50
	RbF		1.49	"	"	27.18	104.47	3.8434[5]	0.280[5]	0.127[5]	0.297	1048[33]	221[5]	48
	MgO		0.72	1.40	4	11.25	40.31	3.583[6]	1.628[6]	1.311[6]	0.178	3125[32]	955[36]	96
	CaO		1.00	"	"	16.76	56.08	3.346[7]	1.14[7]	0.814[7]	0.186	2887[32]	670*	91
	SrO		1.13	"	"	20.69	103.62	5.009[7]	0.88[7]	0.591[7]	0.177	2693[32]	457[37]	90
	BaO		1.36	"	"	25.59	153.34	5.992[8]	0.61[8]	0.355[8]	0.152	2291[32]	291*	75
Fluorite	CaF_2	8-4	1.12	1.31	2	24.55	78.08	3.181[9]	0.845[40]	0.427[40]	0.270	1691[32]	514[38]	67
	SrF_2		1.25	"	"	29.37	125.62	4.277[10]	0.713[40]	0.350[40]	0.273	1673[31]	380[10]	66
	PbF_2		1.29	"	"	31.47	245.19	7.79[11]	0.611[11]	0.230[11]	0.250	1097[31]	221[11]	55
	BaF_2		1.42	"	"	35.89	175.34	4.886[9]	0.581[40]	0.255[40]	0.272	1593[31]	282[39]	62
	UO_2		1.00	1.38	8	24.62	270.03	10.97[12]	2.13[12]	0.874[12]	0.170	3151[32]	394*	95
	ThO_2		1.04	"	"	26.38[13]	264.04	10.01	1.93[14]	0.972[14]	0.165	3493[32]	424*	103
Rutile	MgF_2	6-3	0.72	1.30	2	19.61	62.31	3.178[15]	1.019[40]	0.547[40]	0.260	1536[32]	626[44]	67
	NiF_2		0.69	"	"	20.08	96.71	4.815[42]	1.197[43]	0.452[43]	0.312		459*	62
	CoF_2		0.735	"	"	21.11	96.93	4.592[16]	0.835[16]	0.392[16]	0.229	1475[31]	428*	59
	MnF_2		0.82	"	"	23.67	92.93	3.926[15]	0.883[15]	0.30[15]	0.271	1129[31]	393*	55
	SiO_2		0.40	1.36	8	14.01	60.08	4.287[17]	2.49[41]	2.04[41]	0.114		1144*	108
	GeO_2		0.54	"	"	16.64	104.59	6.286[18]	2.589[18]	1.509[18]	0.140	†1116[47]	774*	102
	TiO_2		0.605	"	"	18.80	79.90	4.25[13]	2.155[19]	1.1244[19]	0.132	2103[32]	782*	94
	SnO_2		0.690	"	"	21.56	150.69	6.990[20]	2.123[20]	1.018[20]	0.149	1903[32]	555*	96
Perovskite	$KMgF_3$	12-6-6	1.60 0.72	1.33	1.5	38.23	120.41	3.15[21]	0.756[40]	0.489[40]	0.301	1070[47]	570[49]	69
	$KNiF_3$		1.60 0.69	"	"	38.84[45]	154.81	3.985	0.851[46]	0.456[46]	0.344	1130[47]	479*	67
	$KZnF_3$		1.60 0.75	"	"	40.13[45]	161.47	4.023	0.800[46]	0.392[46]	0.334	875[47]	438*	63
	$KCoF_3$		1.60 0.745	"	"	40.58[45]	155.03	3.82	0.787[46]	0.369[46]	0.333		435*	61
	$RbCoF_3$		1.73 0.745	"	"	42.34[45]	201.40	4.756	0.801[46]	0.397[46]	0.353		397*	65
	$KMnF_3$		1.60 0.82	"	"	44.16	151.04	3.42[22]	0.649[23]	0.325[23]	0.298	1032[48]	418*	60
	$RbMnF_3$		1.73 0.82	"	"	45.73	197.40	4.317[24]	0.675[24]	0.341[24]	0.321	986[48]	386[23]	64
	$CdTiO_3$		1.31 0.605	1.40	6	32.90[25]	208.30	6.331	2.12[26]	0.98[26]	0.182		590*	90
	$CdSnO_3$		1.31 0.69	"	"	36.65[27]	279.09	7.615	1.89[28]	0.87[28]	0.180		489*	90
	$SrTiO_3$		1.40 0.605	"	"	35.87	183.52	5.116[29]	1.744[30]	1.17[30]	0.162	1910[48]	691*	102

a. $\psi = KV^*/Z_cZ_ae^2$ where $V^* = 2\overline{M}/\rho = 2\overline{V}$

b. $A = a\theta_D\overline{M}^{\frac{1}{2}}$ where $a = V^{*1/3}$ = mean lattice parameter

* θ_D calculated from room temperature values of the elastic constants.

† T_m for the quartz polymorph of GeO_2

Table 5.1 (Continued)

1. Shannon and Prewitt (1969).
2. Shannon and Prewitt (1970).
3. Miller and Smith (1964).
4. Marshall and Miller (1967).
5. Cleavelin *et al.* (1972).
6. Spetzler (1969).
7. Son and Bartels (1972).
8. Vetter and Bartels (1973).
9. Wong and Schuele (1968).
10. Gerlich (1964b).
11. Wasilik and Wheat (1965).
12. Wachtman *et al.* (1964).
13. Robie *et al.* (1966).
14. Macedo, Capps and Wachtman (1964).
15. Haussühl (1968).
16. Hart and Stevenson (1970).
17. Mizutani *et al.* (1972).
18. Wang and Simmons (1973).
19. Manghnani, Fisher and Brower (1972).
20. Chang and Graham (1975).
21. Reshchikova (1969).
22. Beckman and Knox (1961).
23. Aleksandrov, Reshchikova and Beznosikov (1966).
24. Melcher and Bolef (1969).
25. Roth (1967).
26. Liebermann (1976).
27. Smith (1960).
28. Liebermann (1974a).
29. Swanson, Fuyat and Ugrinic (1954).
30. Bell and Rupprecht (1963).
31. Wicks and Block (1963).
32. Robie and Waldbaum (1968).
33. Weast (1972).
34. Briscoe and Squire (1957).
35. Lewis, Lehoczky and Briscoe (1967).
36. θ_D calculated from elastic moduli of Anderson and Andreatch (1966).
37. Johnston, Thrasher and Kearney (1970).
38. Huffman and Norwood (1960).
39. Gerlich (1964a).
40. This work.
41. Liebermann *et al.* (1976).
42. Calculated from lattice parameters in Wyckoff (1963).
43. Wu (1974).
44. θ_D calculated from elastic moduli of Aleksandrov *et al.* (1969) at 173°K.
45. Molar volume calculated from the lattice parameter given in Rousseau *et al.* (1974).
46. Rousseau *et al.* (1974).
47. Levin *et al.* (1964).
48. Levin *et al.* (1969).
49. θ_D calculated from elastic moduli of Reshchikova (1969) at 120°K.

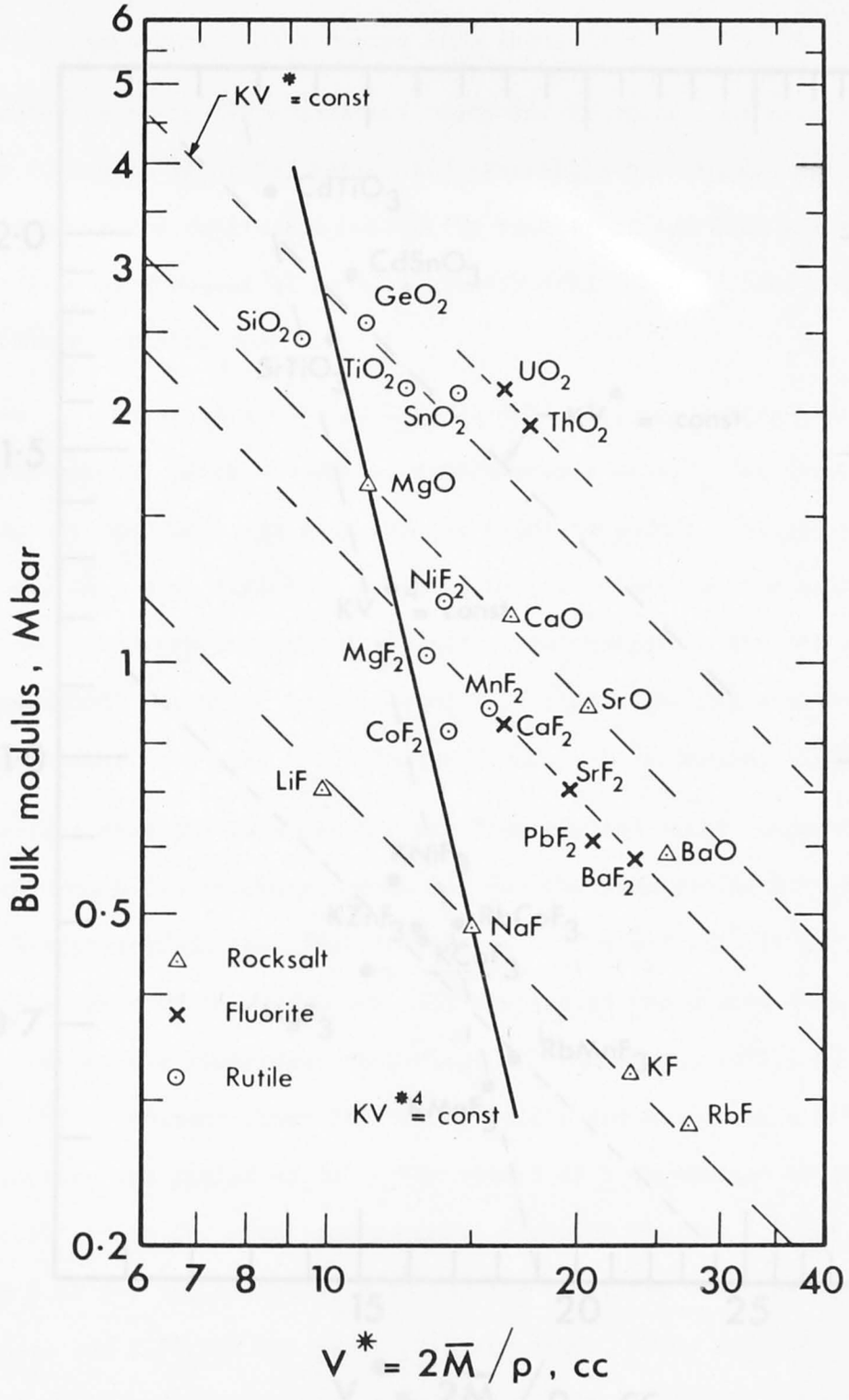

Figure 5.1: Log-log plot of bulk modulus (K) versus molar volume per ion pair ($2\overline{M}/\rho$) for oxides and fluorides in the rocksalt, fluorite and rutile structures. The KV* = constant lines for oxides and fluorides in the three structures are indicated by dashed lines of gradient -1. The solid line of gradient -4 represents the constant mean atomic weight relationship KV^{*4} = constant for $\overline{M}$ = 20-21.

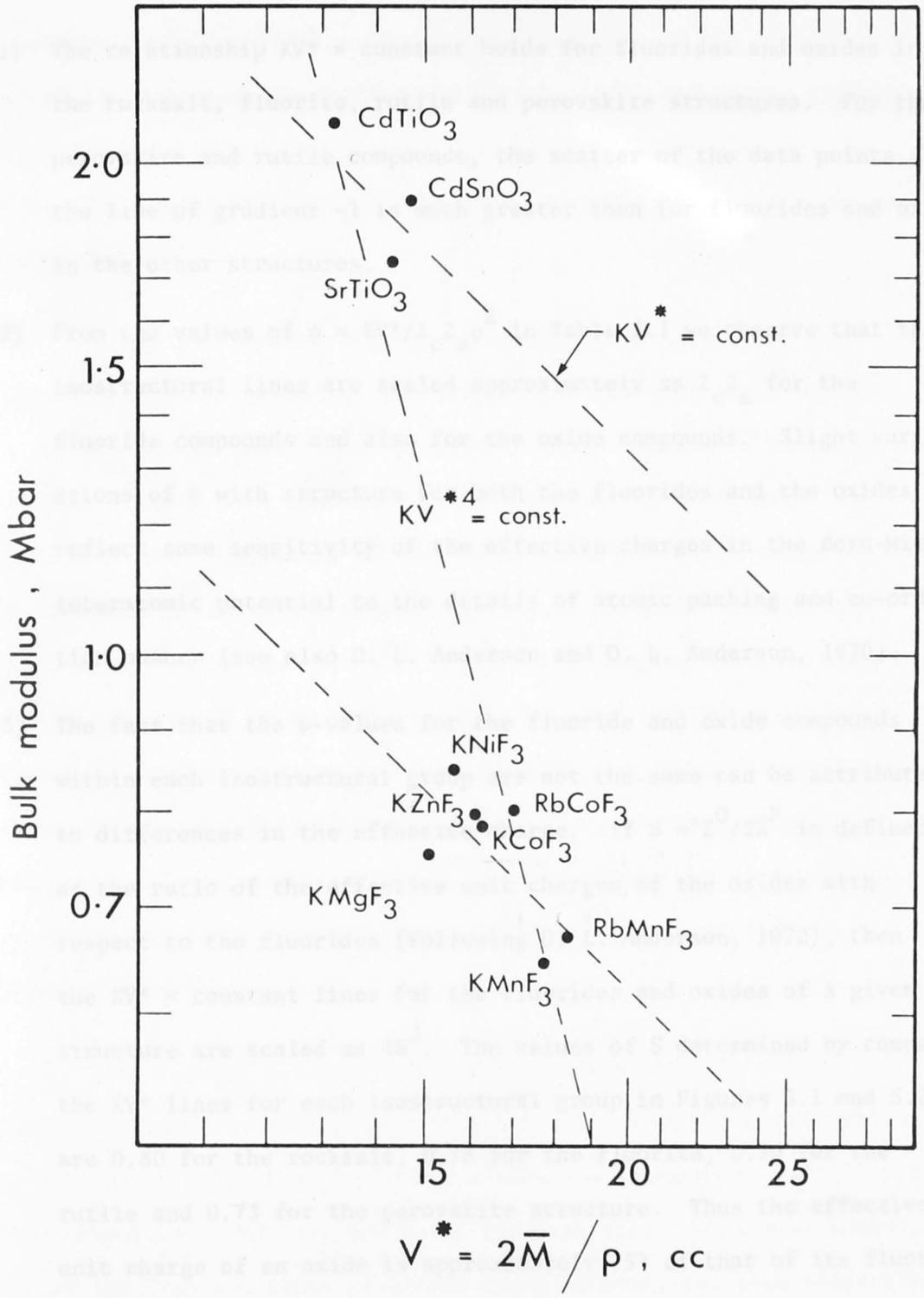

Figure 5.2: Log-log plot of bulk modulus (K) versus molar volume per ion pair ($2\bar{M}/\rho$) for oxides and fluorides in the perovskite structure. The dashed lines represent the KV^* = constant and KV^{*4} = constant relationships, and are labelled accordingly.

Three important trends emerge from these data:

(1) The relationship KV* = constant holds for fluorides and oxides in the rocksalt, fluorite, rutile and perovskite structures. For the perovskite and rutile compounds, the scatter of the data points about the line of gradient -1 is much greater than for fluorides and oxides in the other structures.

(2) From the values of $\psi = KV^*/Z_c Z_a e^2$ in Table 5.1 we observe that the isostructural lines are scaled approximately as $Z_c Z_a$ for the fluoride compounds and also for the oxide compounds. Slight variations of ψ with structure for both the fluorides and the oxides reflect some sensitivity of the effective charges in the Born-Mie interatomic potential to the details of atomic packing and co-ordination number (see also D. L. Anderson and O. L. Anderson, 1970).

(3) The fact that the ψ-values for the fluoride and oxide compounds within each isostructural group are not the same can be attributed to differences in the effective charge. If $S = Z^O/2Z^F$ is defined as the ratio of the effective unit charges of the oxides with respect to the fluorides (following O. L. Anderson, 1972), then the KV* = constant lines for the fluorides and oxides of a given structure are scaled as $4S^2$. The values of S determined by comparing the KV* lines for each isostructural group in Figures 5.1 and 5.2 are 0.80 for the rocksalt, 0.78 for the fluorite, 0.70 for the rutile and 0.73 for the perovskite structure. Thus the effective unit charge of an oxide is approximately 75% of that of its fluoride analogue for all the structures considered.

It is interesting to compare our values of S with those derived from the more rigorous lattice dynamical calculations. Using a shell model, Axe (1965) and Axe and Pettit (1966) derived values of S = 0.73 for the fluorite structure (CaF_2 and ThO_2). Katiyar and Krishnan (1969)

employed a rigid ion model and concluded that S = 0.77 for the rutile structure (MgF_2 and TiO_2). Recent determinations of the effective charges for rutile fluorides (Striefler and Barsch, 1973) and rutile oxides (Striefler and Barsch, 1975) from a least squares fit over all the available elastic and optical data lead to values of S in the range 0.57-0.74.

Since the relative effective charges do not appear to depend on structure for the rocksalt, fluorite, rutile and perovskite structures, it should thus be possible to predict the bulk modulus of an oxide from the bulk modulus of a fluoride of the same crystal structure. In particular the bulk moduli of the corresponding fluoride-oxide pairs in the Goldschmidt modelling scheme (for which the molar volumes are comparable) are related by $(K^O/K^F) = 4S^2$. A similar idea was suggested by Haussühl (1968) in considering MgF_2-TiO_2 and LiF-MgO as analogue pairs. A word of caution is warranted here though; even though the scaling factor $4S^2$ is virtually the same for all the structures considered, the prediction of bulk moduli is bound to be uncertain for those structures which exhibit large scatter about the lines of gradient (-1) in the log-log K-V* plot.

From Figures 5.1 and 5.2 we can conclude that the rutile and perovskite isostructural groups do not fit the KV* = constant systematics as well as we suggested previously (Jones and Liebermann, 1974). For the perovskites, this may be due to the fact that the lattice potential energy involves two types of cation-anion interaction, each characterised by its own repulsive potential. The requirement that the bracketed term in equation (5.2) be a slowly varying function of r_0 (Anderson, 1972) might not be satisfied and deviation from the systematics would occur.

For the rutile-structure oxides, a rigid ion model with central forces only is not satisfactory, and the effects of bond bending must

be incorporated into the model (Striefler and Barsch, 1975). Striefler and Barsch's theoretical values of the bulk modulus agree very well with the experimental values for GeO_2, TiO_2 and SnO_2, and their model predicts reasonable values for the pressure derivatives of the elastic moduli. We can thus assume that it provides a reasonable explanation for the deviations of the rutile oxides on a log-log K-V plot. In general, the deviations from the predicted systematics result from the non-applicability of a simple model rather than from experimental uncertainties. Stishovite (rutile SiO_2) is an exception to this in that a wide range of experimental values of bulk modulus have been reported. Ultrasonically-determined values for polycrystalline samples range from 3.46 Mbar (Mizutani et al., 1972) to 2.49 Mbar, the value used here (Liebermann et al., 1976) while Striefler and Barsch (1976) predict a value of 3.145 Mbar on the basis of their lattice dynamical calculations.

The rigid ion model has also been applied to the rutile fluorides (Striefler and Barsch, 1973), although the predicted and experimental values of bulk modulus are not in such good agreement in this case. In particular the model predicts that K_S should decrease monotonically with increasing molar volume for the sequence of fluorides MgF_2, NiF_2, CoF_2 and MnF_2 which is not observed (see Figure 5.1). It is possible that the effects of bond bending may also be important in the rutile fluorides. Another complication is introduced for the rutile and perovskite fluorides containing transition metal ions, since these compounds undergo magnetic transitions at low temperatures (e.g., Aleksandrov et al., 1966; Melcher and Bolef, 1969; Melcher, 1970). The "non-magnetic" compounds MgF_2 and $KMgF_2$ have very similar values of ψ to those of the rocksalt and fluorite fluorides. Despite these discrepancies, our earlier discussion demonstrated that the relative effective charge of the oxides with respect to the fluorides appears to be virtually independent of structure, co-ordination number and details of the atomic interactions.

Another aspect of bulk modulus-volume systematics is given by O. L. Anderson and Nafe (1965) (see also O. L. Anderson and Soga, 1967) who proposed that oxides and silicates of common mean atomic weight $\overline{M}$ = 20-21 would be characterized by the relationship KV^{*4} = constant. In Figure 5.1, the bulk moduli of compounds with $\overline{M}$ = 20-21 (SiO_2, MgF_2, MgO, NaF) are indeed scaled as the inverse fourth power of the volume; this is an important result since this group of compounds contains both oxides and fluorides of different crystal structures. For other values of $\overline{M}$ the $K \sim V^{*-4}$ scaling is not as evident. However, for the rocksalt structure pairs MgO-NaF ($\overline{M}$ = 20-21), CaO-KF ($\overline{M}$ = 28-29), and SrO-RbF ($\overline{M}$ = 52) this relationship holds very well as indicated in Table 5.2; the members of each pair have comparable $\overline{M}$ since they are composed of adjacent elements in the Periodic Table which are very close in atomic weight. This alternative modelling scheme, on the basis of common $\overline{M}$ rather than ionic radii, is implicit in the approach of Son and Bartels (1972) who chose their pairs on the basis of the same closed shell ion core configuration.

5.3 Shear modulus-volume systematics

There is no simple theoretical basis for shear modulus-volume systematics as there is for the bulk modulus, which can be described in terms of thermodynamic variables. Davies (1975) has demonstrated that the empirical relationship μV^n = constant holds for the alkali halides, rocksalt oxides and fluorite fluorides, where n is a constant approximately equal to 4/3. According to Davies, oxides in the rutile and corundum structures are also consistent with this relationship.

In Figure 5.3 we have plotted shear modulus, μ, versus volume on a log-log plot for oxides and fluorides in the rocksalt, fluorite, rutile and perovskite structures. In addition to the features pointed out by Davies we can make some further comments on Figure 5.3 in the framework

Table 5.2: KV^{*4} Systematics for Rocksalt Fluorides and Oxides

Compound	$\overline{M}$	KV^{*4}
LiF	13.0	0.06
MgO	20.2	0.26
NaF	21.0	0.24
CaO	28.0	0.90
KF	29.1	0.90
SrO	51.8	1.61
RbF	52.2	1.53
BaO	76.7	2.62

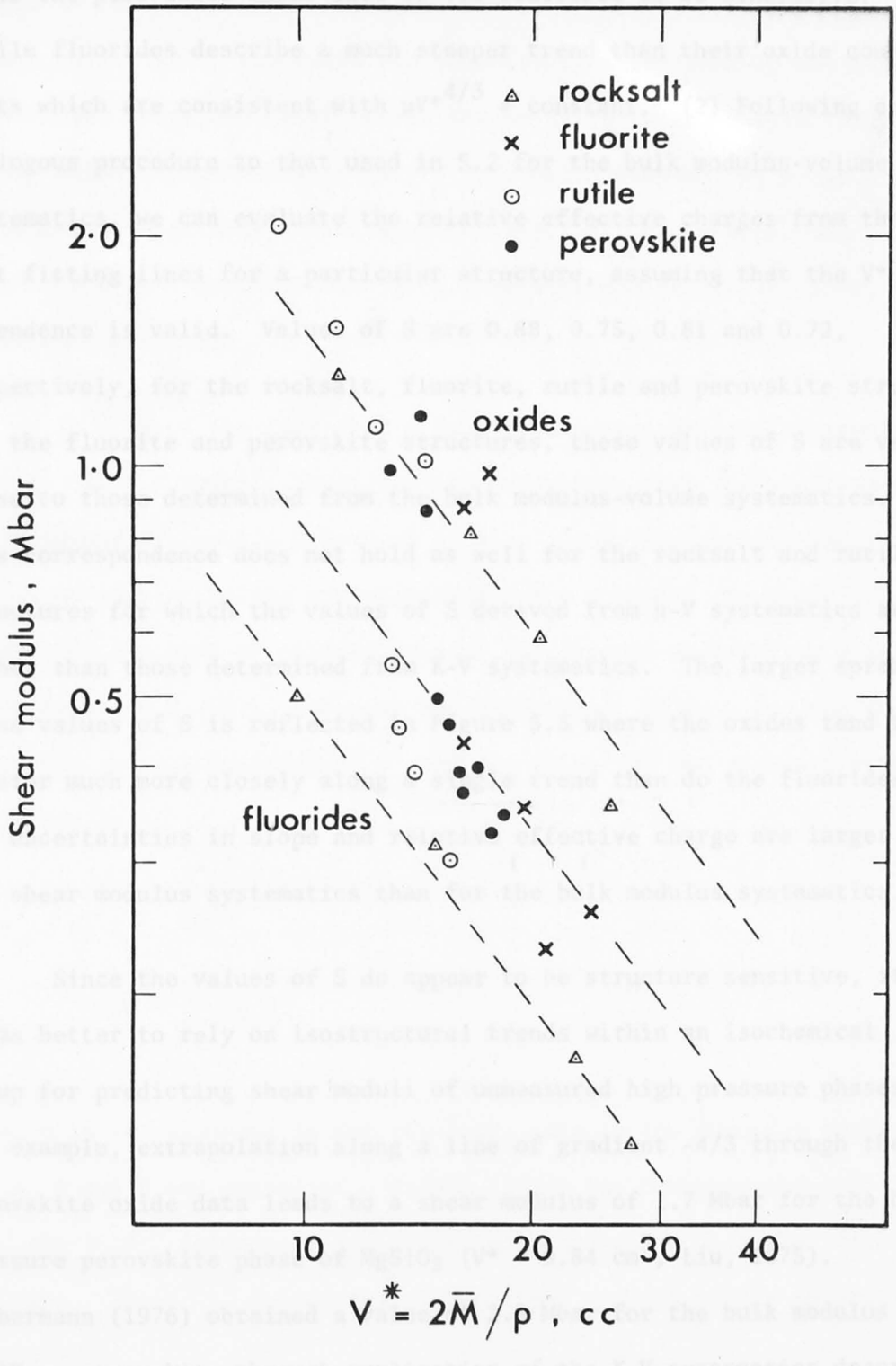

Figure 5.3: Log-log plot of shear modulus (μ) versus molar volume per ion pair ($2\bar{M}/\rho$) for oxides and fluorides in the rocksalt, fluorite, rutile and perovskite structures. The data of Table 5.1 for a particular structure are plotted in order of increasing molar volume. The dashed lines of gradient -4/3 represent the relationship $\mu V^{4/3}$ = constant.

of the fluoride-oxide modelling scheme: (1) the perovskite fluorides follow a well defined trend which is steeper than the lines of gradient -4/3, while the perovskite oxide data is too scattered to be conclusive. The rutile fluorides describe a much steeper trend than their oxide counterparts which are consistent with $\mu V^{*4/3}$ = constant. (2) Following an analogous procedure to that used in 5.2 for the bulk modulus-volume systematics, we can evaluate the relative effective charges from the best fitting lines for a particular structure, assuming that the $V^{*-4/3}$ dependence is valid. Values of S are 0.88, 0.75, 0.81 and 0.72, respectively, for the rocksalt, fluorite, rutile and perovskite structures. For the fluorite and perovskite structures, these values of S are very close to those determined from the bulk modulus-volume systematics. This correspondence does not hold as well for the rocksalt and rutile structures for which the values of S derived from μ-V systematics are higher than those determined from K-V systematics. The larger spread in these values of S is reflected in Figure 5.3 where the oxides tend to cluster much more closely along a single trend than do the fluorides. The uncertainties in slope and relative effective charge are larger for the shear modulus systematics than for the bulk modulus systematics.

Since the values of S do appear to be structure sensitive, it seems better to rely on isostructural trends within an isochemical group for predicting shear moduli of unmeasured high pressure phases. For example, extrapolation along a line of gradient -4/3 through the perovskite oxide data leads to a shear modulus of 1.7 Mbar for the high pressure perovskite phase of $MgSiO_3$ (V^* = 9.84 cm^3, Liu, 1975). Liebermann (1976) obtained a value of 2.8 Mbar for the bulk modulus of $MgSiO_3$ - perovskite through application of the K-V systematics described in 5.1. These results indicate the value of systematics in elastic moduli in characterising the elasticity of unknown phases.

An uncertainty implicit in Figure 5.3 relates to the problem of

calculating the elastic moduli of polycrystalline aggregates from the single crystal elastic moduli. Values of the isotropic bulk and shear moduli in Table 5.1 were calculated by the Voigt-Reuss-Hill (VRH) averaging scheme (Hill, 1952) for which the uncertainties measured by the difference between the Voigt and Reuss bounds can be quite large, particularly for highly anisotropic materials (e.g., rutiles). However, in general it is found that the arithmetic average (VRH average) of the upper and lower bounds is a fair approximation (e.g., Meister and Peselnick, 1965, for tetragonal crystals).

In view of the fact that μ is a complicated average of single crystal elastic moduli, it is perhaps surprising that the shear modulus exhibits any systematic behaviour at all. On a very qualitative level, the shear modulus-volume systematics for the rocksalt structure can be understood in terms of calculations of the elastic moduli from a central force model (e.g., O.L. Anderson and Liebermann, 1970). For the cubic structure, μ is a function of c' and c_{44} which for the rocksalt structure are given by

$$c' = \frac{Z^2e^2}{V_0^{4/3}} \{An + B\}$$
$$c_{44} = \frac{Z^2e^2}{V_0^{4/3}} D \qquad (5.5)$$

where n is the exponent in the repulsive term in the Born-Mie potential and A, B and D are constants. Gilman (1963) has demonstrated that c_{44} exhibits a d^{-4} dependence for alkali halides, where d is the interatomic distance. The $V^{-4/3}$ dependence of the shear modulus arises naturally in this model.

5.4 $(\partial c/\partial T)$ systematics

Following the discussion of systematics in the elastic moduli

for fluorides and oxides in the rocksalt, fluorite, rutile and perovskite structures, it is of particular interest to investigate the relationship of $(\partial c/\partial T)$ to crystallographic parameters. Table 5.3 presents the breakdown of $(\partial c/\partial T)_P$ into intrinsic and extrinsic components according to equation (4.5), for the alkali fluorides LiF, NaF, KF and RbF, and for the alkaline earth oxides MgO, CaO, SrO and BaO. We decided to investigate the relationships between $(\partial c/\partial T)$ for these compounds rather than $(\partial \ln c/\partial T) = {}^{1}/c(\partial c/\partial T)$ used by other authors (e.g., Bartels and Vetter, 1972), since $(\partial c/\partial T)_P$ can be discussed in terms of explicit theoretical expressions derived by Mitskevich (1965).

Some important trends and relationships emerge from Table 5.3: (1) In general, for the fluoride series LiF-NaF-KF-RbF, and for the oxide series MgO-CaO-SrO-BaO, $|(\partial c/\partial T)_P|$ decreases with increasing molar volume for the elastic moduli c_{11}, c', c_{44}, K_S and μ. The trends for $(\partial c/\partial T)_V$ are not nearly so uniform; $|(\partial c/\partial T)_V|$ decreases with increasing molar volume for the moduli c', c_{44}, K_S and μ for the fluorides and for the moduli c_{11}, c' and μ for the oxides, but increases with increasing molar volume for c_{44} and K_S for the oxides. $(\partial c_{11}/\partial T)_V$ for the series LiF-NaF-KF-RbF remains approximately constant. (2) The large extrinsic temperature dependence for the moduli, c_{11}, K_S and c' was noted previously for LiF, NaF and MgO in the discussion of Figures 4.2-4.4. The same behaviour is borne out in general for the alkali fluorides and alkaline earth oxides in Table 5.3. For the shear modulus, μ, the intrinsic and extrinsic components of the temperature dependence are approximately equal for both the fluorides and the oxides. (3) The "weakened model" concept introduced by Goldschmidt (1927) suggests that the elastic properties of fluorides should be more temperature sensitive than those of their oxide analogues. For the fluoride-oxide analogue pairs, LiF-MgO, NaF-CaO, KF-SrO, RbF-BaO, Table 5.3 illustrates that for the moduli c_{11}, c', c_{44} and K_S, $|(\partial c/\partial T)_P|$ for the fluoride member of a pair is generally

TABLE 5.3: Intrinsic and extrinsic components of $\left(\frac{\partial c}{\partial T}\right)_P$ for the alkali fluorides and alkaline earth oxides at room temperature

			Intrinsic	Extrinsic	
		$-\left(\frac{\partial c}{\partial T}\right)_P$	$-\left(\frac{\partial c}{\partial T}\right)_V$	$+\alpha_V K_T \left(\frac{\partial c}{\partial P}\right)_T$	$\left(\frac{\partial c}{\partial P}\right)_T$
		(kbar.deg^{-1})	(kbar.deg^{-1})	(kbar.deg^{-1})	
c_{11}	LiF	0.749[1]	0.094	0.655	9.97[2]
	MgO	0.606[3]	0.166	0.44[3]	8.697[3]
	NaF	0.624[1]	0.102	0.522	11.56[2]
	CaO	0.547[4]	0.085[4]	0.462[4]	10.53[5]
	KF	0.481[4,6]	0.093[4,6]	0.388[4,6]	12.26[7]
	SrO	0.352[4]	-0.065[4]	0.417[4]	11.33[5]
	RbF	0.433[4,6]	0.123[4,6]	0.310[4,6]	12.14[8]
	BaO	0.32[9]	-	-	-
c'	LiF	0.38	0.144	0.236	2.73
	MgO	0.34	0.145	0.195	3.64
	NaF	0.336	0.120	0.216	1.985
	CaO	0.266	0.115	0.148	3.4
	KF	0.26	0.094	0.167	5.25
	SrO	0.21	0.064	0.147	4.0
	RbF	0.225	0.099	0.126	4.93
	BaO	0.19	-	-	-
c_{44}	LiF	0.183	0.092	0.091	1.38
	MgO	0.103	0.048	0.055	1.09
	NaF	0.058	0.049	0.009	0.205
	CaO	0.072	0.049	0.024	0.6
	KF	0.027	0.040	-0.013	-0.43
	SrO	0.057	0.062	-0.005	-0.2
	RbF	0.017	0.034	-0.017	-0.7
	BaO	0.16	-	-	-
K_S	LiF	0.242	-0.098	0.340	5.14
	MgO	0.153	-0.042	0.195	3.85
	NaF	0.177	-0.058	0.235	5.18
	CaO	0.192	-0.069	0.262	6.0
	KF	0.134	-0.032	0.166	5.26
	SrO	0.07	-0.15	0.22	6.0
	RbF	0.134	-0.008	0.143	5.57
	BaO	0.07	-	-	-
μ	LiF	0.316	0.169	0.147	2.24
	MgO	0.230	0.107	0.123	2.44
	NaF	0.153	0.116	0.037	0.814
	CaO	0.150	0.075	0.075	1.70
	KF	0.094	0.061	0.033	1.043
	SrO	0.119	0.070	0.049	1.32
	RbF	0.074	0.057	0.017	0.668
	BaO	0.166	-	-	-

TABLE 5.3 (Continued)

1. This work
2. Miller and Smith (1964)
3. Spetzler (1969)
4. Bartels and Vetter (1972)
5. Son and Bartels (1972)
6. Haussühl (1960)
7. Roberts and Smith (1970a)
8. Roberts and Smith (1970b)
9. Vetter and Bartels (1973)

larger than that for the oxide. However, the $(\partial c/\partial T)_P$ for a particular analogue pair are not as dissimilar as one would expect from other evidence of the "weakened model" concept, e.g., the ratio of the bulk moduli (Jones and Liebermann, 1974). (4) An alternative modelling scheme (Son and Bartels, 1972) based on the same closed shell ion core configuration would pair MgO-NaF, CaO-KF and SrO-RbF; $(\partial c/\partial T)_P$ for a pair chosen on this basis are more comparable but not demonstrably more systematic than for pairs with similar ionic radii. A modelling scheme based on ionic radii considerations has more theoretical appeal since properties dependent on geometrical configuration such as the relative effect of nearest neighbour and next nearest neighbour interactions ought to be similar for the members of an analogue pair.

In Table 5.4 we present the intrinsic and extrinsic components of $(\partial c/\partial T)_P$ for the alkaline earth fluorides CaF_2, SrF_2 and BaF_2. Temperature derivatives of the single crystal elastic moduli are not available for their oxide analogues, ThO_2 and UO_2. However we can note some features of the dependence of $(\partial c/\partial T)$ on crystallographic parameters for the fluorides alone. (1) For the fluoride series CaF_2-SrF_2-BaF_2, $|(\partial c/\partial T)_P|$ decreases with increasing molar volume for all the elastic moduli. The $(\partial c/\partial T)_V$ data do not exhibit systematic behaviour except for the modulus c', for which $|(\partial c/\partial T)_V|$ decreases with increasing molar volume. (2) The large extrinsic temperature dependence for the moduli c_{11} and K_S was noted previously in the discussion of Figures 4.5, 4.6 and 4.7. For the single crystal (c' and c_{44}) and isotropic (μ) shear moduli, the intrinsic temperature dependence comprises at least half of the total temperature dependence. (3) For the fluorite structure, the value of $|(\partial c_{11}/\partial T)_P|$ is very much lower than for the rocksalt structure. $|(\partial c'/\partial T)_P|$ and $|(\partial c_{44}/\partial T)_P|$ are comparable in value for the fluorites in contrast to the rocksalt structure where $|(\partial c'/\partial T)_P|$ is much larger than $|(\partial c_{44}/\partial T)_P|$. For the two structures, the values of $|(\partial c_{44}/\partial T)_P|$ are similar.

TABLE 5.4: Intrinsic and extrinsic components of $\left(\frac{\partial c}{\partial T}\right)_P$ for the alkaline earth fluorides at room temperature

			Intrinsic	Extrinsic	
		$-\left(\frac{\partial c}{\partial T}\right)_P$	$-\left(\frac{\partial c}{\partial T}\right)_V$	$+\alpha_V^1 K_T \left(\frac{\partial c}{\partial P}\right)_T$	$\left(\frac{\partial c}{\partial P}\right)_T$
		(kbar.deg^{-1})	(kbar.deg^{-1})	(kbar.deg^{-1})	
c_{11}	CaF_2	0.346[2]	0.0461	0.300	6.05[3]
	SrF_2	0.236[2]	0.0630	0.173	5.25[4]
	BaF_2	0.212[2]	0.0452	0.167	4.82[3]
c'	CaF_2	0.1108	0.0686	0.042	0.852
	SrF_2	0.0573	0.0453	0.012	0.365
	BaF_2	0.0376	0.0437	-0.006	-0.177
c_{44}	CaF_2	0.1212	0.0563	0.0649	1.31
	SrF_2	0.0925	0.0574	0.0351	1.07
	BaF_2	0.0761	0.0492	0.0269	0.777
K_S	CaF_2	0.198	-0.0454	0.243	4.92
	SrF_2	0.159	0.002	0.157	4.76
	BaF_2	0.156	-0.0191	0.175	5.05
μ	CaF_2	0.118	0.058	0.060	1.218
	SrF_2	0.084	0.058	0.026	0.795
	BaF_2	0.061	0.047	0.014	0.39

1. Sirdeshmukh and Deshpande (1964)
2. This work
3. Wong and Schuele (1968)
4. Alterovitz and Gerlich (1970)

The intrinsic and extrinsic temperature dependence for the rutile-structure compounds are given in Tables 5.5 and 5.6. Several important features emerge from Tables 5.6 and 5.7. (1) The trend that was observed for the rocksalt and fluorite structures for $|(\partial c/\partial T)_P|$ to decrease with increasing molar volume is evident here for neither the rutile fluorides nor oxides; in particular, the values of $(\partial c/\partial T)_P$ for TiO_2 seem anomalously high in comparison with GeO_2 and SnO_2. (2) For the rutile fluorides, the extrinsic temperature effect is dominant for the moduli c_{11}, c_{12}, c_{13} and K_S. The intrinsic component dominates the temperature dependence for the shear moduli, c_{66} and μ_S. In general the temperature dependence of the rutile oxides is characterized by similar contributions from the intrinsic and extrinsic components; however, the dominant component is extrinsic for the moduli c_{11}, c_{12}, c_{13} and K_S, and intrinsic for the shear moduli c_{44}, c_{66} and μ_S. (3) As was stated earlier, an underlying concept of the fluoride-oxide modelling scheme was that the physical properties of the fluorides should be more temperature sensitive. From Tables 5.5 and 5.6, we can see that $|(\partial c/\partial T)_P|$ for the fluorides is in general much lower than the corresponding $|(\partial c/\partial T)_P|$ for the oxides. An exception to this is SnO_2 for which all the $(\partial c/\partial T)_P$ are very comparable with those for the fluorides. The major cause of this difference is the fact that the intrinsic temperature dependence for the rutile oxides is much larger than for the fluorides. (4) The temperature behaviour of MgF_2 does however reflect that of TiO_2 in that the ratio of $(\partial c/\partial T)_P$ for TiO_2 relative to MgF_2 lies between 2.5 and 3 for all modes except c_{13}. Similar ratios for other fluoride-oxide pairs do not exhibit such constancy.

In Table 5.7, we have listed the intrinsic and extrinsic components of the $(\partial c/\partial T)_P$ for the perovskites $KMgF_3$ and $SrTiO_3$. The comparisons must be viewed as being rather tentative since the value of α_V is only an estimate for $KMgF_3$ (see Footnote, p. 29). However some comments can

Table 5.5: Intrinsic and extrinsic components of $\left(\frac{\partial c}{\partial T}\right)_P$ for the rutile fluorides at room temperature

		$-\left(\frac{\partial c}{\partial T}\right)_P$	intrinsic $-\left(\frac{\partial c}{\partial T}\right)_V$	extrinsic $+\alpha_V^1 K_T \left(\frac{\partial c}{\partial P}\right)_T$	$\left(\frac{\partial c}{\partial P}\right)_T$
		(kbar.deg^{-1})	(kbar.deg^{-1})	(kbar.deg^{-1})	
C_{11}	MgF_2	0.192[2]	0.0107	0.181	4.8[3]
	NiF_2	0.16[4]	0.037	0.123	4.4[5]
	MnF_2	0.216[6]			
C_{33}	MgF_2	0.322	0.110	0.212	5.6
	NiF_2	0.32	0.166	0.154	5.5
	MnF_2	0.374			
C_{12}	MgF_2	0.194	-0.0366	0.231	6.1
	NiF_2	0.24	-0.009	0.249	8.9
	MnF_2	0.220			
C_{13}	MgF_2	0.086	-0.0574	0.143	3.8
	NiF_2	0.11	0.048	0.062	2.2
	MnF_2	0.163			
C_{44}	MgF_2	0.0745	0.0443	0.119	0.8
	NiF_2	0.02	0.010	0.009	0.33
	MnF_2	0.069			
C_{66}	MgF_2	0.277	0.160	0.117	3.1
	NiF_2	0.26	0.176	0.084	3.0
	MnF_2	0.264			
K_S	MgF_2	0.160	-0.0213	0.181	4.8
	NiF_2	0.18	0.046	0.134	4.8
	MnF_2	0.209			
μ	MgF_2	0.079	0.059	0.020	0.6
	NiF_2	0.028	0.045	-0.017	-0.6
	MnF_2	0.065			

1. α_V for MgF_2 taken from Bailey et al. (1975)
   α_V for NiF_2 taken from RaO (1973).
2. This work.
3. Davies (1976).
4. Wu (1974).
5. Jamieson and Wu (1974).
6. Haussühl (1968).

Table 5.6: Intrinsic and extrinsic components of $\left(\frac{\partial c}{\partial T}\right)_P$ for the rutile oxides at room temperature

		$-\left(\frac{\partial c}{\partial T}\right)_P$	intrinsic $-\left(\frac{\partial c}{\partial T}\right)_V$	extrinsic $+\alpha_V^1 K_T\left(\frac{\partial c}{\partial P}\right)_T$	$\left(\frac{\partial c}{\partial P}\right)_T$
		(kbar.deg^{-1})	(kbar.deg^{-1})	(kbar.deg^{-1})	
C_{11}	GeO_2	0.42[2]	0.187	0.233	6.65[2]
	TiO_2	0.51[3]	0.184[3]	0.326[3]	6.47[3]
	SnO_2	0.20[4]	0.084	0.116	5.25[4]
C_{33}	GeO_2	0.38	0.148	0.232	6.63
	TiO_2	0.90	0.484	0.416	8.34
	SnO_2	0.37	0.236	0.134	6.10
C_{12}	GeO_2	0.46	0.178	0.282	8.05
	TiO_2	0.58	0.123	0.457	9.10
	SnO_2	0.21	0.062	0.148	6.73
C_{13}	GeO_2	0.23	0.087	0.143	4.10
	TiO_2	0.33	0.077	0.253	5.02
	SnO_2	0.132	0.030	0.102	4.65
C_{44}	GeO_2	0.15	0.088	0.062	1.78
	TiO_2	0.22	0.168	0.052	1.10
	SnO_2	0.059	0.04	0.019	0.889
C_{66}	GeO_2	0.38	0.237	0.143	4.10
	TiO_2	0.78	0.457	0.323	6.43
	SnO_2	0.256	0.187	0.069	3.18
K_S	GeO_2	0.36	0.145	0.216	6.15
	TiO_2	0.41	0.067	0.343	6.80
	SnO_2	0.19	0.077	0.113	5.13
μ	GeO_2	0.12	0.077	0.043	1.22
	TiO_2	0.27	0.226	0.044	0.78
	SnO_2	0.067	0.054	0.013	0.61

1. α_V for GeO_2 and SnO_2 taken from RaO (1973).

2. Wang and Simmons (1973).

3. Manghnani et al. (1972).

4. Chang and Graham (1975).

TABLE 5.7: Intrinsic and extrinsic components of $\left(\frac{\partial c}{\partial T}\right)_P$ for the perovskites $KMgF_3$ and $SrTiO_3$ at room temperature

		$-\left(\frac{\partial c}{\partial T}\right)_P$ (kbar.deg^{-1})	Intrinsic $-\left(\frac{\partial c}{\partial T}\right)_V$ (kbar.deg^{-1})	Extrinsic $+\alpha_V^1 K_S\left(\frac{\partial c}{\partial P}\right)_T$ (kbar.deg^{-1})	$\left(\frac{\partial c}{\partial P}\right)_T$
c_{11}	$KMgF_3$	0.509[2]	0.255	0.254	8.93[2]
	$RbMnF_3$	0.44[5]	-	-	-
	$SrTiO_3$	0.867[3]	0.378	0.489	10.21[4]
c'	$KMgF_3$	0.251	0.168	0.083	2.94
	$RbMnF_3$	0.217	-	-	-
	$SrTiO_3$	0.367	0.207	0.160	3.35
c_{44}	$KMgF_3$	0.085	0.048	0.0372	1.31
	$RbMnF_3$	0.028	-	-	-
	$SrTiO_3$	0.161	0.102	0.059	1.24
K_S	$KMgF_3$	0.174	0.032	0.142	5.01
	$RbMnF_3$	0.151	-	-	-
	$SrTiO_3$	0.377	0.102	0.275	5.74
μ	$KMgF_3$	0.159	0.104	0.055	1.93
	$RbMnF_3$	0.095	-	-	-
	$SrTiO_3$	0.295	0.154	0.141	2.95

1. α_V for $SrTiO_3$ taken from Lytle (1964)

   α_V for $KMgF_3$ estimated in Footnote p. 29.

2. This work

3. Bell and Rupprecht (1963)

4. Beattie and Samara (1971)

5. Melcher and Bolef (1969)

still be made on the nature of the temperature dependence of the elastic moduli. (1) For both $KMgF_3$ and $SrTiO_3$, the intrinsic temperature effect is greater than or equal to the extrinsic effect for the modes c_{11}, c' and c_{44}. For $(\partial K_S/\partial T)_P$, the dominant effect is extrinsic, although not as marked as for the rocksalt and fluorite structure. (2) The values of $(\partial c/\partial T)_P$ for a particular mode are larger for $SrTiO_3$ than for $KMgF_3$; similar behaviour was noted for $(\partial c/\partial T)_P$ for the rutile-structure compounds. For the fluorides $KMgF_3$-$RbMnF_3$, $|(\partial c/\partial T)_P|$ decreases with increasing molar volume for all moduli; however more data are required to establish a trend.

It is worth re-stating the most striking conclusions of the preceding comparisons of $(\partial c/\partial T)$ for oxides and fluorides in the rocksalt, fluorite, rutile and perovskite structures. (1) Trends of decreasing $|(\partial c/\partial T)_P|$ with increasing molar volume are observed for the rocksalt and fluorite structure compounds. (2) $(\partial c/\partial T)_P$ values are very similar for the members of a rocksalt-structure fluoride-oxide analogue pair; these similarities are not exhibited by the rutile and perovskite-structure compounds. (3) For all of the compounds considered, $(\partial K_S/\partial T)_P$ is dominated by extrinsic temperature dependence; for $(\partial \mu/\partial T)_P$, the intrinsic component is greater than or equal to the extrinsic component.

The existence of the above trends and similarities for the rocksalt fluorides and oxides prompted us to seek a theoretical explanation for this behaviour. From theoretical lattice dynamical considerations, Mitskevich (1965) derived the following expressions for the temperature dependence of the c_{ij},

$$\left(\frac{\partial c_{11}}{\partial T}\right)_P = -\frac{k}{d_0^3}\,(0.411\Lambda^2 + 3.25\Lambda - 4.8)$$

$$\left(\frac{\partial c_{12}}{\partial T}\right)_P = \frac{k}{d_0^3}\,(0.038\Lambda^2 + 0.46\Lambda - 4.0) \qquad (5.6)$$

$$\left(\frac{\partial c_{44}}{\partial T}\right)_P = -\frac{k}{d_0^3}\,(-0.06\Lambda + 4.8)$$

where k is Boltzmann's constant and Λ is the repulsive parameter in the Born-Mayer potential

$$\Phi(d) = -\frac{A_m Z_c Z_a e^2}{d} + Be^{-\Lambda d/d_0} \qquad (5.7)$$

where d_0 is the equilibrium value of the nearest neighbour distance d, A_m is the Madelung constant and Z_c, Z_a are the valences of the cation and anion respectively. By invoking equilibrium conditions it is easy to show that

$$\Lambda = 2 + \frac{9Vd_0K}{A_m Z_c Z_a e^2} \qquad (5.8)$$

where V is the molecular volume. We demonstrated earlier that the relationship $KV^*/Z_cZ_ae^2$ = constant holds for isostructural series of fluorides and oxides in the rocksalt, fluorite, rutile and perovskite structures (also for halides, sulphides, selenides and tellurides, D. L. Anderson and O. L. Anderson, 1970). We have applied this result to equation (5.8) which leads to

$$\Lambda = 2 + \phi d \qquad (5.9)$$

where ϕ is a constant for the members of an isostructural series. Hence from equations (5.6) and (5.9), $(\partial c_{ij}/\partial T)_P$ should be a function of nearest-neighbour distance only.

In Figure 5.4 we have plotted on a log-log diagram, $|(\partial c/\partial T)_P|$ versus molar volume per ion pair for the moduli c_{11}, c' and c_{44} for the alkali fluorides and the alkaline earth oxides. Both the fluorides and

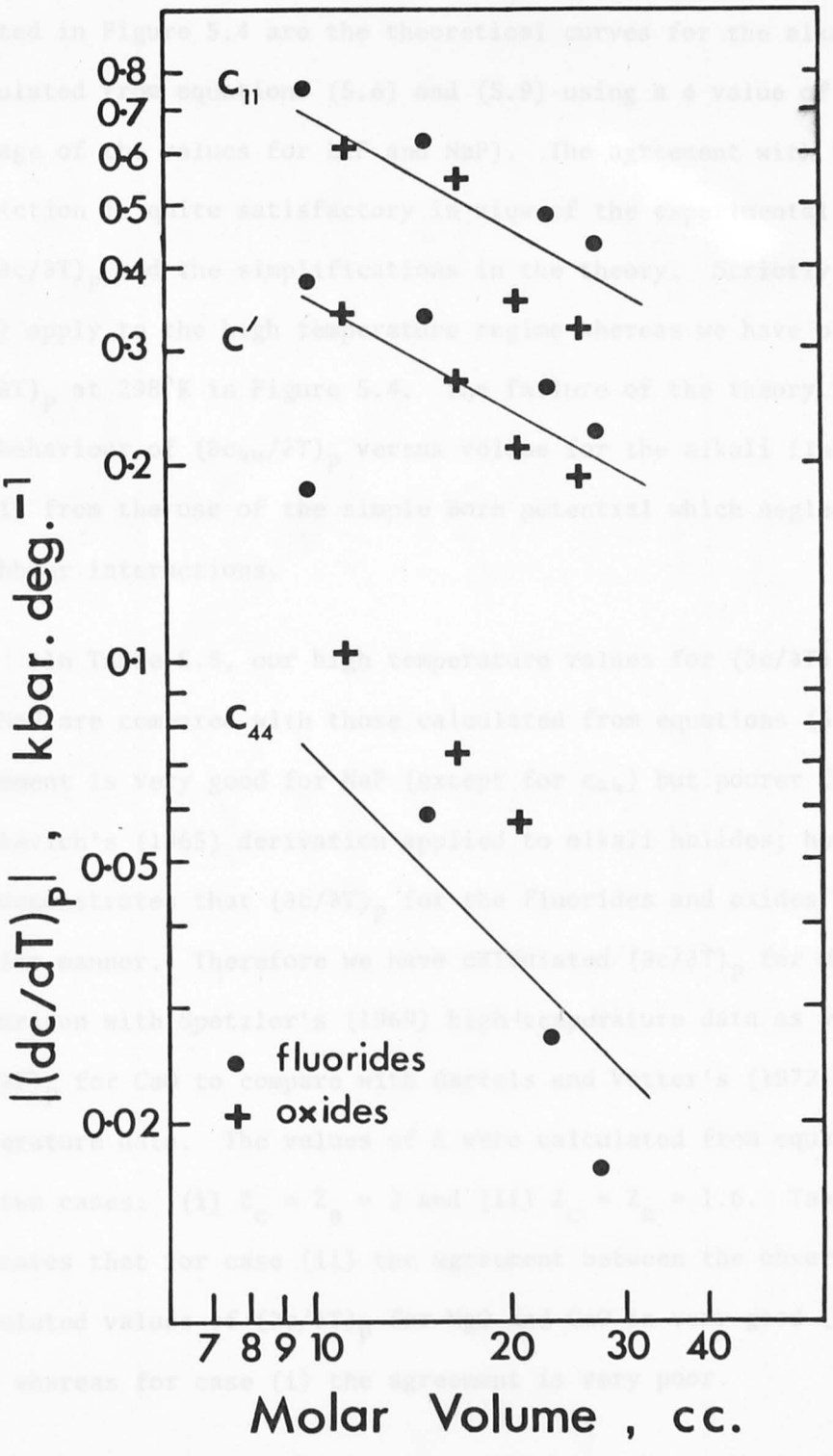

Figure 5.4: Log-log plot of $|(\partial c/\partial T)|_P$ (from Table 5.3) versus molar volume per ion pair for the modes c_{11}, c' and c_{44} for the alkali fluorides and alkaline earth oxides (rocksalt structure). The data points from left to right are LiF-NaF-KF-RbF and MgO-CaO-SrO-BaO respectively. The solid curves are calculated from equations (5.6) and (5.9) using ϕ = 2.63 for the alkali halides.

the oxides describe nearly linear and remarkably similar trends. Also plotted in Figure 5.4 are the theoretical curves for the alkali fluorides calculated from equations (5.6) and (5.9) using a ϕ value of 2.63 (the average of the values for LiF and NaF). The agreement with the theoretical prediction is quite satisfactory in view of the experimental uncertainties in $(\partial c/\partial T)_p$ and the simplifications in the theory. Strictly, equations (5.6) apply to the high temperature regime whereas we have plotted $(\partial c/\partial T)_p$ at 298°K in Figure 5.4. The failure of the theory to describe the behaviour of $(\partial c_{44}/\partial T)_p$ versus volume for the alkali fluorides might result from the use of the simple Born potential which neglects next-nearest neighbour interactions.

In Table 5.8, our high temperature values for $(\partial c/\partial T)_p$ for LiF and NaF are compared with those calculated from equations (5.6). The agreement is very good for NaF (except for c_{44}) but poorer for LiF. Mitskevich's (1965) derivation applied to alkali halides; however Figure 5.4 demonstrates that $(\partial c/\partial T)_p$ for the fluorides and oxides behave in a similar manner. Therefore we have calculated $(\partial c/\partial T)_p$ for MgO for comparison with Spetzler's (1969) high temperature data as well as $(\partial c/\partial T)_p$ for CaO to compare with Bartels and Vetter's (1972) room temperature data. The values of Λ were calculated from equation (5.8) for two cases: (i) $Z_c = Z_a = 2$ and (ii) $Z_c = Z_a = 1.6$. Table 5.8 indicates that for case (ii) the agreement between the observed and calculated values of $(\partial c/\partial T)_p$ for MgO and CaO is very good (except for c_{44}) whereas for case (i) the agreement is very poor.

The concept of an effective charge governing the Coulombic interaction has been discussed by many authors. Son and Bartels (1972) pointed out that the effective charge model made the decomposition of the elastic properties and the repulsive parameters for the oxides appear more like those of the fluorides. Sirdeshmukh and Rao (1975) demonstrated that the use of an effective charge in the calculation of the Gruneisen

Table 5.8: Comparison of calculated and measured values of $(\partial c/\partial T)_P$ for LiF, NaF, MgO and CaO[1]

	d (A^o)	K_S (kbar)	Z	Λ	$\left(\frac{\partial c_{11}}{\partial T}\right)_P$	$\left(\frac{\partial c'}{\partial T}\right)_P$	$\left(\frac{\partial c_{44}}{\partial T}\right)_P$	$\left(\frac{\partial K_S}{\partial T}\right)_P$
					(kbar.deg.$^{-1}$)			
LiF	2.0132[2]	704[2]	1	7.17	-0.70	-0.36	-0.073	-0.22
					(-0.67)[4]	(-0.27)	(-0.22)	(-0.30)
NaF	2.3165[2]	483[4]	1	8.22	-0.55	-0.29	-0.048	-0.17
					(-0.56)[4]	(-0.28)	(-0.075)	(-0.19)
MgO	2.1065[3]	1628[5]	2	5.53	-0.38	-0.19	-0.067	-0.13
			1.6	7.51	-0.63	-0.33	-0.064	-0.19
					(-0,59)[5]	(-0.30)	(-0.122)	(-0.20)
CaO	2.4055[3]	1140[3]	2	6.26	-0.31	-0.16	-0.044	-0.10
			1.6	8.66	-0.54	-0.28	-0.043	-0.16
					(-0.55)[6]	(-0.27)	(-0.072)	(-0.19)

1. $(\partial c/\partial T)_P$ measured at room temperature for CaO and at high temperatures for LiF, NaF and MgO.
2. Miller and Smith (1964)
3. Son and Bartels (1972)
4. This work
5. Spetzler (1969)
6. Bartels and Vetter (1972)

parameter γ for the alkaline earth oxides resulted in agreement with the thermal values of γ. Following Anderson's (1972) discussion of bulk modulus systematics, we have shown earlier in this Chapter that a relative effective charge of the oxides with respect to the fluorides of $S = \frac{Z^O}{2Z^F} = 0.80$ for the rocksalt structure made $KV/Z_c Z_a e^2$ the same constant for all of the rocksalt fluorides and oxides. The good agreement between the observed and calculated values of $(\partial c/\partial T)_P$ for MgO and CaO for $Z_c = Z_a = 1.6$ supports the application of the above result to equation (5.9) where ϕ is now the same constant for both the oxides and fluorides. Equations (5.6) and (5.9) demonstrate that $(\partial c/\partial T)_P$ should be similar for the members of a fluoride-oxide analogue pair chosen on the basis of similar ionic radii (e.g. LiF-MgO, NaF-CaO), the differences arising from the fact that the nearest neighbour distances are not exactly equal (Table 5.8).

While Mitskevich's (1965) theory is limited by its very simple lattice potential, particularly in the description of $(\partial c_{44}/\partial T)_P$, it can be applied in conjunction with the observed bulk modulus systematics to describe some of the observed trends and relationships in a semi-quantitative manner. In particular, this theory demonstrates the importance of the nearest neighbour distance as a parameter controlling the temperature dependence of the elastic moduli.

Following the success of our model incorporating Mitskevich's theory and K-V systematics for the rocksalt structure, it is of interest to investigate its validity for the fluorite structure. No simple equations such as (5.6) have been derived for this structure due to the complexity of evaluating the lattice sums in the potential energy. An added complication is introduced by the fact that the fluorite lattice is non-centrosymmetric. However, the qualitative behaviour of $(\partial c/\partial T)_P$ as a function of nearest neighbour distance can be illustrated in Figure 5.5 which is a log-log plot of $(\partial c/\partial T)_P$ versus molar volume per ion pair.

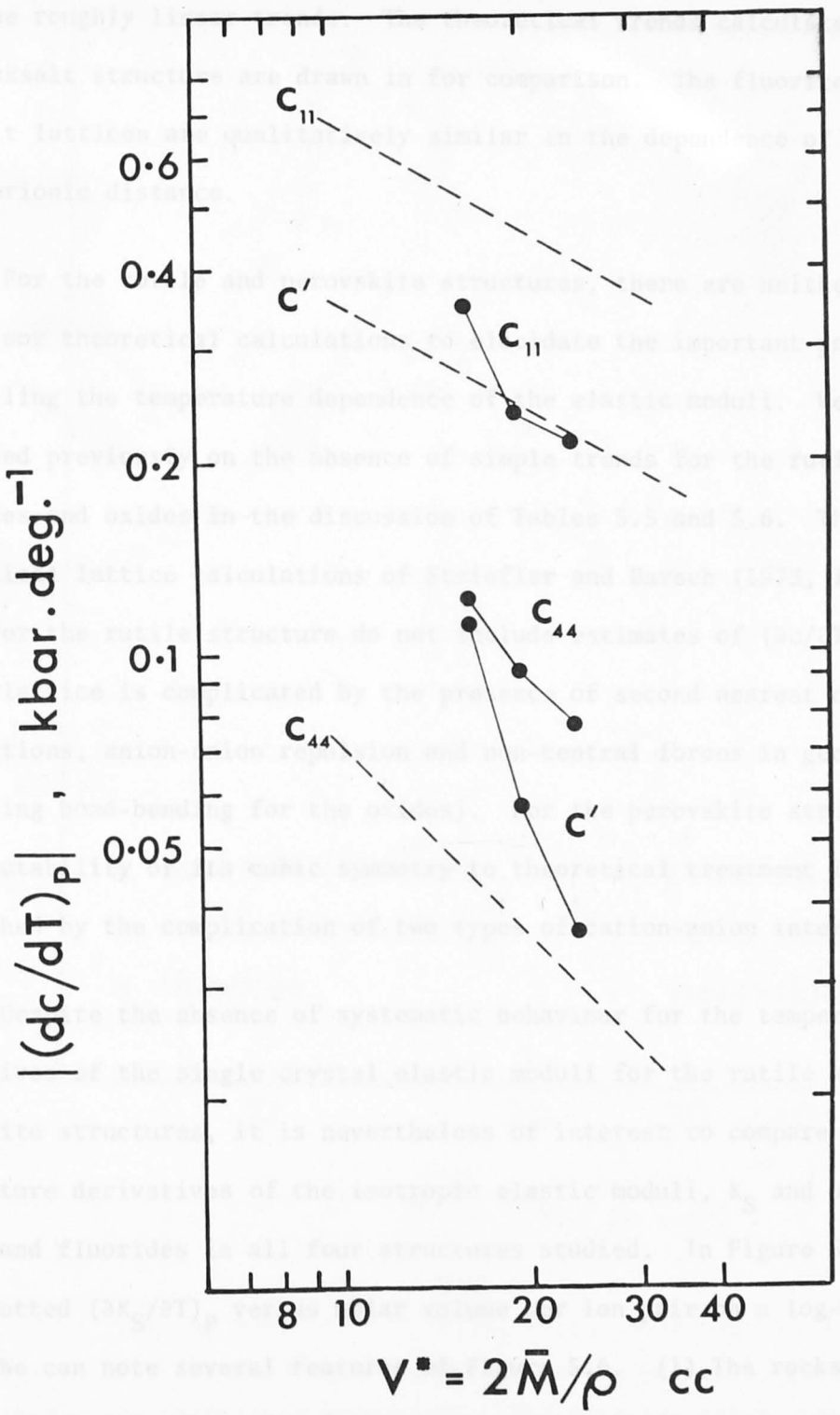

Figure 5.5: Log-log plot of $|(\partial c/\partial T)|_P$ (from Table 5.4) versus molar volume per ion pair for the modes c_{11}, c' and c_{44} for the alkaline earth fluorides (fluorite structure). The data points from left to right are CaF_2-SrF_2-BaF_2. For comparison, the calculated curves for the alkali halides (Figure 5.4) are shown as dashed lines.

We can see that for the modes c_{11}, c' and c_{44} the data for the series CaF_2-SrF_2-BaF_2 are monotonically decreasing with increasing volume and describe roughly linear trends. The theoretical trends calculated for the rocksalt structure are drawn in for comparison. The fluorite and rocksalt lattices are qualitatively similar in the dependence of $(\partial c/\partial T)_P$ on interionic distance.

For the rutile and perovskite structures, there are neither obvious trends nor theoretical calculations to elucidate the important parameters controlling the temperature dependence of the elastic moduli. We commented previously on the absence of simple trends for the rutile fluorides and oxides in the discussion of Tables 5.5 and 5.6. The theoretical lattice calculations of Striefler and Barsch (1973, 1974, 1975) for the rutile structure do not include estimates of $(\partial c/\partial T)_P$. The rutile lattice is complicated by the presence of second nearest neighbour interactions, anion-anion repulsion and non-central forces in general (including bond-bending for the oxides). For the perovskite structure, the tractability of its cubic symmetry to theoretical treatment is outweighed by the complication of two types of cation-anion interaction.

Despite the absence of systematic behaviour for the temperature derivatives of the single crystal elastic moduli for the rutile and perovskite structures, it is nevertheless of interest to compare the temperature derivatives of the isotropic elastic moduli, K_S and μ, for oxides and fluorides in all four structures studied. In Figure 5.6, we have plotted $(\partial K_S/\partial T)_P$ versus molar volume per ion pair on a log-log plot. We can note several features of Figure 5.6. (1) The rocksalt and fluorite-structure fluorides follow a monotonically decreasing trend with increasing molar volume, which is consistent with the earlier discussions involving Mitskevich's theory. The rocksalt oxides scatter quite widely about a similar trend; however, the errors for SrO and BaO are large (50%) (Bartels and Vetter, 1972; Vetter and Bartels, 1973).

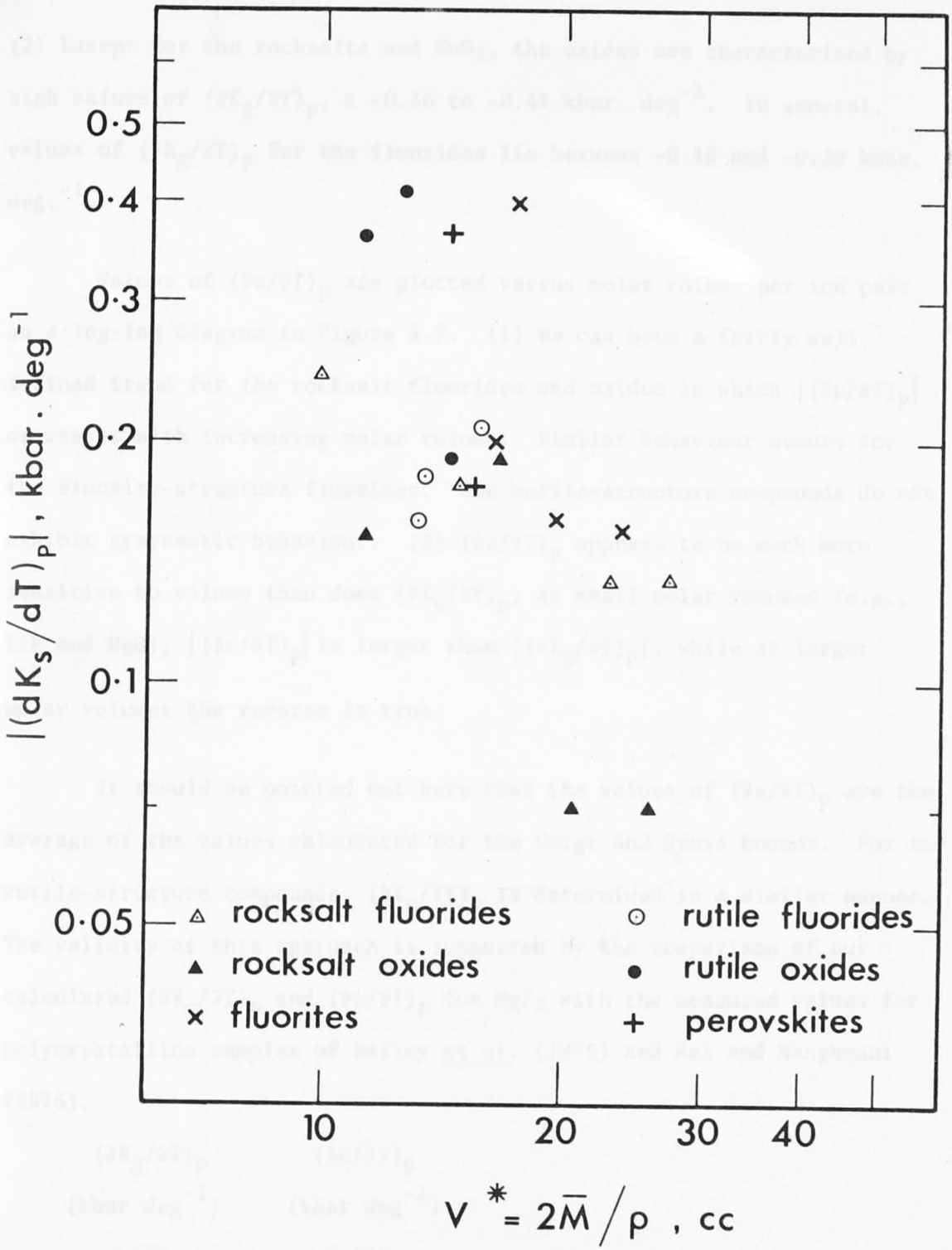

Figure 5.6: Log-log plot of $|(\partial K_S/\partial T)|_P$ versus molar volume per ion pair ($2\bar{M}/\rho$) for fluorides and oxides in the rocksalt, fluorite, rutile and perovskite structures. The data are taken from Tables 5.3-5.7; the molar volumes are listed in Table 5.1. The fluorite and perovskite oxides plot much higher than their fluoride counterparts, so that use of the same symbols for oxides and fluorides causes no confusion. $(\partial K_S/\partial T)_P$ for ThO_2 is taken from Spinner et al. (1963).

(2) Except for the rocksalts and SnO_2, the oxides are characterised by high values of $(\partial K_S/\partial T)_P$, ≅ -0.36 to -0.41 kbar. deg^{-1}. In general, values of $(\partial K_S/\partial T)_P$ for the fluorides lie between -0.15 and -0.20 kbar. $deg.^{-1}$.

Values of $(\partial \mu/\partial T)_P$ are plotted versus molar volume per ion pair on a log-log diagram in Figure 5.7. (1) We can note a fairly well defined trend for the rocksalt fluorides and oxides in which $|(\partial \mu/\partial T)_P|$ decreases with increasing molar volume. Similar behaviour occurs for the fluorite-structure fluorides. The rutile-structure compounds do not exhibit systematic behaviour. (2) $(\partial \mu/\partial T)_P$ appears to be much more sensitive to volume than does $(\partial K_S/\partial T)_P$; at small molar volumes (e.g., LiF and MgO), $|(\partial \mu/\partial T)_P|$ is larger than $|(\partial K_S/\partial T)_P|$, while at larger molar volumes the reverse is true.

It should be pointed out here that the values of $(\partial \mu/\partial T)_P$ are the average of the values calculated for the Voigt and Reuss bounds. For the rutile-structure compounds, $(\partial K_S/\partial T)_P$ is determined in a similar manner. The validity of this approach is supported by the comparison of our calculated $(\partial K_S/\partial T)_P$ and $(\partial \mu/\partial T)_P$ for MgF_2 with the measured values for polycrystalline samples of Bailey et al. (1975) and Rai and Manghnani (1976).

$(\partial K_S/\partial T)_P$ (kbar deg^{-1})	$(\partial \mu/\partial T)_P$ (kbar deg^{-1})		
0.160	0.079		This work
0.154	0.098		Bailey et al. (1975)
0.160	0.092	A	Rai and Manghnani (1976)
0.155	0.088	B	

Thus we can perhaps expect that the values of $(\partial K_S/\partial T)_P$ and $(\partial \mu/\partial T)_P$ for polycrystalline aggregates should reflect any existing trends for the derivatives of the single crystal moduli.

We can examine Figure 5.6 and 5.7 in the framework of the fluoride-

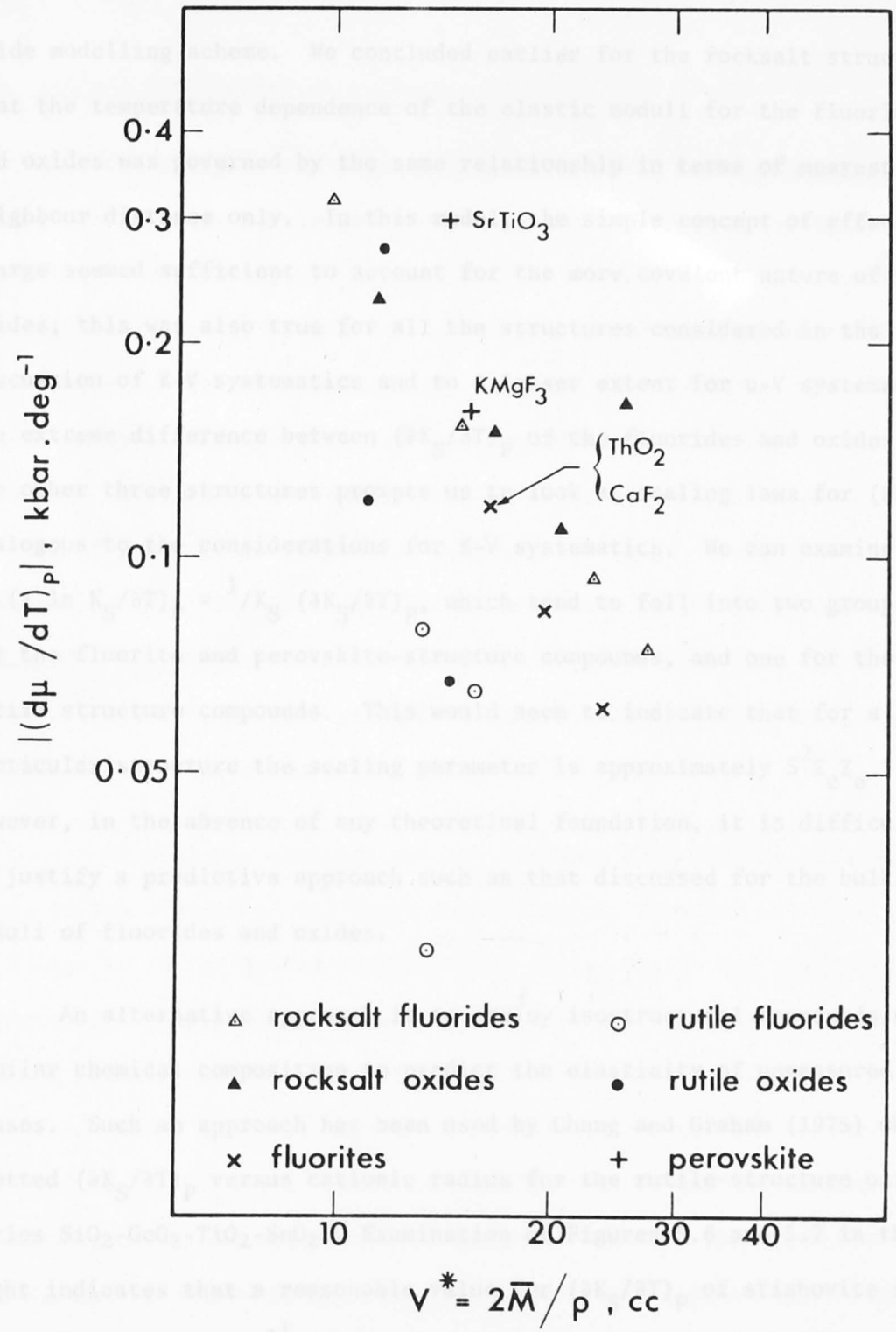

Figure 5.7: Log-log plot of $|(\partial\mu/\partial T)|_p$ versus molar volume per ion pair ($2\bar{M}/\rho$) for fluorides and oxides in the rocksalt, fluorite, rutile and perovskite structures. The data are taken from Tables 5.3-5.7; the molar volumes are listed in Table 5.1. $(\partial\mu/\partial T)_p$ for ThO_2 is taken from Spinner et al. (1963).

oxide modelling scheme. We concluded earlier for the rocksalt structure that the temperature dependence of the elastic moduli for the fluorides and oxides was governed by the same relationship in terms of nearest neighbour distance only. In this model, the simple concept of effective charge seemed sufficient to account for the more covalent nature of the oxides; this was also true for all the structures considered in the discussion of K-V systematics and to a lesser extent for μ-V systematics. The extreme difference between $(\partial K_S/\partial T)_P$ of the fluorides and oxides for the other three structures prompts us to look at scaling laws for $(\partial K_S/\partial T)_P$, analogous to the considerations for K-V systematics. We can examine values of $(\partial \ln K_S/\partial T)_P = {}^1/K_S \ (\partial K_S/\partial T)_P$, which tend to fall into two groups, one for the fluorite and perovskite-structure compounds, and one for the rutile structure compounds. This would seem to indicate that for a particular structure the scaling parameter is approximately $S^2Z_cZ_a$. However, in the absence of any theoretical foundation, it is difficult to justify a predictive approach such as that discussed for the bulk moduli of fluorides and oxides.

An alternative approach is to employ isostructural compounds of similar chemical composition to predict the elasticity of unmeasured phases. Such an approach has been used by Chang and Graham (1975) who plotted $(\partial K_S/\partial T)_P$ versus cationic radius for the rutile-structure oxide series SiO_2-GeO_2-TiO_2-SnO_2. Examination of Figures 5.6 and 5.7 in this light indicates that a reasonable value for $(\partial K_S/\partial T)_P$ of stishovite should be -0.38±0.1 kbar. deg^{-1}. This is certainly consistent with the value of -0.35 kbar. deg^{-1} for $(\partial K_S/\partial T)_P$ obtained by Graham (1973) from the reduction of shock wave data for stishovite. A similar estimate can be made for $(\partial K_S/\partial T)_P$ for the perovskite-structure polymorph of $MgSiO_3$. The systematics for $(\partial \mu/\partial T)_P$ for the rutile and perovskite structures are too inconclusive to enable predictions to be made for stishovite and $MgSiO_3$-perovskite.

5.5 $(\partial c/\partial P)$ systematics

The study of the relationship of $(\partial c/\partial P)_T$ to crystallographic parameters has been furthered by the discussion of Davies (1975). Davies demonstrated for the alkali halides that $K' = (\partial K/\partial P)_{T,P=0}$ is remarkably constant, and that $K\mu'/\mu$ where $\mu' = (\partial \mu/\partial P)_{T,P=0}$ decreases monotonically with increasing cationic radius. K' does not vary systematically for the oxides and silicates, although a tendency of $K\mu'/\mu$ for a particular structure to decrease with increasing cationic radius was noted by Davies. In view of the results of central force models (e.g., O. L. Anderson and Liebermann, 1970) that account for the behaviour of $(\partial c'/\partial P)_T$ and $(\partial c_{44}/\partial P)_T$ for simple cubic lattices, Davies postulated that the trends he observed for $K\mu'/\mu$ were probably a simple, though as yet undetermined, function of crystal structure.

We will now consider our new pressure data for the perovskite $KMgF_3$ in the context of the above relationships, together with the values of K' and $K\mu'/\mu$ for oxides and fluorides in the rutile and perovskite structures. In Figure 5.8 we have plotted K' and $K\mu'/\mu$ versus a mean lattice spacing per ion pair. For K', no systematic trend can be discerned except that, in general, K' is larger for the oxides than for the fluorides. We can at least conclude that K' should lie between 5 and 7 for stishovite and the perovskite phase of $MgSiO_3$. The trend for $K\mu'/\mu$ for the rutile oxides is approximately linear as described by Davies. MgF_2 lies fairly close to this trend, in contrast to NiF_2 for which μ' is negative. The low values of μ' seem to be characteristic of the rutile structure (see Tables 5.5 and 5.6). Extrapolation along the rutile oxide trend leads to a value between 2 and 3 for $K\mu'/\mu$ for stishovite. In the absence of sufficient data to define a trend for the perovskites and in view of the fact that $K\mu'/\mu$ appears to decrease with increasing interionic distance, we can place a lower limit of 3 on $K\mu'/\mu$ for the perovskite-structure $MgSiO_3$.

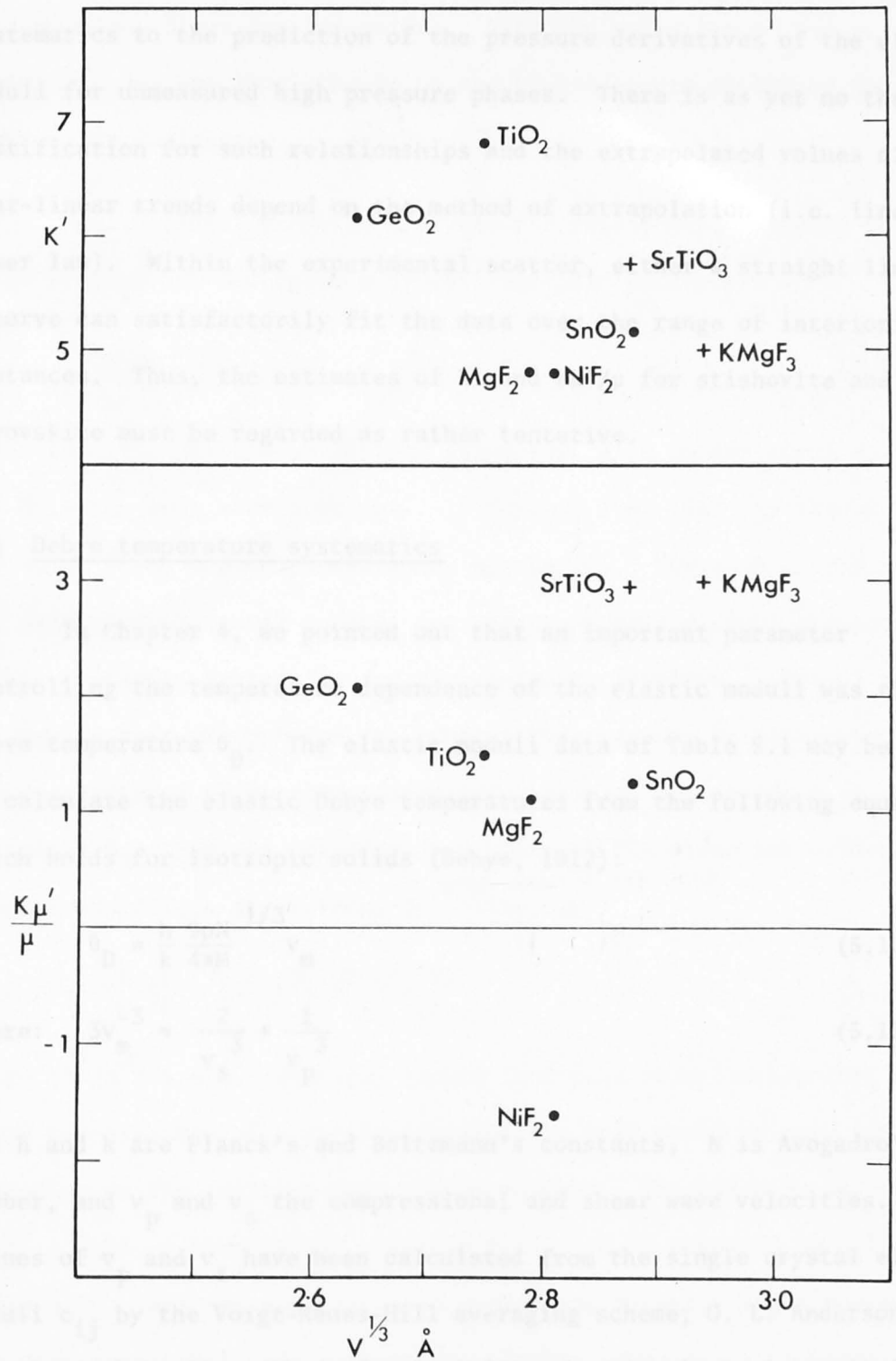

Figure 5.8: Plot of K' and Kμ'/μ versus mean atomic spacing, $V^{1/3}$, where V is the volume per ion pair, for fluorides and oxides in the rutile and perovskite structures. Values of K' and μ' are listed in Tables 5.5-5.7, while those for K and μ appear in Table 5.1. The volume per ion pair is calculated from the molar volume listed in Table 5.1.

It is wise to be cautious in the application of the above systematics to the prediction of the pressure derivatives of the elastic moduli for unmeasured high pressure phases. There is as yet no theoretical justification for such relationships and the extrapolated values along near-linear trends depend on the method of extrapolation (i.e. linear or power law). Within the experimental scatter, either a straight line or a curve can satisfactorily fit the data over the range of interionic distances. Thus, the estimates of K' and $K\mu'/\mu$ for stishovite and $MgSiO_3$-perovskite must be regarded as rather tentative.

5.6 Debye temperature systematics

In Chapter 4, we pointed out that an important parameter controlling the temperature dependence of the elastic moduli was the Debye temperature θ_D. The elastic moduli data of Table 5.1 may be used to calculate the elastic Debye temperatures from the following equation, which holds for isotropic solids (Debye, 1912):

$$\theta_D = \frac{h}{k}\left(\frac{9\rho N}{4\pi M}\right)^{1/3} v_m \qquad (5.10)$$

where: $$3v_m^{-3} = \frac{2}{v_s^3} + \frac{1}{v_p^3} \qquad (5.11)$$

and h and k are Planck's and Boltzmann's constants, N is Avogadro's number, and v_p and v_s the compressional and shear wave velocities. The values of v_p and v_s have been calculated from the single crystal elastic moduli c_{ij} by the Voigt-Reuss-Hill averaging scheme; O. L. Anderson (1963) has shown that this method of calculating the elastic θ_D is equivalent to the more rigorous method of averaging the eigenfrequencies over all possible normal modes and directions of the crystal. Wherever possible, the Debye temperatures given in Table 5.1 have been calculated using the elastic constant data near 0°K; in the other cases, room temperature elastic data were employed so that the values of θ_D will be underestimated.

In Table 5.9 we also list the ratios of the Debye temperatures for the corresponding fluorides and oxides. With the exception of the pairs containing BaO and ThO_2, the θ_D of the fluorides are 65-80% of those for their oxide analogues.

Gmelin (1970) proposed a systematic relationship between the Debye temperature and certain crystallographic parameters:

$$\theta_D = \frac{A}{a\bar{M}^{1/2}} \qquad (5.12)$$

where $a = V^{*1/3}$ is a mean lattice parameter, A is an empirical constant, and $\bar{M}$ is the mean atomic weight. In Table 5.1 we list the values of $A = a\theta_D\bar{M}^{1/2}$ for the compounds under discussion. For each of the fluoride and oxide isostructural groups, the values of this product are approximately constant, especially for the rocksalt structure. Some of the scatter in this product for the other structures may be attributable to the necessity of using room temperature elastic constant data to calculate θ_D. For the corresponding pairs of fluorides and oxides, the Debye temperatures should thus be related by:

$$\theta_D^F/\theta_D^O = (A^F/A^O)(\bar{M}^O/\bar{M}^F)^{1/2} \qquad (5.13)$$

where $(A^F/A^O) \approx 0.6$. We might expect from this relationship that the Debye temperatures of a particular analogue pair could be very similar, depending on the relative mean atomic weights. For LiF-MgO, for instance, $\bar{M}^O/\bar{M}^F = 1.55$ so that (5.13) predicts $\theta_D^F/\theta_D^O = 0.75$ compared to 0.77 in Table 5.9. Thus for some analogue pairs, the fluoride might not be expected to exhibit high temperature elastic behaviour at substantially lower temperatures than the oxide.

Table 5.9: Ratios of Melting (T_m) and Debye (θ_D) Temperatures for Oxide-Fluoride Analogue Pairs

Pair	T_m^F/T_m^O	θ_D^F/θ_D^O
LiF-MgO	0.36	0.77
NaF-CaO	0.44	0.73
KF-SrO	0.42	0.72
RbF-BaO	0.46	0.76
KF-BaO	0.49	1.12
CaF_2-ThO_2	0.48	1.21
MgF_2-TiO_2	0.73	0.79
MnF_2-SnO_2	0.59	0.72
$KMgF_3$-$SrTiO_3$	0.56	0.79

CHAPTER 6

SUMMARY OF CONCLUSIONS

6.1 Introduction

6.2 High temperature elasticity

6.3 Systematics in elastic moduli and their pressure and temperature derivatives

6.4 Final conclusions on the fluoride-oxide modelling scheme

CHAPTER 6

SUMMARY OF CONCLUSIONS

6.1 Introduction

Goldschmidt's modelling scheme based on crystal chemical considerations is the origin of both the germanate-silicate and fluoride-oxide analogue concepts. The success of the germanate modelling scheme in predicting the high pressure phases of silicates and in examining their elasticity prompted investigation of the fluoride-oxide modelling scheme in the context of high temperature elasticity. There were two aspects to our approach. The first involved examination of the temperature dependence of the elastic moduli in the framework of equations of state to determine whether the fluorides exhibited "high temperature" elastic behaviour at lower absolute temperatures than the oxides. This would enable evaluation of high temperature derivatives at accessible laboratory temperatures, using fluoride models. Our second aim was to determine the relationship between the temperature derivatives of the elastic moduli for the fluorides and oxides, with a view to predicting the high temperature elastic behaviour of the oxides.

The scarcity of data and the dubious quality of some of the existing data made the above comparisons impossible. We therefore developed the capacity to measure the elastic moduli as a function of temperature, using the precise pulse superposition technique, for single crystal fluorides crystallising in the rocksalt, fluorite, rutile and perovskite structures. Our new data are in good agreement with data from other investigators at room temperature and are demonstrably superior to existing high temperature data. Evaluation of our data in the context of high temperature equations of state and systematics in the elastic moduli and their pressure and temperature derivatives lead to the following conclusions.

6.2 High temperature elasticity

Classical lattice dynamic theories predict that the elastic moduli should exhibit a linearly decreasing dependence on temperature for temperatures greater than the Debye temperature, θ_D. These theories are couched in terms of volume and temperature as the independent variables so that the prediction of high temperature linearity applies strictly to constant volume rather than constant pressure space. Examination of our new high temperature data demonstrates:

(1) The fluorides do not appear to exhibit "high temperature" elastic behaviour at substantially lower absolute temperatures than do the oxides. This was illustrated for the fluoride-oxide analogue pairs, LiF-MgO and MgF_2-TiO_2. This result is not inconsistent with the relative magnitude of the Debye temperatures.

(2) In the experimental temperature range, the c-T data at constant pressure (1 bar) continue to exhibit curvature, rather than the predicted linearity. For CaF_2, SrF_2, BaF_2 and MgF_2, the deviation from linearity is consistent with the experimental variables being P and T, and can be largely eliminated by the correction to constant volume. However, for the c' and c_{44} modes for LiF and NaF, the curvature is in the opposite sense, and correction to constant volume merely accentuates the deviation from linearity. This demonstrated concave upward curvature in the c-T plot must have important implications for lattice dynamical theories.

6.3 Systematics in elastic moduli and their pressure and temperature derivatives

Our new data were combined with data from the literature in order to examine established and postulated elasticity systematics in terms of the fluoride-oxide modelling scheme.

(1) Fluorides are excellent models for the oxides using bulk modulus-volume systematics. A uniform relative effective charge of S = 0.75 of the fluorides with respect to the oxides for all of the structures considered permits the prediction of the bulk modulus of an oxide from that of its fluoride analogue. The data for the more complex rutile and perovskite structures do not fit the KV = constant systematics quite as well as the data for the rocksalt and fluorite structures.

(2) A systematic trend of $\mu V^{*4/3}$ = constant is evident in a shear modulus-volume plot, although there is no theoretical foundation for such a trend. An analogous evaluation of the relative effective charge leads to values of S which are more structure sensitive, thus disallowing the fluoride-oxide predictive approach for shear moduli. Consideration of the isostructural trends for the oxides leads to a value of μ of 1.7 Mbar for the perovskite-structure polymorph of $MgSiO_3$.

(3) Several very interesting features emerge from the examination of the temperature derivatives of the elastic moduli for the fluorides and oxides. (a) The rocksalt fluorides and oxides and the fluorite fluorides exhibit trends of decreasing $|(\partial c/\partial T)_P|$ with increasing molar volume; such trends are not in evidence for the rutile-structure compounds. (b) The values of $(\partial c/\partial T)_P$ are very similar for the members of a rocksalt fluoride-oxide analogue pair; analogue pairs for the other structures do not exhibit such similarity. (c) For all the structures considered, $(\partial K_S/\partial T)_P$ is dominated by extrinsic temperature dependence; in some cases e.g., the alkali fluorides, K_S actually increases very slowly with temperature at constant volume. In contrast, for $(\partial \mu/\partial T)_P$, the intrinsic component is at least as important as the extrinsic component. The above result leads us to speculate that static lattice models which describe the effect of volume change on the elastic moduli might provide reasonable values for $(\partial K_S/\partial T)_P$.

A simple model incorporating Mitskevich's theory with K-V systematics was employed to explain the observed behaviour for $(\partial c/\partial T)_P$ for the rocksalt fluorides and oxides in terms of nearest-neighbour distance only. The values of $(\partial K_S/\partial T)_P$ and $(\partial \mu/\partial T)_P$ were plotted versus molar volume for all the structures considered. As expected from our model, the rocksalt fluorides and oxides and fluorite fluorides exhibited systematic trends in these plots. In general, and excluding the rocksalt structure, values of $|(\partial K_S/\partial T)_P|$ are very much higher for the oxides than for the fluorides and appear to be scaled as $S^2 Z_c Z_a e^2$. Using an isostructural, isochemical predictive approach, values of $(\partial K_S/\partial T)_P = 0.38 \pm 0.1$ kbar. deg^{-1} were estimated for both stishovite and the perovskite-phase of $MgSiO_3$.

6.4 Final conclusions on the fluoride-oxide modelling scheme

The fluoride-oxide modelling scheme centred on the structural correspondences between fluoride-oxide analogue pairs with similar ionic radii. The "weakened model" concept suggested that the difference in physical properties could be attributed to the fact that the valence charges of the fluorides were half those for the oxides. This model was shown to give a good representation of the bulk moduli of the fluorides relative to those of the oxides, although an effective charge was invoked to account for the partial covalency of the oxides. The shear moduli of fluorides and oxides also appear to be related in an analogous manner.

The similarity in the temperature derivatives of the elastic moduli for fluoride-oxide analogue pairs in the rocksalt structure can be explained in terms of a simple model where the interionic distance is the only parameter. Here again, the simple concept of an effective charge is sufficient to account for the more covalent nature of the oxides. However, for the fluorite, rutile and perovskite structures, such similarities in the values of $(\partial c/\partial T)_P$ for a fluoride-oxide analogue pair do not appear. It must be assumed for these structures that the

higher degree of covalency for the oxides plays a much more important role in determining $(\partial c/\partial T)_p$. In the absence of a theoretical basis for these differences in $(\partial c/\partial T)_p$ for the fluorides and oxides, it is wiser to examine isostructural, isochemical relationships for predicting the elasticity of unmeasured phases.

As a predictive tool for the high temperature elasticity of the oxides, the fluoride-oxide analogue scheme is limited. Only for the rocksalt structure can we estimate values of $(\partial c/\partial T)_p$ for the oxides from those of the fluorides. In addition, we have shown that the fluorides do not exhibit high temperature elastic behaviour at significantly lower absolute temperatures than their oxide analogues. However, in the absence of good single crystals of oxides and silicates, measurement of fluoride structural analogues does provide information on the relationship of elasticity to crystallographic parameters for a particular structure. The study of simple ionic compounds in which the forces are fairly well understood is a particularly useful one in increasing our understanding of the behaviour of solids as a function of temperature and pressure. The value of our results for the temperature dependence of the elastic moduli lies in the fact that we have measured structural analogues of important mantle phases.

The limited success of the fluoride-oxide modelling scheme prompts suggestions for the direction of future research: (1) The study of analogue compounds isostructural and isochemical with high pressure phases, to avoid difficulties raised in the fluoride-oxide modelling scheme by the difference in bonding type. (2) Development of the theoretical basis for systematics in the pressure and temperature derivatives of the elastic moduli. In particular, the modified rigid ion models of Striefler and Barsch (1973, 1974, 1975) might be extended to provide theoretical estimates of $(\partial c/\partial T)_p$. (3) Development of

experimental techniques to measure the elasticity of high pressure phases of analogue compounds in situ after synthesis as a function of pressure and temperature. A further possibility is the extension of the temperature range of measurement of the elastic moduli at constant pressure by the use of improved bonding techniques.

APPENDIX A

CALCULATION OF CRYSTAL MISORIENTATION EFFECTS

The relationship between the misoriented axes and the crystallographic axes is illustrated in Figure A.1, where, following Waterman (1959), $\{y_i\}$ are the pure mode axes and $\{x_i\}$ are the misoriented axes. The polar misorientation angle θ together with the angle ϕ are given in Table A.1 for the propagation directions of interest for each crystal.

Waterman has derived expressions for the fractional change in velocity, $(\Delta v/v)$, arising from the misorientation, in terms of the angles θ and ϕ. We have used these expressions directly in calculating the relative change in the elastic moduli, c, for crystals with cubic and tetragonal symmetry.

The effect of crystal misorientation on the temperature derivatives of the elastic moduli, $\dot{c}$, can be calculated as follows:

$$\frac{\Delta\dot{c}}{\dot{c}} = \frac{\dot{c}-\dot{c}_o}{\dot{c}} = \frac{\frac{\partial}{\partial T}(\rho(v+\Delta v)^2) - \frac{\partial}{\partial T}(\rho v^2)}{\frac{\partial}{\partial T}(\rho(v+\Delta v)^2)} \qquad (A.1)$$

Neglecting terms of order $(\Delta v)^2$, equation (A.1) becomes

$$\frac{\Delta\dot{c}}{\dot{c}} = \frac{\frac{\partial}{\partial T}[\rho v^2 + 2\rho v\Delta v - \rho v^2]}{\frac{\partial}{\partial T}(\rho(v+\Delta v)^2)}$$

$$= \frac{2\rho v^2 \frac{\partial}{\partial T}\left(\frac{\Delta v}{v}\right)}{\frac{\partial}{\partial T}(\rho+\Delta v)^2)} + 2\left(\frac{\Delta v}{v}\right)\frac{\frac{\partial}{\partial T}(\rho v^2)}{\frac{\partial}{\partial T}(\rho(v+\Delta v)^2)}$$

$$\approx \frac{2\dot{c}}{\dot{c}}\frac{\partial}{\partial T}\left(\frac{\Delta v}{v}\right) + 2\left(\frac{\Delta v}{v}\right) \qquad (A.2)$$

Waterman's equations for $(\Delta v/v)$ can then be differentiated with respect to T to evaluate $\frac{\partial}{\partial T}\left(\frac{\Delta v}{v}\right)$ in (A.2).

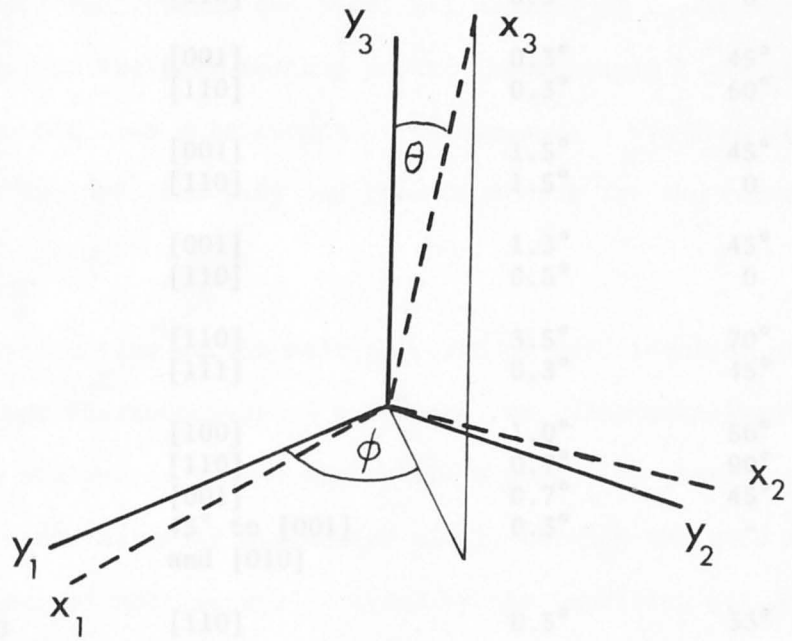

Figure A.1: Relationship between the misoriented axes and the crystallographic axes for crystals of cubic and tetragonal symmetry.

TABLE A.1: Misorientation angles† for each of the seven crystals studied

Compound	Direction	θ	ϕ
LiF	[001]	0.3°	45°
	[110]	0.3°	0
NaF	[001]	0.3°	45°
	[110]	0.3°	60°
CaF_2	[001]	1.5°	45°
	[110]	1.5°	0
SrF_2	[001]	1.3°	45°
	[110]	0.5°	0
BaF_2	[1$\bar{1}$0]	3.5°	70°
	[1$\bar{1}$1]	0.3°	45°
MgF_2	[100]	1.0°	56°
	[110]	0.7°	90°
	[001]	0.7°	45°
	45° to [001] and [010]	0.3°	-
$KMgF_3$	[110]	0.5°	33°

† θ and ϕ are defined in Figure A.1

APPENDIX B

CALIBRATION OF THERMOCOUPLES

The melting point of gold and the boiling point of water were used as calibration points for the platinum-platinum 10% rhodium thermocouples. The initial and final calibration of thermocouple 1 were made against the gold melting point; thermocouple 2 was calibrated with thermocouple 1 as a reference. Thermocouple 2 was used for the measurements for SrF_2 and BaF_2 and thermocouple 1 for the remainder of the crystals.

The calibration at the melting point of gold involved placement of two adjacent thermocouples in a furnace: one, the uncalibrated thermocouple and one, a thermocouple with a gold wire completing the junction. As the assembly was heated slowly through the gold melting point, evidence of melting was provided by the levelling out of the "gold" thermocouple temperature (see Figures B.1 and B.2). This temperature was taken to be 1064.4°C (Weast, 1972) and the corresponding temperature as measured by the unknown thermocouple was noted. Thermocouple 1 was estimated to be correct to within 2°C. Subsequent calibration indicated that thermocouples 1 and 2 agreed almost exactly with each other. Figures B.1 and B.2 illustrate that thermocouple 1 was not contaminated during the experimental runs.

Both thermocouples were calibrated against the boiling point of distilled water and were found to be correct to within 1°C. The barometric pressure was taken into account in estimating the corrected boiling point of water according to the tabulations in Weast (1972).

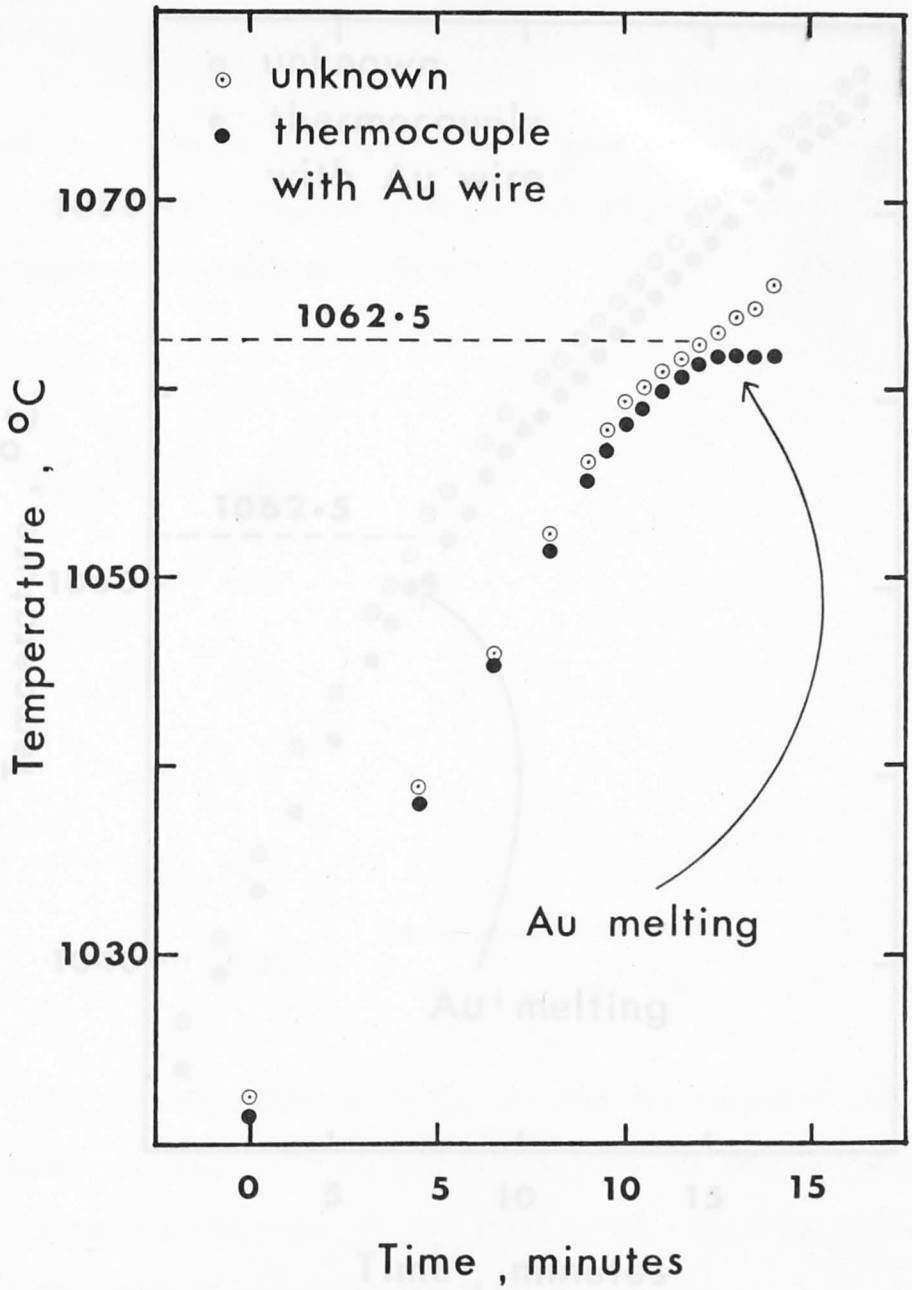

Figure B.1: Initial calibration of thermocouple 1 against the melting point of gold.

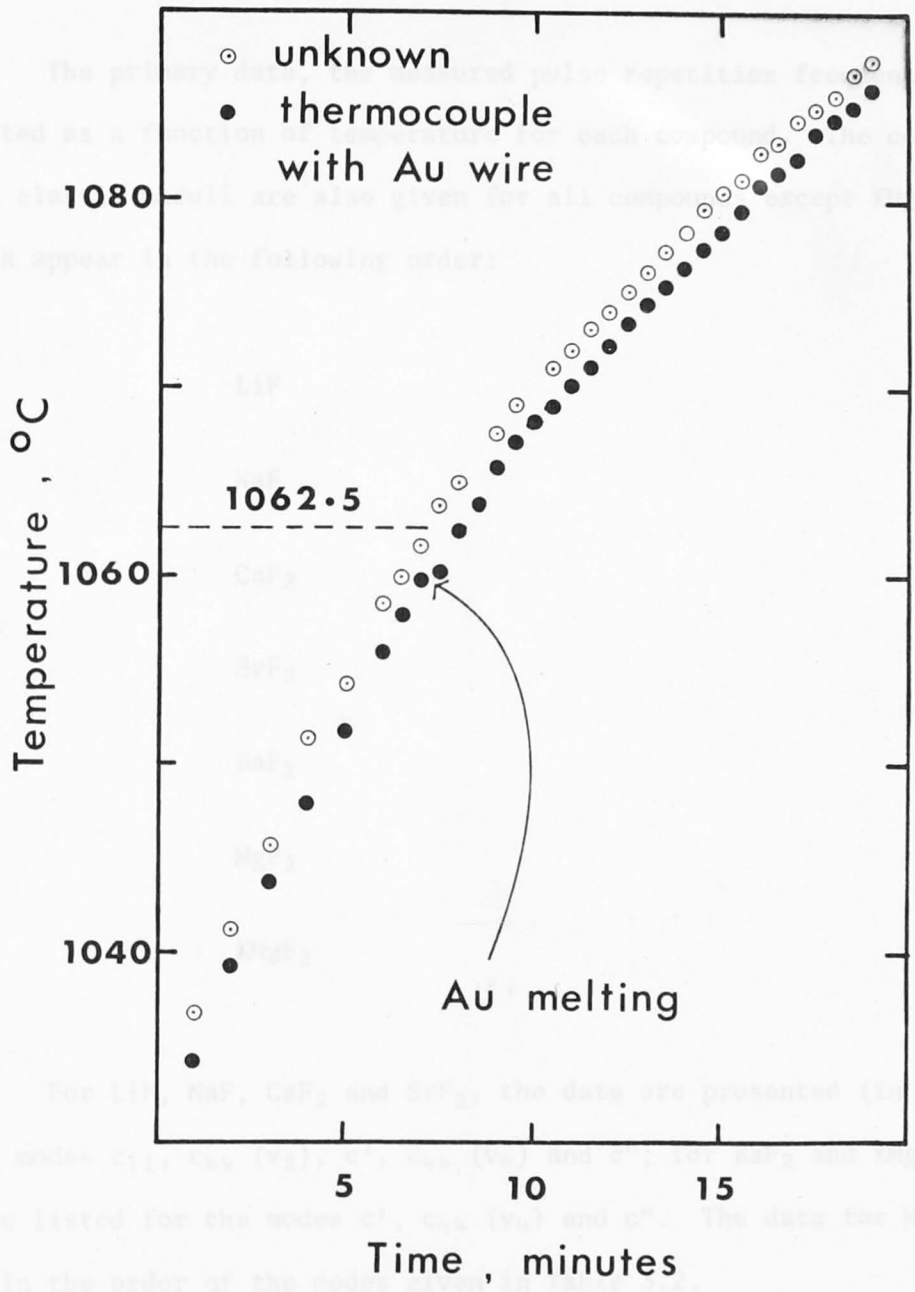

Figure B.2: Final calibration of thermocouple 1 against the melting point of gold.

APPENDIX C

RAW DATA

The primary data, the measured pulse repetition frequencies, are listed as a function of temperature for each compound. The corresponding elastic moduli are also given for all compounds except $KMgF_3$. The data appear in the following order:

LiF

NaF

CaF_2

SrF_2

BaF_2

MgF_2

$KMgF_3$

For LiF, NaF, CaF_2 and SrF_2, the data are presented (in order) for the modes c_{11}, c_{44} (v_2), c', c_{44} (v_4) and c"; for BaF_2 and $KMgF_3$, the data are listed for the modes c', c_{44} (v_4) and c". The data for MgF_2 appear in the order of the modes given in Table 3.2.


LiF

RAW DATA FOR LITHIUM FLUORIDE

C = C11 , MODE IS P [001]

LENGTH (298) = .2894 INCHES , DENSITY(298) = 2.6413 GM/CC

TEMPERATURE (DEGREES K)	FREQUENCY (KHZ)	MODULUS,C (MBAR)
294.3	448.29	1.147308
309.4	446.31	1.136609
312.4	445.88	1.134333
319.9	444.78	1.128435
321.9	444.49	1.126863
323.1	444.35	1.126133
324.5	444.15	1.125041
325.6	443.94	1.123986
326.4	443.88	1.123627
326.5	443.83	1.123370
326.8	443.78	1.123106
326.9	443.76	1.123001
327.1	443.72	1.122790
327.2	443.69	1.122660
327.3	443.69	1.122606
327.3	443.66	1.122479
327.4	443.63	1.122349
327.6	443.62	1.122283
327.9	443.56	1.121976
327.9	443.58	1.122052
327.9	443.56	1.121976
327.8	443.56	1.121954
332.1	443.26	1.119263
334.9	442.65	1.117660
337.9	442.25	1.114953
341.2	441.79	1.112508
344.5	441.38	1.110317
346.7	441.09	1.108774
348.3	440.83	1.107406
349.1	440.74	1.106923
350.5	440.57	1.106015
351.5	440.42	1.105198
352.1	440.31	1.104623
352.2	440.28	1.104494
352.5	440.25	1.104332
352.5	440.21	1.104131
352.5	440.19	1.104056
352.6	440.17	1.103952
352.6	440.15	1.103851
352.6	440.15	1.103851
352.6	440.13	1.103751
352.6	440.13	1.103751
352.5	440.13	1.103755
352.3	440.14	1.103788
352.3	440.15	1.103813

TEMPERATURE (DEGREES K)	FREQUENCY (KHZ)	MODULUS,C (MBAR)
424.6	430.21	1.051753
424.1	430.06	1.051040
423.2	430.31	1.052296
422.6	430.22	1.051882
422.2	430.44	1.052950
422.1	430.49	1.053223
421.9	430.50	1.053260
421.8	430.53	1.053455
421.8	430.56	1.053553
421.7	430.56	1.053606
421.6	430.57	1.053635
421.6	430.56	1.053610
427.1	429.78	1.049551
440.9	427.76	1.039152
443.7	427.37	1.037120
444.3	427.28	1.036708
444.7	427.22	1.036400
445.4	427.13	1.035911
446.9	426.93	1.034880
447.4	426.88	1.034617
448.4	426.74	1.033898
450.2	426.51	1.032735
450.2	426.51	1.032687
450.2	426.50	1.032662
449.9	426.50	1.032675
449.9	426.50	1.032675
480.4	422.28	1.011125
489.9	420.98	1.004493
491.6	420.76	1.003373
494.2	420.42	1.001621
495.4	420.24	1.000713
498.8	419.72	.998145
501.3	419.38	.996400
501.4	419.35	.996230
501.5	419.33	.996155
501.4	419.32	.996111
501.3	419.32	.996115
501.3	419.32	.996115
500.9	419.33	.996180
506.1	418.78	.993375
506.7	418.67	.992781
508.8	418.42	.991508
513.4	417.71	.987978
515.9	417.36	.986218
516.4	417.31	.985937

351.6	440.33	1.104793	518.3	416.99	.984370
355.1	439.88	1.102376	520.0	416.77	.983260
357.8	439.50	1.100367	520.8	416.65	.982684
359.5	439.24	1.098975	522.0	416.49	.981832
359.8	439.19	1.098738	522.3	416.44	.981631
363.2	438.70	1.096156	528.4	415.73	.978008
363.6	438.65	1.095865	533.5	414.99	.974291
366.3	438.22	1.093613	540.0	414.06	.969656
366.6	438.18	1.093426	543.6	413.53	.967023
370.3	437.69	1.090838	544.5	413.35	.966190
372.5	437.37	1.089182	547.3	412.99	.964343
372.6	437.34	1.089004	549.5	412.63	.962616
372.8	437.33	1.088971	549.4	412.65	.962690
372.8	437.33	1.088922	549.0	412.65	.962684
372.6	437.30	1.088805	548.7	412.67	.962813
372.6	437.31	1.088830	548.3	412.72	.963064
372.5	437.30	1.088809	554.3	411.97	.959336
372.3	437.31	1.088891	554.3	411.94	.959197
372.2	437.32	1.088920	554.3	411.94	.959197
371.6	437.38	1.089243	554.3	411.94	.959197
371.5	437.40	1.089371	560.5	411.12	.955119
371.3	437.42	1.089478	566.0	410.36	.951335
371.3	437.44	1.089528	569.6	409.79	.948541
371.5	437.44	1.089520	570.4	409.72	.948206
371.5	437.44	1.089520	575.6	408.97	.944517
371.6	437.42	1.089467	576.0	406.92	.944223
377.2	436.72	1.085763	576.2	408.90	.944145
381.3	436.16	1.082795	576.3	408.88	.944071
384.1	435.77	1.080749	593.2	406.49	.932326
387.3	435.29	1.078244	593.2	406.50	.932372
391.5	434.72	1.075231	593.3	406.47	.932253
394.2	434.37	1.073394	612.0	403.90	.919705
397.9	433.82	1.070555	612.0	403.90	.919659
398.4	433.74	1.070165	612.2	403.89	.919628
398.6	433.72	1.070009	637.8	400.01	.900974
398.7	433.69	1.069907	638.8	399.94	.900593
398.7	433.69	1.069857	640.0	399.78	.899844
398.6	433.69	1.069861	640.5	399.72	.899552
398.4	433.69	1.069894	641.2	399.62	.899049
397.6	433.78	1.070394	642.6	399.44	.898201
397.5	433.81	1.070497	643.6	399.32	.897596
397.5	433.81	1.070546	644.6	399.19	.896991
397.6	433.81	1.070542	645.6	398.94	.895825
397.6	433.82	1.070567	646.2	398.93	.895731
401.2	433.42	1.068426	646.3	398.90	.895592
407.9	432.46	1.063432	646.8	398.84	.895301
637.8	400.06	.901154	647.4	398.78	.894984
411.7	431.86	1.060356	647.8	398.74	.894832
413.9	431.65	1.059237	648.7	398.60	.894165
414.3	431.57	1.058828	650.4	398.38	.893104
420.8	430.81	1.054842	485.3	421.65	1.007884
423.6	430.40	1.052722			

RAW DATA FOR LITHIUM FLUORIDE

C = C44 , MODE IS S [001] RANDOM POL.

LENGTH (298) = .2894 INCHES , DENSITY(298) = 2.6413 GM/CC

TEMPERATURE (DEGREES K)	FREQUENCY (KHZ)	MODULUS,C (MBAR)	TEMPERATURE (DEGREES K)	FREQUENCY (KHZ)	MODULUS,C (MBAR)
294.0	334.79	.639903	408.5	329.82	.618546
299.0	334.56	.638908	414.1	329.57	.617478
304.5	334.37	.638042	415.1	329.53	.617286
307.3	334.24	.637507	415.7	329.49	.617160
313.2	333.99	.636429	431.3	328.85	.614398
321.8	333.62	.634837	432.3	328.80	.614169
322.1	333.60	.634774	434.4	328.69	.613708
324.9	333.51	.634334	435.0	328.67	.613600
325.7	333.49	.634240	435.6	328.62	.613418
326.2	333.46	.634135	438.0	328.51	.612950
338.6	332.92	.631796	441.2	328.33	.612202
339.4	332.90	.631703	441.5	328.34	.612232
340.0	332.87	.631576	441.7	328.31	.612134
343.1	332.74	.631015	442.0	328.31	.612090
344.4	332.66	.630703	443.0	328.26	.611917
346.6	332.56	.630275	443.7	328.22	.611714
349.0	332.47	.629900	444.9	328.17	.611498
349.5	332.45	.629795	446.2	328.11	.611262
349.6	332.44	.629774	446.5	328.08	.611143
349.9	332.44	.629729	446.9	328.06	.611059
350.0	332.42	.629689	447.7	328.02	.610891
350.2	332.40	.629609	448.1	327.99	.610770
350.4	332.39	.629548	449.3	327.94	.610555
352.6	332.33	.629272	450.2	327.87	.610291
355.0	332.23	.628840	450.9	327.85	.610181
357.0	332.15	.628493	451.3	327.83	.610097
358.1	332.10	.628261	453.2	327.76	.609809
359.0	332.06	.628109	463.0	327.33	.607936
360.7	331.98	.627768	466.0	327.21	.607417
361.1	331.96	.627665	466.4	327.17	.607296
365.1	331.79	.626952	466.9	327.17	.607246
365.7	331.74	.626750	468.6	327.07	.606852
366.9	331.70	.626572	470.0	326.99	.606540
368.5	331.63	.626290	471.3	326.93	.606267
369.1	331.60	.626164	472.7	326.85	.605917
370.1	331.56	.625990	474.7	326.74	.605479
371.6	331.49	.625654	484.6	326.26	.603457
372.0	331.47	.625608	484.7	326.26	.603436
373.5	331.40	.625291	485.1	326.22	.603297
373.7	331.38	.625211	485.2	326.22	.603276
374.3	331.36	.625122	492.7	325.88	.601870
374.6	331.35	.625077	494.6	325.81	.601564
374.5	331.34	.625042	498.7	325.60	.600668
374.7	331.33	.625019	501.6	325.47	.600134
381.3	331.07	.623870	506.2	325.22	.599060

382.3	331.03	.623697	508.5	325.15	.598744
383.3	330.99	.623523	513.9	324.85	.597541
386.3	330.83	.622871	520.5	324.51	.596086
389.6	330.67	.622194	524.9	324.30	.595222
390.9	330.62	.621938	530.6	324.01	.594030
391.9	330.60	.621859	531.0	324.00	.593965
392.3	330.56	.621699	532.2	323.94	.593696
392.4	330.56	.621716	533.4	323.85	.593335
399.1	330.25	.620378	534.2	323.81	.593187
399.7	330.22	.620232	536.5	323.69	.592670
399.6	330.21	.620216	536.8	323.67	.592607
402.5	330.11	.619773	548.6	323.14	.590364
403.1	330.08	.619628	562.6	322.49	.587627
404.3	330.01	.619375	563.6	322.38	.587218
407.6	329.88	.618811			

RAW DATA FOR LITHIUM FLUORIDE

C = (C11-C12)/2 , MODE IS S [110] POL. [1-10]

LENGTH (298) = .2837 INCHES , DENSITY(298) = 2.6413 GM/CC

TEMPERATURE (DEGREES K)	FREQUENCY (KHZ)	MODULUS,C (MBAR)
295.0	245.92	.331774
303.2	244.88	.328886
307.6	244.27	.327209
313.2	243.19	.324255
320.3	242.55	.322468
322.5	242.17	.321454
322.5	242.18	.321481
322.5	242.18	.321474
322.5	242.18	.321488
325.6	241.85	.320565
333.9	240.73	.317520
346.1	239.11	.313116
347.1	238.69	.312020
346.9	238.71	.312068
346.8	238.73	.312114
346.4	238.92	.312635
345.9	238.95	.312719
345.6	239.01	.312873
345.5	239.03	.312927
345.4	239.06	.312987
345.2	239.08	.313048
344.9	239.10	.313116
344.6	239.14	.313211
344.3	239.17	.313313
344.1	239.21	.313407
363.1	236.75	.306789
368.8	235.99	.304761
374.9	235.14	.302497
375.1	235.12	.302443
399.5	231.67	.293389
421.1	228.78	.285870
421.2	228.78	.285869
427.9	227.95	.283719
428.2	227.91	.283629
428.4	227.87	.283521
433.6	227.17	.281731
433.8	227.15	.281661
434.1	227.09	.281534
439.9	226.37	.279688
450.5	224.95	.276157
450.6	224.91	.275958
450.6	224.91	.275952
450.6	224.90	.275946
450.6	224.90	.275946
450.6	224.90	.275946

TEMPERATURE (DEGREES K)	FREQUENCY (KHZ)	MODULUS,C (MBAR)
521.8	215.45	.252497
521.7	215.47	.252551
521.7	215.49	.252581
521.6	215.49	.252599
521.5	215.50	.252618
521.6	215.50	.252629
521.6	215.50	.252629
521.5	215.50	.252630
521.9	215.46	.252526
538.7	213.30	.247297
544.3	212.55	.245495
545.2	212.43	.245220
546.5	212.25	.244797
548.5	211.98	.244147
548.5	211.95	.244089
548.5	211.95	.244084
548.5	211.95	.244084
548.5	211.95	.241603
557.1	210.91	.241398
557.5	210.83	.241165
558.4	210.73	.239857
562.6	210.17	.239453
563.6	210.00	.238719
566.2	209.69	.237525
569.9	209.18	.235773
575.4	208.44	.235726
575.5	208.42	.235727
575.4	208.42	.229782
595.7	205.87	.229532
596.6	205.76	.228880
598.7	205.48	.228812
598.8	205.45	.228722
598.9	205.41	.228720
599.1	205.41	.228717
598.9	205.41	.228729
598.8	205.41	.227234
604.6	204.76	.227105
605.2	204.71	.225571
610.5	204.04	.224930
612.6	203.76	.222957
619.1	202.90	.222615
620.3	202.75	.222240
621.5	202.58	.221755
623.3	202.37	.221760
623.3	202.37	.221732
623.4	202.36	

474.3	221.82	.268185	623.4	202.36	.221732
474.7	221.77	.268066	626.5	202.02	.220961
476.4	221.52	.267431	629.1	201.72	.220261
477.9	221.26	.266781	629.6	201.61	.220032
477.9	221.26	.266781	630.8	201.47	.219698
477.9	221.27	.266811	631.8	201.32	.219377
477.8	221.28	.266831	633.4	201.13	.218946
481.1	220.90	.265885	634.8	200.94	.218524
483.8	220.50	.264906	637.2	200.65	.217863
485.8	220.23	.264230	637.9	200.53	.217600
501.2	218.29	.259418	639.3	200.37	.217228
502.4	218.10	.258971	640.1	200.26	.216992
505.1	217.72	.258034	641.8	200.03	.216476
505.1	217.69	.257969	642.2	199.98	.216353
505.1	217.72	.258017	643.5	199.82	.215983
504.9	217.71	.258013	643.8	199.78	.215904
504.7	217.72	.258033	645.5	199.58	.215443
504.6	217.73	.258046	645.8	199.51	.215294
504.5	217.74	.258088	646.6	199.44	.215151
503.8	217.85	.258351	649.4	199.09	.214362
503.7	217.86	.258370	649.4	199.07	.214314
503.7	217.86	.258370	649.5	199.06	.214281
508.6	217.30	.256990	649.4	199.05	.214260
512.1	216.80	.255777	649.3	199.06	.214283
513.1	216.66	.255442	649.2	199.07	.214316
515.7	216.34	.254660	649.2	199.14	.214461
516.6	216.21	.254332	649.5	199.09	.214361
517.5	216.07	.254005	650.4	199.01	.214180
520.9	215.60	.252871	650.9	198.95	.214040
522.1	215.45	.252494	652.6	198.76	.213619
523.6	215.25	.252021	655.7	198.32	.212642
523.3	215.24	.251989	657.7	198.00	.211920
521.9	215.43	.252449	658.4	197.99	.211902

RAW DATA FOR LITHIUM FLUORIDE

C = C44 , MODE IS S [110] POL. [001]

LENGTH (298) = .2999 INCHES , DENSITY(298) = 2.6413 GM/CC

TEMPERATURE (DEGREES K)	FREQUENCY (KHZ)	MODULUS,C (MBAR)
294.0	322.58	.637931
294.0	322.58	.637931
294.0	322.57	.637911
340.4	320.70	.629560
340.6	320.67	.629458
374.6	319.17	.622836
374.6	319.17	.622797
422.6	317.03	.613398
482.1	314.33	.601577
482.8	314.37	.601732
525.0	312.38	.593069
524.9	312.33	.592863
579.7	309.63	.581270
616.6	307.74	.573218
629.2	307.12	.570571
629.8	307.10	.570481
630.2	307.08	.570377
630.2	307.06	.570340

RAW DATA FOR LITHIUM FLUORIDE

C = (C11+C12+2C44)/2 , MODE IS P [110]

LENGTH (298) = .2837 INCHES , DENSITY(298) = 2.6413 GM/CC

TEMPERATURE (DEGREES K)	FREQUENCY (KHZ)	MODULUS,C (MBAR)	TEMPERATURE (DEGREES K)	FREQUENCY (KHZ)	MODULUS,C (MBAR)
294.3	513.65	1.447466	495.2	494.67	1.332517
297.1	513.46	1.446292	496.4	494.53	1.331724
298.4	513.32	1.445414	497.5	494.41	1.331016
304.3	512.87	1.442631	497.5	494.38	1.330855
308.3	512.49	1.440249	497.5	494.37	1.330828
310.3	512.32	1.439226	497.5	494.37	1.330828
312.9	512.11	1.437951	497.4	494.38	1.330867
319.3	511.53	1.434333	496.1	494.40	1.331067
322.4	511.23	1.432530	509.3	493.24	1.324043
323.6	511.09	1.431688	510.6	493.08	1.323138
323.6	511.10	1.431716	515.3	492.55	1.320033
323.6	511.09	1.431688	519.7	492.03	1.317001
323.7	511.09	1.431683	521.2	491.88	1.316140
323.8	511.08	1.431622	521.5	491.84	1.315883
323.9	511.07	1.431562	521.3	491.81	1.315733
324.1	511.06	1.431496	521.3	491.81	1.315760
324.3	511.04	1.431374	521.1	491.83	1.315878
324.4	511.02	1.431257	520.8	491.87	1.316109
325.9	510.90	1.430485	520.8	491.87	1.316109
343.4	509.36	1.421051	520.6	491.92	1.316388
345.5	509.17	1.419916	520.5	491.94	1.316447
350.9	508.62	1.416528	520.3	491.94	1.316512
351.6	508.51	1.415908	520.6	491.94	1.316495
351.8	508.49	1.415759	520.7	491.94	1.316463
351.8	508.47	1.415704	520.7	491.92	1.316356
351.6	508.47	1.415713	520.8	491.90	1.316270
351.8	508.47	1.415704	521.2	491.88	1.316140
351.6	508.47	1.415713	525.3	491.44	1.313530
351.6	508.49	1.415797	534.9	490.33	1.307089
351.5	508.49	1.415802	542.6	489.65	1.303030
351.5	508.50	1.415858	544.6	489.43	1.301719
353.4	508.36	1.414984	544.6	489.43	1.301719
358.4	507.88	1.412065	544.4	489.44	1.301783
359.9	507.72	1.411100	544.3	489.46	1.301869
361.7	507.56	1.410094	543.9	489.47	1.301998
364.1	507.29	1.408502	543.1	489.53	1.302336
365.6	507.12	1.407510	542.3	489.58	1.302648
367.8	506.91	1.406207	544.8	489.47	1.301893
368.9	506.79	1.405486	551.7	488.79	1.297938
369.8	506.68	1.404830	552.6	488.74	1.297568
384.0	505.63	1.398296	562.6	487.74	1.291744
384.0	505.63	1.398296	564.6	487.55	1.290596
384.3	505.60	1.398087	565.3	487.49	1.290239
384.9	505.51	1.397614	567.7	487.17	1.288407
385.4	505.48	1.397395	570.3	486.88	1.286723

385.6	505.42	1.397026	570.2	486.88	1.286756
396.7	504.35	1.390549	570.2	486.89	1.286782
396.4	504.38	1.390785	570.2	486.90	1.286809
395.6	504.46	1.391240	570.2	486.90	1.286809
395.4	504.48	1.391360	581.8	485.82	1.280462
395.4	504.49	1.391388	585.2	485.50	1.278578
395.3	504.49	1.391393	589.1	485.12	1.276324
395.4	504.49	1.391388	591.9	484.79	1.274451
394.5	504.54	1.391738	593.9	484.58	1.273204
426.1	501.44	1.373026	593.5	484.54	1.273069
426.3	501.36	1.372604	592.9	484.58	1.273262
426.3	501.36	1.372604	592.4	484.65	1.273712
426.2	501.35	1.372555	591.4	484.73	1.274165
425.7	501.36	1.372636	591.2	484.76	1.274308
422.7	501.62	1.374245	591.1	484.77	1.274392
421.8	501.69	1.374676	591.1	484.79	1.274498
420.1	501.87	1.375697	591.2	484.78	1.274413
419.9	501.90	1.375899	591.2	484.78	1.274465
419.8	501.92	1.375987	591.4	484.78	1.274401
419.8	501.92	1.376042	591.6	484.77	1.274363
419.8	501.93	1.376069	591.6	484.75	1.274258
419.8	501.92	1.376042	596.9	484.38	1.271977
419.9	501.92	1.375982	602.3	483.78	1.268512
446.8	499.37	1.360673	605.8	483.49	1.266838
447.1	499.35	1.360520	608.8	483.12	1.264723
447.7	499.28	1.360107	612.3	482.78	1.262737
448.1	499.19	1.359622	614.5	482.60	1.261666
448.9	499.17	1.359443	616.5	482.29	1.259901
448.6	499.20	1.359612	617.7	482.22	1.259465
448.6	499.22	1.359759	618.3	482.10	1.258802
448.4	499.25	1.359906	618.3	482.10	1.258776
448.4	499.24	1.359851	617.9	482.10	1.258852
471.3	496.92	1.346038	617.9	482.12	1.258957
470.9	496.93	1.346087	618.5	482.12	1.258895
470.7	496.97	1.346342	627.5	481.35	1.254370
470.6	496.99	1.346456	629.3	481.16	1.253247
470.6	497.00	1.346483	630.8	480.99	1.252298
470.4	497.01	1.346575	632.7	480.78	1.251065
470.4	497.01	1.346575	634.9	480.53	1.249608
470.6	497.02	1.346591	637.3	480.25	1.248034
470.4	497.03	1.346629	638.2	480.15	1.247487
470.6	497.02	1.346591	639.7	480.00	1.246592
470.7	497.01	1.346559	641.1	479.87	1.245859
470.7	497.01	1.346504	642.5	479.70	1.244867
470.8	497.00	1.346472	643.4	479.58	1.244216
475.5	496.64	1.344266	643.5	479.56	1.244106
475.9	496.62	1.344109	643.5	479.58	1.244158
476.4	496.53	1.343648	643.6	479.56	1.244100
476.7	496.52	1.343551	643.6	479.55	1.244023
476.7	496.50	1.343443	643.6	479.53	1.243945
476.8	496.48	1.343329	643.7	479.54	1.243991
476.7	496.47	1.343307	643.7	479.54	1.243965
476.6	496.49	1.343421	643.7	479.53	1.243939
476.4	496.49	1.343432	643.7	479.54	1.243965
476.1	496.52	1.343584	645.9	479.35	1.242873
474.9	496.62	1.344218	647.5	479.17	1.241818
475.6	496.62	1.344179	648.9	479.01	1.240905
477.3	496.46	1.343166	652.8	478.62	1.238651
479.6	496.24	1.341850	656.1	478.19	1.236202

486.4	495.60	1.338019	657.2	477.99	1.235154
488.6	495.37	1.336710	658.4	477.80	1.234074
490.3	495.19	1.335591	661.2	477.43	1.231995
492.8	494.91	1.333970			

NaF

RAW DATA FOR SODIUM FLUORIDE

C = C11 , MODE IS P [001]

LENGTH (298) = .3731 INCHES , DENSITY(298) = 2.8062 GM/CC

TEMPERATURE (DEGREES K)	FREQUENCY (KHZ)	MODULUS,C (MBAR)
293.6	311.12	.975825
305.5	310.10	.969062
318.7	308.85	.960846
326.6	308.09	.955870
329.3	307.79	.953922
329.4	307.78	.953857
337.5	307.05	.949076
346.7	306.13	.943099
348.1	305.99	.942191
360.4	304.87	.934904
368.3	304.11	.929989
376.7	303.29	.924703
376.9	303.26	.924513
394.7	301.57	.913647
395.5	301.48	.913075
400.7	301.02	.910116
408.5	300.33	.905687
413.1	299.87	.902759
452.5	296.05	.878576
452.9	296.03	.878444
462.9	295.14	.872825
475.8	293.98	.865531
481.7	293.31	.861386
492.4	292.34	.855325
505.9	291.06	.847379
512.6	290.41	.843356
514.0	290.26	.842443
515.6	290.13	.841632
527.4	289.00	.834673
528.8	288.78	.833353
528.5	288.81	.833537
540.4	287.73	.826894
547.4	287.06	.822796
558.7	286.00	.816331
568.7	285.02	.810390
569.9	284.89	.809607
572.2	284.70	.808445
572.0	284.68	.808339
572.1	284.69	.808392
581.9	283.78	.802882
589.3	283.06	.798547
595.8	282.45	.794875
596.2	282.40	.794579
598.5	282.15	.793090
607.0	281.36	.788349
609.5	281.10	.786802
609.9	281.05	.786508
610.3	281.02	.786325
611.2	280.92	.785733
618.3	280.28	.781901
619.6	280.15	.781128
622.8	279.83	.779229
624.1	279.70	.778458
627.0	279.41	.776740
631.1	279.02	.774424

RAW DATA FOR SODIUM FLUORIDE

C = C44 , MODE IS S [001] RANDOM POL.

LENGTH (298) = .3731 INCHES , DENSITY(298) = 2.8062 GM/CC

TEMPERATURE (DEGREES K)	FREQUENCY (KHZ)	MODULUS,C (MBAR)	TEMPERATURE (DEGREES K)	FREQUENCY (KHZ)	MODULUS,C (MBAR)
298.3	167.23	.281889	563.5	162.94	.264910
310.7	167.07	.281236	564.7	162.92	.264831
318.2	166.96	.280796	566.0	162.89	.264718
323.0	166.88	.280482	567.2	162.87	.264639
342.5	166.58	.279289	573.7	162.76	.264206
343.2	166.58	.279282	578.1	162.67	.263862
347.9	166.50	.278969	580.1	162.64	.263741
351.2	166.46	.278803	590.4	162.46	.263036
355.6	166.40	.278565	592.0	162.43	.262920
363.7	166.27	.278045	594.1	162.39	.262765
369.3	166.17	.277655	597.8	162.33	.262527
380.4	166.00	.276977	606.7	162.15	.261839
395.1	165.77	.276063	608.3	162.12	.261722
405.4	165.61	.275425	611.4	162.06	.261491
420.6	165.37	.274471	618.3	161.93	.260989
438.2	165.09	.273358	623.3	161.85	.260671
447.0	164.95	.272802	624.4	161.82	.260561
450.3	164.89	.272568	627.3	161.77	.260364
468.9	164.59	.271378	628.7	161.74	.260251
473.1	164.52	.271101	630.8	161.70	.260096
488.0	164.28	.270148	632.6	161.67	.259978
498.5	164.09	.269408	636.3	161.60	.259708
505.2	163.96	.268906	637.4	161.57	.259598
530.0	163.55	.267285	642.4	161.49	.259279
536.4	163.43	.266819	666.1	161.04	.257544
539.0	163.38	.266626	649.0	161.37	.258813
545.6	163.26	.266159	649.9	161.34	.258706
547.5	163.22	.266007	653.2	161.28	.258473
547.3	163.22	.266009	654.4	161.26	.258394
546.5	163.23	.266051	657.2	161.21	.258199
546.7	163.23	.266049	659.0	161.17	.258048
553.3	163.12	.265614	660.3	161.15	.257968
559.0	163.01	.265190	661.4	161.12	.257859
562.4	162.96	.264988	662.7	161.10	.257778

RAW DATA FOR SODIUM FLUORIDE

C = (C11-C12)/2 , MODE IS S [110] POL. [1-10]

LENGTH (298) = .2485 INCHES , DENSITY(298) = 2.8062 GM/CC

TEMPERATURE (DEGREES K)	FREQUENCY (KHZ)	MODULUS,C (MBAR)
294.2	287.10	.368631
310.3	285.13	.363386
322.7	283.60	.359361
321.1	283.74	.359709
324.7	283.33	.358640
336.7	281.84	.354727
346.0	280.65	.351619
359.8	278.87	.347025
365.2	278.25	.345411
381.0	276.26	.340290
389.1	275.23	.337658
389.3	275.18	.337533
440.8	268.69	.321171
450.5	267.45	.318105
451.4	267.31	.317755
453.2	267.08	.317192
462.8	265.87	.314217
466.1	265.47	.313220
466.7	265.40	.313053
470.9	264.85	.311705
480.0	263.69	.308855
486.6	262.92	.306966
492.0	262.17	.305162
493.8	261.94	.304616
499.3	261.25	.302939
504.7	260.57	.301291
506.3	260.35	.300762
513.1	259.48	.298665
517.9	258.91	.297306
518.3	258.85	.297163
519.3	258.68	.296755
519.6	258.66	.296699
517.5	258.96	.297414
530.4	257.31	.293493
533.9	256.92	.292538
535.6	256.76	.292182
536.7	256.53	.291632
555.4	254.19	.286105
555.5	254.16	.286036
559.9	253.62	.284772
560.4	253.57	.284631
562.0	253.35	.284129
563.4	253.17	.283702
565.0	252.97	.283234
568.4	252.51	.282174
571.4	252.13	.281277
572.4	252.01	.280997
576.0	251.57	.279971
576.1	251.54	.279909
582.6	250.73	.278028
587.0	249.89	.276120
593.1	249.37	.274901
597.9	248.75	.273455
607.4	247.57	.270760
612.5	246.92	.269271
617.5	246.30	.267853
618.2	246.21	.267654
619.0	246.11	.267427
620.2	245.98	.267124
621.0	245.86	.266859
621.9	245.73	.266566
622.8	245.60	.266289
623.3	245.55	.266164
625.5	245.26	.265503
627.3	245.17	.265286
629.1	244.82	.264506
630.4	244.64	.264101
634.1	244.18	.263064
634.4	244.13	.262952
636.1	243.90	.262447
636.7	243.88	.262385
637.1	243.79	.262192
637.2	243.76	.262126
643.1	243.05	.260529
644.3	242.87	.260134
644.9	242.81	.259987
646.3	242.62	.259579
647.5	242.47	.259222
648.6	242.36	.258979
649.3	242.25	.258740

RAW DATA FOR SODIUM FLUORIDE

C = C44 , MODE IS S [110] POL. [001]

LENGTH (298) = .2530 INCHES , DENSITY(298) = 2.8062 GM/CC

TEMPERATURE (DEGREES K)	FREQUENCY (KHZ)	MODULUS,C (MBAR)
296.3	247.44	.283798
318.4	246.97	.282504
322.9	246.85	.282210
328.4	246.73	.281877
341.0	246.48	.281169
346.6	246.35	.280835
350.1	246.25	.280556
357.5	246.11	.280170
364.7	245.92	.279673
365.6	245.91	.279635
365.5	245.90	.279619
365.9	245.90	.279610
372.1	245.76	.279247
376.6	245.67	.278975
380.5	245.57	.278708
383.9	245.49	.278504
386.1	245.44	.278380
387.1	245.42	.278302
389.1	245.37	.278179
407.5	244.93	.277000
427.9	244.46	.275726
430.1	244.41	.275584
431.6	244.36	.275461
437.7	244.23	.275098
442.4	244.09	.274733
446.3	244.00	.274494
456.7	243.74	.273798
460.3	243.66	.273580
466.1	243.51	.273186
471.1	243.40	.272862
479.2	243.18	.272291
480.1	243.17	.272254
486.2	243.02	.271856
510.0	242.42	.270256
518.5	242.18	.269619
523.8	242.06	.269292
527.8	241.96	.269030
540.8	241.65	.268192
547.2	241.48	.267735
571.1	240.84	.266050
574.7	240.74	.265775
575.5	240.73	.265738
575.3	240.72	.265719
575.0	240.72	.265717

RAW DATA FOR SODIUM FLUORIDE

C = (C11+C12+2C44)/2 , MODE IS P [110]

LENGTH (298) = .2418 INCHES , DENSITY(298) = 2.8062 GM/CC

TEMPERATURE (DEGREES K)	FREQUENCY (KHZ)	MODULUS,C (MBAR)
297.2	458.60	.890402
318.6	456.87	.883095
328.6	455.94	.879208
345.5	454.44	.872906
369.1	452.60	.865139
381.4	451.49	.860540
397.9	449.97	.854260
440.3	446.46	.839620
440.7	446.42	.839476
441.4	446.36	.839208
452.1	445.47	.835535
460.6	444.81	.832745
478.6	443.25	.826338
496.6	441.67	.819675
500.7	441.33	.818475
516.3	440.26	.813963
518.6	440.46	.814624
532.1	438.67	.807573
536.1	438.29	.806036
553.3	436.77	.799843
557.6	436.37	.798210
570.2	435.40	.794261
573.4	435.09	.793000
592.1	433.48	.786482
622.1	431.00	.776439


CaF2

RAW DATA FOR CALCIUM FLUORIDE

C = C11 , MODE IS P [001]

LENGTH (298) = .2884 INCHES , DENSITY(298) = 3.1830 GM/CC

TEMPERATURE (DEGREES K)	FREQUENCY (KHZ)	MODULUS,C (MBAR)	TEMPERATURE (DEGREES K)	FREQUENCY (KHZ)	MODULUS,C (MBAR)
296.8	491.53	1.650723	479.5	482.54	1.584409
311.2	490.87	1.645811	495.9	481.64	1.577885
312.6	490.87	1.645717	497.2	481.58	1.577443
312.7	490.81	1.645358	506.1	481.10	1.573930
314.7	490.74	1.644754	506.5	481.06	1.573686
316.2	490.65	1.644133	507.6	481.01	1.573350
317.7	490.62	1.643848	514.0	480.67	1.570851
318.0	490.59	1.643670	514.3	480.65	1.570709
319.3	490.51	1.643056	545.5	478.85	1.557786
330.3	490.04	1.639565	548.0	478.71	1.556780
331.2	489.97	1.639032	553.0	478.44	1.554867
347.0	489.26	1.633737	554.3	478.37	1.554363
347.7	489.21	1.633378	576.2	477.11	1.545325
348.0	489.20	1.633334	577.8	477.03	1.544746
348.6	489.18	1.633180	578.9	476.97	1.544316
348.9	489.15	1.632969	589.2	476.38	1.540109
349.1	489.15	1.632929	590.0	476.33	1.539788
350.1	489.12	1.632760	591.4	476.25	1.539185
363.4	488.45	1.627787	598.5	475.84	1.536269
363.7	488.41	1.627510	598.9	475.81	1.536092
364.4	488.38	1.627285	610.8	475.13	1.531258
365.0	488.35	1.627097	611.4	475.09	1.530945
368.9	488.15	1.625592	619.3	474.62	1.527654
369.1	488.14	1.625518	620.4	474.56	1.527194
389.3	487.15	1.618173	621.0	474.51	1.526882
389.4	487.13	1.618103	633.2	473.82	1.521957
407.4	486.26	1.611640	634.3	473.76	1.521499
409.9	486.12	1.610621	637.2	473.59	1.520331
410.8	486.09	1.610389	637.5	473.57	1.520192
421.6	485.54	1.606382	639.7	473.42	1.519147
422.2	485.48	1.605930	645.1	473.10	1.516926
422.9	485.47	1.605871	651.3	472.71	1.514164
423.5	485.46	1.605750	653.9	472.56	1.513075
437.9	484.71	1.600259	657.8	472.40	1.511939
438.6	484.67	1.600001	659.2	472.31	1.511311
451.5	484.03	1.595232	659.8	472.27	1.511033
452.4	483.99	1.595000	660.4	472.22	1.510723
452.7	483.96	1.594759	662.6	472.08	1.509715
455.5	483.83	1.593764	665.4	471.91	1.508525
456.6	483.78	1.593459	673.0	471.48	1.505498
471.8	482.94	1.587294	673.4	471.43	1.505164
472.7	482.90	1.586998	678.8	471.09	1.502797
473.8	482.83	1.586529	679.5	471.04	1.502484

RAW DATA FOR CALCIUM FLUORIDE

C = C44 , MODE IS S [001] RANDOM POL.

LENGTH (298) = .2884 INCHES , DENSITY(298) = 3.1830 GM/CC

TEMPERATURE (DEGREES K)	FREQUENCY (KHZ)	MODULUS,C (MBAR)	TEMPERATURE (DEGREES K)	FREQUENCY (KHZ)	MODULUS,C (MBAR)
296.0	222.66	.338732	536.2	213.36	.309338
320.6	221.72	.335694	538.3	213.27	.309061
321.3	221.69	.335629	539.1	213.25	.308983
321.5	221.68	.335582	542.9	213.10	.308534
322.1	221.67	.335548	543.1	213.08	.308489
332.7	221.27	.334278	557.4	212.51	.306734
332.9	221.26	.334247	558.3	212.48	.306626
343.3	220.87	.332996	571.3	211.94	.304987
343.4	220.86	.332965	571.9	211.92	.304925
350.9	220.59	.332083	581.3	211.56	.303791
351.1	220.58	.332036	582.2	211.52	.303684
373.0	219.73	.329325	587.5	211.30	.302999
374.1	219.68	.329182	591.0	211.16	.302586
375.4	219.63	.329023	591.2	211.15	.302556
376.1	219.61	.328958	598.9	210.83	.301582
380.7	219.42	.328370	599.8	210.78	.301447
381.1	219.42	.328338	606.0	210.53	.300687
394.3	218.92	.326761	610.2	210.36	.300156
395.1	218.90	.326681	610.3	210.35	.300127
395.6	218.88	.326632	616.5	210.09	.299340
399.3	218.73	.326158	617.8	210.06	.299245
399.7	218.72	.326110	624.2	209.79	.298429
400.3	218.70	.326076	624.8	209.76	.298339
416.4	218.07	.324066	626.2	209.72	.298215
416.3	218.07	.324067	627.8	209.65	.298005
431.9	217.48	.322185	628.6	209.61	.297899
432.5	217.44	.322092	632.5	209.45	.297402
434.7	217.35	.321809	633.1	209.43	.297341
436.5	217.29	.321603	637.3	209.25	.296785
443.7	217.03	.320780	641.7	209.08	.296271
443.9	217.02	.320749	642.6	209.04	.296166
445.0	216.98	.320622	645.5	208.92	.295819
445.3	216.97	.320591	646.9	208.86	.295625
463.3	216.25	.318346	649.2	208.77	.295353
464.4	216.22	.318220	656.5	208.47	.294436
465.7	216.16	.318049	657.5	208.42	.294290
473.2	215.87	.317139	662.8	208.22	.293702
473.6	215.85	.317092	665.9	208.09	.293313
473.8	215.84	.317061	667.8	208.02	.293102
475.8	215.76	.316797	672.3	207.82	.292507
503.8	214.65	.313321	673.0	207.80	.292431
505.3	214.58	.313134	675.1	207.70	.292163
525.6	213.81	.310681	675.3	207.69	.292134
526.6	213.75	.310557	677.2	207.61	.291895
527.8	213.71	.310417	677.7	207.59	.291835
535.1	213.40	.309448	678.5	207.56	.291717
535.8	213.38	.309399			

RAW DATA FOR CALCIUM FLUORIDE

C = (C11-C12)/2 , MODE IS S [110] POL. [1-10]

LENGTH (298) = .2948 INCHES , DENSITY(298) = 3.1830 GM/CC

TEMPERATURE (DEGREES K)	FREQUENCY (KHZ)	MODULUS,C (MBAR)
295.5	290.94	.604294
324.0	290.25	.601080
324.6	290.23	.600989
333.0	290.03	.600055
334.1	290.00	.599917
335.9	289.96	.599729
352.3	289.56	.597866
353.0	289.54	.597774
377.0	288.94	.594987
377.4	288.94	.594961
399.4	288.39	.592427
399.7	288.38	.592382
399.9	288.37	.592317
400.6	288.35	.592226
421.0	287.81	.589756
421.6	287.79	.589686
439.5	287.33	.587518
441.5	287.29	.587348
444.4	287.21	.586960
446.4	287.14	.586667
446.8	287.12	.586601
447.0	287.12	.586557
467.6	286.55	.583967
469.0	286.52	.583826
474.9	286.37	.583113
475.6	286.34	.583001
477.6	286.26	.582627
477.7	286.26	.582626
478.0	286.24	.582581
478.9	286.22	.582487
483.9	286.10	.581889
486.3	286.03	.581571
489.7	285.93	.581137
492.6	285.85	.580772
500.9	285.61	.579681
501.4	285.59	.579593
503.8	285.53	.579296
504.9	285.49	.579159
508.3	285.41	.578767
522.1	285.01	.576953
527.6	284.86	.576269
529.5	284.81	.576020
534.9	284.65	.575297
537.9	284.55	.574871
539.6	284.51	.574686
542.8	284.42	.574258
544.7	284.36	.574009
544.9	284.35	.573986
548.9	284.24	.573466
550.9	284.18	.573196
552.4	284.13	.572993
554.9	284.06	.572676
556.0	284.03	.572499
557.4	283.98	.572298
558.9	283.94	.572096
570.1	283.60	.570590
572.7	283.53	.570252
574.2	283.48	.570050
577.6	283.37	.569561
580.9	283.28	.569133
582.5	283.22	.568890
584.6	283.15	.568579
585.2	283.13	.568490
594.5	282.88	.567358
599.0	282.74	.566713
599.8	282.71	.566602
602.6	282.63	.566243
604.3	282.57	.565979
604.5	282.56	.565956
605.2	282.54	.565866
607.1	282.49	.565599
609.1	282.43	.565351
611.4	282.36	.565039
614.1	282.28	.564662
614.7	282.26	.564593
618.2	282.15	.564085
619.2	282.11	.563931
620.9	282.06	.563708
622.5	282.00	.563446
623.0	281.95	.563239
627.3	281.85	.562760
627.8	281.83	.562714
628.5	281.81	.562604
630.1	281.76	.562363
630.6	281.74	.562296

RAW DATA FOR CALCIUM FLUORIDE

C = C44 , MODE IS S [110] POL. [001]

LENGTH (298) = .2948 INCHES , DENSITY(298) = 3.1830 GM/CC

TEMPERATURE (DEGREES K)	FREQUENCY (KHZ)	MODULUS,C (MBAR)
295.5	217.75	.338507
340.6	216.14	.333205
341.6	216.12	.333144
341.1	216.12	.333128
342.0	216.08	.332998
342.3	216.07	.332973
350.0	215.78	.332040
350.1	215.78	.332032
348.5	215.78	.332035
349.0	215.78	.332024
359.0	215.40	.330784
359.9	215.37	.330686
359.9	215.34	.330609
364.6	215.18	.330076
368.1	215.05	.329652
374.1	214.81	.328881
380.0	214.61	.328211
382.1	214.53	.327966
386.8	214.34	.327359
392.4	214.15	.326715
394.9	214.05	.326384
396.3	214.00	.326221
405.6	213.63	.325041
405.9	213.62	.325016
408.5	213.58	.324867
407.5	213.56	.324806
407.5	213.55	.324791
412.5	213.37	.324191
412.5	213.37	.324191
414.4	213.36	.324162
413.6	213.33	.324062
440.3	212.32	.320795
440.5	212.31	.320763
442.6	212.29	.320695
449.9	211.96	.319659
450.0	211.95	.319636
474.7	211.00	.316570
475.0	210.99	.316537
477.5	210.94	.316391
481.8	210.73	.315707
489.4	210.42	.314721
492.8	210.28	.314284
505.5	209.80	.312763
514.5	209.44	.311608
526.2	208.98	.310168
543.9	208.30	.308020
555.5	207.84	.306560
559.9	207.66	.306011
566.0	207.44	.305302
570.0	207.35	.305004
572.3	207.20	.304549
573.9	207.13	.304339
580.1	206.90	.303625
589.3	206.51	.302420
593.6	206.36	.301927
600.6	206.06	.301006
603.5	205.95	.300656
610.0	205.69	.299857
614.0	205.52	.299346
619.5	205.32	.298702
621.7	205.22	.298402
623.9	205.13	.298124
628.6	204.93	.297524
629.6	204.90	.297400
631.8	204.82	.297174
633.6	204.75	.296965
634.5	204.72	.296849
634.5	204.70	.296791
634.8	204.69	.296760
635.0	204.68	.296752
635.2	204.68	.296728
635.5	204.67	.296704
635.6	204.66	.296667
635.7	204.65	.296638
636.0	204.64	.296614
636.2	204.63	.296583
636.3	204.63	.296575
637.1	204.60	.296504
637.9	204.57	.296404
639.6	204.50	.296189

RAW DATA FOR CALCIUM FLUORIDE

C = (C11+C12+2C44)/2 , MODE IS P [110]

LENGTH (298) = .2948 INCHES , DENSITY(298) = 3.1830 GM/CC

TEMPERATURE (DEGREES K)	FREQUENCY (KHZ)	MODULUS,C (MBAR)	TEMPERATURE (DEGREES K)	FREQUENCY (KHZ)	MODULUS,C (MBAR)
301.7	440.46	1.384840	603.5	423.37	1.270534
301.5	440.47	1.384909	607.0	423.15	1.269105
322.9	439.37	1.377363	613.5	422.72	1.266355
323.3	439.35	1.377289	615.4	422.60	1.265577
340.7	438.46	1.371149	619.0	422.38	1.264148
341.0	438.44	1.371015	623.1	422.11	1.262406
358.3	437.53	1.364852	624.0	422.08	1.262198
359.1	437.48	1.364517	624.6	422.03	1.261881
376.6	436.55	1.358200	626.3	421.94	1.261260
377.9	436.48	1.357725	629.6	421.72	1.259873
396.6	435.46	1.350822	632.5	421.55	1.258768
397.7	435.40	1.350385	635.1	421.37	1.257643
410.1	434.67	1.345514	635.6	421.35	1.257508
410.6	434.63	1.345251	636.0	421.33	1.257347
411.3	434.59	1.344982	637.1	421.26	1.256865
421.0	434.08	1.341498	637.4	421.24	1.256737
421.6	434.03	1.341232	641.1	421.01	1.255311
435.6	433.24	1.335922	642.0	420.97	1.254985
438.6	433.10	1.334934	644.3	420.81	1.253961
450.6	432.40	1.330281	651.5	420.36	1.251090
452.5	432.33	1.329760	652.2	420.31	1.250741
453.6	432.26	1.329295	652.8	420.28	1.250574
484.9	430.44	1.317147	653.3	420.25	1.250380
485.3	430.42	1.317043	654.5	420.17	1.249838
505.6	429.22	1.309041	655.0	420.14	1.249674
506.3	429.17	1.308714	656.4	420.06	1.249125
509.2	429.01	1.307678	657.8	419.97	1.248577
514.8	428.67	1.305429	659.4	419.86	1.247875
533.1	427.62	1.298405	661.2	419.76	1.247226
533.6	427.57	1.298116	663.3	419.62	1.246360
537.1	427.35	1.296700	664.7	419.53	1.245753
538.7	427.27	1.296134	668.7	419.30	1.244266
544.2	426.96	1.294050	671.2	419.10	1.242974
544.5	426.93	1.293889	672.5	419.01	1.242401
551.2	426.53	1.291255	673.3	418.98	1.242229
552.1	426.47	1.290893	674.0	418.94	1.242000
555.1	426.30	1.289740	678.5	418.65	1.240116
556.0	426.26	1.289439	679.5	418.58	1.239671
561.4	425.93	1.287304	680.3	418.53	1.239322
565.7	425.69	1.285688	681.8	418.42	1.238684
569.1	425.65	1.285400	682.8	418.35	1.238240
573.2	425.22	1.282615	684.8	418.21	1.237322
575.6	425.08	1.281695	687.0	418.05	1.236309
579.3	424.83	1.280102	688.9	417.97	1.235750
584.8	424.51	1.278002	689.9	417.90	1.235306
599.4	423.60	1.272103	695.0	417.53	1.232968
601.3	423.49	1.271323			

SrF_2

RAW DATA FOR STRONTIUM FLUORIDE

C = C11 , MODE IS P [001]

LENGTH (298) = .3019 INCHES , DENSITY(298) = 4.2820 GM/CC

TEMPERATURE (DEGREES K)	FREQUENCY (KHZ)	MODULUS,C (MBAR)
294.2	352.06	1.248416
294.2	352.06	1.248451
309.7	351.60	1.244854
323.7	351.15	1.241397
349.8	350.32	1.235026
353.3	350.22	1.234217
369.4	349.68	1.230131
378.1	349.40	1.227988
398.5	348.74	1.222906
419.1	348.05	1.217680
423.7	347.87	1.216359
435.9	347.49	1.213408
436.4	347.47	1.213258
459.6	346.69	1.207343
460.2	346.67	1.207190
481.8	345.92	1.201409
500.7	345.26	1.196380
519.8	344.58	1.191200
539.7	343.88	1.185887
540.3	343.86	1.185733
559.6	343.16	1.180390
560.4	343.14	1.180230
581.0	342.38	1.174459
601.6	341.61	1.168536
602.1	341.60	1.168418
635.8	340.33	1.158744
629.3	340.56	1.160525
621.5	340.87	1.162857
633.5	340.42	1.159365
633.8	340.41	1.159321
646.3	339.92	1.155534
653.2	339.65	1.153496
659.0	339.44	1.151834
661.0	339.37	1.151288
662.2	339.31	1.150907
666.8	339.13	1.149469
669.7	339.01	1.148605

RAW DATA FOR STRONTIUM FLUORIDE

C = C44 , MODE IS S [001] RANDOM POL.

LENGTH (298) = .3019 INCHES , DENSITY(298) = 4.2820 GM/CC

TEMPERATURE (DEGREES K)	FREQUENCY (KHZ)	MODULUS,C (MBAR)	TEMPERATURE (DEGREES K)	FREQUENCY (KHZ)	MODULUS,C (MBAR)
295.7	178.10	.319498	471.0	173.69	.302956
295.8	178.10	.319488	472.7	173.64	.302789
307.0	177.83	.318465	494.4	173.07	.300651
308.2	177.80	.318342	501.9	172.86	.299911
318.3	177.55	.317398	519.4	172.40	.298174
326.6	177.34	.316615	536.4	171.93	.296476
340.1	177.00	.315335	550.3	171.57	.295118
342.2	176.95	.315128	588.6	170.53	.291300
351.9	176.71	.314235	592.7	170.43	.290911
362.6	176.44	.313222	595.4	170.34	.290609
376.3	176.09	.311911	611.7	169.90	.288969
381.0	175.97	.311453	618.6	169.72	.288295
395.0	175.61	.310135	632.2	169.33	.286871
399.6	175.50	.309687	640.1	169.11	.286070
412.6	175.16	.308438	643.5	169.02	.285729
415.5	175.09	.308177	653.3	168.75	.284725
425.6	174.83	.307191	655.7	168.68	.284486
433.6	174.61	.306401	657.9	168.62	.284273
446.1	174.29	.305211	659.1	168.58	.284127
451.6	174.15	.304673			

RAW DATA FOR STRONTIUM FLUORIDE

C = (C11-C12)/2 , MODE IS S [110] POL. [1-10]

LENGTH (298) = .3068 INCHES , DENSITY(298) = 4.2820 GM/CC

TEMPERATURE (DEGREES K)	FREQUENCY (KHZ)	MODULUS,C (MBAR)
293.5	196.30	.400836
293.6	196.30	.400835
293.6	196.30	.400835
309.6	196.10	.399929
310.7	196.09	.399861
322.0	195.94	.399179
322.6	195.93	.399145
331.3	195.82	.398622
348.9	195.59	.397585
361.6	195.42	.396824
362.0	195.41	.396781
388.0	195.06	.395183
410.6	194.75	.393769
428.5	194.50	.392657
443.4	194.28	.391676
444.3	194.27	.391629
445.0	194.27	.391594
464.0	194.00	.390380
469.4	193.92	.390019
485.3	193.68	.388945
486.9	193.67	.388862
497.7	193.50	.388106
500.1	193.46	.387947
529.0	193.04	.386031
531.6	193.00	.385859
543.9	192.81	.384985
544.7	192.80	.384938
554.7	192.65	.384241
555.3	192.64	.384186
565.1	192.49	.383500
601.9	191.91	.380853
601.8	191.91	.380864
585.8	192.15	.381963
586.2	192.15	.381940
602.1	191.91	.380841
603.7	191.88	.380706
610.7	191.76	.380189
612.7	191.73	.380040
626.2	191.50	.378968
632.9	191.39	.378482
637.9	191.31	.378101
639.8	191.28	.377962
642.4	191.24	.377765
651.1	191.12	.377214
655.2	191.06	.376931
656.8	191.03	.376795
659.7	190.99	.376594
661.3	190.96	.376447
662.7	190.94	.376352
663.9	190.91	.376230

RAW DATA FOR STRONTIUM FLUORIDE

C = C44 , MODE IS S [110] POL. [001]

LENGTH (298) = .3068 INCHES , DENSITY(298) = 4.2820 GM/CC

TEMPERATURE (DEGREES K)	FREQUENCY (KHZ)	MODULUS,C (MBAR)	TEMPERATURE (DEGREES K)	FREQUENCY (KHZ)	MODULUS,C (MBAR)
295.2	175.25	.319462	511.0	169.78	.298731
318.9	174.66	.317179	512.7	169.75	.298580
330.0	174.38	.316117	534.1	169.17	.296442
344.0	174.03	.314789	535.3	169.15	.296338
353.7	173.78	.313855	552.0	168.71	.294688
370.4	173.37	.312292	553.9	168.66	.294509
386.7	172.95	.310680	580.6	167.95	.291848
404.7	172.50	.308981	580.7	167.94	.291830
405.4	172.49	.308933	590.4	167.67	.290805
421.1	172.10	.307446	592.1	167.64	.290671
421.4	172.09	.307417	610.3	167.15	.288854
424.3	172.02	.307152	611.4	167.13	.288768
432.8	171.80	.306321	623.9	166.78	.287479
432.8	171.80	.306321	629.8	166.62	.286880
449.5	171.39	.304769	633.7	166.52	.286487
449.6	171.38	.304733	643.7	166.23	.285416
450.0	171.37	.304704	647.3	166.14	.285068
463.2	171.03	.303432	655.1	165.93	.284308
463.3	171.03	.303413	656.6	165.89	.284141
485.3	170.46	.301267	659.9	165.81	.283829
486.4	170.43	.301172	664.3	165.68	.283363
487.7	170.40	.301041			

RAW DATA FOR STRONTIUM FLUORIDE

C = (C11+C12+2C44)/2 , MODE IS P [110]

LENGTH (298) = .3068 INCHES ; DENSITY(298) = 4.2820 GM/CC

TEMPERATURE (DEGREES K)	FREQUENCY (KHZ)	MODULUS,C (MBAR)
293.8	335.03	1.167598
293.8	335.04	1.167633
293.8	335.03	1.167598
307.0	334.55	1.163980
317.8	334.16	1.161072
334.5	333.53	1.156429
334.7	333.51	1.156287
342.8	333.21	1.154025
346.7	333.06	1.152915
359.7	332.56	1.149252
375.3	331.97	1.144889
375.7	331.96	1.144778
388.6	331.47	1.141125
413.5	330.49	1.133982
413.6	330.49	1.133911
423.3	330.10	1.131116
447.5	329.20	1.124439
452.7	328.99	1.122933
468.4	328.31	1.117935
486.9	327.58	1.112572
503.1	326.92	1.107734
505.2	326.83	1.107111
532.0	325.72	1.098946
548.9	325.03	1.093916
565.4	324.37	1.088993
571.6	324.05	1.086718
587.3	323.44	1.082211
603.3	322.70	1.076822
629.9	321.57	1.068520
640.9	321.10	1.065064
644.2	320.97	1.064066
651.9	320.62	1.061571
657.1	320.40	1.059882
660.4	320.26	1.058883
665.0	320.06	1.057411
669.2	319.87	1.055985
671.6	319.76	1.055245
672.6	319.72	1.054881
673.6	319.67	1.054584

BaF_2

RAW DATA FOR BARIUM FLUORIDE

C = (C11-C12)/2 , MODE IS S [110] POL. [1-10]

LENGTH (298) = .3131 INCHES , DENSITY(298) = 4.8870 GM/CC

TEMPERATURE (DEGREES K)	FREQUENCY (KHZ)	MODULUS,C (MBAR)	TEMPERATURE (DEGREES K)	FREQUENCY (KHZ)	MODULUS,C (MBAR)
296.5	142.92	.252525	581.5	139.96	.240495
296.3	142.92	.252526	586.5	139.92	.240314
311.5	142.77	.251953	590.0	139.88	.240178
322.0	142.67	.251527	595.8	139.79	.239828
329.3	142.60	.251251	599.2	139.75	.239667
341.2	142.49	.250782	600.3	139.74	.239625
346.0	142.44	.250597	604.1	139.70	.239460
360.3	142.30	.250026	605.0	139.69	.239403
366.0	142.25	.249793	607.2	139.66	.239284
381.2	142.09	.249181	611.3	139.61	.239083
382.1	142.09	.249150	617.0	139.55	.238845
394.9	141.96	.248621	618.1	139.53	.238786
410.1	141.81	.248008	620.2	139.50	.238668
419.6	141.70	.247594	633.2	139.34	.238018
445.1	141.45	.246551	635.5	139.31	.237898
460.8	141.29	.245889	640.0	139.27	.237728
473.8	141.15	.245330	643.3	139.23	.237542
502.5	140.84	.244080	646.9	139.19	.237387
519.1	140.66	.243340	648.5	139.16	.237290
533.5	140.50	.242692	655.2	139.07	.236925
541.0	140.42	.242357	657.3	139.05	.236824
562.8	140.17	.241373	658.7	139.03	.236754
575.5	140.02	.240769	663.1	138.97	.236533
576.2	140.02	.240747			

RAW DATA FOR BARIUM FLUORIDE

C = C44 , MODE IS S [110] POL. [001]

LENGTH (298) = .3131 INCHES , DENSITY(298) = 4.8870 GM/CC

TEMPERATURE (DEGREES K)	FREQUENCY (KHZ)	MODULUS,C (MBAR)	TEMPERATURE (DEGREES K)	FREQUENCY (KHZ)	MODULUS,C (MBAR)
298.7	144.06	.256585	534.2	139.18	.238166
298.7	144.07	.256594	541.1	139.02	.237573
309.7	143.85	.255780	554.9	138.72	.236441
321.3	143.60	.254830	565.7	138.50	.235620
322.3	143.59	.254780	580.9	138.17	.234379
329.5	143.46	.254271	594.3	137.86	.233253
341.1	143.22	.253376	600.3	137.73	.232772
347.1	143.09	.252875	602.3	137.69	.232632
357.9	142.88	.252073	607.2	137.58	.232218
367.5	142.68	.251332	611.3	137.49	.231869
371.1	142.59	.250995	616.7	137.36	.231427
380.3	142.42	.250327	618.7	137.32	.231269
400.3	142.00	.248748	623.3	137.22	.230892
411.6	141.78	.247898	628.3	137.11	.230487
411.7	141.76	.247841	634.7	136.96	.229946
420.3	141.59	.247197	636.3	136.93	.229825
433.1	141.33	.246188	640.9	136.83	.229457
436.4	141.25	.245924	642.4	136.79	.229312
456.1	140.85	.244397	644.6	136.74	.229137
461.3	140.74	.243993	649.3	136.64	.228751
480.5	140.33	.242438	651.9	136.58	.228532
495.2	140.01	.241267	653.6	136.54	.228386
501.2	139.89	.240790	653.9	136.53	.228359
511.7	139.67	.239957	655.1	136.50	.228266

RAW DATA FOR BARIUM FLUORIDE

C = (C11+C12+2C44)/2 , MODE IS P [110]

LENGTH (298) = .3131 INCHES , DENSITY(298) = 4.8870 GM/CC

TEMPERATURE (DEGREES K)	FREQUENCY (KHZ)	MODULUS,C (MBAR)	TEMPERATURE (DEGREES K)	FREQUENCY (KHZ)	MODULUS,C (MBAR)
296.3	273.60	.925514	477.5	267.19	.878966
296.3	273.60	.925514	478.0	267.17	.878856
309.2	273.16	.922295	493.2	266.60	.874798
320.5	272.77	.919447	539.4	264.89	.862509
331.9	272.35	.916430	539.8	264.88	.862434
346.1	271.84	.912689	556.6	264.24	.857901
355.5	271.53	.910388	576.2	263.53	.852788
362.9	271.26	.908430	593.2	262.85	.848004
375.7	270.81	.905192	601.4	262.53	.845704
397.0	270.06	.899747	609.9	262.21	.843429
397.1	270.06	.899712	620.3	261.81	.840561
423.1	269.13	.893045	632.8	261.31	.837065
423.0	269.14	.893080	640.0	261.05	.835214
436.1	268.67	.889716	642.5	260.94	.834477
440.1	268.53	.888669	651.9	260.58	.831931
460.5	267.79	.883364	653.1	260.53	.831580
460.9	267.79	.883322			

—— MgF_2 ——

RAW DATA FOR MAGNESIUM FLUORIDE

C = C11 , MODE IS P [100]

LENGTH (298) = .2727 INCHES , DENSITY(298) = 3.1770 GM/CC

TEMPERATURE (DEGREES K)	FREQUENCY (KHZ)	MODULUS,C (MBAR)	TEMPERATURE (DEGREES K)	FREQUENCY (KHZ)	MODULUS,C (MBAR)
297.0	480.56	1.408040	479.9	474.60	1.369378
297.2	480.55	1.408006	496.8	473.99	1.365472
309.3	480.24	1.405960	498.7	473.92	1.365024
310.8	480.20	1.405664	508.1	473.61	1.362993
326.0	479.76	1.402732	518.1	473.22	1.360546
326.3	479.72	1.402520	530.5	472.80	1.357815
336.0	479.47	1.400878	535.4	472.60	1.356523
342.7	479.22	1.399213	543.5	472.30	1.354641
358.1	478.74	1.396074	552.0	472.00	1.352721
360.7	478.65	1.395551	570.1	471.28	1.348171
370.9	478.33	1.393432	578.9	470.90	1.345790
371.6	478.31	1.393300	583.3	470.72	1.344657
385.7	477.81	1.390077	587.8	470.55	1.343579
391.7	477.54	1.388402	599.7	470.10	1.340728
395.7	477.47	1.387877	603.3	469.95	1.339786
405.4	477.13	1.385685	608.3	469.77	1.338641
408.0	477.03	1.385075	618.6	469.29	1.335660
444.4	475.90	1.377645	620.7	469.19	1.335069
445.9	475.87	1.377466	623.3	468.99	1.333869
446.8	475.83	1.377243	632.1	468.62	1.331554
448.5	475.77	1.376828	634.8	468.53	1.330978
469.2	474.96	1.371673	642.3	468.22	1.329037
474.5	474.79	1.370599	643.5	468.17	1.328724
479.1	474.63	1.369541			

RAW DATA FOR MAGNESIUM FLUORIDE

C = C66 , MODE IS S [100] POL. [010]

LENGTH (298) = .2727 INCHES , DENSITY(298) = 3.1770 GM/CC

TEMPERATURE (DEGREES K)	FREQUENCY (KHZ)	MODULUS,C (MBAR)	TEMPERATURE (DEGREES K)	FREQUENCY (KHZ)	MODULUS,C (MBAR)
297.0	396.24	.957318	448.0	387.89	.915180
297.0	396.24	.957318	448.0	387.88	.915156
297.2	396.24	.957315	451.0	387.69	.914214
312.2	395.45	.953259	461.1	387.13	.911399
318.1	395.12	.951559	479.0	386.07	.906144
325.7	394.72	.949522	500.2	384.84	.900058
339.3	393.96	.945669	524.1	383.46	.893251
351.3	393.28	.942231	533.0	382.91	.890554
365.3	392.60	.938768	548.0	382.06	.886352
380.5	391.62	.933886	554.8	381.67	.884462
392.8	391.03	.930892	569.0	380.94	.880886
414.0	389.83	.924895	580.2	380.19	.877203
414.0	389.83	.924895	597.6	379.18	.872302
430.4	388.92	.920289	614.2	378.17	.867382
435.3	388.56	.918559	629.9	377.26	.863015

RAW DATA FOR MAGNESIUM FLUORIDE

C = C44 , MODE IS S [100] POL. [001]

LENGTH (298) = .2727 INCHES , DENSITY(298) = 3.1770 GM/CC

TEMPERATURE (DEGREES K)	FREQUENCY (KHZ)	MODULUS,C (MBAR)	TEMPERATURE (DEGREES K)	FREQUENCY (KHZ)	MODULUS,C (MBAR)
295.3	304.98	.567130	345.3	304.14	.563576
295.3	304.99	.567149	353.0	304.01	.563008
306.4	304.81	.566402	361.0	303.86	.562400
309.7	304.75	.566151	366.4	303.76	.561964
322.1	304.54	.565263	369.0	303.71	.561774
329.3	304.42	.564755	371.0	303.67	.561627
339.6	304.24	.564015	371.7	303.67	.561584

RAW DATA FOR MAGNESIUM FLUORIDE

C = (C11+C12+2C66)/2 , MODE IS P [110]

LENGTH (298) = .2456 INCHES , DENSITY(298) = 3.1780 GM/CC

TEMPERATURE (DEGREES K)	FREQUENCY (KHZ)	MODULUS,C (MBAR)	TEMPERATURE (DEGREES K)	FREQUENCY (KHZ)	MODULUS,C (MBAR)
298.0	653.92	2.115377	335.6	651.32	2.097408
298.0	653.93	2.115442	349.0	650.36	2.090793
308.2	653.25	2.110780	355.1	649.93	2.087829
312.7	652.93	2.108568	357.9	649.72	2.086421
314.0	652.82	2.107783	373.5	648.57	2.078497
326.4	651.93	2.101606	373.5	648.57	2.078529
333.6	651.46	2.098343			

RAW DATA FOR MAGNESIUM FLUORIDE

C = (C11-C12)/2 , MODE IS S [110] POL. [1-10]

LENGTH (298) = .2456 INCHES , DENSITY(298) = 3.1780 GM/CC

TEMPERATURE (DEGREES K)	FREQUENCY (KHZ)	MODULUS,C (MBAR)	TEMPERATURE (DEGREES K)	FREQUENCY (KHZ)	MODULUS,C (MBAR)
295.0	226.64	.254108	471.9	226.74	.253616
294.9	226.64	.254109	485.2	226.72	.253515
323.0	226.69	.254123	500.9	226.69	.253403
328.9	226.70	.254122	512.0	226.68	.253322
336.1	226.71	.254116	534.8	226.64	.253122
340.6	226.72	.254109	541.5	226.62	.253060
347.7	226.73	.254115	560.9	226.58	.252885
362.6	226.74	.254078	563.8	226.57	.252839
368.1	226.75	.254067	586.0	226.50	.252595
384.6	226.75	.254023	591.0	226.48	.252517
398.0	226.77	.254002	599.7	226.45	.252422
410.6	226.77	.253950	603.1	226.43	.252374
425.4	226.76	.253878	614.5	226.41	.252255
433.6	226.76	.253844	624.3	226.36	.252122
448.0	226.75	.253762	637.0	226.33	.251975
457.0	226.75	.253713	647.2	226.26	.251795

RAW DATA FOR MAGNESIUM FLUORIDE

C = C44 , MODE IS S [110] POL. [001]

LENGTH (298) = .2456 INCHES , DENSITY(298) = 3.1780 GM/CC

TEMPERATURE (DEGREES K)	FREQUENCY (KHZ)	MODULUS,C (MBAR)	TEMPERATURE (DEGREES K)	FREQUENCY (KHZ)	MODULUS,C (MBAR)
294.8	338.83	.567993	344.7	337.92	.564479
295.0	338.83	.567991	353.3	337.75	.563852
294.8	338.83	.567993	356.4	337.68	.563590
306.4	338.64	.567239	367.6	337.46	.562757
309.5	338.58	.567011	370.6	337.40	.562530
320.7	338.37	.566227	377.1	337.26	.562022
322.6	338.33	.566060	383.3	337.13	.561534
331.0	338.18	.565485	389.0	337.01	.561083
337.2	338.06	.565029	393.6	336.92	.560742

RAW DATA FOR MAGNESIUM FLUORIDE

C = C33 , MODE IS P [001]

LENGTH (298) = .2794 INCHES , DENSITY(298) = 3.1780 GM/CC

TEMPERATURE (DEGREES K)	FREQUENCY (KHZ)	MODULUS,C (MBAR)	TEMPERATURE (DEGREES K)	FREQUENCY (KHZ)	MODULUS,C (MBAR)
294.6	566.29	2.053108	514.3	556.62	1.980155
305.2	565.89	2.050052	515.6	556.53	1.979457
313.3	565.53	2.047324	527.4	556.00	1.975483
321.3	565.22	2.045033	529.8	555.87	1.974588
333.3	564.70	2.041054	538.4	555.32	1.970531
343.9	564.28	2.037858	541.1	555.18	1.969490
345.4	564.19	2.037221	562.7	554.17	1.961877
352.6	563.87	2.034764	562.7	554.18	1.961947
365.3	563.32	2.030636	571.1	553.72	1.958612
365.6	563.31	2.030523	592.9	552.82	1.951785
380.6	562.67	2.025641	599.0	552.42	1.948885
381.1	562.64	2.025489	602.3	552.26	1.947696
391.4	562.21	2.022195	617.3	551.51	1.942168
405.8	561.54	2.017184	624.1	551.16	1.939543
406.4	561.51	2.016959	625.4	551.10	1.939061
419.0	560.93	2.012519	625.8	551.08	1.938948
420.0	560.89	2.012215	636.4	550.53	1.934847
435.6	560.21	2.007120	636.8	550.50	1.934629
436.1	560.18	2.006897	639.9	550.32	1.933376
436.4	560.17	2.006785	640.0	550.32	1.933374
442.1	559.93	2.005007	652.0	549.85	1.929777
455.5	559.33	2.000491	652.8	549.79	1.929411
456.9	559.26	1.999966	653.3	549.78	1.929296
476.5	558.36	1.993205	655.5	549.68	1.928518
477.8	558.29	1.992684	655.9	549.66	1.928405
489.9	557.60	1.987520	657.8	549.55	1.927597
492.0	557.49	1.986700	664.0	549.21	1.925130
506.8	556.78	1.981424	665.9	549.12	1.924463
509.8	556.63	1.980305	668.7	549.00	1.923534

RAW DATA FOR MAGNESIUM FLUORIDE

C = C44 , MODE IS S [001] RANDOM POL.

LENGTH (298) = .2794 INCHES , DENSITY(298) = 3.1780 GM/CC

TEMPERATURE (DEGREES K)	FREQUENCY (KHZ)	MODULUS,C (MBAR)	TEMPERATURE (DEGREES K)	FREQUENCY (KHZ)	MODULUS,C (MBAR)
301.7	297.56	.566831	472.3	294.17	.553249
300.5	297.57	.566894	484.1	293.91	.552235
296.6	297.64	.567176	500.5	293.54	.550787
296.6	297.64	.567176	500.9	293.53	.550747
309.0	297.44	.566344	516.9	293.21	.549433
311.6	297.37	.566105	517.2	293.19	.549356
317.0	297.27	.565683	531.8	292.85	.548049
317.2	297.27	.565683	549.2	292.47	.546543
325.8	297.10	.565000	554.5	292.37	.546106
335.3	296.92	.564295	570.9	291.99	.544624
336.3	296.91	.564234	576.9	291.84	.544035
347.3	296.70	.563389	580.2	291.76	.543701
358.1	296.49	.562565	592.4	291.49	.542652
358.3	296.49	.562545	596.0	291.40	.542299
371.4	296.23	.561502	599.2	291.33	.542004
383.9	295.99	.560520	609.6	291.06	.540983
400.3	295.65	.559198	616.4	290.90	.540335
400.5	295.65	.559160	620.7	290.81	.539960
415.3	295.35	.557978	632.2	290.56	.538991
415.8	295.33	.557919	635.0	290.49	.538699
434.0	294.96	.556421	640.3	290.36	.538207
434.4	294.96	.556400	643.0	290.28	.537915
448.8	294.67	.555241	644.8	290.25	.537776
450.5	294.63	.555101	648.2	290.17	.537462
467.5	294.26	.553610	654.1	290.02	.536875
467.3	294.27	.553668	656.8	289.95	.536602

RAW DATA FOR MAGNESIUM FLUORIDE

C = [C11+C12+2C44+SQRT[(C11-C33)**2+4*((C13+C44)**2)]]/4

MODE IS P [45 DEGREES TO [001] AND [100]]

LENGTH (298) = .2752 INCHES , DENSITY(298) = 3.1770 GM/CC

TEMPERATURE (DEGREES K)	FREQUENCY (KHZ)	MODULUS,C (MBAR)	TEMPERATURE (DEGREES K)	FREQUENCY (KHZ)	MODULUS,C (MBAR)
295.8	534.08	1.771197	489.0	526.90	1.719952
295.8	534.08	1.771197	507.5	526.22	1.715078
307.3	533.69	1.768383	512.4	526.04	1.713764
309.5	533.62	1.767908	515.8	525.89	1.712776
317.8	533.35	1.765887	539.9	524.91	1.705831
328.9	532.96	1.763116	549.6	524.50	1.702918
337.4	532.62	1.760728	571.6	523.62	1.696777
350.6	532.21	1.757717	588.4	522.93	1.691894
362.3	531.79	1.754738	588.7	522.92	1.691823
375.0	531.31	1.751244	598.7	522.53	1.689039
380.5	531.07	1.749581	604.5	522.25	1.687128
400.4	530.32	1.744229	616.2	521.71	1.683340
413.9	529.76	1.740297	620.4	521.52	1.682049
421.1	529.44	1.738043	625.1	521.32	1.680683
436.6	528.93	1.734347	647.9	520.38	1.674065
440.1	528.81	1.733440	650.3	520.27	1.673302
453.1	528.34	1.730114	653.3	520.13	1.672331
469.9	527.66	1.725301	654.8	520.03	1.671621

RAW DATA FOR MAGNESIUM FLUORIDE

C = [C11+C12+2C44-SQRT[(C11-C33)**2+4*((C13+C44)**2)]]/4

MODE IS S [45 DEGREES TO [001] AND [100]]

LENGTH (298) = .2752 INCHES , DENSITY(298) = 3.1770 GM/CC

TEMPERATURE (DEGREES K)	FREQUENCY (KHZ)	MODULUS,C (MBAR)	TEMPERATURE (DEGREES K)	FREQUENCY (KHZ)	MODULUS,C (MBAR)
295.7	291.25	.526728	353.1	289.87	.521407
295.5	291.24	.526711	357.4	289.76	.520985
311.4	290.88	.525298	360.7	289.67	.520660
317.7	290.72	.524665	366.7	289.49	.519958
338.6	290.22	.522755	372.1	289.35	.519440
338.4	290.22	.522756	374.0	289.31	.519249
348.4	289.99	.521867			

RAW DATA FOR MAGNESIUM FLUORIDE

C = [C44+C66]/2 , MODE IS S [45 DEGREES TO [001] AND [100] POL. [010]

LENGTH (298) = .2752 INCHES , DENSITY(298) = 3.1770 GM/CC

TEMPERATURE (DEGREES K)	FREQUENCY (KHZ)	MODULUS,C (MBAR)
296.2	350.76	.763963
296.0	350.76	.763965
311.9	350.18	.761304
312.8	350.15	.761166
327.2	349.60	.758652
327.2	349.59	.758609
327.5	349.58	.758585
335.9	349.27	.757145
344.1	348.95	.755687
354.3	348.56	.753910
363.9	348.20	.752269
368.3	348.01	.751409
372.9	347.83	.750613
373.3	347.81	.750502

$KMgF_3$

RAW DATA FOR POTASSIUM MAGNESIUM FLUORIDE

C = (C11-C12)/2 , MODE IS S [110] POL. [1-10]

LENGTH (298) = .1937 INCHES , DENSITY(298) = 3.151 GM/CC

TEMPERATURE (DEGREES K)	FREQUENCY (KHZ)	TEMPERATURE (DEGREES K)	FREQUENCY (KHZ)
294.0	393.66	423.3	381.13
294.0	393.65	425.9	380.88
303.3	392.82	434.7	380.01
312.5	391.90	439.0	379.66
320.4	391.10	448.6	378.72
323.1	390.87	451.8	378.44
332.1	389.97	460.8	377.55
343.7	388.82	460.8	377.53
354.6	387.78	475.0	376.16
356.7	387.53	478.0	375.82
368.4	386.42	480.5	375.60
373.4	385.94	491.6	374.49
385.7	384.81	495.4	374.11
386.9	384.63	498.7	373.81
390.1	384.33	511.6	372.52
401.5	383.24	518.8	371.78
405.6	382.83	539.7	369.83
419.1	381.53	543.0	369.40
422.5	381.17		

RAW DATA FOR POTASSIUM MAGNESIUM FLUORIDE

C = C44 , MODE IS S [110] POL. [001]

LENGTH (298) = .1937 INCHES , DENSITY(298) = 3.151 GM/CC

TEMPERATURE (DEGREES K)	FREQUENCY (KHZ)	TEMPERATURE (DEGREES K)	FREQUENCY (KHZ)
294.3	404.95	467.8	400.39
294.3	404.97	468.3	400.37
302.2	404.81	478.2	400.04
319.0	404.33	481.0	400.02
326.4	404.16	484.9	399.92
336.6	403.78	494.2	399.58
345.6	403.53	498.3	399.54
357.9	403.27	499.5	399.44
361.4	403.15	513.5	399.05
370.9	402.92	513.7	399.12
373.4	402.84	521.1	398.82
376.1	402.78	531.1	398.63
381.2	402.62	531.2	398.63
398.4	402.19	533.0	398.58
400.9	402.12	543.5	398.26
411.9	401.79	551.2	398.09
425.3	401.49	552.9	398.03
429.8	401.33	555.0	397.99
435.6	401.15	560.1	397.87
440.0	401.12	563.3	397.77
440.5	401.11	565.6	397.72
443.4	400.96	571.9	397.52
450.9	400.84	578.2	397.33
456.6	400.71	580.7	397.26
456.9	400.69	589.2	397.01
459.8	400.60	597.4	396.79
460.2	400.58		

RAW DATA FOR POTASSIUM MAGNESIUM FLUORIDE

C = (C11+C12+2C44)/2 , MODE IS P [110]

LENGTH (298) = .1937 INCHES , DENSITY(298) = 3.151 GM/CC

TEMPERATURE (DEGREES K)	FREQUENCY (KHZ)	TEMPERATURE (DEGREES K)	FREQUENCY (KHZ)
298.0	680.66	444.8	670.17
308.6	679.84	448.0	670.00
312.6	679.60	454.0	669.59
318.9	679.14	473.0	668.05
327.3	678.64	478.6	667.74
332.6	678.22	497.7	666.37
343.0	677.55	500.1	666.28
350.3	676.98	516.3	665.25
350.7	677.00	521.6	665.01
352.9	676.78	534.4	664.16
362.7	676.25	539.7	663.78
372.3	675.59	555.4	662.82
372.7	675.60	558.1	662.55
382.0	674.98	563.0	662.41
391.4	674.00	593.6	660.19
407.6	672.92	601.4	659.58
428.5	671.53	603.1	659.37
428.4	671.44	620.5	658.11
435.3	670.95	624.8	657.84

BIBLIOGRAPHY

Abramowitz, M. and Stegun, I. A., (eds.), 1965. Handbook of mathematical functions, Dover Publications, Inc., New York.

Aleksandrov, K. S., Reshchikova, L. M. and Beznosikov, B. V., 1966. Behaviour of the elastic constants of $KMnF_3$ single crystals near the transition of puckering, Phys. Stat. Sol., 18:K17-K20.

Aleksandrov, K. S., Shabanova, L. A. and Zinenko, V. I., 1969. Elastic constants of MgF_2 single crystals, Phys. Stat. Sol., 33:K1-K3.

Alterovitz, S. and Gerlich, D., 1970. Third-order elastic moduli of strontium fluoride, Phys. Rev., 1B:2718-2723.

Anderson, D. L., 1967. A seismic equation of state, Geophys. J. R. astr. Soc., 13:9-30.

Anderson, D. L. and Anderson, O. L., 1970. The bulk modulus-volume relationship for oxides, J. Geophys. Res., 75:3494-3500.

Anderson, D. L. and Kanamori, H., 1968. Shock-wave equations of state for rocks and minerals, J. Geophys. Res., 73:6477-6502.

Anderson, D. L. Sammis, C. and Jordan, T., 1971. Composition and evolution of the mantle and core, Science, 171:1102-1112.

Anderson, O. L., 1963. A simplified method for calculating the Debye temperature from elastic constants, J. Phys. Chem. Solids, 24:909-917.

Anderson, O. L., 1966. Derivation of Wachtman's equation for the temperature dependence of elastic moduli of oxide compounds, Phys. Rev., 144:553-557.

Anderson, O. L., 1972. Patterns in elastic constants of minerals important to geophysics, in E. C. Robertson (ed.), The nature of the solid earth, McGraw-Hill, Chapt. 21:575-613.

Anderson, O. L., 1973. Comments on the power law representation of Birch's law, J. Geophys. Res., 78: 4901-4914.

Anderson, O. L. and Andreatch, P., Jr., 1966. Pressure derivatives of elastic constants of single-crystal MgO at 23° and -195.8°C, J. Am. Ceram. Soc., 49: 404-409.

Anderson, O. L. and Liebermann, R. C., 1970. Equations for the elastic constants and their pressure derivatives for three cubic lattices and some geophysical applications, Phys. Earth Planet. Inter., 3:61-85.

Anderson, O. L. and Nafe, J. E., 1965. The bulk modulus-volume relationship for oxide compounds and related geophysical problems, J. Geophys. Res., 70:3951-3963.

Anderson, O. L. and Soga, N., 1967. A restriction to the law of corresponding states, J. Geophys. Res., 72:5754-5757.

Austin, J. B., 1952. Thermal expansion of nonmetallic crystals, J. Am. Ceram. Soc., 35:243-253.

Axe, J. D., 1965. Long-wave lattice dynamics of the fluorite structure, Phys. Rev., 139: A1215-A1220.

Axe, J. D. and Pettit, G. D., 1966. Infrared dielectric dispersion and lattice dynamics of uranium dioxide and thorium dioxide, Phys. Rev., 151:676-680.

Bailey, D. M., Calderwood, F. W., Greiner, J. D., Hunter, O., Jr., Smith, J. F. and Schiltz, R. J., Jr., 1975. Reproducibilities of some physical properties of MgF_2, J. Am. Ceram. Soc., 58:489-492.

Bartels, R. A. and Vetter, V. H., 1972. The temperature dependence of the elastic constants of CaO and SrO, J. Phys. Chem. Solids, 33:1991-1992.

Beattie, A. G. and Samara, G. A., 1971. Pressure dependence of the elastic constants of $SrTiO_3$, J. Appl. Physics, 42:2376-2381.

Beckman, O. and Knox, K., 1961. Magnetic properties of $KMnF_3$.I Crystallographic studies, Phys. Rev., 121:376-380.

Bell, R. O. and Rupprecht, G., 1963. Elastic constants of strontium titanate, Phys. Rev., 129:90-94.

Bensch, W. A., 1972. Third-order elastic constants of NaF, Phys. Rev., 6B:1504-1509.

Bevington, P. R., 1969. Data reduction and error analysis for the physical sciences, McGraw-Hill.

Birch, F., 1960. The velocity of compressional waves in rocks to 10 kilobars, 1, J. Geophys. Res., 65:1083-1102.

Birch, F., 1961a. The velocity of compressional waves in rocks to 10 kilobars, 2, J. Geophys. Res., 66:2199-2224.

Birch, F., 1961b. Composition of the earth's mantle, Geophys. J. R. astr. Soc., 4:295-311.

Born, M., 1943. The thermodynamics of crystal lattices. I Discussion of the methods of calculation, Proc. Cambridge Phil. Soc., 39:100-103.

Born, M. and Bradburn, M., 1943. The thermodynamics of crystal lattices. II Calculation of certain lattice sums occurring in thermodynamics, Proc. Cambridge Phil. Soc., 39:104-113.

Bradburn, M., 1943. The thermodynamics of crystal lattices.III The equation of state for a face-centred cubic lattice, Proc. Cambridge Phil. Soc., 39:113-127.

Brielles, J. and Vidal, D., 1975. Variation des constantes élastiques de la fluorine CaF_2 avec la pression jusqu'à 12 kbar, High Temperatures - High Pressures, 7:29-33.

Briscoe, C. V., and Squire, C. F., 1957. Elastic constants of LiF from 4.2°K to 300°K by ultrasonic methods, Phys. Rev., 106:1175-1177.

Chang, E. and Graham, E. K., 1975. The elastic constants of cassiterite SnO_2 and their pressure and temperature dependence, J. Geophys. Res., 80:2595-2599.

Chernov, Y. M. and Stepanov, A. V., 1961. The temperature dependence of the elastic constants of LiF monocrystals, Sov. Phys.-Solid State, 3:2097-2098.

Chung, D. H., 1974. General relationships among sound speeds I. New experimental information, Phys. Earth Planet Inter., 8:113-120.

Cleavelin, C. R., Pederson, D. O., and Marshall, B. J., 1972. Elastic constants of RbF from 300 to 4.2°K, Phys. Rev., 5B:3193-3198.

Cook, R. K., 1957. Variation of elastic constants and static strains with hydrostatic pressure: a method for calculation from ultrasonic measurements, J. Acoust. Soc. Amer., 29:445-449.

Coughanour, L. W., Roth, R. S., Marzullo, S. and Sennett, F. E., 1955. Solid-state reactions and dielectric properties in the system magnesia-lime-tin oxide-titania, J. Res. Natl. Bur. Stds. U.S., 54:149.

Cutler, H. R. Gibson, J. J. and McCarthy, K. A., 1968. The elastic constants of magnesium fluoride, Solid State Communications, 6:431-433.

Davies, G. F., 1973. Quasi-harmonic finite strain equations of state of solids, J. Phys. Chem. Solids, 34:1417-1429.

Davies, G. F., 1975. The estimation of elastic properties from analogue compounds, Geophys. J. R. astr. Soc., in press.

Davies, G. F., 1976. Personal communication.

Davies, G. F. and Gaffney, E. S., 1973. Identification of high pressure phases of rocks and minerals from Hugoniot data, Geophys. J. R. astr. Soc., 33:165-183.

Debye, P., 1912. Zur Theorie der spezifischen Wärmen, Ann. Phys., 39:789-839.

Douglas, T. B., 1959. Thermodynamic properties of lithium, beryllium, magnesium, aluminium, and their compounds with hydrogen, oxygen, nitrogen, fluorine and chlorine, Unpublished report.

Frisillo, A. L. and Barsch, G. R., 1972. Measurement of single-crystal elastic constants of bronzite as a function of pressure and temperature, J. Geophys. Res., 77:6360-6384.

Fritz, I. J., 1974. Pressure and temperature dependence of the elastic properties of rutile (TiO_2), J. Phys. Chem. Solids, 35:817-826.

Furth, R., 1944. Proc. Roy. Soc. London, 183:87.

Garber, J. A. and Granato, A. V., 1975. Fourth-order elastic constants and the temperature dependence of second-order elastic constants in cubic materials, Phys. Rev., 11B:3998-4007.

Gerlich, D., 1964a. Elastic constants of barium fluoride between 4.2 and 300°K, Phys. Rev., 135:A1331-A1333.

Gerlich, D., 1964b. Elastic constants of strontium fluoride between 4.2 and 300°K, Phys. Rev., 136:A1366-A1368.

Gerlich, D., 1968. Third-order elastic moduli of barium fluoride, Phys. Rev., 168:947-952.

Gilman, J. J., 1963. Strength of ceramic crystals, U.S. National Bureau Standards Monograph 59:79-102.

Gmelin, E., 1970. Thermal properties of alkaline earth oxides II Analysis of experimental results for MgO, CaO, SrO, and BaO, Z. Naturforsch, 25a:887-893.

Goldschmidt, V. M., 1927. Geochemische Verteilungsgesetze der Elemente VIII. Untersuchungen über Bau und Eigenschaften von Krystallen, Skr. Nor. Vidensk.-Akad. Oslo, I, Math.-Naturvidensk. K., 1926, 2 no. 8:1-156.

Gow, M. M., 1944. The thermodynamics of crystal lattices IV The elastic constants of a face-centred cubic lattice with central forces, Proc. Cambridge Phil. Soc., 40:151-166.

Graham, E. K., 1973. On the compression of stishovite, Geophys. J. R. astr. Soc., 32:15-34.

Grüneisen, E., 1926. The state of a solid body, translation of "Zurstand des festen Körpers". Handbuch der Physik, Bd. 10, Julius Springer (Berlin), 1926, pp. 1-52. NASA Republication RE2-18-59W.

Hart, S. and Stevenson, R. W. H., 1970. The elastic compliances of CoF_2, J. Phys. D. : Appl. Phys., 3:1789-1795.

Haussühl, S., 1960. Thermo-elastische Konstanten der Alkalihalogenide vom NaCl-Typ, Z. Phys., 159:223-229.

Haussühl, S., 1963. Das elastische Verhalten von Flusspat und strukturverwandten Kristallen, Phys. Stat. Solidi, 3:1072-1076.

Haussühl, S., 1968. Elastisches und thermoelastisches Verhalten von MgF_2 und MnF_2, Phys. Stat. Sol., 28:127-130.

Hill, R., 1952. The elastic behaviour of a crystalline aggregate, Proc. Phys. Soc. London (A), 65:349-354.

Ho, P. S. and Ruoff, A. L., 1967. Pressure dependence of the elastic constants and an experimental equation of state for CaF_2, Phys. Rev., 161:864-869.

Huffman, D. R. and Norwood, M. H., 1960. Specific heat and elastic constants of calcium fluoride at low temperatures, Phys. Rev., 117:709-711.

Jackson, I.N.S., 1976. Phase equilibria in oxide and silicate analogue systems: studies of melting and polymorphic phase transformations, Ph.D. Thesis, A.N.U.

Jackson, I. N. S. and Liebermann, R. C., 1974. Melting and elastic shear instability of alkali halides, J. Phys. Chem. Solids, 35:1115-1119.

Jamieson, J. C. and Wu, A. Y., 1974. The pressure dependence of the elastic constants of NiF_2, personal communication.

JANAF Thermochemical Tables, 2nd ed., 1971. NSRDS-NBS 37, Washington.

Johnston, D. L., Thrasher, P. H. and Kearney, R. J., 1970. Elastic constants of SrO, J. Appl. Phys., 41:427-428.

Jones, L. E. A. and Liebermann, R. C., 1974. Elastic and thermal properties of fluoride and oxide analogues in the rocksalt, fluorite, rutile and perovskite structures, Phys. Earth Planet. Inter., 9:101-107.

Katiyar, R. S. and Krishnan, R. S., 1969. Lattice dynamics of crystals having the rutile structure, J. Ind. Inst. Sci., 51:121-133.

Kittel, C., 1971. (4th edition). Introduction to solid state physics, John Wiley and Sons, Inc., New York.

Leibfried, G. and Hahn, H., 1958. Zur Temperaturabhängigkeit der elastischen Konstanten von Alkalihalogenidkristallen, Z. Physik, 150:497-525.

Leibfried, G. and Ludwig, W., 1961. Theory of anharmonic effects in crystals, in Solid State Physics, edited by F. Seitz and D. Turnbull (Academic, New York), 12:275-444.

Levin, E. M., Robbins, C. R. and McMurdie, H. F., 1964. Phase diagrams for ceramists, American Ceramic Society, Columbus, Ohio.

Levin, E. M., Robbins, C. R. and McMurdie, H. F. 1969. Phase diagrams for ceramists. 1969 Supplement, American Ceramic Society, Columbus, Ohio.

Lewis, J. T., Lehoczky, A. and Briscoe, C. V., 1967. Elastic constants of the alkali halides at 4.2°K, Phys. Rev., 161:877-887.

Liebermann, R. C., 1972. Compressional velocities of polycrystalline olivine, spinel, and rutile minerals, Earth Planet. Sci. Letters, 17:263-268.

Liebermann, R. C., 1974a. Unpublished data.

Liebermann, R. C., 1974b. Elasticity of pyroxene-garnet and pyroxene-ilmenite phase transformations in germanates, Phys. Earth Planet. Inter., 8:361-374.

Liebermann, R. C., 1975. Elasticity of olivine (α), beta (β), and spinel (γ) polymorphs of germanates and silicates, Geophys. J. R. astr. Soc., 42:899-929.

Liebermann, R. C., 1976. Elasticity of the ilmenite-perovskite phase transformation in $CdTiO_3$, Earth Planet. Sci. Letters, 29:326-332.

Liebermann, R. C. and Ringwood, A. E., 1973. Birch's law and polymorphic phase transformations, J. Geophys. Res., 78:6926-6932.

Liebermann, R. C., Ringwood, A. E. and Major, A., 1976. Elasticity of stishovite, submitted to Earth Planet. Sci. Letters.

Liebermann, R. C., Ringwood, A. E., Mayson, D. J. and Major, A., 1975. Hot-pressing of polycrystalline aggregates at very high pressure for ultrasonic measurements, Proc. 4th International Conf. High Pressure, Kyoto, 1974, pp. 495-502, Physico-Chemical Society of Japan.

Liu, L., 1975. Post-oxide phases of forsterite and enstatite, Geophys. Res. Letters, 2:417-419.

Liu, L., 1976. The high pressure phases of $MgSiO_3$, Earth Planet. Sci. Letters, in press.

Lytle, F. W., 1964. X-ray diffractometry of low-temperature phase transformations in strontium titanate, J. Appl. Phys., 35:2212-2215.

McSkimin, H. J., 1961. Pulse superposition method for measuring ultrasonic wave velocities in solids, J. Accoust. Soc. Am., 33:12-16.

McSkimin, H. J., 1964. Ultrasonic methods for measuring the mechanical properties of liquids and solids, in W. P. Mason (ed.) Physical Acoustics, Vol. 1A, Academic Press, Chapter 4, 271-334.

McSkimin, H. J., and Andreatch, P., 1962. Analysis of the pulse superposition method for measuring ultrasonic wave velocities as a function of temperature and pressure, J. Acoust. Soc. Am., 34:609-615.

Macedo, P. M., Capps, W. and Wachtman, J. B., Jr., 1964. Elastic constants of single crystal ThO_2 at 25°C, J. Am. Ceram. Soc., 47:651.

Madan, M. P., 1971. Temperature dependence of the bulk modulus of alkali halides, J. Appl. Phys., 42:3888-3893.

Manghnani, M. H., Fisher, E. S. and Brower, W. S., Jr., 1972. Temperature dependence of the elastic constants of single crystal rutile between 4° and 583°K, J. Phys. Chem. Solids, 33:2149-2159.

Marshall, B. J. and Miller, R. E., 1967. Elastic constants of KF from 300° to 4.2°K, J. Appl. Phys., 38:4749-4750.

Megaw, H. D., 1939. The thermal expansion of crystals in relation to their structure, Z. Krist., 100:58-76.

Meister, R. and Peselnick, L., 1966. Variational method of determining effective moduli of polycrystals with tetragonal symmetry, J. Appl. Phys., 37:4121-4125.

Melcher, R. L., 1970. Magnon-phonon interactions in MnF_2, J. Appl. Phys., 41:1412-1414.

Melcher, R. L. and Bolef, D. I., 1969. Ultrasonic propagation in $RbMnF_3$. I Elastic properties, Phys. Rev., 178:864-873.

Miller, R. A. and Smith, C. S., 1964. Pressure derivatives of the elastic constants of LiF and NaF, J. Phys. Chem. Solids, 25:1279-1292.

Mitskevich, V. V., 1965. Temperature coefficients of elastic constants of alkali halide crystals, Sov. Phys.-Solid State, 6:2405-2409.

Mizutani, H., Hamano, Y. and Akimoto, S., 1972. Elastic-wave velocities of polycrystalline stishovite, J. Geophys. Res., 77:3744-3749.

Musgrave, M. J. P., 1970. Crystal acoustics, Holden-Day, San Francisco.

Nikanorov, S. P. and Stepanov, A. V., 1963. Temperature dependence of the elastic constants of single crystals of potassium chloride and sodium fluoride, Sov. Phys.-Solid State, 4:1889-1895.

Nikanorov, S. P., Kardashev, B. K. and Kas'kovich, N. S., 1968. Temperature dependence of elastic constants of calcium fluoride, Sov. Phys.-Solid State, 10:703-705.

Rai, C. S. and Manghnani, M. H., 1976. Pressure and temperature dependence of the elastic moduli of polycrystalline MgF_2, submitted for publication.

Rao, K. V. Krishna, 1973. Thermal expansion and crystal structure, American Institute of Physics Conference Proceedings (U.S.A.), 17:219-230.

Reshchikova, L. M., 1969. Elastic properties of a $KMgF_3$ single crystal, Sov. Phys.-Solid State, 10:2019-2020.

Ringwood, A. E., 1970. Phase transformations and the constitution of the mantle, Phys. Earth Planet. Inter., 3:109-155.

Roberts, R. W. and Smith, C. S., 1970a. Ultrasonic parameters in the Born model of the sodium and potassium halides, J. Phys. Chem. Solids, 31:619-634.

Roberts, R. W. and Smith, C. S., 1970b. Ultrasonic parameters in the Born model of the rubidium halides, J. Phys. Chem. Solids, 31:2397-2400.

Robie, R. A. and Waldbaum, D. R., 1968. Thermodynamic properties of minerals and related substances at 298.15°K (25.0°C) and one atmosphere (1.013 bars) pressure and at higher temperatures, Geol. Surv. Bull. 1259:1-256, U.S. Dept. Inter.

Robie, R. A., Bethke, P. M., Toulmin, M. S. and Edwards, J. L., 1966. X-ray crystallographic data, densities, and molar volumes of minerals, in S. P. Clark (ed.), Handbook of Physical Constants, Geol. Soc. Am. Mem., 97, Sect. 5:27-73.

Rosenberg, H. M. and Wigmore, J. K., 1967. The elastic constants of potassium magnesium fluoride, Phys. Letters, 24A:317.

Roth, R. S., 1957. Classification of perovskite and other ABO_3-type compounds, J. Res. Natl. Bur. Standards, U.S., 58:75-88.

Rousseau, M., Nouet, J. and Zarembowitch, A., 1974. Interatomic force constants studies of AMF_3 perovskite-type crystals, J. Phys. Chem. Solids, 35:921-926.

Roy, D. M., Roy, R. and Osborn, E. F., 1953. Fluoride model systems: III The system NaF-BeF_2 and the polymorphism of Na_2BeF_4 and BeF_2, J. Am. Ceram. Soc., 36:185-190.

Roy, D. M., Roy, R., and Osborn, E. F., 1954. Fluoride model systems: IV The systems LiF-BeF_2, and PbF_2-BeF_2, J. Am. Ceram. Soc., 37:300-305.

Schreiber, E., Anderson, O. L. and Soga, N., 1973. Elastic constants and their measurement, McGraw-Hill.

Shankland, T. J., 1972. Velocity-density systematics: derivation from Debye theory and the effect of ionic size, J. Geophys. Res., 77:3750-3758.

Shankland, T. J. and Chung, D. H., 1974. General relationships among sound speeds, II Theory and discussion, Phys. Earth Planet. Inter., 8:121-129.

Shannon, R. D. and Prewitt, C. T., 1969. Effective ionic radii in oxides and fluorides, Acta Crystallogr., B25:925-946.

Shannon, R. D. and Prewitt, C. T., 1970. Revised values of effective ionic radii, Acta. Crystallogr. B26:1046-1048.

Sirdeshmukh, D. B. and Deshpande, V. T., 1964. Temperature variation of the lattice constants and the coefficients of thermal expansion of some fluorite type crystals, Indian J. Pure Appl. Physics, 2:405-407.

Sirdeshmukh, D. B. and Rao, B. K., 1975. The effective charge model and the Grüneisen constant of some oxides, J. Phys. Chem. Solids, 36:355.

Slagle, O. D. and McKinstry, H. A., 1967. Temperature dependence of the elastic constants of the alkali halides. I. NaCl, KCl, and KBr, J. Appl. Phys., 38:437-446.

Smith, J. V., 1960. The system cadmium oxide-stannic oxide, Acta. Crystallogr., 13:749-752.

Soga, N. and Anderson, O. L., 1967. High-temperature elasticity and expansivity of forsterite and seatite, J. Am. Ceram. Soc., 50:239-242.

Soga, N., Schreiber, E. and Anderson, O. L., 1966. Estimation of bulk modulus and sound velocities of oxides at very high temperatures, J. Geophys. Res., 71:5315-5320.

Son, P. R. and Bartels, R. A., 1972. CaO and SrO single crystal elastic constants and their pressure derivatives, J. Phys. Chem. Solids, 33:819-828.

Spetzler, H. A. W., 1969. Effect of temperature and pressure on elastic properties of polycrystalline MgO, Ph.D. thesis, Calif. Inst. Technol. Calif.

Spetzler, H., 1970. Equation of state of polycrystalline and single crystal MgO to 8 kilobars and 800°K, J. Geophys. Res., 75:2073-2087.

Spinner, S., Stone, L. and Knudsen, F. P., 1963. Temperature dependence of the elastic constants of thoria specimens of varying porosity, J. Res. Natl. Bur. Standards, U.S., 67C:93-100.

Srivastava, K. K. and Merchant, H. D., 1973. Thermal expansion of alkali halides above 300°K, J. Phys. Chem. Solids, 34:2069-2073.

Stern, E. A., 1958. Theory of the anharmonic properties of solids, Phys. Rev., 111:786-797.

Striefler, M. E. and Barsch, G. R., 1973. Elastic and optical properties of rutile-structure fluorides in the rigid-ion approximation, Phys. Stat. Sol. (b), 59:205-217.

Striefler, M. E. and Barsch, G. R., 1974. Optical mode gammas, pressure derivatives of elastic and dielectric constants, and stability of rutile structure fluorides in the rigid ion approximation, Phys. Stat. Sol. (b), 64:613-625, Erratum, Phys. Stat. Sol. (b), 67:417-418.

Striefler, M. E. and Barsch, G. R., 1975. Elastic, optical, and dielectric properties and their pressure derivatives of rutile-structure oxides in a modified rigin ion approximation, Phys. Stat. Sol. (b), 67:143-156.

Striefler, M. E. and Barsch, G. R. 1976. Elastic and optical properties of stishovite, submitted to J. Geophys. Res.

Susse, C., 1961. Mesure des constantes élastiques du fluorure de lithium et du périclase en fonction de la température et de la pression, J. Rech. Centre Natl. Rech. Sci. (Paris), 54:23-59.

Swanson, H. E., Fuyat, R. F. and Ugrinic, G. M., 1954. Standard X-ray diffraction powder patterns, U.S. National Bureau Standards Circular 539 Vol. III:44.

Thilo, E. and Lehmann, H. A., 1949. Chemische Untersuchungen von Silikaten. XII Über das System LiF-BeF_2 und seine Beziehungen zum System MgO-SiO_2, Z. Anorg. Chem., 258:332-355.

Thomsen, L., 1970. On the fourth-order anharmonic equation of state of solids, J. Phys. Chem. Solids, 31:2003-2016.

Thomsen, L., 1972. The fourth-order anharmonic theory: elasticity and stability, J. Phys. Chem. Solids, 33:363-378.

Thomsen, L. and Anderson, O. L., 1969. On the high-temperature equation of state of solids, J. Geophys. Res., 74:981-991.

Touloukian, Y. S., (ed.), 1967. Thermophysical properties of high temperature solid materials, Vol. 5. Non-oxides and their solutions and mixtures, including miscellaneous ceramic materials, Thermophysical Properties Research Center, Purdue University, MacMillan.

Truell, R., Elbaum, C. and Chick, B. B., 1969. Ultrasonic methods in solid state physics, Academic Press, Inc. (London) Ltd.

Vallin, J., Marklund, K., Sikström, J. O. and Beckman, O., 1966. Elastic properties of NaF, Arkiv för Fysik, 32:515-527.

Varshni, Y. P., 1970. Temperature dependence of the elastic constants, Phys. Rev., 10B:3952-3958.

Vetter, V. H. and Bartels, R. A., 1973. BaO single crystal elastic constants and their temperature dependence, J. Phys. Chem. Solids, 34:1448-1449.

Vidal, D., 1974. Mesure des constantes élastiques du fluorure de calcium monocristallin de 20 à 850°C, C. R. Acad. Sc. Paris, 279B:345-347.

Wachtman, J. B., Jr., Tefft, W. E., Lam, D. G., Jr. and Apstein, C. S., 1961. Exponential temperature dependence of Young's modulus for several oxides, Phys. Rev., 122:1754-1759.

Wachtman, J. B., Jr., Wheat, M. L., Anderson, H. J., and Bates, J. L., 1965. Elastic constants of single crystal UO_2 at 25°C, J. Nucl. Mater., 16:39-41.

Wang, H. and Simmons, G., 1973. Elasticity of some mantle crystal structures 2. Rutile GeO_2, J. Geophys. Res., 78:1262-1273.

Wasilik, J. H. and Wheat, M. L., 1965. Elastic constants of cubic lead fluoride at room temperature, J. Appl. Phys. 36:791-793.

Waterman, P. C., 1959. Orientation dependence of elastic waves in single crystals, Phys. Rev., 113:1240-1253

Weast, R. C. (ed.), 1972. Handbook of Chemistry and Physics, Chemical Rubber Co., Cleveland, Ohio, U.S.A.

Wicks, C. E. and Block, F. E., 1963. Thermodynamic properties of 65 elements - their oxides, halides, carbides and nitrides, U.S. Bur. Mines, Bull. 605:1-146.

Wong, C. and Schuele, D. E., 1968. Pressure and temperature derivatives of the elastic constants of CaF_2 and BaF_2, J. Phys. Chem. Solids, 29:1309-1330.

Wu, A. Y., 1974. The elastic properties of NiF_2 single crystal, personal communication.

Wyckoff, R. W. G., 1963. Crystal structures, Volume 1, 2nd edition, Interscience Publishers.

ERRATA

Page 5, line 18	"behavior" should be "behaviour".
Page 9, line 14	"viscocity" should be "viscosity".
Table 5.1, Ref. 12	"1964" should be "1965".
Ref. 25	"1967" should be "1957".
Table 5.8	"d" should be "d_o".

Physics of the Earth and Planetary Interiors, 9 (1974) 101–107

ELASTIC AND THERMAL PROPERTIES OF FLUORIDE AND OXIDE ANALOGUES IN THE ROCKSALT, FLUORITE, RUTILE AND PEROVSKITE STRUCTURES

LEONIE E.A. JONES and ROBERT C. LIEBERMANN
Research School of Earth Sciences, Australian National University, Canberra, A.C.T. (Australia)

(Submitted for publication March 19, 1974; accepted May 31, 1974)

Fluorides are considered as models for the physical properties of oxides on the basis of Goldschmidt's crystal chemical arguments. The well-established bulk modulus (K)–volume (V) relationship KV = constant is shown to hold for fluorides and oxides belonging to the four isostructural series. The bulk moduli of equivolume oxides and fluorides are scaled as $4S^2$, where $S = Z^O/2Z^F$ is the ratio of the effective unit charges and is approximately 77% for all of the crystal structures. The fluorides have distinctly lower melting and Debye temperatures which offers the possibility of using these compounds as models for the high-temperature elastic behaviour of their oxide analogues.

1. Introduction

The concept of fluoride and oxide analogue compounds was first introduced by Goldschmidt (1927) on the basis of a number of crystal chemical considerations: (a) the similarity in ionic radii of O^{2-} and F^-; (b) the applicability of the rigid ion model to compounds containing the O^{2-} and F^- ions, which have relatively low polarizabilities resulting in their ionic radii being almost independent of coordination number; and (c) the correspondence of the crystal structures of oxide and fluoride compounds in which the cations are also of comparable ionic radii. Notable examples of this modelling concept are LiF–MgO (rocksalt structure) CaF_2–ThO_2 (fluorite structure), MgF_2–TiO_2 (rutile structure), and BeF_2–SiO_2 (α-quartz and coesite structures).

Goldschmidt (1927) also suggested that because of their lower ionic charge fluorides should be "weakened" models of their oxide analogues and thus be characterized by lower melting temperature, lower hardness and lower refractive index. Subsequent investigations by Roy et al. (1953, 1954) and Thilo and Lehmann (1949), have demonstrated close similarities in the phase diagrams of binary fluoride and oxide systems at atmospheric pressure with the fluoride systems exhibiting much lower solidus and liquidus temperatures. Recently, Jackson and Liebermann (1974) have shown that the fusion curves of rocksalt fluorides and oxides at high pressure may be correlated in a similar manner.

The purpose of this paper is to examine the elastic and thermal properties of fluoride and oxide compounds crystallizing in the rocksalt, fluorite, rutile, and perovskite structures in the framework of systematics proposed by previous investigators. We also compare the melting and Debye temperatures of the model pairs to evaluate the possibility of using fluoride data to predict the high-temperature elasticity of their oxide analogues.

2. Data and discussion

The central feature of the entire modelling scheme is the similarity of the ionic radii of O^{2-} and F^- for various coordination numbers listed below (after Shannon and Prewitt, 1970).

Coordination number	Ionic radii (Å)	
	O^{2-}	F^-
II	1.35	1.285
III	1.36	1.30
IV	1.38	1.31
VI	1.40	1.33

Simple fluoride and oxide compounds whose cations have comparable ionic radii and ionic charge ratios of 1/2 exhibit the same crystal structure. In addition, a number of binary compounds which obey this model-

TABLE I
Crystal structures of some fluorides and oxides

Crystal structure	Fluoride	Oxide
Olivine	Na_2BeF_4	Ca_2SiO_4
Phenacite	Li_2BeF_4	Zn_2SiO_4
Pyroxene	$LiBeF_3$	$MgSiO_3$
Diopside	$LiNaBe_2F_6$	$CaMgSi_2O_6$
Perovskite	$KMnF_3$	$BaTiO_3$
Spinel	Li_2NiF_4	Mg_2SnO_4
Strontium plumbate	Na_2NiF_4	Ca_2SnO_4

ling formula and whose crystal structures are of interest in geophysical discussions of the earth's interior are listed in Table I. Of particular interest is the close correspondence of the ionic radii of Be^{2+} and Si^{4+} (0.27Å and 0.26Å, respectively, for 4-fold coordination (Shannon and Prewitt, 1970)) which permits the fluoride–oxide model system to be extended to fluoroberyllates and silicates. One disadvantage is that trivalent cations have no place in this scheme, so that it is difficult to model the corundum and garnet structures.

In Table II we list all the fluorides and oxides of the rocksalt, fluorite, rutile and perovskite structures for which elastic constant data are available. Table II also contains coordination numbers, ionic radii, densities (ρ), molecular weights (M), molar volumes (V), and the isotropic elastic bulk (K) and shear (μ) moduli, all determined at room temperature and atmospheric pressure.

2.1. *Elastic properties systematics*

Several previous studies have demonstrated that the relationship KV = constant holds for isostructural series of halides, oxides, sulfides, selenides, and tellurides (O.L. Anderson and Nafe, 1965; D.L. Anderson, 1967; O.L. Anderson and Soga, 1967; D.L. Anderson and O.L. Anderson, 1970; and O.L. Anderson, 1972). This behaviour is consistent with a simple Born-Mie interatomic potential with power law repulsion leading to $KV^{4/3}$ = constant, which is indistinguishable from the empirical result. Following O.L. Anderson and Nafe (1965), we present in Fig. 1 the data of Table II as a log-log plot of bulk modulus versus molar volume per ion pair ($V^* = 2\overline{M}/\rho$ = $2\overline{V}$, where $\overline{M}$ and $\overline{V}$ are the mean atomic weight and volume, respectively).

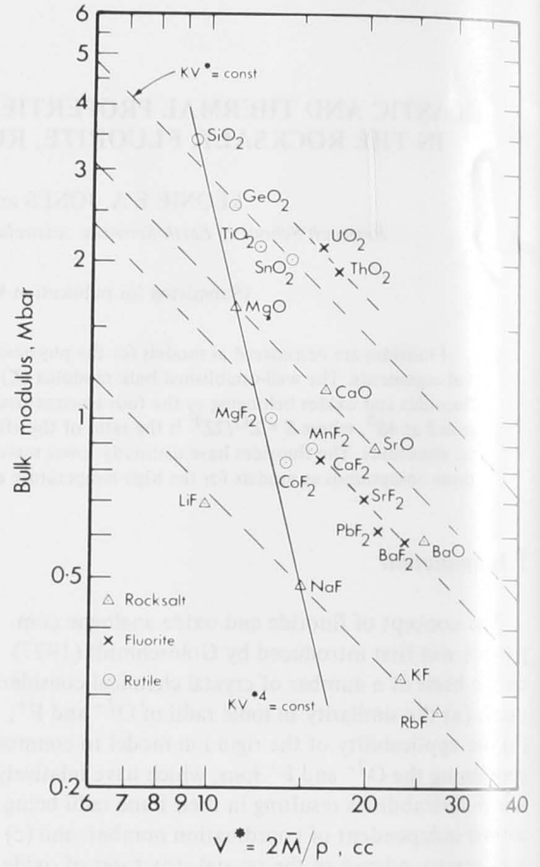

Fig. 1. Log-log plot of bulk modulus (K) versus molar volume per ion pair ($2\overline{M}/\rho$) for oxides and fluorides in the rocksalt, fluorite and rutile structures. (To avoid confusion, the perovskite structure is excluded.) The KV^* = constant lines for oxides and fluorides in the three structures are indicated by dashed lines of gradient −1. The solid line of gradient −4 represents the constant mean atomic weight relationship KV^{*4} = constant for $\overline{M}$ = 20–21.

Three important trends emerge from this data:

(1) The relationship KV^* = constant holds for fluorides and oxides crystallizing in the rocksalt, fluorite, rutile and perovskite structures.

(2) From the values of $\psi = KV^*/Z_cZ_ae^2$ in Table II we observe that the isostructural lines are scaled as Z_cZ_a for the fluoride compounds and also for the oxide compounds, where Z_c and Z_a are the valence charges of the

cation and anion. The constancy of the values (within 10%) for each set of chemical compounds in different crystal structures implies that the effective charges in the Born-Mie interatomic potential are relatively insensitive to coordination number and to the details of the atomic packing (see also D.L. Anderson and O.L. Anderson, 1970).

(3) The fact that the ψ-values for the fluoride and oxide compounds within each isostructural group are not the same may be attributable to differences in the effective charge. If $S = Z^O/2Z^F$ is defined as the ratio of the effective unit charges of the oxides with respect to the fluorides (following O.L. Anderson, 1972), then the KV^* = constant lines for the fluorides and oxides of a given structure are scaled as $4S^2$. The values of S determined by comparing the KV^* lines for each structural group in Fig. 1 are 0.80 for the rocksalt, 0.78 for the fluorite, 0.74 for the rutile and 0.74 for the perovskite structures. Thus the effective unit charge of an oxide is approximately 77% of that of its fluoride analogue for all the structures considered.

It is interesting to compare our values of S with those derived from the more rigorous lattice dynamical calculations. Using a shell model, Axe (1965) and Axe and Pettit (1966) derived values of $S = 0.73$ for the fluorite structure (CaF_2 and ThO_2). Katiyar and Krishnan (1969) employed a rigid ion model and concluded that $S = 0.77$ for the rutile structure (MgF_2 and TiO_2). Recent determinations of the effective charges for rutile fluorides (Striefler and Barsch, 1973) and rutile oxides (M.E. Striefler and G.R. Barsch, private communication, 1974) from a least-squares fit over all the available elastic and optical data lead to values of S in the range 0.57–0.74.

Since the relative effective charges of the fluorides and oxides do not appear to depend on coordination number or crystal field, it should thus be possible to predict the bulk modulus of an oxide from the bulk modulus of a fluoride of the same crystal structure. In particular the bulk moduli of the corresponding fluoride–oxide pairs in the Goldschmidt modelling scheme (for which the molar volumes are comparable) are related by $(K^O/K^F) = 4S^2$. A similar idea was suggested by Haussühl (1968) in considering MgF_2–TiO_2 and LiF–MgO as analogue pairs.

Another aspect of bulk modulus systematics is given by O.L. Anderson and Nafe (1965) (see also O.L. Anderson and Soga, 1967) who proposed that data for oxides and silicates of common mean atomic weight $\bar{M}$ = 20–21 would be characterized by the relationship KV^{*4} = constant. In Fig. 1, the bulk moduli of compounds with $\bar{M}$ = 20–21 (SiO_2, MgF_2, MgO, NaF) are indeed scaled as the inverse fourth power of the volume; this is an important result since this group of compounds contains both oxides and fluorides of different crystal structures. For other values of $\bar{M}$, the $K \sim V^{*-4}$ scaling is not as evident. However, for the rocksalt structure pairs MgO–NaF ($\bar{M}$ = 20–21), CaO–KF ($\bar{M}$ = 28–29), and SrO–RbF ($\bar{M}$ = 52) this relationship holds very well as indicated in Table III; the members of each pair have comparable $\bar{M}$ since they are composed of adjacent elements in the Periodic Table which are very close in atomic weight. This alternative modelling scheme, on the basis of common $\bar{M}$ rather than ionic radii, is implicit in the approach of Son and Bartels (1972) who chose their pairs on the basis of the same closed shell ion core configuration.

2.2. *High-temperature elasticity*

In presenting the concept of fluorides as "weakened" models of oxides, Goldschmidt (1927) cited the melting points of the phenacites Li_2BeF_4 (470°C) and Zn_2SiO_4 (1510°C) to illustrate the greater temperature sensitivity of the physical properties of the fluorides. We list in Table II the melting temperatures at atmospheric pressure for the compounds under consideration in this paper. The ratios of the melting points of the fluorides to those of their oxide analogues T_m^F/T_m^O are given in Table IV; with the exception of MgF_2–TiO_2, this ratio is less than 0.6 for all of the analogue pairs.

In discussing the temperature dependence of the elastic properties, the Debye temperature θ_D is a significant parameter since Leibfried and Ludwig (1961) have shown that for $T > \theta_D$ the bulk modulus should decrease linearly with increasing temperature. The elastic moduli data of Table II may be used to calculate the elastic Debye temperatures from the following equation, which holds for isotropic solids (Debye, 1912):

$$\theta_D = \frac{h}{k}\left(\frac{9\rho N}{4\pi M}\right)^{1/3} \upsilon_m$$

where: $3\upsilon_m^{-3} = \left(\frac{2}{\upsilon_s^3} + \frac{1}{\upsilon_p^3}\right)$

TABLE II
Summary of elastic and thermal properties of fluorides and oxides

Structure	Compound	CN	Ionic radii[1,2] (Å)		$Z_c Z_a$	Molar volume (cm^3)	M (g)	ρ (g/cm^3)	Elastic moduli (Mbar)		ψ[a]	T_m	θ_D	A[b]
			cation(s)	anion					K_s	μ_s		(°K)	(°K)	
Rocksalt	LiF	6–6	0.74	1.33	1	9.83	25.94	2.639[3]	0.696[3]	0.490[3]	0.267	1120[31]	734[34]	57
	NaF		1.02	1.33	1	14.98	41.99	2.804[3]	0.482[3]	0.313[3]	0.281	1269[32]	491[35]	56
	KF		1.38	1.33	1	23.00	58.10	2.526[4]	0.323[4]	0.164[4]	0.289	1130[31]	327[4]	50
	RbF		1.49	1.33	1	27.18	104.47	3.8434[5]	0.280[5]	0.127[5]	0.297	1048[33]	221[5]	48
	MgO		0.72	1.40	4	11.25	40.31	3.583[6]	1.628[6]	1.311[6]	0.178	3125[32]	955[36]	96
	CaO		1.00	1.40	4	16.76	56.08	3.346[7]	1.14[7]	0.814[7]	0.186	2887[32]	670*	91
	SrO		1.13	1.40	4	20.69	103.62	5.009[7]	0.88[7]	0.591[7]	0.177	2693[32]	457[37]	90
	BaO		1.36	1.40	4	25.59	153.34	5.992[8]	0.61[8]	0.355[8]	0.152	2291[32]	291*	75
Fluorite	CaF_2	8–4	1.12	1.31	2	24.55	78.08	3.181[9]	0.841[9]	0.426[9]	0.268	1691[32]	514[38]	67
	SrF_2		1.25	1.31	2	29.37	125.62	4.277[10]	0.699[10]	0.346[10]	0.267	1673[31]	380[10]	66
	PbF_2		1.29	1.31	2	31.47	245.19	7.79[11]	0.611[11]	0.230[11]	0.250	1097[31]	221[11]	55
	BaF_2		1.42	1.31	2	35.89	175.34	4.886[9]	0.584[9]	0.255[9]	0.272	1593[31]	282[39]	62
	UO_2		1.00	1.38	8	24.62	270.03	10.97[12]	2.13[12]	0.874[12]	0.170	3151[32]	394*	95
	ThO_2		1.04	1.38	8	26.38[13]	264.04	10.01	1.93[14]	0.972[14]	0.165	3493[32]	424*	103
Rutile	MgF_2	6–3	0.72	1.30	2	19.61	62.31	3.178[15]	1.015[15]	0.546[15]	0.258	1536[32]	621*	67
	CoF_2		0.735	1.30	2	21.11	96.93	4.592[16]	0.835[16]	0.392[16]	0.229	1475[31]	428*	59
	MnF_2		0.82	1.30	2	23.67	92.93	3.926[15]	0.883[15]	0.30[15]	0.271	1129[31]	393*	55
	SiO_2		0.40	1.36	8	14.01	60.08	4.287[17]	3.46[17]	1.29[17]	0.157		930*	88
	GeO_2		0.54	1.36	8	16.64	104.59	6.286[18]	2.589[18]	1.509[18]	0.140		774*	102
	TiO_2		0.605	1.36	8	18.80	79.90	4.25[13]	2.155[19]	**1.124**[19]	0.132	2103[32]	782*	94
	SnO_2		0.69	1.36	8	21.55	150.69	6.992[20]	2.03[20]	0.98[20]	0.142	1903[32]	545*	94
Perovskite	$KMgF_3$	12–6–6	1.60 0.72	1.33	1.5	38.23	120.41	3.15[21]	0.753[21]	0.471[21]	0.299		548*	67
	$KMnF_3$		1.60 0.82	1.33	1.5	44.16	151.04	3.42[22]	0.649[23]	0.325[23]	0.298		418*	60
	$RbMnF_3$		1.73 0.82	1.33	1.5	45.73	197.40	4.317[24]	0.675[24]	0.341[24]	0.321		386[23]	64
	$CdTiO_3$		1.31 0.605	1.40	6	32.90[25]	208.30	6.331	2.00[26]	0.98[26]	0.171		589*	90
	$CdSnO_3$		1.31 0.69	1.40	6	36.65[27]	279.09	7.615	1.89[26]	0.87[26]	0.180		489*	90
	$CaSnO_3$		1.35 0.69	1.40	6	36.47[28]	206.77	5.673	1.15[26]	0.85[26]	0.109		555*	87
	$SrTiO_3$		1.40 0.605	1.40	6	35.87	183.52	5.116[29]	1.744[30]	1.17[30]	0.162		691*	102

[a] $\psi = KV^*/Z_c Z_a e^2$; $V^* = 2\bar{M}/\rho = 2\bar{V}$
[b] $A = a\theta_D\sqrt{\bar{M}}$; $a = V^{1/3}$ = mean lattice parameter.
* θ_D calculated from room temperature values of the elastic constants.

1. Shannon and Prewitt (1969)
2. Shannon and Prewitt (1970)
3. Miller and Smith (1964)
4. Marshall and Miller (1967)
21. Reshchikova (1969)
22. Beckman and Knox (1961)
23. Aleksandrov et al. (1966)
24. Melcher and Bolef (1969)

θ_D calculated from room temperature values of the elastic constants.

1. Shannon and Prewitt (1969)
2. Shannon and Prewitt (1970)
3. Miller and Smith (1964)
4. Marshall and Miller (1967)
5. Cleavelin et al. (1972)
6. Spetzler (1969)
7. Son and Bartels (1972)
8. Vetter and Bartels (1973)
9. Wong and Schuele (1968)
10. Gerlich (1964b)
11. Wasilik and Wheat (1965)
12. Wachtman et al. (1965)
13. Robie et al. (1966)
14. Macedo et al. (1964)
15. Haussühl (1968)
16. Hart and Stevenson (1970)
17. Mizutani et al. (1972)
18. Wang and Simmons (1973)
19. Manghnani et al. (1972)
20. Liebermann (1973)
21. Reshchikova (1969)
22. Beckman and Knox (1961)
23. Aleksandrov et al. (1966)
24. Melcher and Bolef (1969)
25. Roth (1957)
26. Liebermann (1974)
27. Smith (1960)
28. Coughanour et al. (1955)
29. Swanson et al. (1954)
30. Bell and Rupprecht (1963)
31. Wicks and Block (1963)
32. Robie and Waldbaum (1968)
33. Weast (1972)
34. Briscoe and Squire (1957)
35. Lewis et al. (1967)
36. θ_D calculated from elastic constants of Anderson and Andreatch (1966)
37. Johnston et al. (1970)
38. Huffman and Norwood (1960)
39. Gerlich (1964a)

TABLE III
KV^{*4} systematics for rocksalt fluorides and oxides

Compound	$\overline{M}$	KV^{*4}
LiF	13.0	0.06
MgO	20.2	0.26
NaF	21.0	0.24
CaO	28.0	0.90
KF	29.1	0.90
SrO	51.8	1.61
RbF	52.2	1.53
BaO	76.7	2.62

TABLE IV
Ratios of melting (T_m) and Debye (θ_D) temperatures for oxide-fluoride analogue pairs

Pair	T_m^F/T_m^O	θ_D^F/θ_D^O
LiF–MgO	0.36	0.77
NaF–CaO	0.44	0.73
KF–SrO	0.42	0.72
RbF–BaO	0.46	0.76
KF–BaO	0.49	1.12
CaF_2–ThO_2	0.48	1.21
MgF_2–TiO_2	0.73	0.79
MnF_2–SnO_2	0.59	0.72
$KMgF_3$–$SrTiO_3$	–	0.79

and h and k are Planck's and Boltzmann's constants, N is Avogadro's number, and v_p and v_s the compressional and shear wave velocitites. The values of v_p and v_s have been calculated from the single crystal elastic moduli c_{ij} by the Voigt-Reuss-Hill averaging scheme; O.L. Anderson (1963) has shown that this method of calculating the elastic θ_D is equivalent to the more rigorous method of averaging the eigenfrequencies over all possible normal modes and directions of the crystal. Wherever possible, the Debye temperatures given in Table II have been calculated using the elastic constant data near 0°K; in the other cases, room temperature elastic data were employed so that the values of θ_D will be underestimated. In Table III we also list the ratios of the Debye temperatures for the corresponding fluorides and oxides. With the exception of the pairs containing BaO and ThO_2, the θ_D of the fluorides are 65–80% of those for their oxide analogues.

Gmelin (1970) proposed a systematic relationship between the Debye temperature and certain crystallographic parameters:

$$\theta_D = \frac{A}{a\bar{M}^{1/2}}$$

where $a = V^{*1/3}$ is a mean lattice parameter, A is an empirical constant, and $\bar{M}$ is the mean atomic weight. In Table II we list the values of $A = a\theta_D\bar{M}^{1/2}$ for the compounds under discussion. For each of the fluoride and oxide isostructural groups, the values of this product are approximately constant, especially for the rocksalt structure. Some of the scatter in this product for the other structures may be attributable to the necessity of using room temperature elastic constant data to calculate θ_D. For the corresponding pairs of fluorides and oxides, the Debye temperatures should thus be related by:

$$\theta_D^F/\theta_D^O = (A^F/A^O)(\bar{M}^O/\bar{M}^F)^{1/2}$$

so that θ_D for the oxide may be predicted from θ_D for its fluoride analogue.

The scaling of the thermal properties of the fluoride and oxide analogues offers several distinct advantages in studying fluoride models:

(a) It is experimentally possible to measure the elastic properties of fluoride compounds to much greater fractions of their melting temperatures.

(b) Their lower Debye temperatures imply that the fluorides should exhibit the linear K vs T high-temperature behaviour at lower absolute temperatures.

(c) Their lower melting temperatures facilitate the fabrication of hot-pressed polycrystalline aggregates of the binary fluorides with crystal structures of interest to geophysics; in lieu of single crystals of these compounds, these aggregate specimens may be used for high-temperature elasticity measurements by ultrasonic techniques.

3. Summary

Goldschmidt's (1927) crystal chemical modelling scheme has been employed to examine the relationship of elastic and thermal properties of fluoride and oxide compounds with the rocksalt, fluorite, rutile and perovskite structures. The bulk moduli are inversely proportional to volume for the fluorides and oxides of each crystal structure. The approximate constancy of the relative effective charge as a scaling factor for the bulk moduli of fluorides and oxides of a particular structure offers the possibility that the elasticity of oxide compounds with other crystal structures could be predicted from the data for the corresponding fluorides. In addition, the lower elastic moduli of the fluorides may enable us to measure the second-order pressure derivatives which are difficult to obtain for the oxides even with the most sophisticated ultrasonic techniques.

The lower melting and Debye temperatures of the fluorides and fluoroberyllates support our interest in utilizing these compounds as models for the high-temperature elasticity of their oxide and silicate analogues. An ultrasonic program is currently underway in our laboratory to measure the elastic properties of LiF to high temperatures; these data will permit a detailed comparison with the MgO data of Spetzler (1969), as well as evaluation of the higher order terms in various finite strain equations of state (e.g. Thomsen, 1972; Davies, 1973).

By model studies of this type, we are endeavouring to estimate the high-temperature properties of oxides and silicates, just as others (see Ringwood (1970) for a comprehensive review) have employed germanates as high-pressure models for the physical and crystal chemical properties of their silicate analogues.

Acknowledgements

We thank A.E. Ringwood for suggesting that the oxide–fluoride modelling scheme of Goldschmidt might

be applicable to discussions of high-temperature elasticity, and I.N.S. Jackson and A.E. Ringwood for comments on this paper. We are grateful to M.E. Striefler and G.R. Barsch for permission to use their data on the rutile oxides prior to publication.

References

Aleksandrov, K.S., Reshchikova, L.M. and Beznosikov, B.V., 1966. Phys. Stat. Sol., 18: k17–k20.
Anderson, D.L., 1967. Geophys. J., 13: 9–30.
Anderson, D.L. and Anderson, O.L., 1970. J. Geophys. Res., 75: 3494–3500.
Anderson, O.L., 1963. J. Phys. Chem. Solids, 24: 909–917.
Anderson, O.L., 1972. In: E.C. Robertson (Editor), The Nature of the Solid Earth. McGraw-Hill, Chapt. 21: 575–613.
Anderson, O.L. and Andreatch, P., Jr., 1966. J. Am. Ceram. Soc., 49: 404–409.
Anderson, O.L. and Nafe, J.E., 1965. J. Geophys. Res., 70: 3951–3963.
Anderson, O.L. and Soga, N., 1967. J. Geophys. Res., 72: 5754–5757.
Axe, J.D., 1965. Phys. Rev., 139: A1215–A1220.
Axe, J.D. and Pettit, G.D., 1966. Phys. Rev., 151: 676–680.
Beckman, O. and Knox, K., 1961. Phys. Rev., 121: 376–380.
Bell. R.O. and Rupprecht, G., 1963. Phys. Rev., 129: 90–94.
Briscoe, C.V. and Squire, C.F., 1957. Phys. Rev., 106: 1175–1177.
Cleavelin, C.R., Pederson, D.O. and Marshall, B.J., 1972. Phys. Rev., 5B: 3193–3198.
Coughanour, L.W., Roth, R.S., Marzullo, S. and Sennett, F.E., 1955. J. Res. Natl. Bur. Stds., 54: 149.
Davies, G.F., 1973. J. Phys. Chem. Solids, 34: 1417–1429.
Debye, P., 1912. Ann. Phys., 39: 789–839.
Gerlich, D., 1964a. Phys. Rev., 135A: 1331–1333.
Gerlich, D., 1964b. Phys. Rev., 136A: 1366–1368.
Gmelin, E., 1970. Z. Naturforsch., 25a: 887–893.
Goldschmidt, V.M., 1927. Skr. Nor. Vidensk.–Akad. Oslo, I, Math.-Naturvidensk. K., 1926, 2 no. 8: 1–156.
Hart, S. and Stevenson, R.W.H., 1970. J. Phys. D: Appl. Phys. 3: 1789–1795.
Haussühl, S., 1968. Phys. Stat. Sol., 28: 127–130.
Huffman, D.R. and Norwood, M.H., 1960. Phys. Rev., 117: 709–711.
Jackson, I.N.S and Liebermann, R.C., 1974. J. Phys. Chem. Solids, in press.
Johnston, D.L., Thrasher, P.H. and Kearney, R.J., 1970. J. Appl. Phys., 41: 427–428.
Katiyar, R.S. and Krishnan, R.S., 1969. J. Ind. Inst. Sci., 51: 121.
Lewis, J.T., Lehoczky, A. and Briscoe, C.V., 1967. Phys. Rev., 161: 877–887.
Liebermann, R.C., 1973. Phys. Eart Planet. Inter., 7: 461–465.
Liebermann, R.C., 1974. Unpublished data.
Leibfried, G. and Ludwig, W., 1961. Solid State Phys., 12: 275–444.
Macedo, P.M., Capps, W. and Wachtman, J.B., Jr., 1964. J. Am. Ceram. Soc., 47: 651.
Manghnani, M.H., Fisher, E.S. and Brower, W.S., Jr., 1972. J. Phys. Chem. Solids, 33: 2149–2159.
Marshall, B.J. and Miller, R.E., 1967. J. Appl. Phys., 38: 4749–4750.
Melcher, R.L. and Bolef, D.I., 1969. Phys. Rev., 178: 864–873.
Miller, R.A. and Smith, C.S., 1964. J. Phys. Chem. Solids, 25: 1279–1292.
Mizutani, H., Hamano, Y. and Akimoto, S., 1972. J. Geophys. Res., 77: 3744–3749.
Reshchikova, L.M., 1969. Sov. Phys. – Solid State, 10: 2019–2020.
Ringwood, A.E., 1970. Phys. Earth Planet. Inter., 3: 109–155.
Robie, R.A. and Waldbaum, D.R., 1968. Geol. Surv. Bull. 1259. U.S. Dep. Inter.
Robie, R.A., Bethke, P.M., Toulmin, M.S. and Edwards, J.L., 1966. In: S.P. Clark (Editor), Handbook of Physical Constants. Geol. Soc. Am. Mem., 97, Sect. 5: 27–73.
Roth, R.S., 1957. J. Res. Natl. Bur. Stds., 58: 75–88.
Roy, D.M., Roy, R. and Osborn, E.F., 1953. J. Am. Ceram. Soc., 36: 185–190.
Roy, D.M., Roy, R., and Osborn, E.F., 1954. J. Am. Ceram. Soc., 37: 300–305.
Shannon, R.D. and Prewitt, C.T., 1969. Acta Crystallogr., B25: 925–946.
Shannon, R.D. and Prewitt, C.T., 1970. Acta Crystallogr., B26: 1046–1048.
Smith, J.V., 1960. Acta Crystallogr., 13: 749–752.
Son, P.R. and Bartels, R.A., 1972. J. Phys. Chem. Solids, 33: 819–828.
Spetzler, H.A.W., 1969. Effect of Termperature and Pressure. on Elastic Properties of Polycrystalline MgO. Thesis, Calif. Inst. Technol., Calif.
Striefler, M.E. and Barsch, G.R., 1973. Phys. Stat. Sol., B, 59: 205–217.
Swanson, H.E., Fuyat, R.F. and Ugrinic, G.M., 1954. N.B.S. Circ., 539 Vol. III, 44.
Thilo, E. and Lehmann, H.A., 1949. Z. Anorg. Chem., 258: 332.
Thomsen, L., 1972. Phys. Earth Planet. Inter., 5: 282–294.
Vetter, V.H. and Bartels, R.A., 1973. J. Phys. Chem. Solids, 34: 1448–1449.
Wachtman, J.B., Jr., Wheat, M.L., Bates, J.L., and Anderson, H.J., Nucl. Mater., 16: 39–41.
Wang, H. and Simmons, G., 1973. J. Geophys. Res., 78: 1262–1273.
Wasilik, J.H. and Wheat, M.L., 1965. J. Appl. Phys., 36: 791–793.
Weast, R.C. (Editor), 1972. Handbook of Chemistry and Physics. Chemical Rubber Co., Cleveland, Ohio.
Wicks, C.E. and Block, F.E., 1963. Bur. Mines, Bull. 605.
Wong, C. and Schuele, D.E., 1968. J. Phys. Chem. Solids, 29: 1309–1330.